Phase Behaviour of Asymmetric Mixtures for the Net Zero Transition

Riley Vernon Latcham

A thesis submitted in partial fulfilment of the requirements for the degree of Doctor of Philosophy in Chemical Engineering of Imperial College London and the Diploma of Imperial College London

Department of Chemical Engineering
Imperial College London
London SW7 2AZ, United Kingdom

April 2025

Originality Declaration

I herewith certify that all material in this dissertation which is not my own work has been properly acknowledged.

Riley Vernon Latcham

Copyright Declaration

‘The copyright of this thesis rests with the author. Unless otherwise indicated, its contents are licensed under a Creative Commons Attribution-Non Commercial 4.0 International Licence (CC BY-NC).

Under this licence, you may copy and redistribute the material in any medium or format. You may also create and distribute modified versions of the work. This is on the condition that: you credit the author and do not use it, or any derivative works, for a commercial purpose.

When reusing or sharing this work, ensure you make the licence terms clear to others by naming the licence and linking to the licence text. Where a work has been adapted, you should indicate that the work has been changed and describe those changes.

Please seek permission from the copyright holder for uses of this work that are not included in this licence or permitted under UK Copyright Law.’

“My propositions serve as elucidations in the following way: anyone who understands me eventually recognises them as nonsensical, when he has used them—as steps—to climb beyond them. (He must, so to speak, throw away the ladder after he has climbed up it.) He must transcend these propositions, and then he will see the world aright.”

— Ludwig Wittgenstein
Tractatus Logico-Philosophicus

Foreword

This thesis is the culmination of four and a half years of work and serves to support the two causes that I care most deeply about: the pursuit of curiosity and the mitigation of the problems that have come about as a result of the progress it brings.

Each chapter in this thesis is preceded by a quote which I hope conveys succinctly the theme underlying its contents. It is recommended that they be read first as presented, then, upon the completed reading of the corresponding chapter, the reader is invited to reflect upon them once more.



Acknowledgements

Scientific research does not happen in a vacuum; it is dependent not only on the work of a given researcher but also on the many people who have supported and influenced them. To acknowledge and thank all of them feels to be a challenge eclipsed only by the greatest of those that will follow in these pages. I shall do my best, but, as shall be evident throughout (such as months spent on problems that would be solved in moments if only my eyes crossed the right line on a paper), I am by no means perfect, and no inclusion nor exclusion is absolute.

First of all, I must acknowledge my supervisor, Martin Trusler, who provided much guidance and inspiration, both during my PhD and in the preceding project which led me to embark upon it, as well as constant support and understanding in matters professional and personal. The achievements of this work are in no small part due to his openness to trying new things combined with the wealth of knowledge and equipment he possesses. It is one thing to know that something can be built, at least on paper, and another to actually pursue it. I would also like to thank Martin for funding much of the research itself and for providing ample opportunity to present and learn at conferences.

It would be remiss not to note the great impact of the many members of the Thermophysics group throughout my time. I have a great appreciation for my senior colleagues, Nadine Moustafa, Ziqing Pan, Kaiqiang “Victor” Zhang, Humera Ansari, Malyanah Mohd Taib, and their predecessors, who helped to define the group as it was when I joined. Of no less importance are the newer members who joined after I did, Hossam Qusty, Iusiph Eiubovi, David Uko, Yasser Aljeshi, Lillian Ladu, Lu Ai, and Miriam Hauser; as well as those who are joint members with other groups, Kleio Zervidi, Mohammed Saleh, Chao Sun, and Hao Pei. I know that the group will be in safe hands with them.

I would like to especially thank two of my fellow members, not to diminish all those others, who have done much to make the journey of myself and others easier. First, Qiaoyun Chen, who has proceeded along these same years as I; through the woes of experimental struggles and the triumph of overcoming them, from a fellow new starter in the group to one of those older members to whom those who succeed us seek advice. Second, Carsten Wedler, who taught us all much in his years with the group, setting an excellent example both in academia and in life.

There are many more who have been a part of our group for but a short time, whether visiting students and researchers such as “GC”, Keming, Xuehui, Zhiming, Sijia, Davide, and Giulia; masters students whom I have had the pleasure of assisting such as Yuyan, Hongbiao, and Wenqi; or undergraduates, notably Luc Paoli, who helped develop parts of both in-house and open source software used in this work. There are also my predecessors with the apparatus at the core of this work, Olivia Fandiño, David Vega-Maza, Saif Al Ghafri, and Lorena Souza, whose efforts I directly built upon.

While we in the Thermophysics group are primarily experimentalists, I appreciate greatly all that I have learned from the MSE group, very much our modelling complement. Some, such as Amparo Galindo and George Jackson, who once provided me with my formal introduction

to basic thermodynamics during my time as an undergraduate, have gone on to help me learn to carve out my own niche during this PhD. A special acknowledgement must be given to Andrew Haslam, who has contributed so much, from his teachings on SAFT and thermodynamics more generally, to support of Clapeyron (a software package that is used extensively within this work), and, of course, the MSE seminars over which he so carefully presides. I would, no doubt, have progressed far less in my understanding of thermodynamics if it were not for his dedication to academia on all fronts.

I owe much of my knowledge of sustainability and the transition towards net zero (TNZ) emissions to the TNZ seminar series, which have afforded me endless opportunities to learn more about this complex and diverse field. It has been an honour to be a contributor to this series, as well as an organiser of it towards the end of my time at Imperial. I am endlessly thankful to my colleagues and predecessors on the team, Carsten, Ronny Pini, Hassan Azzan, Adam Ward, Lucy Barton, Tristan Spreng, Asheeka “Ash” Padhiar, and Bhavna Patel, as well as all of the major supporters and regulars. I have immense gratitude to Geoffrey “Geoff” Maitland, who has championed this series since its inception more than a decade ago.

I would also like to extend thanks to other members of Chemical Engineering department who have helped research thrive. The likes of Gavin Barnes in the mechanical workshop and Chin Lang in the electronics workshop who, alongside their colleagues, helped manufacture and repair various custom pieces of equipment; Ed Bailey, who helped in pump repairing; Ben Kistnah and Sergio Macias Buenano, who kept the stores, and by extension the labs, stocked; Perminder Amrit and Severine Toson, whose work kept everyone safe; and Paul Fennell, for space in one of his labs. I have appreciated the culture of innovation that Omar Matar, Sandro Macchietto, and others promote, especially in the extension of research to developed processes.

There are countless individuals with whom I had beneficial conversations and for whom I wish I had the space to acknowledge. To cover but a few, Markus Richter and the others from Bochum and Chemnitz; Paul Stanwix and the others from UWA; Aaron Rowane and others from NIST; and Signe Kjelstrup and others from the nanothermodynamics community. I would especially like to thank Pierre Walker (and the broader Clapeyron team) and Ian Bell, who have both championed accessible open source thermodynamics software in recent years.

Those mentioned thus far have largely had a direct academic impact, though others have had more personal impacts that cannot be understated. If there is one person this work could not have been achieved without, it is undoubtedly my partner, Deepali. Words cannot begin to capture how grateful I am for the support which she has provided me with, standing by me ceaselessly through the most difficult and wonderful of times alike. I must also acknowledge the many years of deeply personal support I have received from my family; it has been quite the journey. I would like to especially acknowledge my father, Clive, for always teaching me that it is better to do what is right above what is easy, and for helping to fund my academic journey. I am grateful, also, to my partner’s family, who have welcomed me into their lives with such kindness.

Finally, I would like to thank you, the reader, who has picked up this manuscript in the pursuit of curiosity of one form or another, thereby contributing to the completion of its overarching purpose. Should you find its contents interesting, I direct you then towards the works of those whom I have mentioned above and throughout this work; I am certain that you will not regret it. And, when something catches your eye and compels you down different avenues than I (to think that which has never crossed my mind), we will be one step closer to understanding the truth behind these pages.

Abstract

Understanding the thermophysical properties of fluids is crucial to the effective development of industrial processes and is dependent on models optimised against reliable experimental data that are always in short supply. Veridical since antiquity, the accelerating impact of climate change and unsustainable processes have promoted it to a problem of the utmost importance and urgency. The transition towards sustainability and net zero greenhouse gas emissions requires the resolution of many known unknowns and the dissolution of unknown unknowns. Of especial significance is the behaviour of the consistently asymmetric mixtures formed by carbon dioxide (CO_2) and hydrogen (H_2). This work provides some essential fragments of the information required; investigating the phase behaviour of mixtures of carbon dioxide with methanol and with isobutane, and of hydrogen with isobutane, alongside the behaviour of hydrogen mixtures more broadly. Low uncertainty experimental measurements have extended the range of available data and have been applied to optimise and assess thermodynamic models suitable for use in process design and simulation. A methodology by which such measurements may be conducted has been developed to allow for unprecedented levels of automation, necessary to address knowledge gaps with sufficient haste. The possibility of apparatuses capable of autonomously exploring entire phase spaces, including self-calibration and some density measurement, has been demonstrated.

Contents

Chapter 1: Introduction 18
1.1 Industry, Energy, and their Impacts 19
1.1.1 The Development of Industry and the Usage of Energy 19
1.1.2 Climate Change 20
1.1.3 Net Zero Emissions and Sustainability More Generally 22
1.2 Sustainable Processes 25
1.2.1 Carbon Capture, Utilisation, and Storage 25
1.2.2 Other Sustainable Processes 30
1.3 Scope and Objectives 32
1.3.1 Mixtures Selected for Investigation 33
Chapter 2: Chemical Engineering Thermophysics 37
2.1 Introduction to Thermophysics 38
2.2 Cubic Equations of State 43
2.3 Alternative Equations of State 49
2.4 Practical Considerations for the use of Thermodynamic Models 52
Chapter 3: Phase Behaviour of Mixtures 55
3.1 The Behaviour of Asymmetric Mixtures 56
3.2 Mixtures with CO_2 62
3.2.1 Isobutane + CO_2 62
3.2.2 Methanol + CO_2 63
3.3 Mixtures with H_2 67
3.3.1 General Phase Behaviour of H_2 Mixtures 67
3.3.2 Introduction to Literature Data for H_2 Mixtures 69
3.3.3 Mixtures with Organic Compounds 73
3.3.4 Mixtures with Inorganic Compounds 76
3.3.4 Critical Behaviour of H_2 Mixtures 79
Chapter 4: Experimental Methods 83
4.1 Phase Behaviour Apparatus 84
4.1.1 Apparatus as Presented Initially 84
4.1.2 Modifications Made to the Apparatus 87
4.1.3 General Operating Procedure 92
4.2 Detector Calibration 94
4.2.1 Theory of the Composition Measurement Method 94

4.2.2 Calibration with Gas Loop Sampling 99
4.2.3 Calibration Against Synthetic Mixtures 103
4.3 Additional Considerations 114
4.3.1 Materials 114
4.3.2 Control, Data Acquisition & Processing, and Automation 116
4.3.3 Uncertainty 119
Chapter 5: Results & Discussion 122
5.1 Isobutane + CO_2 123
5.1.1 Experimental Results 123
5.1.2 Modelling Results 124
5.2 Isobutane + H_2 126
5.2.1 Experimental Results 126
5.2.2 Modelling Results 131
5.2.3 Critical behaviour 135
5.3 Methanol + CO_2 139
5.3.1 Experimental Results 139
5.3.2 Volumetric Data 146
5.3.3 Modelling Results 149
Chapter 6: Conclusions & Recommendations 160
6.1 Summary and Conclusions 161
6.2 Recommendations for Future Work 164
6.2.1 Further Experimental Investigations 164
6.2.2 Further Apparatus Development 166
6.2.3 Further Model Investigations 166
References 169

List of Figures

Figure 2.1: pT projection of the phase diagram of pure CO_2 in the vicinity of the critical point, showing the saturation curve —, thermal conductivity — and speed of sound — Widom-like lines, and the critical isochore – –, calculated using the EoS of Span & Wagner [207], along with the boundary ⋯ of $T_r \geq 1$, $p_r \geq 1$

Figure 2.2: A p_rV_r projection of the van der Waals EoS shown in reduced terms for three reduced temperatures, — $T_r = 0.9$ (● roots of the cubic equation at the saturation pressure), — $T_r = 1$ (♦ critical point), — $T_r = 1.1$

Figure 2.3: The molecular structure of isobutane, showing how it is treated within a group contribution approach, consisting of three primary CH_3 groups ● and one tertiary CH group ●

Figure 3.1: Typical p_rT_r projections of (a) type (I or 1^P), (b) (II or 1^P1^Z), and (c) (III or 1^C1^Z) mixtures, showing the pure component saturation curves —/— up to the critical points, mixture critical curves – –, VLLE curves ⋯, and shaded regions illustrating how solidification may constrain the fluid coexistence region

Figure 3.2: Typical pxy isotherms for (a) type I mixtures, (b) type III mixtures at temperatures between the critical points of either component, showing the saturated liquid — and vapour — curves, with x_1/y_1 referring to the mole fraction of the more volatile component

Figure 3.3: pxy projection for methanol + CO_2 at T = (298.15 ± 0.03) K showing the data available in the literature. Note that for clarity all datasets are represented by the same symbol

Figure 3.4: Distribution of the datasets published over time, showing (a) the year and number of datapoints included and (b) the cumulative number of datapoints as a function of time over the past century

Figure 3.5: Mixture critical curves of several hydrogen binaries as a function of reduced temperature and pressure. — — Helium [419], - - - N_2 [420], – – CO [423], — — methane [422], - - - ethane [424], – – CO_2 [426], — — methanol [512], - - - water [491] , —— isobutane (this work, discussed later in Section 5.2.3), ○ represents experimental data (filled ● in the case of data from this work), ■ represents the estimated intersection of the critical curve with the SFFE line, and ● represents the critical point of the less volatile component, please note this is hydrogen in the case of hydrogen + helium

Figure 4.1: Simplified P&ID diagram of the VLE apparatus used in this work as it was initially, as shown in [305], reproduced with permission

Figure 4.2: P&ID of the GC setup, showing the switching valves in their off position and numbered as they are in the GC itself, with the main carrier gas stream highlighted blue. In this work V2 and V3 were on the on position, such that column 2 was bypassed and the TCD used as the detector

Figure 4.3: Simplified cutaway view of the cell and ROLSI valves. LR: liquid ROLSI, VR: vapour ROLSI, EM: electromagnet, S: spring, P: piston, PS: piston seal, C: capillary, CT: coaxial tube, LT: liquid tube, SB: stirrer bar, SS: supporting structure, CL: cell lid, RR: retaining ring, OR: O-ring, CB: cell body. The pressure fittings, bath structure and working fluid, ROLSI insulation, and heated lines are not shown and the scale of the ROLSI internals has been exaggerated for visibility

Figure 4.4: Simplified P&ID diagram of the VLE apparatus used in this work as it was during measurements of isobutane with CO_2 and with H_2, adapted from [305], as shown in [138]

Figure 4.5: Simplified P&ID diagram of the VLE apparatus used in this work as it was during measurements of methanol with CO_2, adapted from [138, 305]

Figure 4.6: Chromatogram showing peaks produced by CO_2 samples withdrawn through a ROLSI valve with increasing valve opening time, with sample size ranging from approximately 35 nmol to 8.5 µmol

Figure 4.7: Calculated peaks using the EMG distribution with an area of 40000 units for varied values of variance and skewness, — $s_p^2 = 0.0001$ $\gamma = 0.1$, — $s_p^2 = 0.01$ $\gamma = 0.1$, - - $s_p^2 = 0.0001$ $\gamma = 1$, — — $s_p^2 = 0.01$ $\gamma = 1$

Figure 4.8: Sample amount calculated for varied values of variance and skewness for a peak of area 40000 units, using the optimised parameters for CO_2 ($a_i = 2885$, $b_i = -50.36$), — $\gamma = 0.1$, — $\gamma = 1$, note the x-axis is log scaled

Figure 4.9: Gas loop filling density against peak area for (a) isobutane and (b) CO_2 when using helium as the carrier gas, showing experimental points ○ and the calculated calibration curves, — loop 1, — loop 2

Figure 4.10: Relative deviations of the measured loop filling densities from the calibration equation for (a) isobutane and (b) CO_2 when using helium as the carrier gas

Figure 4.11: Gas loop filling density against peak area for (a) isobutane and (b) H_2 when using argon as the carrier gas, showing experimental points ○ and the calculated calibration curves, — loop 1, — loop 2

Figure 4.12: Relative deviations of the measured loop filling densities from the calibration equation for (a) isobutane and (b) H_2 when using argon as the carrier gas

Figure 4.13: Relative response factor of methanol compared to CO_2 as a function of ROLSI valve opening time for four mixtures prepared in the VVC, x_{CO2} = ● 0.268, ■ 0.400, ♦ 0.499, ▲ 0.600

Figure 4.14: Example chromatograms from VVC methanol + CO_2 calibrations (a) with and (b) without heating the sample return path, showing peaks produced by repeated sampling. Note that CO_2 has the lower retention time (ie it is the first in each pair of peaks) and that the sample

sizes were not the same for (a) and (b) so the absolute magnitude of the signal should not be compared here

Figure 4.15: Calibration curves for methanol — and CO_2 - - (a) across the entire relevant range and (b) for small peak areas, where the non-linearity due to adsorption is most notable

Figure 4.16: Deviations of sampled compositions from the synthetic mixture compositions for different optimised versions of the calibration equation, (a) no adsorption and CO_2 parameters taken from gas sample loop calibrations, (b) no adsorption and CO_2 parameters also regressed, (c) adsorption treated with a simple constant offset, (d) adsorption modelled using a Langmuir-like term. Each point represents the average of a sequence of samplings, typically consisting of 25 samples, x_{CO2} = ● 0.4802, ■ 0.4132, ♦ 0.5703, ▲ 0.9480

Figure 4.17: Comparison between the deviations for the single site adsorption of methanol alone ● and for the competitive single site adsorption of both methanol and CO_2 ■, as a function of the methanol peak area

Figure 4.18: The main control panel of the control and data acquisition program, as it appeared at the end of a sequence of low temperature methanol + CO_2 measurements across 7 state points. Part of this panel was developed by Souza [533], while the majority was added in this work (note that the underlying workings are not visible in this view)

Figure 5.1: pxy diagrams for [CO_2 (1) + isobutane (2)] at (a) 310 K, (b), 280 K, and (c) 240 K, showing the experimental data from this work ●, as well as the data of Nagata et al. [337] at 310 K ○, Besserer and Robinson [334] at 310.93 K ◇, Weber [332, 333] at 310.93 K □ and 280 K △. Also shown are the predictions of PR-vdW - - - and PR-mWS-NRTL — and those of EPPR78 – –, SAFT-γ-Mie – ·· –, and GERG-2008 – · –

Figure 5.2: pxy diagrams for [H_2 (1) + isobutane (2)] at (a) 190 K, (b), 240 K, (c) 280 K, (d) 311 K, (e) 339 K, (f) 363 K, (g) 375 K, (h) 390 K, and (i) 400 K, showing the experimental data from this work ●, as well as the data of Dean and Tooke [176] at (311 and 339) K ○ and the predictions of PR-vdW —

Figure 5.3: pxy diagram for [H_2 (1) + isobutane (2)] at 390 K, showing the experimental data from this work ●, as well as the predictions of PR-vdW — and those of EPPR78 – – and GERG-2008 – · –

Figure 5.4: pT diagram for isobutane + H_2, showing the vapour curves of pure isobutane — and H_2 — predicted by the EoS of Bücker & Wagner and of Leachman et al., the critical points of pure isobutane ◆ and H_2 ◆, the experimentally estimated mixture critical points ●, and the mixture critical loci predicted by PR-vdW —, EPPR78 – –, and GERG-2008 – · –

Figure 5.5: Near critical region of [H_2 (1) + isobutane (2)] at (390 and 400) K in terms of the pressure p and reduced critical composition $z_1/z_{1,c}$, showing the predictions of the scaling law — as well as the experimental data for the liquid ○ and vapour ● compositions

Figure 5.6: pT projection of the mixture critical curve – for isobutane + H_2 predicted by the PR-vdW EoS using BIPs optimised against the experimental data up to 20 MPa, including the isobutane critical point and the two experimentally estimated mixture critical points ●

Figure 5.7: pxy diagrams for [CO_2 (1) + methanol (2)] at temperatures of (a) (228 to 231) K, (b), (237 to 242) K, (c) (247 to 251) K, (d) (272 to 274) K, showing the experimental data from this work ●, as well as the values available in literature ○/○

Figure 5.8: pxy diagrams for [CO_2 (1) + methanol (2)] at 298.15 K, showing the experimental analytical liquid ● and vapour ● data and synthetic ◆ data from this work, as well as the values available in literature ○/○, and the best fit obtained with PR-mWS-NRTL — (near to the limit where unphysical VLLE predictions appear). Please note that the vapour data shown were ultimately not included in the final dataset

Figure 5.9: Cell pressure as a function of the volume of methanol swept by the pump, showing measured points ●, model calculations ●, and polynomial best fits – –

Figure 5.10: Saturated liquid densities for methanol + CO_2 at T = 298.15 K, showing the pure component vapour ● and liquid ● densities, experimental measurements ●, literature data of Brunner [363], Chang et al [412], and Benzanehtek et al [383], and an example of typical PR-vdW model predictions –/– encountered during optimising only for pTxy data, in this case without volume translation to emphasise the difficulty in capturing liquid densities with cubic EoS (note that a prediction of liquid-liquid separation appears as a horizontal line). Also shown are the predictions of SAFT-γ-Mie – – using the literature parameters

Figure 5.11: Density of compressed liquid methanol + CO_2 against composition during cell filling at T = 298.15 K, showing measured densities ● (with expanded (k = 2) uncertainties) and the densities expected in the case of ideal mixing ●

Figure 5.12: Parameter space for PR-vdW at T = 298.15 K when minimising the sum squared error in composition against the data produced in this work, shown as (a-c) an error heatmap increasingly focussed on the near-optimal region and (d) projected l_{ij} – error plane, with multiple local minima visible. Regions of lower error are shown in dark blue (note colour bars are excluded as relative values are of greater importance here) and the located minimum ● is indicated

Figure 5.13: Optimal values of the BIPs k_{ij} ○ and l_{ij} ○ in the PR-vdW model as a function of temperature (for ~1 K groupings), showing the optimised polynomial functions of temperature ···/···. Note for T > 450 K there is an additional point where the (473.15 and 477.6) K data have been grouped together, to supplement the data scarcity and scatter in that region

Figure 5.14: pxy diagram for methanol + CO_2 at (230 to 298.15) K, showing experimental data from this work ○ and predictions of PR-vdW –/–

Figure 5.15: pxy diagram for methanol + CO_2 at (230 to 298.15) K, showing experimental data from this work ○ and predictions of SAFT-γ-Mie –/– when using literature unlike interaction parameters [570]

Figure 5.16: pxy diagram for methanol + CO_2 at (a) 230 K, (b) 240 K, (c) 250 K, and (d) 273.15 K showing experimental data from this work ○ and predictions of SAFT-γ-Mie –/– when using literature unlike parameters or when optimising both unlike parameters

Figure 5.17: pxy diagram for methanol + CO_2 at (230 to 298.15) K, showing experimental data from this work ○ and predictions of PSRK –/–

Figure 5.18: pxy diagram for methanol + CO_2 at (230 to 298.15) K, showing experimental data from this work ○ and predictions of the EoS of Blackham & Lemmon –/–

Figure 5.19: pxy diagram for methanol + CO_2 at 298.15 K, showing exp data ● and predictions of PR-mWS-NRTL —, PSRK – –, SAFT-γ-Mie - - - (with literature BIP values), and Blackham & Lemmon – · –

List of Tables

Table 2.1: Conjugate pairs of variables that contribute to the energy of real systems, adapted from [188, 189]

Table 3.1: Pure component parameters: critical temperature T_c, pressure p_c, and density ρ_c, as well as molar mass M, acentric factor ω, and triple point temperature T_t [207, 282-284, 305]; real and adjusted (*) critical points for hydrogen are listed, see [305] for details

Table 3.2: Previous investigations into the phase behaviour of isobutane + CO_2 including the temperature and pressure ranges covered

Table 3.3: Previous investigations into the phase behaviour of methanol + CO_2 including the temperature and pressure ranges covered

Table 3.4: Previous investigations into the density of methanol + CO_2 including the temperature ranges covered and whether the data are for saturated vapour (SV), liquid (SL), or compressed fluid single-phase (CF) density

Table 3.5: Availability of data for considered binary mixtures of hydrogen with different groups of molecules

Table 3.6: Overview of available data sets for the phase behaviour of binary mixtures with hydrogen

Table 4.1: Equations of state used to calculate gas loop densities for calibration, their relative uncertainties, and references

Table 4.2: Optimised calibration constants for the components investigated in this work with their respective carrier gases

Table 4.3: Compositions of the methanol + CO_2 calibration mixtures, as determined from the preparation of the synthetic mixture $x_{CO2,synth}$ as well as the average values obtained from sampling with the liquid $x_{CO2,\ Liq\ ROLSI}$ and vapour $x_{CO2,\ Vap\ ROLSI}$ ROLSI valves

Table 4.4: Optimised calibration constants for CO_2 and methanol using the adsorption corrected calibration equation, helium as the carrier gas, and different values for either ROLSI valve for methanol

Table 4.5: Optimised conditions for the GC and sampling system used in methanol + CO_2 measurements and the resultant retention times for each component

Table 4.6: Description of the materials used and their mole fraction purities

Table 4.7: Quality of the methanol batches as specified and as per the certificate of analysis for their particular lots, given on a mass fraction basis to the resolution provided

Table 4.8: Standard uncertainties of the relevant measured quantities

Table 5.1: Experimental phase behaviour data for [CO_2 (1) + isobutane (2)], the temperature, T, pressure, p, liquid, x_1, and vapour, y_1, compositions and their combined standard uncertainties, $u_c(x_1)$ and $u_c(y_1)$

Table 5.2: Optimised constants for the temperature dependent binary interaction parameters for the two PR EoS models for isobutane + CO_2

Table 5.3: Experimental phase behaviour data for [H_2 (1) + isobutane (2)], the temperature, T, pressure, p, liquid, x_1, and vapour, y_1, compositions and their combined standard uncertainties, $u_c(x_1)$ and $u_c(y_1)$

Table 5.4: Optimised constants for the temperature dependent binary interaction parameters for PR-vdW EoS model for isobutane + H_2

Table 5.5: Estimated critical pressure, p_c, and composition, $z_{1,c}$, for [H_2 (1) + isobutane (2)] at experimental temperatures, T

Table 5.6: Values of the parameters used in the determination of critical points using the critical scaling laws and estimation of near critical uncertainties

Table 5.7: Experimental phase behaviour data for [CO_2 (1) + methanol (2)], the temperature, T, pressure, p, liquid, x_1, compositions, their standard uncertainties, $u(x_1)$, and their combined standard uncertainties, $u_c(x_1)$

Table 5.8: Rough saturated liquid density data obtained in this work at T = 298.15 K

Table 5.9: Low uncertainty compressed liquid density data obtained in this work at T = 298.15 K during preparation of the fourth synthetic calibration mixture, including the expanded (k = 2) uncertainties in composition and density, as well as relative expanded uncertainties for the latter

Table 5.10: Optimised constants for the temperature dependent binary interaction parameters for the PR-vdW EoS for methanol + CO_2 across the entire temperature range

Table 5.11: Newly optimised constants for the temperature dependence of the unlike interaction parameters for SAFT-γ-Mie for methanol + CO_2 for temperatures between (230 and 273.15) K

Chapter 1: Introduction

“Phlebas the Phoenician, a fortnight dead, forgot the cry of gulls, and the deep sea swell and the profit and loss. A current under sea picked his bones in whispers. As he rose and fell he passed the stages of his age and youth entering the whirlpool. Gentile or Jew, O you who turn the wheel and look to windward, consider Phlebas, who was once handsome and tall as you.”

— T.S. Eliot
The Waste Land IV: “Death by Water”

1.1 Industry, Energy, and their Impacts

1.1.1 The Development of Industry and the Usage of Energy

The story prefacing this work begins with onset of industrialisation, at least, when scope is restricted sensibly. At this time, the scales at which people could harness energy and matter ceased to be negligible within the overall global mass and energy balances. It is also the origin of modern chemical engineering. The two are deeply intertwined, as are their benefits and consequences.

Technological development, much like learning and, pertinently, climate change, is an exponential process. The building up of infrastructure and understanding allows for further development to proceed at a faster rate, which, combined with economies of scale, provides impetus for a runaway feedback loop. It is here that the crux of the issues underlying the following discussions rests: the ability to utilise something does not require that the usage be sustainable (whether across the span of a second, a decade, or up to the limit of infinite time).

Industrialisation allowed the processing of material at unprecedented scales, increasing in a manner that is roughly proportional to the energy required. Improvements in efficiency, such as with the development of the steam engine (and early thermodynamics with it), in many cases resulted ultimately in greater usage of energy and materials as noted as early as 1865 by Jevons [1]. Jevons' work was especially concerned with the usage and potential depletion of supplies of coal, however it is echoed throughout the anthropogenic use of energy [2].

Coal, like wood before it, was initially primarily limited to heating [3]. The development of thermodynamic cycles allowed for this thermal energy to do "work", and their combination could then be dispatched to process chemicals. For example, coal could be heated in the presence of steam and limited oxygen (O_2) to produce Town gas [4], a gaseous mixture rich in hydrogen (H_2) and carbon monoxide (CO). Coal could provide the thermal energy required, both to sustain the reaction and to heat steam that could do work on turbines that, in turn, rotate compressors to do work on the Town gas, such that it may be conveyed through conduits for downstream use in producing light or heat. This process would also produce limited amounts of ammonia (NH_3) [5], with the incorporated nitrogen (N_2) coming from the atmospheric air fed in to provide oxygen.

Fixed nitrogen, of which ammonia is a prominent example, is essential for the growth of biological organisms, yet the necessary breaking of the triple bond between nitrogen atoms is energy intensive. Growing populations and limited natural supplies of fixed nitrogen produced similar concerns of sustainability as were voiced with coal [6]. The solution to this problem stands as one of the greatest achievements of the 20th century: the Haber-Bosch process [7].

Coal could be gasified as before, but instead of burning the resulting mixture, it could be used as synthesis gas (syngas) from which more complex chemicals could be produced. Mixing this syngas with atmospheric air and performing the water-gas shift reaction and scrubbing could produce a high purity stream of nitrogen and hydrogen. Raising this mixture to high pressure (*eg* 20 MPa), in the presence of a catalyst, would promote the reaction to form

ammonia in accordance with Le Chatelier's principle. Such ammonia could then be reacted further to produce fertilisers in a way that remains responsible for feeding most of the world's population today, more than a century later [7]. It should be noted, for future reference, that the high pressures involved (especially in the presence of hydrogen) were thought to be unmanageable by most in industry at the time [8], yet engineering overcame this challenge mightily.

The use of old carbonaceous energetic materials (fossil fuels), and their derivatives, grew and evolved substantially in the 20th century, providing the necessary energy and chemicals for socioeconomic growth. Many processes found extensive use during periods of war and some, such as the Bergius process, eventually ceased to exist [9] when the available feedstocks changed and new processes were developed. A notable example that remains relevant especially to the discussion that follows is the Fischer-Tropsch process for synthetic hydrocarbon production [10]. Natural gas, a methane-rich fossil fuel, has displaced the majority of coal usage, including as a source of hydrogen for the aforementioned reactions, with the majority of hydrogen now produced via steam-methane reforming [11]. Synthetic polymers would eventually be developed and applied both to everyday life and industry with great benefit [12].

Concerns around the use of these processes remained focussed on the finite, effectively non-renewable, supply of feedstocks. Would coal run out? Would oil? Would natural gas? It was long evident that unsustainable growth would always be a concern; the broader considerations were only just beginning to be understood. It was now that a greater concern reared its head, one for which all of the world could bear witness.

1.1.2 Climate Change

Anthropogenic climate change represents one of the greatest obstacles facing humanity today. The reality of it is generally accepted worldwide and virtually unanimously accepted within the scientific community [13], while the consequences of this climate change have become ever more widely recognised with much attention focused on preventing the growth of this problem.

While theories of small-scale climate change have existed since antiquity [14], it was not until the early 19th century that the potential for global climate change was realised. In 1824, Fourier theorised that the atmosphere played a significant role in warming the planet and recognised that human activities could influence global temperatures and change the climate [15]. By 1838, Pouillet had proposed that carbon dioxide (CO_2) and water vapour may warm the atmosphere by trapping infrared (IR) radiation and, in 1959, Tyndall's research into the absorption of IR radiation by various gases would give further credence to this theory [16].

The first significant calculations of the potential effect of this newly discovered global warming effect were performed in 1896 by Svante Arrhenius who found that doubling the level of carbon dioxide in the atmosphere would result in a warming of 5-6 °C, though modern estimates are lower [17]. It is worth noting that at the time of this startling observation atmospheric carbon

dioxide was 295 ppm [18], while in 2020 (at the start of this work) this had risen considerably to ~413 ppm and by 2025 to ~427 ppm [19]. The concept would gain the name “the greenhouse effect” in 1909 [20, 21], but would be met with heavy scepticism for many years to come. The development of spectroscopy further established the capacity of carbon dioxide to absorb IR radiation, and correlations between rising temperatures and atmospheric CO_2 levels were made, though largely ignored [22].

Despite the criticism, the evidence in favour of the greenhouse effect and the overarching concept of man-made climate change continued to grow, bolstered by new and more accurate techniques and the advent of computing. In 1960 and 1961 Keeling published his work on what would come to be called the “Keeling Curve” [23], showing the clear rise in atmospheric CO_2 and accelerating the acceptance of Arrhenius’ work after more than half a century of doubt. Many chemicals would go on to be identified as greenhouse gases, such as methane, oxides of nitrogen, and a number of refrigerants.

In the 21st Century, the mechanics and consequences of climate change are much better understood. The most immediately apparent issues result directly from the global temperature increase that greenhouse gases cause, for instance many organisms are not suited to higher temperatures and are incapable of adapting within a short timescale [24]. A large fraction of the world’s seasonal ice deposits has been melting earlier and to greater extent than seen historically, resulting in a feedback loop that has consistently decreased total ice coverage [25]. Sea levels have risen, driven both by the flow of terrestrially bound water to the ocean (*eg* melting glaciers) and the thermal expansion of water, and threaten to submerge vast areas of land. Weather has become more variable and extreme [26]. Food supplies are under threat [27, 28]. There is a litany of less direct effects, for instance, malaria-carrying mosquitoes are thriving in an ever growing area [29]. In contrast to these widespread issues, there are some regions that stand to benefit from climate change, for instance northern Russia expects to see reduced energy usage [30], but these cases are relatively few.

The general scientific consensus from around the late 20th Century onwards was that anthropogenic climate change was indeed possible and of potentially significant concern, with organisations such as the Intergovernmental Panel on Climate Change (IPCC), set up in 1988, encouraging research and government action [31]. Public opinion, however, lagged substantially behind, in part due to the actions of companies who understood the issue as early as 1977 [32] but had a vested interest in downplaying the consequences. Today, much of the world has come to acknowledge the existence of climate change, though a non-negligible fraction of people still question its anthropogenic nature [33].

The prevention and treatment of the problems of anthropogenic climate change is widely expected to be an expensive endeavour, especially in scenarios in which serious action is delayed [34]. The long term gains are considerable and cannot be neglected, and the resulting scientific advances will have widespread impact. The costs of unsustainable growth must always be paid; if society will not enforce payment, thermodynamics will do so unilaterally.

Serious international attempts to combat climate change have been gaining traction, most notably resulting in the ratification of several multinational agreements beginning in earnest in

1972 with the United Nations Conference on the Human Environment in Stockholm. All 113 countries in attendance opted to adopt the Stockholm Declaration, agreeing to take responsibility for their effects on the environment and officially recognising the fundamental human right to a safe and healthy environment [35]. This marked a turning point in climate science and demonstrated that a multilateral approach to fighting climate change was indeed possible. Building upon this momentum, the 1985 Vienna Convention for the Protection of the Ozone Layer and resultant 1987 Montreal Protocol on Substances that Deplete the Ozone Layer gained widespread support, and in 2009 became the first universally ratified treaties of the United Nations, ratified by all 196 countries at the time and the Holy See (by their definition).

1992 saw the creation of the United Nations Framework Convention on Climate Change (UNFCCC) [36], the first major multilateral agreement explicitly aimed at controlling atmospheric greenhouse gas concentrations in general. At the centre of this was an agreement by signatory nations to stabilise their greenhouse gas emission at 1990 levels by the year 2000 [37]. At the first Conference of the Parties, held in 1995, to discuss the implementation of the UNFCCC, it was concluded that this goal was “not adequate” and in 1997 the Kyoto Protocol was adopted [38], the first of two significant extensions to the UNFCCC. In 2010 the overarching target was changed to focus on limiting global warming to below +2 °C relative to pre-industrial levels.

The Kyoto Protocol was succeeded by the Paris Agreement, which came into effect in late 2016 [39]. Like the Kyoto Protocol before it, this agreement seeks to improve upon the goals of the UNFCCC with stricter targets and, in theory, better regulation. The Paris Agreement stipulates that the warming should be kept “well below” +2 °C and ideally limited to +1.5 °C. The achievability of these goals is questionable [40], but, should the past be any indication, it is likely new agreements will have to be negotiated. Warming had reached +1.1 °C in the 2011-2020 period [41] and, in the 12 month period ending August 2024, the average warming peaked at +1.6 °C [42] following an El Niño. The rate of warming appears to be accelerating.

1.1.3 Net Zero Emissions and Sustainability More Generally

One of the most significant driving forces for anthropogenic climate change is the release and subsequent accumulation of greenhouse gases in the atmosphere. There is a wide range of direct and indirect greenhouse gases, whose properties and effects vary but are often simplified to global warming potential and longevity in the atmosphere.

The concept of the global warming potential (GWP) is used to normalise the magnitude of a given gas’s ability to cause global warming, with CO_2 being the reference, providing quick insight. However, different gases are capable of remaining in the atmosphere for longer or shorter periods, their potency varies with time, and there are indirect effects resulting from (among other things) degradation products. For example, the IPCC estimates that methane has a global warming potential 84 times that of CO_2 20 years after its release into the atmosphere [43], but this degrades over time to a GWP of 28 over 100 years and then down

to 7.6 over 500 years [44]. Hydrogen has no direct global warming potential itself and is short lived in the atmosphere, yet has a 100 year GWP of 11.6 as a result of indirect effects [45].

Significant greenhouse gases are CO_2, methane, and volatile fluorinated compounds. CO_2 is most familiar, a direct product of carbonaceous fuel combustion, though the production of cement and steel are responsible for more than 13% of overall CO_2 emissions [46]. There are no significant growing natural sources of CO_2 (*ie* all non-anthropogenic CO_2 entering the atmosphere is part of the normal carbon cycle). Methane is notably different in this regard, as natural sources account for around 40% of its emissions [47], with the majority coming from wetlands, where it is produced by microbes, and the remainder from various smaller sources. One of these sources is methane clathrates, methane trapped in a solid ice-like structure, the impact of which is still under debate [48]. Concerns have been expressed about the possibility of feedback loops leading to a “clathrate gun” scenario, as there are vast natural deposits of such clathrates that are bordering on thermodynamic instability as temperatures rise. The anthropogenic methane emissions come primarily from the agricultural (40%) and energy (37%) sectors [47]. Fugitive emissions of methane, that is to say, unintended emissions occurring during production, handling, and use, are a major concern with serious implications for feasibility of climate action. For example, it is, overall, more environmentally friendly (and generally more efficient) to extract and burn coal locally than to produce natural gas in the US and transport it across the globe in liquified form at low temperature (liquified natural gas, LNG) [49], as a result of current fugitive emission levels in the US (primarily avoidable emissions resulting from lax regulations). Finally, there are emissions of volatile fluorinated compounds, primarily related to refrigeration. These will be discussed further below and are responsible for approximately one tenth of the warming experience thus far [41].

The fine details and mechanics of the effects these compounds have on the environment are beyond the scope of this work and the curious reader is directed to the extensive works of bodies such as the IPCC [41, 50-55], now in its seventh assessment cycle, for a suitable starting point. Note that not all compounds with non-negligible atmospheric interactions promote warming, and some may mask the true extent of warming, like sulphurous compounds whose lifetimes are much shorter than the positive GWP compounds they are often emitted alongside.

The most readily apparent solution to climate change is to greatly reduce greenhouse gas emissions and to remove historical emissions from the atmosphere; the intricacies of this are non-trivial and highly constrained. There are two broad options: directly reducing or removing the emissions sources, or offsetting/accounting for them in such a way that the there is no overall net impact. In practice, a mix is required [52, 55]. The literal complete removal of all anthropogenic emission sources would require the abandonment of all non-natural processes; impractical and, more crucially, unenforceable. At the other extreme, one could make no adjustments from ‘business as usual’ except to respond to every emission with a commensurate removal of greenhouse gases from the atmosphere; a similarly impractical (due to mass and energy constraints) and unenforceable (if equity is desired) approach.

An exemplary case of the broader complexities faced is the concept of planting trees to offset emissions. On the face of it, this is an apparently simple and effective approach: trees take

energy from an external (depending on where one draws system boundaries) source, sunlight, and use it to reduce CO_2 into more usable forms of carbon, including perhaps sequestering some of it within themselves. Reality is not kind to this concept [56, 57]. To express but a few reasons:

- Trees are carbon positive in their early life
- The carbon they process is either used (and re-released as CO_2) or typically converted to methane by microbial action at the end of their lives
- Trees are ubiquitous with capturing and using carbon yet are not the main biological group to do so (a title that instead adorns marine microbes) nor the most efficient
- The logistics and realisation of planting trees have associated emissions, including secondary and tertiary emissions, such as those involved with transporting workers and those in powering a computer on which plans may be made
- Effort and expenditure directed towards the planting of trees cannot also be used elsewhere
- The most efficient implementation, the maximally verticalised use of a very limited number of species, has the greatest potential to disrupt existing ecosystems and is immensely vulnerable to disease and broader ailments (including the effects of warming temperatures)
- The realisation of the concept may have unknown consequences that may only be recognised once it is too late, much as the solution to many human problems through the use of energy has led to the current situation
- The monitoring, reporting, and verification of the emissions offset are borderline intractable

Almost-paradoxical complexities like this are found in all aspects of climate change mitigation and typically grow in scale as their realities are appreciated. The energy polylemma is one of the better discussed broad examples [58-60]. Risk management and reasonable compromise are essential, thus the route pursued is a balanced one [61] (albeit woefully inadequate thus far). The overarching target is to ensure that, regardless of how it is achieved, the impact of emissions (whether CO_2 or something that may be expressed in CO_2 equivalent terms) must balance to have no further net contributions: the concept of net zero greenhouse gas emissions (simply: net zero) [52]. Beyond this is the realm of net negative emissions, which seek to reverse the harm already done by legacy emissions. The underlying concepts for net zero and negative emissions are identical, so little distinction shall be made in this work and net zero will be the preferentially used term.

Simply hitting net zero does not ensure that all forms of climate change cease nor does it necessitate that all processes be sustainable, as has been alluded to already. The scale of the problem to be addressed is far beyond individual comprehension, and the timescale within which progress must be made shrinks as the problem accelerates. Humans are exceptionally talented at producing CO_2, the only other compound processed on a comparable scale is water. Note here that water has its own plethora of sustainability issues [62, 63].

All solutions require the use of energy and key materials, such water, cement, iron, lithium, and copper. All can only be produced at finite scale, with new projects taking finite time to be commissioned (typically on the order of years), and all potential uses are in direct competition.

Any new processes take time to mature. Taking all of this into consideration, the mitigation of climate change represents the largest and most complex task ever undertaken and must be carried out at unparalleled pace. Focus now turns to (a non-exhaustive) discussion of how this may be achieved.

1.2 Sustainable Processes

1.2.1 Carbon Capture, Utilisation, and Storage

One of the major cornerstones underpinning the management of climate change is the concept of carbon capture, utilisation, and storage (CCUS) [64-68]. CCUS is a broadly applicable approach that is the most mature and scalable form of "engineered" (in contrast to nature-based) carbon abatement [64]. It remains in need of much further development, despite its relative maturity, from fundamental science and process design to regulation and insurance [69, 70]. It may be divided into two primary subcategories, defined by the processes following the carbon capture stage, where carbon dioxide may either be stored or go on to serve a specific function, called carbon capture and storage (CCS) and carbon capture and utilisation (CCU), respectively. While many more-overarching approaches contain elements of both of these, specific processes normally focus on just one.

Both CCS and CCU both begin with capturing carbon dioxide. For point source capture (*eg* capturing the flue gas produced by a combined cycle gas turbine) this is often split into two major types: pre-combustion and post-combustion [71]. For cases of the latter where the source is does not involve combustion, as in the case of cement manufacture [72], the term may be viewed as post-CO_2-production, though the term post-combustion remains prevalent in literature.

Pre-combustion carbon capture aims to remove carbon dioxide from a process before it would normally have been generated. When hydrocarbons are combusted in air the two main products are water and, of course, carbon dioxide. Instead of this, pre-combustion capture begins by reacting the fuel to produce a syngas mixture containing mainly hydrogen and carbon dioxide, along with by-products such as carbon monoxide. The hydrogen can be separated from this mixture and used as fuel, where its combustion will yield only water vapour. Meanwhile, the carbon dioxide can be separated, compressed, and either stored or utilised in ways that will be discussed below. Capturing carbon in this way has advantages and disadvantages. For instance, hydrogen burns much more cleanly than traditional fuels, with exhausts that are simpler to manage. On the other hand, hydrogen's low density can complicate transportation and storage, while also having increased safety risks [73], and higher flame temperatures make drop-in replacement challenging.

Post-combustion carbon capture is the most common approach considered and implemented today and can be added to many processes retroactively [65, 67]. Here, one burns fuel as in traditional processes, producing a relatively dirty exhaust as a result of incomplete combustion and impurities present in the fuel and air streams. This exhaust is then processed to remove components such as ash and sulphurous compounds, before separating out carbon dioxide

and leaving behind a relatively clean exhaust. This approach is also conceptually identical to other forms of point source capture that do not involve combustion, differing mainly in which impurities are present and the temperature of the feed stream.

There is a subset of post-combustion capture known as oxy-fuel processes [67]. Instead of burning fuel in air, one uses high purity oxygen that has been extracted from the air by upstream processes. This allows for significantly cleaner and more complete combustion, resulting in an exhaust stream that is primarily carbon dioxide and water vapour, significantly simplifying the downstream separation of CO_2. This process can be combined with electrolytic hydrogen production, wherein oxygen is a byproduct, to yield a good example of process integration helpful in the net zero transition.

Point source capture is the only variety of CCS to have reached large scale deployment, with ~40 Mt of CO_2 captured and stored this way yearly, though the total stored has yet to breach 1 Gt and progress is lagging well behind targets [41]. For reference, accounting for "business as usual" emissions with CCS alone would require ~50 Gtpa, three orders of magnitude higher, while balanced approaches that heavily implement low-emissions energy sources and process efficiency improvements would require ~10 Gtpa [69]. At the other extreme there is direct air capture (DAC/DACCS), wherein CO_2 is captured from atmospheric air wherein it is much more dilute [74]. This process is more energy intensive and roughly an order of magnitude more expensive, however it is the only negative emissions technology that is both sufficiently scalable to account for hard to decarbonise sectors and robustly quantifiable [64]. A growing number of multinational conglomerates are joining the voluntary carbon market and attempting to offset their emissions, primarily reliant on DAC, and are paying on the order of several hundred dollars per tonne of CO_2 [74] compared to the ~$50 per tonne achievable in point source capture [75]. The cost of DAC is expected to continue to drop steadily in the near future [74, 76, 77] due to the relative infancy of the technology and the growing interest in it that is accelerating with the rate of climate change.

The separation of CO_2 from whatever stream it is present in is carried out using either absorption, adsorption, or to a lesser extent, membranes (alternatives such as cryogenic separation are possible but rarely implemented to date). The classic process for comparison in contemporary technoeconomic assessments is the reactive absorption with aqueous monoethanolamine (MEA) solution [78], though real extant processes prefer blends that are often proprietary. In this process, CO_2 is brought into contact with an aqueous MEA solution where it reacts to form carbamates and carbonates, then passed to a desorption column to regenerate the MEA and produce a CO_2-rich outlet stream. The enthalpy of reaction is high, such that processes of this type are (at first approximation) assessed based upon the reboiler duty required. Not all absorptive capture processes are reactive, physisorption is also possible and well established, for example in the Rectisol process [79]. This simple and flexible process [80], originally specific to acid gas sweetening (wherein CO_2 is such an acid gas), uses low temperature (~230 K) methanol to absorb the CO_2 at low (<1 MPa) pressures, with regeneration achieved through simple pressure and/or temperature swings. Adsorption-based processes, such as those using zeolites or metal organic frameworks [77], are the solid-fluid equivalent to the purely fluid-based absorption processes, and may similarly rely on either physisorption or chemisorption. These approaches are especially beneficial when handling

dilute gas streams, as in the extreme case of DACCS [81]. Membrane-based processes are the most distinct in their mechanism and may theoretically have negligible thermal energy requirements. In practice, they are not widely used for CCUS, involve non-negligible pressure duties and the membranes themselves are almost always polymeric or built upon a polymeric support [82], and thus susceptible to CO_2 induced swelling resulting in loss of performance.

High selectivity is desired in all capture processes, especially in comparison to nitrogen, carbon monoxide, and methane. Water is not handled trivially as an impurity by any of these processes, increasing energy requirements overall, but may be removed upstream (for example using desiccants such molecular sieves or silica gel). Almost all sorbents and membranes face issues with degradation, only avoided by stable molecules like methanol, and purge and makeup streams may be required in any case. Degradation may be driven by specific impurities and not all potential impurities are present in a given process, thus a degree of tailoring is beneficial. There may also be strict requirements on impurity tolerances that may otherwise result in corrosion or unwanted phase separations downstream of the capture process [83].

Regardless of the capture technique considered, one is left with carbon that must then go somewhere. The bulk of the burden lies in carbon storage, as this is what primarily contributes to climate change mitigation. Where the store may be, what it might involve, and how permanent it is, are not inherently set.

When deciding on a means to store carbon, one must consider carefully the planned duration of storage and the uncertainties associated with it. It is not possible to say with certainty if any method will be truly permanent, however such a strict requirement is not necessary as such infinite timescales are irrelevant when addressing a problem that is occurring over a short finite time. This slackens the requirement to simply needing to be sufficiently certain that the storage endures for long enough to have been worthwhile, on balance. In a system with many stores of differing nature, this requirement is that the average failure/reemission rate and extent be acceptable. This requirement is still vague, yet its form is one that may have meaningful values ascribed to it, even if the reasoning behind any particular set of values is imperfect. For example, the target could be that 95% of stores retain, on average, 95% of the CO_2 initially stored within them, after 100 years. This is a quantifiable, verifiable, and (not to be neglected) insurable requirement. It is similar to what has been successfully applied in other sectors, such as the storage of nuclear waste or the sealing of natural gas reservoirs. Further discussion is neglected for brevity and because it is an area of ongoing debate.

The form this store might take is another important consideration. In principle, storage could be in either a manufactured structure or a naturally occurring one, however, the sheer volume of carbon to be stored renders the former impractical. Instead, one can rely on various existing underground geological formations, effectively naturally occurring storage tanks, a vastly less labour intensive approach with storage capacities of scales incomparable to any artificial structures.

While conventional forms of storage, like tanks, are generally large uninterrupted volumes encompassed by an impermeable barrier, geological storage takes a very different form. The

rock formations considered for carbon storage typically consist of porous rock containing many microscopic interconnected voids beneath a layer of denser cap rock [84]. CO_2 can be injected into these formations, permeating through the porous rock and occupying any available pore space, while the impermeable cap rock keeps the CO_2 trapped and unable to return to the atmosphere. Such structures are, of course, less space efficient than conventional forms of storage on a volume stored per total volume basis, but, at the massive scales considered, one can store vast quantities of CO_2. There are two main types of formations that are suitable for this storage: saline aquifers and depleted oil and gas reservoirs, although deep coal seams also represent a notable potential storage volume [85].

The most explored of these options is storage in oil and gas fields. The reason for this is simple, geological stores are not just unoccupied volumes, they contain fluids that must be displaced. For reservoirs containing oil and gas, the CO_2 displaces these more valuable fluids, which can be recovered, processed, and sold, providing an economic incentive to carbon sequestration. The most common implementation of this process is known as enhanced oil recovery (EOR), which has been applied since 1972 [86], beginning with the Sleipnir field (whose subsurface CO_2 plume has been characterised over time). Enhanced oil recovery can be a form of both carbon storage and carbon utilisation, dependant on whether or not notable quantities of CO_2 remain trapped within the rock. In either case, the fuel produced may to go on to be combusted with the CO_2 emissions being released to atmosphere, making the environmental benefits of such processes questionable [87]. There are more than just financial benefits to storing carbon in reservoirs, depleted or otherwise. Many such formations have been explored in great detail and have existing infrastructure that can be repurposed, and one can benefit from decades of operational experience.

On the other hand, detailed understanding of saline aquifers is less developed. Additionally, exploration and development of these aquifers lack the great financial incentive that benefit oil and gas fields. In spite of this, saline aquifers hold a lot of promise. They represent the largest available geological store of CO_2, with capacity for an estimated (1 to 10) Tt of CO_2, potentially more than oil and gas reservoirs and coalbeds combined [85]. They are also more likely to have public opinion in their favour; as the effects of climate change are realised and public (and political) support of fossil fuel production wanes, the more challenging it grows to continue EOR. The same cannot necessarily be said for the extraction of all valuable contents of geological formations, such as helium or hydrogen.

Coupled to the question of the form of the store itself is the matter of what form should the carbon be in while stored. When injected into the subsurface it is typically as a compressed liquid-like phase or dissolved in aqueous solution (*eg* formation brine). The movement of this CO_2 is complex and formation dependent, for instance it will certainly not move isotropically and may rise or sink depending on the depth of the formation (as a result of barotropy). Furthermore, geological structures are interconnected, especially when faults are present. For certain structures, such as those rich in olivine [88], the CO_2 will mineralise to form solid carbonates, the permanence of which is practically assured on timescales relevant to life on Earth. At an extreme, the carbon may be returned to its original hydrocarbon state, such as synthetic oil; while a poetic example of lessons learned and mistakes corrected, this approach

is not practical. This is not to say that synthetic hydrocarbons as an overarching family are not practical however, as is seen with CCU [89].

Carbon capture and utilisation is a concept that, in some ways, attempts to go a step beyond the goals of the more tradition approaches of CCS. In place of storage, it considers how undesirable carbon may be able to benefit the world by giving it purpose anew.

There are many different ways in which one could utilise carbon once it has been captured, and it should be noted that CCU is not inherently carbon neutral nor negative. Consider the case of carbonating beverages with captured carbon where, upon a brief period of storage, CO_2 is re-emitted to atmosphere. A similar, more practical case is the production of synthetic fuels intended to be combusted. Here, CO_2 could be captured, converted into fuel, and used to produce energy, leaving it in the same form it started as. Should one repeat this process indefinitely, the chemical recycling of CO_2 would be established, resulting in little to no new primary emissions overall [90]. If this energy would previously have been produced by conventional means from fossil fuels, some amount of emissions can be said to have been successfully abated, however caution is advised not to equate all instances of CO_2 emitted or avoided. There are, of course, also many cases where a clearer positive impact is achieved, with nature inspiring some simple examples. For instance, carbon may be incorporated into cement and concrete in various ways [91] where it may remain for hundreds of years, though it is challenging to monitor and verify what happens to the carbon, especially as the average modern building is not built to last a century. A similar set of concerns surrounds the use of trees in construction, though in this case the longevity is more assured than in their natural environment. These examples help illustrate the three route major routes one may consider for industrial scale CCU: non-transformative utilisation, chemical synthesis, and biomass cultivation.

One form of non-transformative technique has been mentioned already, due to some overlap with CCS, which is enhanced oil recovery. Here carbon is put to use in an effective, albeit environmentally questionable, way, only requiring that it be compressed and transported to an injection site. As with the beverage example also, these approaches often do not accomplish notable emissions reductions.

Therefore, to ensure a more meaningful impact, one turns to transformative techniques, beginning with chemical synthesis. Chemical synthesis involving CO_2 is by no means new, most notably when it is part of a syngas mixture along with CO, H_2, and water, where it is used in processes like Fischer-Tropsch [10]. The more recent developments come in the form of synthesis using captured carbon under the umbrella of CCU. CO_2 is now increasingly being used to produce carbon-neutral and low-carbon fuels such as alcohols [92], which can even be upgraded to more conventional fuels like gasoline [93] (often called efuels). Alternatively, one could produce non-fuel industrial chemicals such as polycarbonates, like PPC [94], acetic acid [95], urea [96], or PVC. Chemical synthesis from CO_2 can also be done, partially or entirely, via biological routes, where it is a feedstock for biomass. The photosynthetic processes of plants provide a highly efficient means of converting CO_2 to more valuable forms, whether this be carried out by trees, vats of microalgae, or anywhere in between. Further processing can then yield more useful products, for instance the pyrolysis of biomass

producing bio-oil [97]. The concept of bioenergy with carbon capture and storage (BECCS) takes this further, burning the biomass or its derivatives then capturing and sequestering the emissions. This is a rare instance of a form of negative emissions technology that may be economically viable without subsidy, though biomass is in high demand for many other "green" processes, as well as for food [98].

1.2.2 Other Sustainable Processes

CCUS has a crucial role in decarbonisation, but it is not the only one, nor do all unsustainable processes involve CO_2. The strongest workhorse in the transition to net zero emissions is undoubtedly electrification and the complementary growth of low emission energy sources such as solar, wind, and nuclear power [69]. That said, the majority of considerations in electrification are solved problems with demonstrated functionality and known physical behaviour. Further, there is an economic drive behind electrification, with solar power now being the cheapest form of electricity and existing agreements such as the United Kingdom's (UK) Contracts for Difference scheme [99] guaranteeing a minimum (strike) price.

Not all things may be electrified; for instance, one cannot (beyond the realm of exotic physics) make plastic out of electricity. All fossil fuel derived products, an especially pervasive group in modern society, must find alternative carbon sources if they are to continue to be used into the distant future. Carbon dioxide may fill this role, through CCU, though it is not the only source of carbon, and it remains that such approaches depend on efficient handling of a broad range of mixtures relating not only to CO_2 but also to hydrogen.

Improvements to general process efficiency remain a priority, both for established processes and new sustainable alternatives. Jevons' paradox endures in some of these situations; however, the aim is to have processes that are fundamentally sustainable, which necessarily avoid negative outcomes. For example, it is desirable to produce hydrogen more efficiently, as the roughly (100 to 130) Mt are produced annually [100], involving a non-negligible fraction of worldwide primary energy usage and resulting emissions [101]. Less than 1% of global hydrogen production is currently from low emissions sources (primarily methane-derived hydrogen with CCS [100]). Escalating usage of hydrogen in this manner is at odds with net zero targets [11, 102-106], however the vision of hydrogen production and usage in the coming decades is drastically different from that which has come before. Countries such as the UK have committed to ambitious low carbon hydrogen production plans [107]. The IEA report that approximately 25% of hydrogen production in 2030 is expected to be low-carbon, based on currently announced projects, and that this number is growing significantly year-on-year [100]. This paints an encouraging future for the 'clean' use of hydrogen, should the expected emission reductions be achieved and excessive fugitive emissions be avoided.

There is also a growing interest in naturally occurring hydrogen, often termed gold or white hydrogen, as evidence mounts that significant quantities of hydrogen exists in subsurface formations and deeper, within the mantle [108]. The competitiveness of this production route remains unclear at this stage, though the case for it is well founded in natural gas extraction. One can only wonder where the world would be should such deposits have been explored

before the widespread production of fossil fuels. There are many different hydrogen production routes that have been proposed, often described in “colours” as above [109-113], though usage is inconsistent and overlapping. Not all forms are equally environmentally friendly [112], or necessarily environmentally friendly at all, notably grey hydrogen production from methane without CCS (the currently predominant route) involves both the intentional emission of CO_2 and the fugitive emission of methane and hydrogen. Such a route makes little economic sense for energy conversion, worse in every practical respect compared to the normal combustion of methane, and is instead the current standard explicitly because hydrogen has not (for the intervening years between Town gas’s replacement and now) been used outside of where it is chemically required [100].

The most publicly prominent role of hydrogen in the net zero transition is as an energy carrier [114-119], though this should not be taken to mean that this is where it is best suited. It is in many ways analogous to natural gas and familiar from its legacy in Town gas; it is readily transported and reacted on demand to release its chemical energy as heat (which can in turn be converted to electrical energy) or directly as electrical power using fuel cells. Production of hydrogen by electrolysis of water is a promising route to energy storage; evening out power-supply curves [120-123], such as during *dunkelflautes*, and answering the dispatchable power problem. At the largest scale, underground hydrogen storage (UHS) utilising vast subsurface reservoir formations has a potential capacity commensurate with the projected demand of at least 1000 TWh that might be required by some estimates [100]. A major criticism of its use as an energy carrier is the inefficiencies in conversion compared to fully electric systems where green electrons from renewable sources are used directly. Nevertheless, there remain situations in which a chemical fuel is preferable: at a small scale, this can apply to off-grid locations; while at a much larger scale, it can provide energy storage more efficiently, on much longer timescales and with less environmental impact than batteries. To facilitate transportation and storage, hydrogen may also be converted into other chemicals, such as ammonia, methanol, methane [124], or liquid organic hydrogen carriers [125].

Where hydrogen’s prominence is more assured is in industry, where it is often required chemically. The efficient large-scale production of industrial commodities such as ammonia and methanol will always require the large-scale handling of hydrogen, regardless of the means by which this hydrogen is produced. In the near term, hydrogen will still be required for refining of petrochemicals, then after in the production and refining of efuels and other industrial chemicals that would normally be derived from fossil fuels. Hydrogen may also be used to help decarbonise the production of cement [126] and in iron and steel making [127, 128], where hydrogen might replace carbon as a reducing agent.

Many more green processes featuring hydrogen and CO_2 may be developed, however the scale of these processes is negligible in comparison to those mentioned, which collectively represent significant fractions of global energy usage and greenhouse-gas emissions [52]. The development of novel sustainable processes remains essential to industrial advancement and the potential for their future importance can never be ruled out (as this would require non-sequiturial knowledge of unknown unknowns or a perfect understanding of fundamental and emergent behaviours), though this does not compel prioritisation. Regardless of whether they

are novel or long established, all processes must be designed with the entire life cycle (from cradle to grave) in mind if it is to be sustainable with low uncertainty.

One final group of processes that warrants mention is refrigeration, air conditioning, and other heat-pumping processes. The thermodynamic cycles underlying these processes represent the primary method by which heat may be removed from a system, able to achieve coefficients of performance greater than unity (*ie* they may move more energy than they require as work), far outperforming alternatives like the thermoelectric effect. Refrigeration cycles are present throughout industry as well as domestic and commercial sectors [129], though usage is growing rapidly for the latter two as a result of climate change and the net zero transition [130, 131]. Increasing ambient temperatures require greater use of air conditioning units to maintain safe living spaces in hot climates, while this heat may alternatively be extracted from the environment and used to provide heat in cold climates (where the process unit is often referred to as a heat pump, the distinction being semantic). Several generations of refrigerants, the working fluids for these cycles, have been developed over the years and have themselves seen a "cycle" [132, 133].

First generation refrigerants like ammonia worked but were toxic or otherwise dangerous, such as highly flammable propane. Second generation refrigerants were then non-toxic and non-flammable: partially or fully halogenated chlorofluorocarbons (CFCs) such as dichlorodifluoromethane (R12). This generation were championed by the talented engineer Midgley and served as his second of three notable demonstrations that apparently-brilliant ideas may have unintended consequences (the first being tetraethyl lead and the last the contraption that killed him), a valuable lesson that should always be kept in mind [134, 135]. In this case, it was discovered that CFCs were degrading the ozone layer in the Earth's stratosphere, resulting in the establishment of the aforementioned Montreal protocol [136]. The third generation were the closely related hydrofluorocarbons, whose atmospheric reactions did not have a high ozone depletion potential (ODP), though it would soon be realised that these compounds (like CFCs) had high GWPs. The archetypal example, tetrafluoroethane (R134a) has a 100 year GWP of 1430, while R12 has a GWP of 10900 [137]. It is these high GWPs that allow fluorinated refrigerants to have such an outsized impact on the climate compared to methane and CO_2 which are present at scales several orders of magnitude higher. In turn, HCFs were replaced with low ODP and GWP fourth generation refrigerants. Some of these, such as hydrofluoroolefines, are but a stopgap (appropriate for drop-in use but still with non-negligible GWP), but those that are currently expected to endure are familiar: the "natural" or "green" refrigerants such as CO_2, isobutane, and ammonia [133]. Much research remains to be done for these "green" refrigerants, especially with regards to blends (mixed refrigerants).

1.3 Scope and Objectives

There are two common themes underlying the furthering of sustainable processes and the transition to net zero emissions. First are the industrially pervasive mixtures involving CO_2 and hydrogen. Second are the repeated dire shortcomings in establishing crucial processes, encompassing fundamental understandings of physical behaviours to high level

considerations and large scale deployment, that must be rapidly overcome. As such, this work proceeds with four objectives:

1. Review the literature for the availability of data and models for processes relevant to the net zero transition and sustainable processes more generally, focussing especially on knowledge gaps regarding the phase behaviour of mixtures of CO_2 and/or H_2 with their accompanying compounds.

2. Generate new experimental data on the fluid phase behaviour of selected important asymmetric binary mixtures, ensuring that the measurements cover both uncharted territory and regions sufficiently well studied *a priori* to provide validation. Regions displaying complex behaviour that is challenging to predict but could facilitate efficient separation processes are of especial interest.

3. Improve the methodology with which such experimental data may be generated, especially with regard to realising low uncertainties and high degrees of measurement automation.

4. Assess and optimise thermodynamic models suitable for use in process simulators, and in process design more generally, against the newly generated experimental data and curated literature data.

This work does not seek to determine which processes should be developed and deployed or how, whether within the scope of the net zero transition or in industry more generally; instead, it aims to provide some essential fragments of the information required to make such decisions.

1.3.1 Mixtures Selected for Investigation

The value in investigating the mixtures selected shall only be truly appreciable in later chapters, yet it would be beneficial to raise which particular mixtures are of focus now to serve as exemplary systems in the picture of thermophysics which follows. Please note that some of these justifications have been voiced in papers published [138] and in preparation, and are adapted here in overarching form. This work focuses on three binary mixtures made from four molecules. The first two molecules are apparent: carbon dioxide and hydrogen. These are the more volatile component in each of their respective binary pairs; their less volatile accompaniments are isobutane (for both CO_2 and H_2) and methanol (for CO_2).

Isobutane (2-methylpropane) is the simplest isomeric alkane; a structural isomer of n-butane with a tertiary carbon atom at its centre. The differences in its behaviour compared with n-butane can offer meaningful insights into how isomers behave, helpful both for a deeper understanding of chemical physics and the development of group contribution methods, especially for the functional group CH. Beyond theoretical value, isobutane is a substance of great importance in various existing and nascent processes, including those on the path to net zero.

An increasingly important application of isobutane is in the area of refrigeration, where, under the name R600a, it has become one of the leading “green” or “natural” refrigerants [139]. Isobutane has effectively zero ODP and a low GWP, the direct GWP is 0.006 [50] while the estimates of the indirect GWP are in the rough range of (3 to 7) [140, 141], though largely based on n-butane. It has a simple, stable structure, making it an ideal choice of refrigerant. CO_2 is also a green refrigerant (R744), with zero ODP and a GWP of one by definition. Blends of isobutane with CO_2 have been considered and investigated [142-146] and offer a compromise on important properties, improving positive qualities like coefficient of performance while mitigating the negatives. For instance, isobutane is extremely flammable and so leaks present a fire risk, whereas CO_2 is non-flammable and provides a reduction in mixture flammability. On the other hand, CO_2 cycles operate at relatively high pressure and incur greater capital costs to withstand that pressure, while isobutane cycles operate at a much more moderate pressure. Beneficially, both are non-toxic, unlike ammonia, another potential green refrigerant [139]. Unfortunately, there is currently insufficient thermophysical property data available in the literature to develop refrigeration systems using isobutane + CO_2 blends, in one case forcing propane + CO_2 to be used as a substitute in modelling [142].

Isobutane is present in large scales across the energy and chemical industry. Isobutane is primarily produced from the isomerisation of n-butane [147], the majority of which is then used to produce 2,2,4-trimethylpentane, the fuel additive commonly known as isooctane, in alkylation units. It can also be produced from CO_2 and H_2 [148], either with a more classical route using syngas or a greener approach using captured CO_2 and low-emission hydrogen. Knowledge of the behaviour of isobutane with CO_2 and H_2 is thus highly pertinent to these processes as well as those downstream and ancillary, doubly so with regards to separations therein. These compounds will inevitably continue to persist as minor components and impurities far downstream of their introduction, including potentially in CO_2 and H_2 pipelines. Along a similar vein, research is being conducted into the blending hydrogen and natural gas, wherein isobutane is a relevant constituent under investigation [149, 150]. All considered, investigating the behaviour of isobutane + CO_2 and isobutane + H_2 represents an essential step on many fronts; with the former previously better investigated (and thus more appropriate as a first step) while the latter had extremely little data available.

Methanol is a potential platform chemical for which the chemical synthesis CCU route is a promising option [151, 152], whether it be the final product or an intermediary. Methanol itself is a very important industrial chemical produced at scales matched by few others [153, 154] and sees a broad variety of applications. While it is used in commercial products from denatured alcohol to antifreeze, its industrial uses are most important, where it is used as a feedstock and fuel [155]. It is primarily used in the production of formaldehyde where it may then go on to produce more complex molecules such as polymers [156]. It can be used as a stand-alone fuel, both for combustion engines and fuel cells, including in blends for the former case (such as in China [157]). Perhaps the most notable use as a fuel is in ships [158, 159], where a growing fraction of newly commissioned vessels are leveraging it to decarbonise the sector’s traditionally unfriendly fuels. Growing attention has also been given to the development of methanol-based efuel processes [92] as a potential replacement for traditionally produced fossil fuels.

The ability to produce methanol in a sustainable manner coupled with its capacity of CO_2 chemical recycling leads to an intriguing, unconventional concept, the methanol economy (championed by Asinger and Olah) [151, 154]. This concept is similar to the hydrogen economy and, while it is less developed, it does offer distinct advantages. The methanol economy aims to replace fossil fuels for the purposes of energy storage, fuel, and as a feedstock for many synthetic hydrocarbons. Methanol's greater density, on both mass and energy bases, and liquid form at standard conditions avoid many of the more substantial issues facing the hydrogen economy. Additionally, it's carbon content affords it greater potential to replace fossil fuels industrially. The future infrastructure involving methanol likely may not reach the scales considered in Olah's vision of a methanol economy [160]. Regardless, the processes that are necessary for any realistic expectations of future development (whether following business as usual or the strictest uptake of low emissions technologies) involve methanol at large scales, with estimates from (100 to 500) Mt per annum in the coming decades [161, 162]. Methanol production currently accounts for ~10 % of the CO_2 emissions of the chemical sector [162], thus increased usage must involve low emissions production that cannot be practically achieved without CCUS.

Methanol is conventionally produced from natural-gas-derived syngas, although coal gasification may also provide a starting point [163], in a highly exothermic reaction that requires complex reactors [92]. It is straightforward to switch between feedstocks in principle, through the water-gas shift reaction and reforming/Sabatier reactions, but this incurs an energy penalty. There are two (reversible) reaction pathways, the historically favoured using CO as a reactant while the other uses CO_2 [164-166] (in practice, both reactions are present and both require H_2). The enthalpy of reaction is lower in the latter case [167], simplifying reactor requirements, and the accessibility of CO_2 as a feedstock is expected to grow in future, while CO is currently conveniently produced within the main hydrogen production routes, though the reforming process is energy intensive [168].

Three major routes to decarbonise methanol exist today. The first is to inject CO_2 captured from point sources (*eg* power generation flue gas) into the steam-methane reformer and methanol reactor of an otherwise conventional methanol production process, achieving a degree of CCU and potentially improving process efficiency, as has been pursued by Mitsubishi Heavy Industries and QAFAC [169]. This approach is the most limited, though it may be used in combination with some alternative processes that seek to use conventionally CO-favoured reactions (leveraging greater experience and the potential for retrofitting). The second major route involves such a process, where the syngas feedstock is replaced with a biomass-derived source [170], such as reformed bio-methane (examined by BioMCN) or gasified waste wood products (established by Enerkem) [169]. These biomass-based routes technically using CO_2 as the carbonaceous-feedstock and convert it to CO, though the efficiency penalty is partially alleviated by the high efficiency of biological photosynthesis (and its downstream processes). Much as with BECCS, there are a litany of concerns about the sustainability and environmental impact of the biomass sources, and scale is similarly limited (as the two are in competition). The only route that is sufficiently scalable and decarbonisable is to produce methanol from captured CO_2 and low emission H_2, occasionally termed green methanol production. The concept is similar to that which is applicable to most hydrocarbons and related chemicals. CO_2 may come directly from a point source (as done with flue gas by

Carbon Recycling International (CRI) [89, 92]) or from ambient air (as done with via DACCS in the Haru Oni project [171]). In the latter case, when used in conjunction with H_2 produced from the electrolysis of water, one obtains a source of methanol (and through it, more complex chemicals) that is accessible across the vast majority of the planet and whose feedstocks are virtually undepletable (dependent not on fresh or archaic biomass, but on three of the most abundant elements in the solar system and broader universe).

It is apparent that any practical process relating to methanol must involve, or have involved, a mixture containing both it and CO_2. Understanding this mixture is thus essential, from the initial production and separation of a crude methanol stream to all manner of downstream processes, which may involve a methanol-rich sub-stream used to capture CO_2 such as in Rectisol-like processes. As such, low uncertainty measurements of the behaviour of methanol + CO_2 is crucial and widely applicable, but the large body of extant data is in a problematic state that compels new investigations.

Significant attention will also be placed on hydrogen mixtures more broadly, primarily through literature review and analysis of critical behaviour. Knowledge/understanding of the behaviour of hydrogen mixtures is far less developed than for other industrial mixtures, in juxtaposition to its importance in the ongoing net zero transition. Even for common mixtures such H_2 with light alkanes, there is scant thermophysical property data available in the literature, much of which is antiquated [172-176] and lacking details of experimental uncertainty. For example, for phase behaviour (the most commonly studied property), it has been found that, for all binary hydrogen mixtures combined, there are little more than four times as many datasets as there are for just methanol + CO_2, even when including the many single-point datasets for hydrogen mixtures. The situation for higher order mixtures is even more dire. The phase behaviour of the main components of syngas (H_2 + CO + CO_2), a mixture that has repeatedly come up thus far as being both essential and commonly used, has only three studies available in the literature totalling only 98 datapoints [177-179] (though it should be noted that there is an as-of-yet unpublished dataset produced by the original version of apparatus in this work [180], prior to the commencement of this work).

It is not uncommon to see recent works which handle either modelling or measurement of hydrogen mixtures that do not explicitly comment on or compare to prior data/models or mistakenly claim there are none (as recently seen, for instance, with H_2 + isobutane [181]). This is, in part, due to the limited scope and currency of reviews in the literature. The lack of data coupled with shortcomings in the communication of available data and models presents a significant hurdle in the development of hydrogen-containing processes; a problem exacerbated by the non-trivial asymmetry presented by these mixtures. This affects both those under conditions typical today and those increasingly prevalent in the near future, where high pressure pipelines and the use of liquid hydrogen render hydrogen accessible at temperatures between (20 and 300) K and pressures up to 200 MPa. Detailed review and discussion would thus be of great benefit.

Chapter 2: Chemical Engineering Thermophysics

“Ce qui est simple est toujours faux. Ce qui ne l’est pas est inutilisable.” (“What is simple is always wrong. What is not is unusable.”)

— Paul Valéry

2.1 Introduction to Thermophysics

The development of thermophysical theories has been propelled by two strong “forces”: curiosity about the nature of physical systems and technological development. These “forces” are coherent, especially within the domain of engineering, and aim to produce evermore meaningful descriptions of what is. In the first chapter it has been established that there is a great need for further technological development in order for the world to smoothly transition to net zero emissions. Thermophysics is one of the tools that engineers must employ, so this chapter shall explain firstly what “thermophysics” is and then how it is applied in practice.

This work pertains to (a subset of) the science of thermodynamic and, more generally, physical properties. The latter refers to measurable characteristics of systems governed by universal relations. This meaning is broad; examples of physical properties within chemical engineering are given for the classical case of the distillation of a binary (two component) mixture, listed non-exhaustively in increasing order of complexity:

- The intermolecular potential between two molecules, either an identical pair or one molecule of each component
- The resultant density of a fluid consisting of those molecules under some specified conditions
- The amount of energy needed to change the temperature of that fluid, called its heat capacity
- The reboiler duty required to heat the contents of the distillation column sufficiently to produce a fluid of the desired composition at the outlet of the column
- The capital and operating costs of building, using, and eventually decommissioning the distillation column

The development of industrial processes is ultimately determined/governed/informed by the more complex of such properties, but they are dependent on the more fundamental properties [182, 183]. Physical properties like the first three are examples of thermodynamic properties, describing the interrelation of energy and matter at equilibrium. The related properties at disequilibrium are termed the transport properties. Together, these fall under the umbrella of thermophysics [184] (though it should be noted that the term thermodynamics is sometimes extended to cover thermophysics, with transport phenomena being referred to as non-equilibrium thermodynamics).

Only a small amount of basic thermophysics will be discussed here, as many works have covered the field in detail [184-187]. The behaviour of matter within a system can be described in terms of its energy, which can, in turn, be described in terms of different energetic contributions. The internal energy U is given by

$$dU = \sum X_j dY_j \tag{2.1}$$

where X_j is the state variable for the energetic contribution j, and Y_j is the partial derivative of U with respect to X_j, together forming conjugate pairs of natural variables.

Numerous types of energy and work are possible in the real world [188], several of which are listed in table 2.1, however the corresponding thermodynamic space is impractically large and

not all energetic contributions are non-negligible for a given application. A convenient approximation is the set (T,p,$\mu_{1:N}$), which may be described in combinations of ensembles, as these state variables are those that are most relevant to industrial processes. Here, μ_i is the chemical potential of the i^{th} species in a system of N components.

Table 2.1: Conjugate pairs of variables that contribute to the energy of real systems, adapted from [188, 189]

Category	Intensive X_j	Extensive Y_j
Thermal	Temperature T	Entropy S
Mechanical	Pressure p	Volume V
	Surface tension* γ	Area A
	Stress ε	Strain σ
	Gravitational potential ψ	Mass m
Electromagnetic	Electric potential φ_i	Charge Q_i
	Electric field $\boldsymbol{E}$	Electric moment $\boldsymbol{P}$
	Magnetic field $\boldsymbol{B}$	Magnetic moment $\boldsymbol{m}$
Chemical	Chemical potential μ_i	Amount n_i

*note that the usage of surface tension can vary significantly in terms of scale and dimensionality (*eg* if it is represented as a tensor), for instance the IUPAC gold book [190] makes no stipulations

These variables are related to each other with a finite number of degrees of freedom F, dictated by the phase rule, derived from the combinatorial geometry of convex polytopes [189]. The general form of the phase rule may be written as

$$F = j - P + 1 \tag{2.2}$$

where j is the number of the number of relevant conjugate pairs and P is the number of equilibrium phases [189], note that other ways of writing it are possible [191-194]. For the thermodynamic space (T,p,$\mu_{1:N}$) the phase rule can (when system size effects are neglected) be reduced to the classical Gibbs phase rule

$$F = N - P + 2 \tag{2.3}$$

The intricacies and limitations of the classical rule were discussed in great detail within the original work of Gibbs [195], though it remains effective in most general applications. Careful consideration should be taken when applying the phase rule to avoid overcounting or neglecting constraints (such as in the case of reactions). The particular choice of variables, how they may be added and/or substituted, is complicated [188, 191]. Significant deviations from the classical phase rule will not be discussed here and can be found in the literature, for example the stress-based phase transition in vanadium dioxide [196], magnetism-based transition in helium-3 [197], or the more common cases in colloidal systems [194, 198, 199].

Knowledge of a subset of the extant thermodynamic variables allows for the determination of a larger set of thermodynamic variables through Euler and cross derivatives, such as the Maxwell relations. This allows experimental measurements of carefully selected properties to provide a great deal of information about a compound, for instance the speed of sound in a fluid provides a great deal of information about its volumetric properties [200].

The majority of this work shall assume that the set (T,p,$\mu_{1:N}$) is a sufficient approximation of the real system, though the existence and relevance of the broader thermodynamic space is

occasionally evident. For example, within the experimental methods, the location of fluid surfaces is important and the minimisation of the surface area is both crucial and often rate limiting (both in this work and similar works [201, 202]). Similarly, in industrial applications, the electrolysis of water to produce green hydrogen is dependent on electrochemical potentials. Additionally, in both cases, the mass of fluids produce buoyant forces and beneficially promote settling.

As mentioned, thermodynamic properties are equilibrium properties. A system is said to be in stable equilibrium when it has achieved its minimum free energy, when there are local minima in the energy there are also metastable states, with transitions between states occurring spontaneously when the transition would decrease the Gibbs free energy G

$$G = U + pV - TS \tag{2.4}$$

which, for future reference, is closely related to the Helmholtz free energy A

$$A = U - TS \tag{2.5}$$

A convenience of equilibrium properties is that temporal energetic contributions may be neglected. This is not to say that time (or its conjugate, frequency) does not exist, and changes may occur at small scales, such as individual molecules changing velocity under the influence of intermolecular interactions, but the system displays time-reversible symmetry (wherein the derivative of the overall internal energy with respect to time is zero).

In this work, the transitions of interest are spontaneous changes in the number of stable phases (the concept of phase equilibria). Focus is placed on equilibria involving fluid phases. The distinction between different fluid states is non-trivial; the terms gas, vapour, liquid, and supercritical fluid are commonly used but are only understood contextually [184]. The following are but a few examples of the confusion that this can cause. A gas may be taken to mean any fluid above its critical temperature, or simply a low density fluid. A liquid is typically a high density fluid, but need not be the densest fluid in a multiphase system. A vapour is sometimes strictly a low density fluid in coexistence with a higher density phase (fluid or otherwise), though this definition can cause contradictions. A supercritical fluid is often taken to be a fluid above its critical temperature or above both its critical temperature and pressure, though the boundaries are vague and there are frequent overlaps with descriptions used for gases or liquids, additionally it is sometimes described as being a fluid that is indistinguishable from either gas or liquid. Furthermore, there are clear regions in which fluids exhibit “critical enhancements” in some properties, yet these regions do not correspond with any of the preceding definitions. Perhaps the most classical distinction between a liquid and a gas is that both can flow (ie are fluid) but only a gas expands to fill its container, however this definition is meaningless as both liquids and gases expand or contract to fill their container and can be made to transition between each other (or other phases) under suitable conditions.

The most meaningful common distinctions between fluid phases are all made on relative terms and apply only to limited cases. For example, for pure simple compounds that adhere to the classical Gibbs phase rule, there may only be two coexisting fluid phases wherever there is one degree of freedom, where one phase is consistently more dense, viscous, and has higher intermolecular potential energy but lower kinetic energy. This phase is what is commonly termed the liquid, while the other is the gas or vapour. The rigor of this definition disappears when applied to mixtures, where an arbitrarily large number of fluid phases may form (though

in practice it is rare for there to be more than four). For example, there is no longer any requirement for a phase that generally appears to be a gas (a gas-like phase) to be less dense than a phase that generally appears to be a liquid (a liquid-like phase), whether referring to density on a mass or molar basis (it should be noted that density is preferentially used to refer to molar density in this work). The distinction beyond the critical point, for pure fluids or mixtures, is similarly problematic.

It is possible to simply refer to all of these phases simply as fluids, however this reduces the information that may be conveyed about a given phase. Relative definitions are used for the remainder of this work; the term liquid shall be used to refer to a liquid-like state, vapour and gas to refer to a gas-like state, and simply “fluid” only when there is sufficient ambiguity. Such usage may be considered correct when the objects/concepts to which the terms are applied may pass a “duck test” based on contextually reasonable/meaningful descriptors. Much like the aforementioned usage of descriptors of fluid states, to pass such a test for the which the descriptor is “duck” an object should “walk like a duck, swim like a duck, and quack like a duck”. For instance, if a fluid is above its critical temperature (debatably gas-like), has a high (liquid-like) density, but an unusually high (supercritical-fluid-like) thermal conductivity, then it does not appear that said fluid is truly liquid-like or gas-like, thus the use of a more conservative term like fluid may be justified. Note, also, that the fluid is not likely to be a duck, however the descriptors selected were perhaps inappropriate to make that particular assessment.

An inexact example shall be given for illustration, using the near-critical phase diagram of pure CO_2, shown in Figure 2.1. In this pT projection, the black curve represents the vapour-liquid coexistence (or saturation) curve for CO_2, which terminates at the critical point. Fluid states whose properties are entirely consistent with those of a liquid or a gas exist on either side of this curve and persist at temperatures and pressures above the critical point. The pT region exceeding the critical point is shown bounded by dotted lines, while it is challenging to draw boundaries for strictly liquid/gas-like behaviour. It is perhaps simplest to instead illustrate a bounded region within which a fluid can confidently be said to be neither entirely liquid-like or gas-like (instead, in this case, supercritical-fluid-like). To do so requires some criteria for assessment, in this case based on the location of Widom-like lines (as in literature [203-205], though alternative criteria exist [206]), each defined as the loci of an inflection point in a thermodynamic property. The blue curve is the Widom-like line for the thermal conductivity (in this case the boundary between unconfidently liquid-like and confidently not liquid-like) while the red is the corresponding line for the speed of sound (in this case the boundary between unconfidently gas-like and confidently not gas-like). The dashed black curve is the critical isochore (the pT isochore for a system at the critical density).

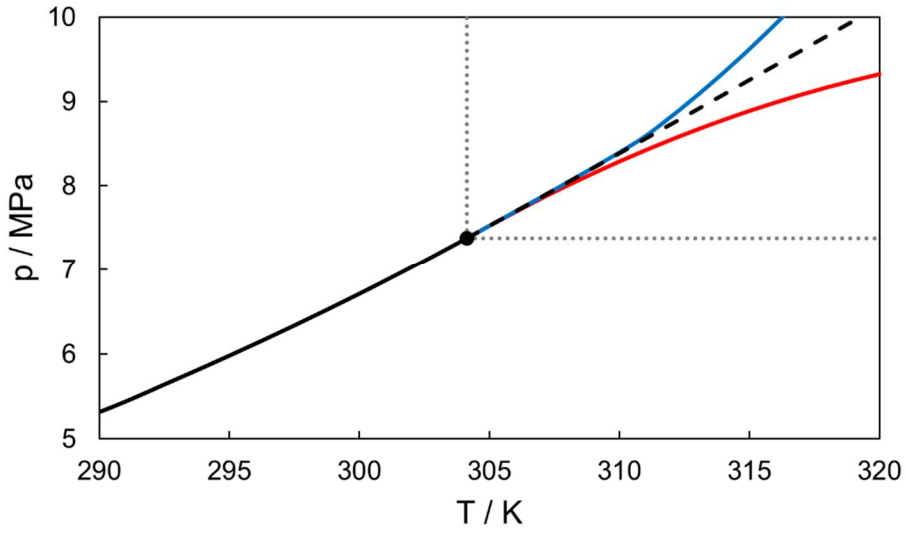


Figure 2.1: pT projection of the phase diagram of pure CO_2 in the vicinity of the critical point, showing the saturation curve —, thermal conductivity — and speed of sound — Widom-like lines, and the critical isochore – –, calculated using the EoS of Span & Wagner [207], along with the boundary ⋯ of $T_r \geq 1$, $p_r \geq 1$

We move now to how one applies knowledge of thermophysics to further process development. Simply observing the behaviour of thermodynamic and other physical properties under specific conditions provides a first step, but such a discrete and finite description is of little practical use. Models, that is to say relationships by which a set of quantities may be mapped onto other quantities, are required to proceed beyond this. Such models may vary tremendously, from *ab initio* relationships based on fundamental principles to purely empirical models. The simplest way in which one may try to determine the value of a property under specified, but unstudied, conditions is to interpolate (or less reliably, extrapolate) it from known values under a different set of conditions, however such a method provides little understanding of the underlying mechanisms governing the properties and eventually requires more work than attempts to describe properties universally.

The type of model that is most important for the behaviours discussed in this work is what is known as an equation of state (EoS) [185], a mathematical description of the dependence of a number j of state variables X such that

$$f\left(X_{1,j}\right) = 0 \tag{2.6}$$

The origins of EoS modelling lie in attempting to develop mechanical devices that utilise working fluids, initially with air [208] but most notably with steam during the advent of steam power [209]. It was observed that, within a system, some properties (which are examples of what would go on to be termed thermodynamic conjugate variables) were related to each other. For example, the volume V of a system is (approximately) proportional to its temperature T and to the amount of substance n within it, while inversely proportional to pressure p. The combination of these observations leads to the most fundamental EoS, the ideal gas equation [210]

$$pV = nRT \tag{2.7}$$

where R is a constant of proportionality known as the gas constant, which is the product of two more fundamental constants: the Avogadro constant N_A and the Boltzmann constant k_B.

This empirically-derived equation, strictly applicable only to an "ideal" gas (distinct from a real gas and other real fluids), is able to describe adequately the behaviour of low density gases, and forms the basis of many EoS [185]. Mathematically, it may only describe one phase for a given set of conditions, as it does not permit multiple values of extensive properties to occur simultaneously. A simple description of a multiphase system, including for mixtures, may be achieved through combination of the ideal gas equation with Henry's law or Raoult's law for an ideal liquid, but the concept of a phase transition is still eluded. To describe fluid phases continuously and allow for the existence of phase transitions, an EoS of mathematical form permitting multiple simultaneous values of at least one extensive property is required, first achieved by van der Waals [211, 212].

2.2 Cubic Equations of State

From this point, the extensive properties within thermodynamic space will be rendered intensive by treating them on a molar basis, for instance the volume is replaced by the molar volume V_m

$$V_m = \frac{V}{n} \tag{2.8}$$

This treatment is convenient but not strictly necessary, and the requirement that the description of multiple phases depends on multiple simultaneous values of extensive properties still applies to these molar-intensified, otherwise extensive, properties.

The ideal gas equation treats molecules as infinitesimally small points, but molecules are known to have a finite volume. For brevity, discussion of the ambiguous nature of this volume in reality, subject to similar ambiguities as surface areas [213, 214], is excluded. Additionally, there are intermolecular forces that attract molecules to each other, up until a sufficiently small separation that a repulsive force takes over, as may be described approximately by a Lennard-Jones-like potential [215]. Such is to say, that the behaviour of molecules is dependent on the presence of other molecules. More strictly, it is also dependent on the presence of external fields [216], but this is similarly neglected for brevity in this work due to the complexity of these interactions and the negligible effect they have under the circumstances considered here.

The molecular volumes and intermolecular attractions were included, in a way, in a modification of the ideal gas equation [211], producing the van der Waals equation of state

$$p = \frac{RT}{V_m - b} - \frac{a}{V_m^2} \tag{2.9}$$

where a is a parameter that arises from intermolecular attractions and b is related to the volume occupied by molecules when treating them as hard (perfectly incompressible) spheres. The first term in this equation is referred to as the repulsive term while the second the attractive term. These two parameters are specific to a given compound and may be obtained directly from experimental pVT measurements.

This equation is a third order polynomial in the molar volume, not readily apparent from the above form, though it may be rearranged to give

$$V_r^3 - \left(\frac{1}{3} + \frac{8T_r}{3p_r}\right)V_r^2 + \left(\frac{3}{p_r}\right)V_r - \frac{1}{p_r} = 0 \tag{2.10}$$

where reduced parameters, p_r, T_r, V_r, have been used for clarity. These reduced parameters and the fraction of that parameter compared to its value at the critical point

$$X_r = \frac{X}{X_c} \tag{2.11}$$

where X represents the parameter being reduced and X_c its value at the critical point.

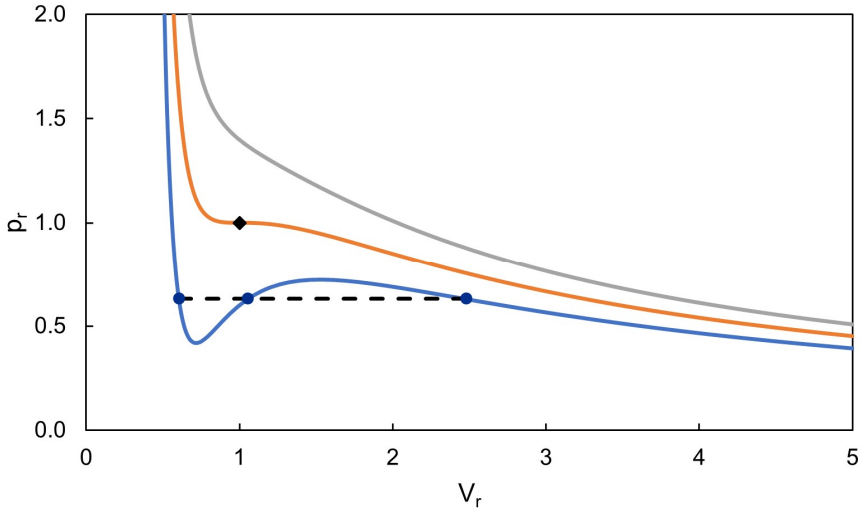


Figure 2.2: A p_rV_r projection of the van der Waals EoS shown in reduced terms for three reduced temperatures, — T_r = 0.9 (● roots of the cubic equation at the saturation pressure), — T_r = 1 (♦ critical point), — T_r = 1.1

This equation is a third order polynomial, also known as a cubic equation. EoS that adopt this general functional form are termed cubic equations of state, though they are occasionally referred to engineering EoS because of the ease and effectiveness of their application, and resulting widespread use in chemical engineering [217]. Their form allows for V_m to assume either one or three values for a given value of temperature and pressure, transitioning smoothly between them at subcritical temperatures, while at supercritical temperatures only one value may be obtained. This behaviour is shown in figure 2.2 for three isotherms: a subcritical isotherm, the critical isotherm, and a supercritical isotherm.

Not all regions where three values of V_m are present are stable, at any one subcritical temperature there may only be one pressure (for pure compounds) for which multiple stable phases can form [218]. This is the saturation pressure, and the locus of V_m at the saturation pressure for varied temperatures is termed the binodal, while the locus of local maxima and minima of V_m form the spinodal. Wherever three simultaneous values of V_m are present, one always lies between the spinodal points, in a region that is both mechanically and thermodynamically unstable, such that no bulk phase may ever exist in equilibrium at this molar volume. As such, cubic EoS may predict either one or two stable phases for pure fluids.

In the multiphase region, the phase with the smaller molar volume is the coexistence or orthobaric liquid, and the phase with the larger molar volume is the coexistence or orthobaric gas, commonly termed the vapour. The unstable intermediate molar volume is not typically used in thermodynamical modelling, though is not uninteresting [219-222].

The qualitative capabilities of the van der Waals equation are remarkable, its only major failing under industrially relevant conditions being the inability to predict the transition to solid phases, though that challenge remains unsurmounted after one and half centuries (with the possible exception of one recent machine-learning based model [223], though non-EoS continuous modelling has been demonstrated [224]). The same cannot be said about its quantitative capabilities, which fall short especially for the liquid phase [217]. Three major approaches have managed to surpass it on this front: empirical corrections focussed mainly on the attractive term, semi-empirical corrections of both the attractive and repulsive terms, and equations of radically different forms that are dependent on increasingly many parameters. The former shall be discussed in this section, while the latter two are discussed in the following section.

The van der Waals EoS has been modified in many different ways, though one of the more notable improvements is the Redlich-Kwong EoS [225], which considered the attraction between molecules to be dependent on temperature. This temperature dependence was further improved by Soave [226], who described the attraction as a function of both temperature and the acentric factor ω (roughly a qualitative description of the sphericity of a molecule), yielding the Soave-Redlich-Kwong (SRK) EoS

$$p = \frac{RT}{V_m - b} - \frac{\alpha a}{V_m\left(V_m + b\right)} \tag{2.12}$$

where α is the alpha function, in this case the version introduced by Soave though others are available [227-230], and is given by

$$\alpha = \left(1 + \kappa\left(1 - \sqrt{T_r}\right)\right)^2 \tag{2.13}$$

where κ is a second order polynomial of the acentric factor, not listed here as it is functionally identical to the version used more extensively in this work, which shall be given below.

The SRK EoS remains widely used industrially alongside a similar equation developed several years later: the Peng-Robinson (PR) EoS [231]

$$p = \frac{RT}{V_m - b} - \frac{\alpha a}{V_m\left(V_m + b\right) + b\left(V_m - b\right)} \tag{2.14}$$

Variants of this equation are the primary modelling focus in this work, and as such shall be discussed in greater detail. The attractive parameter a is given by

$$\alpha = 0.45724\frac{\left(RT_c\right)^2}{p_c} \tag{2.15}$$

and the repulsive parameter b by

$$b = 0.07780\frac{RT_c}{p_c} \tag{2.16}$$

The Soave version of the alpha function is used, taking the same form as previously with κ for this EoS given by

$$\kappa = 0.37464 + 1.54226\omega - 0.26992\omega^2 \tag{2.17}$$

The PR EoS is able to predict liquid densities more accurately than the earlier models [230, 231], but still fails to approach the accuracies of measurements. A further improvement is achieved by simply translating the volumes slightly based on empirical correlations, as was done by Peneloux *et al* [232] for the SRK EoS. The same approach may be applied (with appropriate adjustments) to any cubic EoS. These volume translations may be implemented such that there is no change to calculated compositions of coexisting phases, as is done in this work, or otherwise, with implications for other thermodynamic properties [233]. A notable source of the shortcomings of EoS such as SRK and PR is that only the attractive term is modified from the vdW EoS, a cost that is paid to retain the convenience of its cubic nature.

The models mentioned thus far have been shown as they would be used for pure fluids, to extend them to mixtures requires the introduction of a composition dependence. The most simple approach is to assume that the above models hold true for mixtures when the component specific parameters are replaced with values representing the mixture as a hypothetic pure fluid; this is known as the one fluid approach. The parameters for the hypothetical fluid are calculated from mixing rules, such taking the arithmetic or geometric means as is done in the van der Waals (vdW) mixing rules [211]

$$a = \sum_i \sum_j x_i x_j a_{ij} \tag{2.18}$$

$$b = \sum_i \sum_j x_i x_j b_{ij} \tag{2.19}$$

Here, x_i and x_j are the mole fraction of component i and j, respectively, and a_{ij} and b_{ij} are calculated from the pure component parameters as

$$a_{ij} = (1 - k_{ij})\sqrt{a_i a_j} \tag{2.20}$$

$$b_{ij} = (1 - l_{ij})\frac{b_i + b_j}{2} \tag{2.21}$$

where k_{ij} and l_{ij} are binary interaction parameters (BIPs) matrices, equal to zero for $i = j$, that may be regressed from experimental data. It should be noted that k_{ij} and l_{ij} are symmetric N by N matrices. The combination of this mixing rule with the PR EoS shall be referred to as PR-vdW. When BIPs are set to zero, as was standard until 1953 [234], a model is said to be used in a purely predictive manner. These BIPs have little physical basis, and are effectively used by some as “fudge factors”, though this indelicate description should not be taken to imply that they are not effective.

A semi-predictive approach for estimating BIPs is the group contribution approach [235, 236], wherein the BIPs are described in terms of the functional groups present within the molecules. Two examples of group contribution EoS are used in this work and will be discussed further below. This approach is especially valuable when little to no data exists for a specific compound, but data are available for related compounds such as those within the same homologous series. Small molecules are often treated by a single encompassing group, as is the case for CO_2, H_2, and methanol, while larger molecules are more reliably subdivided, as shown in figure 2.3 for isobutane. It is preferable to fit the group interaction parameters starting

with the simplest molecule for a given group, as such isobutane is the ideal candidate for parameterising the tertiary CH group [138].

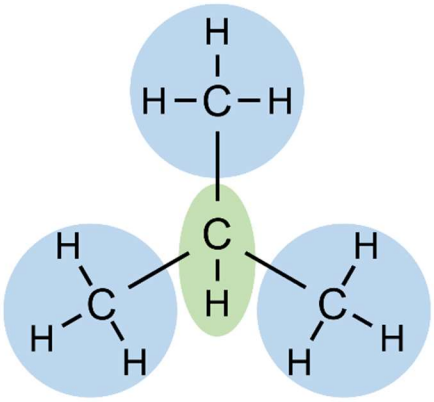


Figure 2.3: The molecular structure of isobutane, showing how it is treated within a group contribution approach, consisting of three primary CH_3 groups ● and one tertiary CH group ●

Regardless of how one obtains BIPs, a model will still be limited by the quality of its mixing rule. The van der Waals mixing rule is effective for many simple systems, but it struggles when it comes to highly non-ideal systems, such as asymmetric mixtures. Many alternative mixing rules have been developed over the years [221, 237, 238]. The most effective are probably those that introduce a description of the excess Gibbs free energy G^E through an activity coefficient model, referred to as a cubic + G^E model. One method of implementing G^E is the traditional $\gamma - \varphi$ method [217], but this is of limited applicability, especially for mixtures that include supercritical components (as are investigated in this work), so this will be neglected in favour of more thermodynamically consistent methods.

One such mixing rule that suitably introduces G^E, which may be calculated from any activity coefficient model with suitable considerations, is the Wong-Sandler (WS) mixing rule [239]

$$\frac{a}{RT} = \frac{QD}{(1-D)} \tag{2.22}$$

$$b = \frac{Q}{(1-D)} \tag{2.23}$$

where Q is given by

$$Q = \sum_i \sum_j x_i x_j \left(b - \frac{a}{RT}\right)_{ij} \tag{2.24}$$

and where the last term is

$$\left(b - \frac{a}{RT}\right)_{ij} = \frac{1}{2}(1-k_{ij})\left(\left(b_i - \frac{a_i \alpha_i}{RT}\right) + \left(b_j - \frac{a_j \alpha_j}{RT}\right)\right) \tag{2.25}$$

where k_{ij} here is a similar, though not identical, BIP to that of the vdW mixing rule. The D term in the mixing rule is given by

$$D = \sum_i x_i \left(\frac{a_i \alpha_i}{b_i RT}\right) + \frac{A^E_\infty}{CRT} \tag{2.26}$$

where C is a constant used for clarity

$$C = \frac{\ln(\sqrt{2}-1)}{\sqrt{2}} \tag{2.27}$$

and A_∞^E is the excess Helmholtz energy at the limit of infinite pressure, approximately equal to G^E [240, 241], calculated from an activity coefficient model. In this case the non-random two-liquid (NRTL) model [242] is used, though the one-fluid van Laar model [243-245] or alternative two-fluid models from the simple Wilson model [246, 247] to the more sophisticated UNIQUAC [248, 249] and COSMOSPACE [250] models may, alternatively, be applied. Here, A_∞^E is given by

$$\frac{A_\infty^E}{RT} = \sum_i x_i \frac{\sum_j x_j \tau_{ji} G_{ji}}{\sum_k x_k G_{ki}} \tag{2.28}$$

where τ_{ij} is an adjustable parameter, formally based on the difference in the interaction energies between like and unlike molecules (but, in practice, of lesser meaning), and G_{ij} is

$$G_{ij} = \exp(-\alpha_{ij}\tau_{ij}) \tag{2.29}$$

where α_{ij} is a further adjustable parameter called the non-randomness parameter. It should be noted that, unlike k_{ij} and l_{ij} in PR-vdW, τ_{ij} is an asymmetric N by N matrix.

These two-fluid models treat mixtures differently to the one-fluid approach mentioned previously. Instead of assuming that the mixture behaves as a hypothetic pure fluid with scale-independent composition, it instead has local composition variations, only realising the overall composition at sufficiently large scales. This approach is not considered theoretically rigorous [217] (though neither is the one fluid approach) but may describe the behaviour of real liquids satisfactorily, including capturing the effects of molecular association in a rudimentary fashion. The NRTL model neglects surface contributions, reducing its predictive capabilities, however, in this work parameter optimisation is favoured. Furthermore, UNIQUAC suffers an inconsistency when used the WS mixing rule for asymmetric mixtures [251], which likely also applies to COSMOSPACE, thus NRTL is more suitable for the mixtures considered here.

A shortcoming of the original WS mixing rule is that it cannot reproduce exactly the behaviour of vdW mixing rule. Orbey and Sandler [252] proposed a modified version of the WS mixing rule (mWS) to rectify this, given specifically for use with a modification of NRTL, for which the vdW mixing rule was a special case. Equation 2.25 is now

$$\left(b - \frac{a}{RT}\right)_{ij} = \frac{b_i + b_j}{2} - (1-k_{ij})\frac{\sqrt{a_i\alpha_i a_j\alpha_j}}{RT} \tag{2.30}$$

and Equation 2.29 is now

$$G_{ij} = b_i \exp(-\alpha_{ij}\tau_{ij}) \tag{2.31}$$

which may reproduce the vdW mixing rule for $l_{ij} = 0$, also known as the one parameter vdW rule, while $l_{ij} \neq 0$ cannot be mapped onto PR-mWS-NRTL. An additional benefit of this form is that it facilitates consistency checking, as any implementation of the model which fails at this reduction would evidently be misprogrammed.

The combination of the PR EoS with the mWS mixing rule utilising the NRTL free energy model (PR-mWS-NRTL) includes four adjustable parameters for a binary mixture (k_{ij}, τ_{12}, τ_{21}, and α_{ij}),

increasing the difficulty of optimisation. A common approach to manage the size of the parameter space is to assume a value of α_{ij} . When setting it to zero NRTL reduces to the Margules model [253], exactly for the original version of NRTL, and something akin to it in the case of the modified version in mWS. The original publication of NRTL included recommended values for different categories of mixtures [242], with a value of 0.3 suggested for many cases of vapour-liquid equilibrium. The original recommendations produce conflicting and ambiguous cases for some systems and numerous systems are best represented by values of α_{ij} outside the range that is consistent with the proposed underlying theory [254], including instances where negative values (ie hyper-random arrangement) performed best [254, 255]. Shortcomings in the applicability of the theory to real mixtures may be responsible, though use in process engineering does not necessarily require rigorous theory. From a mathematical perspective, the primary effect of the sign of α_{ij} within PR-mWS-NRTL is to change the sign of τ_{ij}, and the magnitude of α_{ij} is inversely correlated with the magnitude of τ_{ij}.

An alternative method is to set one of the values of τ_{ij} to be infinitely large, such that the corresponding value of G_{ij} is equal to zero. This not only reduces the cardinality of the parameter space by one but also reduces the number of calculations required, as several terms may now be removed. This special simplified case of the NRTL model will be referred to as sNRTL and the overall model PR-mWS-sNRTL. Strictly, this model describes a seemingly unphysical situation where the local composition around molecules of one type is effectively pure, however it may be used to obtain initial values when optimising PR-mWS-NRTL and will be shown later to perform well for mixtures of methanol + CO_2.

The final cubic EoS used in this work is the Enhanced Predictive Peng-Robinson 78 (EPPR78) model [256-258]. It is another cubic + G^E model, with a van Laar activity coefficient model, utilising a group contribution approach to determine the BIPs. It is especially tailored to petrochemicals, features 40 different functional groups, but is not currently parameterised for alcohols.

2.3 Alternative Equations of State

The models used today are almost exclusively those that have come about since the advent of the digital computer, with one important exception: the virial equation

$$Z = 1 + \frac{B}{V_m} + \frac{C}{V_m^2} + \frac{D}{V_m^3} + \ldots \tag{2.32}$$

where B is the second virial coefficient, C the third virial coefficient, and so on, and Z is the compressibility factor

$$Z = \frac{pV_m}{RT} \tag{2.33}$$

Effectively the deviation from the ideal gas equation, with an ideal gas having Z = 1.

The equation is a Maclaurin series in terms of the molar density (the inverse molar volume), which may be expanded up to infinite terms for exact correctness but is often truncated after the third term. Unlike the other EoS mentioned thus far, the virial equation may be derived rigorously from statistical mechanics, based originally upon the virial theorem though it may

be alternatively derived from the grand canonical ensemble [259]. In the limit of zero density, or when truncated after the first term, it reproduces the ideal gas equation. Each virial coefficient represents the effects of increasingly many-bodied interactions, starting with pairwise interactions for *B* with later terms growing increasingly important at higher densities and in the vicinity of critical points. It should be noted that the virial equation as it is known today is not identical to that originally favoured by Kamerlingh Onnes [260], and that the preceding statement is only true of the modern version.

The virial equation itself is not used within this work, but played a pivotal role both in the history of fluid thermodynamics and in the development of the mixing rules described previously, especially in adhering to the behaviour of the second virial coefficient [217].

The virial equation does not converge at high densities [259], nor is it applicable to complex systems, despite the mathematical requirement that some infinite series must exist that perfectly describes real fluid behaviour. This result is unsurprising as the equation is only statistical-mechanically exact within the simple thermodynamic space (T,p,μ). This shortcoming is emblematic of many of the issues faced by the EoS discussed in this work thus far. Capturing the behaviour of real fluids requires the capacity to describe the impact of all present forms of work (eg polarizability and the resulting molecular association) on the overall system energy. The most successful attempts thus far describe systems in terms of the Helmholtz free energy and fall under the categories of molecular EoS based on perturbation theory and empirical multiparameter EoS.

The molecular EoS are statistical-mechanically based models that describe fluids based upon a reference system with an exact solution and a series of perturbations from that reference system. This approach originates from the works of van der Waals [211], developed further by Barker & Henderson [261, 262] and contemporaries, and was advanced significantly by Wertheim [263-266] with his “thermodynamic perturbation theory” (TPT) [267]. The general form of a perturbative EoS in terms of the Helmholtz free energy can be written as

$$A = A^{\text{ref}} + \sum_i A_i^{\text{pert}} \tag{2.34}$$

where A^{ref} is the Helmholtz energy of the reference fluid and A_i^{pert} is the residual energy contribution from the *i*th perturbation term. This particular expression is not normally used, but illustrates that perturbation theory is capable of achieving what the virial EoS attempted to when extended as an infinite series.

Building upon TPT, Chapman *et al* [268] proposed the statistically associating fluid theory (SAFT) model. This model provides not only a more rigorous description of the behaviour captured by cubic EoS but also allowed for the description of directional molecular association explicitly.

Many variants of the SAFT EoS have been developed; only two closely related recent variants are discussed in this work, SAFT-VR-Mie [269] and SAFT-γ-Mie [270], reviews of other variants can be found in the literature [271-274]. SAFT-VR-Mie treats molecules as chains of spherical segments (note that the chain length may be one for monoatomic molecules) whose interactions are described by the Mie potential, a generalised variable range Lennard-Jones

potential. Soft spherical monomers with Mie repulsion act as the reference fluid, improving upon a similar model from 2006 [275] wherein hard spheres were the reference fluid. The overall Helmholtz free energy is typically written as

$$A = A^{\text{ideal}} + A^{\text{mono}} + A^{\text{chain}} + A^{\text{assoc}} \tag{2.35}$$

where A^{ideal} is the ideal gas Helmholtz free energy, A^{mono} the monomeric contribution, A^{chain} the chain contribution, and A^{assoc} is the contribution from molecular association. Further terms may be added for more complex systems, such as those featuring ions [276], and modifications for positional isomers are also available [277], however these are not necessary for the mixtures considered in this work.

SAFT-γ-Mie is a generalisation of SAFT-VR-Mie as a group contribution approach [270]. Both of these versions of SAFT still require both pure component and mixture interaction parameters to be regressed against experimental data, though the SAFT-γ family express these in terms of functional groups. As such, they may be considered semi-empirical models. In particular, the unlike dispersion energy ε_{kl} is generally treated as an adjustable parameter [270], much like k_{ij} in cubic EoS, as too sometimes is the unlike repulsive exponent λ^{r}_{kl}.

The final category of EoS considered here are the multiparameter EoS, noting that the EoS that bear this name should not be confused with the preceding EoS which often feature multiple adjustable parameters themselves. Multiparameter EoS are entirely empirical models that describe the Helmholtz free energy in terms of an arbitrarily large set of temperature and density dependent functions of arbitrary form. The parameters of such EoS are specific to a given compound or mixture and are not transferable between different compounds as they are not based in any rigorous thermodynamic theory. The loose requirements for these equations result in a range of unphysical predictions [278, 279], such as multiple van der Waals loops [221], but also allow for exceptional performance within the range of conditions under which they were optimised [280], currently capable of exceeding any other model except in the description of helium (for which incomparably accurate *ab initio* models are available up to moderate pressure [281]). The caveat is that the accuracy is dependent on the availability of a large number of experimental datapoints across multiple properties (eg vapour pressure, density, speed of sound), as such these models have negligible predictive capabilities.

Several pure fluid multiparameter EoS [207, 282-284] have been used in this work for the calculation of pure component densities as part of the experimental methods, where the model uncertainties are comparable to experimental uncertainties and at least one order of magnitude better than any other model discussed here. Only one multiparameter EoS for mixtures has been used in this work: GERG-2008 [285], an update to GERG-2004 [286], that is the current ISO standard for single phase properties of natural-gas-like mixtures [287] and generally applicable to multiphase properties. This model is applicable to mixtures of 21 different fluids focused on mixtures found in natural gas but also relevant to the use of hydrogen, to CCUS, and to cryogenic separations.

The general structure of GERG-2008 is

$$\alpha = \alpha^{o} + \sum x_i \alpha^{r}_{oi} + \Delta\alpha^{r} \tag{2.36}$$

where α is the dimensionless Helmholtz free energy, α^{o} is the ideal gas contribution, α^{r}_{oi} is the pure component contribution of component i, and $\Delta\alpha^{r}$ is the departure function. The non-ideal

α terms are functions of density and temperature that have been reduced by reducing functions. Not all mixtures have been optimised to the same extent, for example isobutane + CO_2 has a specifically adjusted reducing function but no departure function, while isobutane + H_2 has no fitting and relies on linear combining rules. Hydrogen mixtures, even those with greater degrees of fitting, are documented to be modelled poorly, though extension of the GERG approach by Beckmüller *et al* [288] has improved the performance for mixtures with four of the other twenty components.

The detailed workings of any multiparameter EoS have been excluded due to the limited relevance and may instead be found in literature [207, 280, 282-284, 289, 290].

2.4 Practical Considerations for the use of Thermodynamic Models

The above models do not have analytical solutions for mixtures and so must be solved numerically for multiphase systems (though cubic EoS have analytical solutions for pure fluid and single-phase mixture properties). The calculations are carried out using computer programs. In research, such programs are often purpose-built standalone programs, either developed in-house by the researcher(s) or by third parties, and may be open or closed in terms of access and/or source code.

In this work, the Peng Robinson models were computed using in-house software, implemented in three different languages for different applications. A VBA implementation in Microsoft Excel was used for BIP optimisation using the non-linear generalised reduced gradient decent method, design of experiments, and general use. A MATLAB implementation was developed for BIP optimisation using grid searching and some general use. The core EoS functionality was also applied elsewhere in the MATLAB-based modelling of DAC process separations by Zervidi [291] and colleagues. A Keysight VEE implementation was developed for the automation of the experimental apparatus, though not fully implemented.

The pure component multiparameter EoS were computed using the Reference Fluid Properties (REFPROP) 10.0 program developed by NIST [292, 293]. All the other EoS used were computed using the open source software package Clapeyron [294] implemented in Julia. Strictly, the usage of Clapeyron required some (in-house) programming, though this simply involved the adaptation of some examples (from the package documentation) as well as the adaptation of part of the MATLAB grid searching program (in the case of SAFT-γ-Mie optimisation).

In industrial applications, such models are often contained within process simulators, such as Aspen [295], gPROMS [296], and Petro-Sim [297]. The majority of process simulators are closed source and costly, presenting a significant barrier to process development especially on the research and development side. Open source options are slowly becoming available, such as DWSIM [298] and OpenModelica [299], and Clapeyron-based simulators are under development [300].

Only the in-house implementations will be discussed in detail, specific details of the third party programs can be found within their respective documentations.

The main numerical method used is what is known as a flash algorithm [301], wherein the pressure, temperature, and overall composition of the system are specified and the equilibrium compositions of any coexisting phases are calculated. The flash algorithm used in this work attempts to find any region with coexisting phases for a given temperature and pressure, regardless of the overall composition specified (including negative flashes), though the specified value affects the speed and feasibility of convergence. Alternative approaches are available [302]. The flash is based on the necessary requirement of equal fugacity, generally suitable for two phase calculations though it is not sufficient to guarantee stability [303] (the requirement that the Gibbs free energy be minimised). It is specifically programmed for one or two phase systems, and preferentially converges to vapour-liquid equilibria over liquid-liquid equilibria.

The BIPs were regressed from experimental data generated in this work and selected literature values through two methods. One was the non-linear generalised reduced gradient method [304], used as implemented in Excel's built-in solver to minimise the sum squared error S in composition between the experimental value x_{exp} and the calculated value $x_{calc.}$

$$S = \sum (x_{\text{calc}} - x_{\text{exp}})^2 \tag{2.37}$$

The ranges of the BIP values were constrained to improve convergence, starting from broad ranges (eg -2 to 2) and increasingly tightened as the near optimal region was identified. A constraint that the flash algorithm must converge successfully was also applied. This approach consistently produced near optimal solutions, albeit typically after many attempts with different initial values and constrains.

The major limitation of smart/dynamic optimisation methods like the one above is that the parameter/solution space is non-convex. The number of local minima (in one or more dimensions) scales with the number of experimental datapoints. The difficulty in finding the optimal solution grows immensely as the cardinality of the space grows. The four BIPs in PR-mWS-NRTL are significantly harder to regress as the flexibility that they offer also results in multiple near-optimal solutions.

The alternative method employed was grid searching the solution space by calculating the error for all potential values of a parameter to a given resolution, effectively optimising by brute force. This approach is much more computationally intense but able to locate the global optimal solution.

The MATLAB model could converge one flash calculation every millisecond on average. Performing a 1000 x 1000 grid search of the error for 100 experimental datapoints, as would be done if optimising PR-vdW, could be done in 28 hours. If one searched the same number of parameter values for each of the four BIPs in PR-mWS-NRTL the calculation would take three millennia. In practice, such a large number of calculations are not required, as one starts with a rough low-resolution search and focusses on a shrinking area of interest with increasing resolution, such that PR-vdW could be fit in less than an hour and PR-mWS-NRTL in about

one week. This approach also has benefits when using temperature dependent BIPs, as one merely fits a function to the locus of optimal solutions at each temperature instead of increasing the number of parameters being simultaneously optimised.

The program was not explicitly written to perform these calculations as fast as possible, improvements to the way the calculations are coded and the use of more efficient programming languages would allow for meaningful improvements, especially should parallelised calculations be used. The combination of these improvements would allow for a minimum of a 100-fold improvement in speed on an typical modern workstation and high power computing clusters may be used for further improvement. A simple test of parallelisation across multiple CPU cores found minimal overhead, such that 10 cores/workers could conduct the same grid search as a single core in approximately one tenth of the time.

It appears that there is little justification for not using a grid search when optimising models for binary mixtures with four parameters or fewer. Only when optimising models with many parameters or for a large number of systems, such that the runtime would be on the order of months, is the reduced quality of optimisation sensible (especially when the data such models are optimised against take months or years to produce per dataset).

The final consideration to be discussed here is the choice of objective function to be minimised during optimisation. The minimisation of sum squared error in composition, given previously, has been used in this work and the preceding works [305, 306]. The first justification for this is that the experimental relative uncertainties of alternative parameters (ie the temperature or pressure) are generally far smaller than for composition, and the second reason is that the particular flash calculations used are designed to output composition for a given pressure. This approach struggles when there are rapid changes in composition for very small changes in pressure, and similarly the use of pressure struggles in the opposite case. Orthogonal distance regression is occasionally used to mitigate this issue [307], accounting for errors in multiple dimensions simultaneously, but requires more computation and was not explored in this work.

Chapter 3: Phase Behaviour of Mixtures

“What could apparently be simpler than a drop of liquid?”

— J.S. Rowlinson
A Drop of Liquid

3.1 The Behaviour of Asymmetric Mixtures

When two or more different compounds are present in a system at once they will assume/display behaviour that differs from either of the compounds when pure. This situation is common; the concept of a truly pure fluid is merely hypothetical at industrially relevant scales. High purities are achievable (for instance, 99.999% pure hydrogen is used in this work), however, the presence of trace impurities is a practical certainty. Radioactivity and quantum mechanics alone are sufficient to ensure this, though impurities are typically process related.

Each additional component increases the cardinality of the thermodynamic space by one and, in doing so, frees up another state variable to contribute to the possible number of coexisting phases [188, 195]. For example, for a specified value of temperature in the space (p,T,μ_1), the classical Gibbs phase rules states that that there is only one pressure for which two phases may coexist. In the space $(p,T,\mu_{1:2})$ there is an additional degree of freedom, such that two-phase equilibria (classically the vapour-liquid equilibria) may occur across a range of pressures for a specific temperature and vice versa.

The additional degree of freedom does not necessitate that the maximum number of phases will occur for any values of the state variables. Phase stability remains dictated by the minimum free energy criteria, which are sufficient to simultaneously satisfy the phase rule. One should consider why it could be energetically favourable for a homogenous mixture to separate into two phases.

A simple exemplary case is a mixture of hard spheres of two different diameters at high packing fraction (*ie* solid-like density), with finite (non-zero) kinetic energy and no attractive forces. If the spheres are of similar diameter then there shall not be a significant difference in the achievable packing fraction, however, once the size ratio is sufficiently large the two sizes of spheres will disrupt each other's packing structures [308]. In this situation, they could achieve more favourable structures (for the same overall composition) by separating into two phases, one richer in spheres of the smaller diameter, the other richer in spheres of the larger diameter. If the difference in size grows even further, then the smaller spheres may also happily sit between the larger spheres. Even for such a simple model system, a wide range of different phases are possible, for which exact solutions are known when the spheres are close-packed [309, 310] *(ie* in the limit of infinite pressure).

Real fluids are not so simple; the analogy still roughly applies but is complicated by additional forces and the flexibility afforded by lower packing fractions (that may go down to the limit of zero density, an ideal gas). Real molecules are not perfectly spherical, their intra and inter-molecular structures are neither isotropic nor time-invariant (even before considering wave-particle duality). This naturally (by definition) gives rise to numerous intermolecular forces due to the potentials within a given thermodynamic space. Some of these forces manifest themselves as what are referred to as bonds, energetically-favourable non-random/anisotropic probabilistic relationships between the positions of molecules. The mechanisms behind differing types of bonds are overlapping, such that one should consider them to all fall on a continuous scale describing the potential energy between molecules [272].

The strongest of those within this work are covalent bonds, the conventional sharing of electrons within a molecule (typically between two atoms), however focus is placed on non-reactive systems.

It is the weaker intermolecular bonds that are the primary interest instead. For instance, there are the forces between spontaneous, induced, and/or permanent dipoles, attracting/coalescing even nominally inert compounds like helium (as in the case of the helium dimer [311]). These forces are especially strong in systems containing molecules with covalent bonds between atoms with appreciable differences in electronegativity, such as hydrogen and oxygen, where lone pairs are present [312]. The hydroxyl group produces forces sufficiently strong that, for the archetypal example of water, the molecules effectively polymerise [313], with the dimer being especially prevalent. This type of bonding is referred to in this work as molecular association (as it is within the SAFT framework [272]), with the particularly common cases involving hydrogen as the less electronegative species often called hydrogen bonding (the distinction is semantic).

When a binary mixture consists of one polar component, such as methanol, and one non-polar component, such hydrogen, the strength of the intermolecular forces between methanol molecules is greater than between the unlike species, promoting their separation much like in the example of unequal hard spheres. Mixtures, like these, with large differences between the pure-component properties are termed asymmetric mixtures. The cases above are examples of asymmetry in size and in polarity (or more specifically, dipole moment, as higher order multipoles may also give rise to asymmetry), though differences in mass, thermal de Broglie wavelength, shape, etc are equally valid. The impact of asymmetries on the phase behaviour of mixtures is most succinctly put by the classical adage “like dissolves like”, the implicit complement to which is “unlike may not necessarily dissolve unlike”.

It is possible to describe all pure compounds and mixtures (both real and hypothetical) within what is known as a global phase diagram [314-321], a necessary result of the universality of physics. This developing field stems from observations of mixtures whose phase space can be meaningfully categorised, with the “types” proposed by van Konynenburg & Scott [322] for binary systems being the most familiar. Their original analysis was specific to the van der Waals fluid (especially, but not exclusively, for equally sized components), allowing for categorisation based purely on pure component parameters and their additivity within the one fluid model, yet is broadly applicable to real binary mixtures [218]. Similar categorisation is possible also for ternary and higher order mixtures [323], but is beyond the scope this work.

The inescapable ambiguity of different fluid states, at least within contemporary understanding, might lead one to suspect that meaningful categorisation of phase behaviour should not be possible. The method of van Konynenburg & Scott avoids this ambiguity by neglecting the particularities of any given phase, instead focussing on the multiplicity and connectivity of critical curves/regions (the loci of critical points) within the thermodynamic space [321, 322]. The thermodynamic spaces for all mixtures of a given type are topologically identical. There are also subtypes depending on the locations of critical curves relative to pure component saturation curves, as in the case of azeotropy, as well as the presence of inflection points in critical curves . The types defined by Bolz et al [321] are more exhaustive [319],

listing 17 basic classes in the original publication within a framework that can be applied to arbitrarily complex fluid behaviour, though without standardised nomenclature for solid equilibria. Typical examples of *pT* diagrams are shown in Figure 3.1, note that the particular shapes of the critical curves shown are not representative of the full set nor is the full scale shown (or often even known).

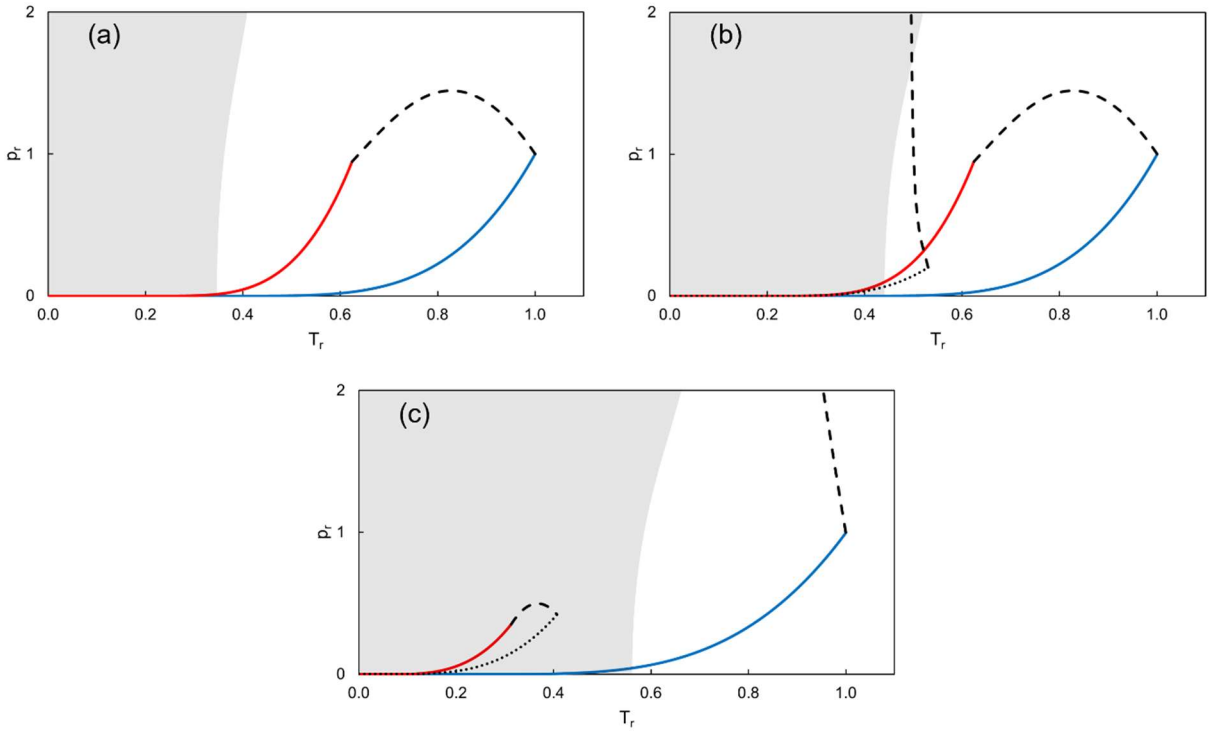


Figure 3.1: Typical p_rT_r projections of (a) type (I or 1^P), (b) (II or 1^Pl^Z), and (c) (III or 1^C1^Z) mixtures, showing the pure component saturation curves —/— up to the critical points, mixture critical curves – –, VLLE curves ···, and shaded regions illustrating how solidification may constrain the fluid coexistence region

The transition between one type of behaviour and another occurs upon the appearance/emergence of a new critical curve, such as in the transition from a type I to type II mixture upon the appearance of a liquid-liquid critical curve, or upon the intersection (change in number of separate/disconnected curves) of two critical curves, such as in the transition from a type II to a type III mixture. This work discusses mixtures showing only type I, II, or III behaviour (though not intentionally), further information about the other types and subtypes may be found in the literature [314-322].

Mixtures of similar compounds produce classical simple phase diagrams with one continuous critical curve between the critical points of the two components and closed *pxy* envelopes, classified as type I or 1^P behaviour. An example is shown in Figures 3.1a and 3.2a. The phase envelopes do not necessarily need to be convex and type I mixtures (as with all other overarching types) may show azeotropy. The critical curve is not a straight line nor is it necessarily monotonic, but commonly connects the pure component critical points with a positive deviation from linearity in the *pT* plane. The curve may also exceed the critical temperature of the less volatile (and thus both) components, referred to in older literature as gas-gas immiscibility of the third kind [218], though this is uncommon. The fluid-fluid

coexistence (or demixing, depending upon one's perspective) typically occurs from around the triple point of the highest freezing (typically, but not exclusively, least volatile) component and connects the two pure component phase spaces, in a region of what is termed vapour-liquid equilibrium. For example, the *pxy* phase envelopes tend to $x = y$ at the limits of $x = 0$ or 1, and terminate at the pure component saturated vapour pressures. At (or more strictly, generally near) the triple point temperature of the highest freezing component there is a region of three phase SVLE which may persist down to around the triple point of the lower freezing component. At temperatures below this, regions of solid fluid equilibria continue to exist, but with no more than one fluid phase (for simple, truly type I mixtures). Looking towards higher temperatures, once the critical temperature of the more volatile component is exceeded there is no longer an uninterrupted region of VLE connecting the two pure components. For example, *pxy* envelopes/projections, such as is shown in Figure 3.2a, now show a smoothly continuous curve, beginning and terminating at the two phase region of the less volatile component, featuring exactly one critical point for a given temperature. This continues up until the critical point of the less volatile component, beyond which is a purely single phase region.

As the asymmetry between the mixture components grows, a new region of fluid-fluid coexistence emerges, as shown in Figure 3.1b, where both fluids are typically liquid-like (as such it is termed liquid-liquid equilibrium, LLE). Such behaviour is classified as type II or $1^{P}l^{X}$ behaviour, where X here denotes unknown or unspecified target/end point. In a fluid only model, like the EoS models in this work, this emerges from the limit of zero temperature [317], type $1^{P}l^{Z}$ behaviour. Real fluid mixtures solidify at temperatures greater than zero, so the occurrence of LLE can be prevented under circumstances where solidification precedes LLE (where the classical Gibbs phase rule applies/is applicable). A complication arises in that the number of intersections of the LLE critical curve with the SFE/SFFE curve does not appear to be constrained. As such, there are systems that are type II within a fluid only model but where solidification precedes LLE under all conditions for the real system, such that it is indistinguishable from a type I system (at first approximation). There can also be systems where a region of LLE appears at its true origin, the upper critical end point (UCEP), with a region of three phase VLLE present. The LL critical curve may then proceed towards greater pressures, not necessarily monotonically with respect to temperature, and will terminate either upon solidification or upon the breakdown of the molecular structures (through reaction, ionisation, etc). For model systems that consider fluid and solid phases but do not consider molecular stability, there is no requirement that the region of LLE/FFE be bound. Similarly, a region of LLE can emerge, away from its theoretical UCEP and three phase coexistence curve, from a region of SFE, ultimately terminating as before. Alternatively, a LL critical curve may emerge from the UCEP, intersect the SLLE curve twice, and have two apparently disconnected regions of LLE, and so on. In any case, a type II mixture nominally has two disconnected critical curves, with the emergent one advancing towards the original as the asymmetry grows.

At a certain point (that only truly exactly occurs for hypothetical fluid mixtures), the two critical curves intersect, and beyond it the connectivity of the critical regions changes. The critical point of the more volatile component now nominally connects to the UCEP and adjacent three phase VLLE curve, as shown in Figure 3.1c. This is type III or, nominally, $1^{C}1^{Z}$ behaviour, though often the second critical curve is either masked or not investigated, where it cannot be

strictly define beyond $1^{C}X^{X}$. Solidification preceding the conditions under which that critical curve would appear is common in real highly asymmetric fluids. Meanwhile, the critical point of the less volatile component connects to a critical curve that follows the path towards greater pressures that the LL critical curve previously had taken. The ultimate path and termination of that critical curve have the same conditions as before; never intersecting the critical point of the more volatile component. As the asymmetry grows, so does the region of demixing. The critical curve initially passes through a pressure minimum, potentially followed by a temperature minimum, though the pressure minimum eventually disappears (as it has in the case shown in Figure 3.1c). Further increases in asymmetry lead to the critical curve departing from the critical point of the less volatile component ever more steeply, until effectively vertical (as in the case of H_2 + water), before gaining a positive slope. Historically this would be the transition from gas-gas immiscibility of the second kind into that of the first kind [218], though this is largely semantic.

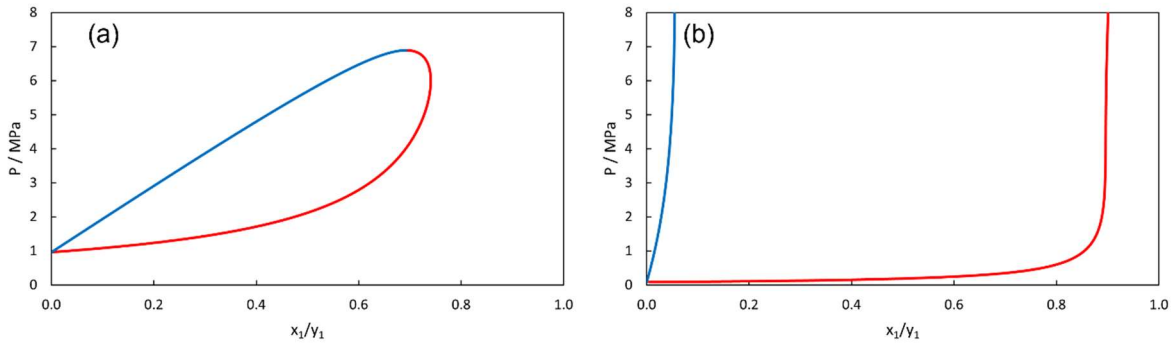


Figure 3.2: Typical pxy isotherms for (a) type I mixtures, (b) type III mixtures at temperatures between the critical points of either component, showing the saturated liquid — and vapour — curves, with x_1/y_1 referring to the mole fraction of the more volatile component

Table 3.1: Pure component parameters: critical temperature T_c, pressure p_c, and density ρ_c, as well as molar mass M, acentric factor ω, and triple point temperature T_t [207, 282-284, 305]; real and adjusted (*) critical points for hydrogen are listed, see [305] for details

Chemical Name	T_c/K	p_c/MPa	ρ_c/(mol/cm^3)	M/(g/mol)	ω	T_t/K
Hydrogen	33.15	1.296	15.508	2.016	-0.219	13.96
Hydrogen*	31.76	1.276	-	-	-0.0626	-
Carbon Dioxide	304.13	7.377	10.625	44.01	0.2239	216.59
Isobutane	407.81	3.629	3.8798	58.12	0.184	113.73
Methanol	512.6	8.104	8.6	32.04	0.5625	175.61

The size of the phase space for type III mixtures is radically different to type I mixtures. For example, if the binary mixture of hydrogen and helium was a type I mixture, one would expect, as per hydrogen's properties as listed in Table 3.1 (note that adjusted critical parameters, for use in modelling at higher temperatures where quantum mechanical effects are less pronounced, determined by fitting the second and third virial coefficients at temperatures between (65 and 500) K [305], are also listed), that its region of fluid-fluid coexistence would begin around 14 K and continue until around 33 K, with mixture critical pressures never exceeding several MPa. In practice, hydrogen + helium is a type III mixture; its FFE has been experimentally shown to continue up to at least 354 K and 7.12 GPa [324], encompassing a

pTx space that is orders of magnitude greater than the former scenario. At temperatures between the pure component critical points, the pxy envelope appears open, as shown in Figure 3.2b.

Type III mixtures often exemplify the difficulty in distinguishing between liquid and gaseous states, producing debate as to what their equilibria should be called, especially at temperatures above the critical points of either component. The terms vapour-liquid equilibria, liquid-liquid equilibria, gas-gas equilibria, and fluid-fluid equilibria have all been applied [325]. In practice there are significant, ill-defined, regions where the behaviour does not meet the liquid-like or gas-like criteria mentioned in the preceding chapter. When referring to type III mixtures in this work, no strict distinction shall be made between the fluid phases, for convenience the term vapour will refer to the phase richer in the more volatile component and liquid will refer to the phase richer in the less volatile component. No inferences beyond this should be assumed, for example the liquid phase is not consistently the most dense phase in mass or molar terms.

The complicated range of options for the presence of FFE regions and their potential intersections with solid regions, especially when clathrate formation is possible, presents a challenge for determining if the entire fluid coexistence region has been explored (and, by extension, what type a given mixture is). When modelling, it is trivial to explore any region of thermodynamic space (though care needs to be taken assess stability) but it is not generally possible to rigorously nor accurately assess solid-fluid behaviour with current theory and models. Furthermore, dense fluids and asymmetric mixtures are often poorly described by models [217, 238]. Experimental investigations can observe the real behaviour with quantifiable uncertainty but are more limited due to technoeconomic considerations, and take far longer. For example, a model may converge a flash in less than a millisecond, while the same flash in an experimental apparatus may take an hour (excluding additional considerations such as sampling). Tracing coexistence regions is helpful, but confirming the presence, or lack thereof, of disconnected regions requires an exhaustive search.

The development of industrial processes require accurate knowledge of the thermophysical properties of the compounds being handled [182], achieved through the use of thermodynamic models that must be based on sufficient reliable experiment data. The most important property for optimising mixture models is the fluid phase behaviour. To confidently obtain an optimal (or near-optimal) fit for a model it is especially preferable to have sufficient data to be able to trace (for instance, by hand) the *pTx* space with a similar uncertainty as is achievable through modelling. A particular model may not necessarily be able to accurately reproduce the real behaviour, but there is sufficient information to make the assessment.

A mixture/system will be referred to as “well studied” (with respect to is phase behaviour/equilibria) when the entire *pTx* space has been covered by experimental measurements, such that one could confidently trace the entire fluid coexistence region(s). An example of such a mixture would be methane + ethane. This differs from whether there is sufficient data to achieve the optimal fit, as is evident from the fact that a perfect predictive model requires no data. In either case, the limiting factor is the amount of available data and their respective uncertainties.

3.2 Mixtures with CO_2

A detailed review of the literature for mixtures containing CO_2 is provided only for the two binary systems investigated in this work: CO_2 with methanol and with isobutane. General reviews of industrially-relevant CO_2 mixtures are available elsewhere already [258, 326-330]. There is substantial overlap between different binary mixtures when considering industrial cases, thus the behaviour of ternary and higher order mixtures is important, however modelling of these is based on binary interactions. Furthermore, data are scarcely available for higher order mixtures, so focus is placed on binary mixtures. The phase behaviour, and thermophysical properties more generally, of CO_2 mixtures have garnered significant attention in the past two decades. Nevertheless, few mixtures have been characterised extensively, especially in comparison to natural-gas-like mixtures.

3.2.1 Isobutane + CO_2

The most well studied of the three mixtures investigated experimentally in this work is that of isobutane with CO_2. There have been seven previous investigations into the phase behaviour of isobutane + CO_2 in the literature, as summarised in Table 2 along with the study from this work, as published [138]. Data had been available covering a range from within 10 K of the critical temperature of isobutane (the less volatile component here) down to 250 K, ~33 K above the triple point temperature of CO_2 (the higher freezing component). The spacing of the data and the agreement between different datasets were sufficient to trace down towards the lower temperature limit, however uncertainties in the behaviour at low temperatures limited applicability in, for example, mixed refrigerant cycles.

A cursory comparison of the critical temperatures and molar masses of the pure components would suggest that this mixture is close to ideal, however the other properties listed (and those excluded) make it clear that there is a more complex asymmetry. For example, the quadrupole moment of CO_2 is significant while that of isobutane is negligible, their intramolecular bonds involve different orbitals, and the molecular structure of CO_2 is linear while isobutane is roughly trigonal pyramidal or tetrahedral. The mixture displays type I/1^P phase behaviour, as is typical of CO_2 + light alkane mixtures, though may alternatively be viewed as type II/$1^P l^X$ with preceding solidification [321]. Considering the position of the melting line of pure CO_2, it is likely, but not shown unequivocally, that solidification precedes a liquid-liquid separation in all cases.

The most recent prior study is that of Wang and Li [331], containing 25 data points with a noticeable scatter. The only other work that covered the low temperature region was Weber's [332]; this data set comprises 76 datapoints that are generally consistent, though there are a small number of apparently erroneous points visible, such as on the 280 K isotherm. A later study by Weber [333] covered higher temperatures, almost up to the critical temperature of isobutane. The data here also appear to be of high quality, with little scatter visible except in the near critical region at T = 394 K. Three of the four isotherms were matched to those in the

earliest study of isobutane + CO_2, that of Besserer and Robinson [334], showing relatively close agreement though there are some minor disagreements for the vapour composition. One isotherm of Besserer and Robinson, at T = 378 K, exhibits some scatter, with two vapour points clearly out of line, but otherwise the data are satisfactory. Robinson, with Leu, later conducted another investigation of the phase behaviour near to the critical point of isobutane [335], including measurements of the mixture critical point for the two temperatures. Nagahama *et al* [336] conducted some measurements only at T = 273 K, however, like Wang and Li's measurements at the same temperature, there is noticeable scatter and the data are not so consistent with those at different temperatures from other reliable studies. Finally, the second most contemporary work, that of Nagata et al [337] reports data along four isotherms at temperatures between (300 and 330) K with only a minor degree of scatter.

Table 3.2: Previous investigations into the phase behaviour of isobutane + CO_2 including the temperature and pressure ranges covered

Authors	Year	T / K	p / MPa	Ref
Besserer & Robinson	1973	311 – 394	0.50 – 7.18	[334]
Nagahama *et al*	1974	273	0.16 – 3.49	[336]
Weber	1985	250 – 280	0.06 – 4.16	[332]
Leu & Robinson	1987	383 – 398	2.46 – 6.00	[335]
Weber	1989	311 – 394	0.57 – 7.40	[333]
Nagata *et al*	2011	300 – 330	0.65 – 6.97	[337]
Wang & Li	2017	263 – 303	0.11 – 3.97	[331]
This Work	2024	240 – 310	0.62 – 6.82	[138]

3.2.2 Methanol + CO_2

The mixture of CO_2 with methanol has been studied more frequently than that with isobutane, by roughly an order of magnitude, yet cannot be considered well studied. It stands as an excellent example of when quantity does not equal quality, exacerbated by cases where brief (in scope and detail of methods) investigations have been conducted to provide validation for apparatuses later used for similar mixtures. It will shortly be apparent that such cases fail to provide low uncertainty validation.

The behaviour of this mixture is not simple, most notably the polarity of methanol causes association between not only methanol molecules but also with CO_2, much like in the case of CO_2 with water. Methanol appears quite distinct in its properties among the series of alcohols, especially as its short chain length prevents significant charge separation. Its behaviour is perhaps best understood when recognising that while it is the first in the series of primary alcohols, there is also a zeroth alcohol: water (hydryl alcohol, if one is to be systematic). Capturing the non-idealities of methanol, CO_2, and their mixtures requires suitable models with complex mixing rules, such as the Wong Sandler rule, or a SAFT-type approach.

CO_2 + water is a type III mixture [338], however methanol presents a lower degree of asymmetry. It has been observed [339] that there is a continuous critical curve between pure methanol and CO_2, thus it is not type III, however it would likely feature LLE in the absence of

solidification. No region of LLE or VLLE has been observed experimentally, however there was not sufficient data available to conclusively rule this out (whether the LLE region is continuous or interrupted by solidification). Data are available down to 213 K, below the triple point of CO_2, with 291 *pTx* data points below 270 K, however only 19 of these are at $x_{CO2} \geq 0.6$, and only six are at $x_{CO2} \geq 0.8$. It is clear that the region of the bubble/liquid curve near to the vapour pressure of pure CO_2 flattens as temperature decreases, necessary for an incipient separation, but further insight was not possible.

The absence of data in this region, exacerbated by the few available points being far spaced, is a frustration for researchers and industry alike. It was not possible to meaningfully assess the performance of a model in these regions, nor low-risk for processes to be designed to utilise the otherwise favourable behaviour. This places substantial limits on the feasibility and efficiency of low temperature methanol + CO_2 processes, such as the Rectisol process, where unanticipated phase separations can be damaging. Furthermore, many available models, such as predictive SRK [340] (similar to EPPR78, but with the parameters for alcohols) or the multiparameter EoS of Blackham and Lemmon [341], predict LLE even in regions where it is confidently known not to occur [342], allowing for the complementary situation in which unaware/uninformed engineers design processes around this unphysical separation. Models which are incapable of predicting LLE, such as one using the Wilson model [343], may avoid the issue entirely but suffer in terms of accuracy.

Table 3.3: Previous investigations into the phase behaviour of methanol + CO_2 including the temperature and pressure ranges covered

Authors	Year	*T* / K	*p* / MPa	Ref
Krichevskii	1941	298.15 - 348.15	0.02 - 9.12	[344]
Krichevskii	1947	273.15 - 348.15	0.69 - 6.97	[345]
Snedeker	1955	308.15 - 308.15	2.23 - 7.82	[346]
Bezdel	1958	223.15 - 458.15	0.1 - 2.94	[347]
Shenderei	1959	213.15 - 247.15	0.1 - 1.57	[348]
Yorizane	1969	243.15 - 273.15	0.2 - 3.33	[349]
Hemmaplardh	1972	288.15 - 333.15	1.64 - 4.33	[350]
Katayama	1975	298.15 - 298.15	0.22 - 6.13	[351]
Ohgaki	1976	298.15 - 313.15	0.58 - 8.06	[352]
Schneider	1978	213.15 - 273.15	0 - 1.69	[353]
Ferrell	1979	258 - 258	0.51 - 1.65	[354]
Semenova	1979	323.15 - 398.15	0.5 - 13	[355]
Lazalde-Crabtree	1980	263.15 - 273.15	1.72 - 1.78	[356]
Takeuchi	1980	223.15 - 273.15	0.3 - 3.04	[357]
Schmelter	1982	273.15 - 273.15	0.49 - 2.99	[358]
Weber	1984	233.15 - 298.15	0.3 - 5.08	[359]
Chang	1985	243.15 - 298.15	0.19 - 5.45	[360]
Galivel-Solastiouk	1986	313.1 - 313.1	2.2 - 3.2	[361]
Langhorst	1987	241.77 - 282.91	0.4 - 3.52	[362]
Brunner	1987	298.15 - 473.15	0.99 - 16.08	[363]
Schroeder	1987	272.9 - 272.9	1.73 - 1.73	[364]
Hong	1988	230 - 330	0.69 - 10.65	[365]

Authors	Year	T / K	p / MPa	Ref
Suzuki	1990	313.4 - 313.4	0.68 - 7.71	[366]
Melzer	1990	253.15 - 298.15	0.04 - 0.05	[367]
Page	1991	333.15 - 393.15	10.58 - 15.56	[368]
Leu	1991	323.2 - 477.6	0.44 - 16.29	[369]
Schroedter	1991	220.06 - 260.05	0.01 - 0.01	[370]
Yong	1992	287.65 - 301.75	5.03 - 6.98	[371]
Roškar	1992	308.15 - 338.15	4.05 - 11.94	[372]
Yoon	1993	313.2 - 313.2	0.7 - 8.21	[373]
Tsuji	1994	353.2 - 353.2	0.72 - 13.6	[374]
Kodama	1996	313.15 - 313.15	2.01 - 7.51	[375]
Reighard	1996	298.45 - 372.65	1.54 - 15.55	[376]
Chang	1997	291.15 - 313.14	0.56 - 8.03	[377]
Joung	1999	313.15 - 313.15	1.8 - 7.9	[378]
Elbaccouch	2000	312.85 - 313.25	1.14 - 7.53	[379]
Yeo	2000	298.15 - 421.15	5.87 - 16.44	[339]
Joung	2001	313.15 - 342.8	0.6 - 12.4	[380]
Zhu	2002	323.15 - 473.15	6 - 16.2	[381]
Laursen	2002	298.15 - 313.15	1.24 - 6.34	[382]
Bezanehtak	2002	278.15 - 308.15	1.5 - 7.43	[383]
Kodama	2002	313.15 - 313.15	7.08 - 9.92	[384]
Secuianu	2003	298.15 - 310.15	0.5 - 7.6	[385]
Secuianu	2003	323.15 - 323.15	6.11 - 9.48	[386]
Xia	2004	313.75 - 395	0.3 - 9.74	[387]
Joedecke	2004	313.73 - 394.99	0.19 - 9.73	[388]
Xie	2005	313.2 - 313.2	0.93 - 7.93	[389]
Schwinghammer	2006	303.15 - 303.15	0.84 - 5.4	[390]
Naidoo	2008	263.15 - 373.15	0.79 - 12.07	[391]
Secuianu	2009	293.15 - 323.15	0.48 - 9.51	[392]
Aida	2010	313.15 - 313.15	0.51 - 7.55	[393]
Tochigi	2010	313.14 - 313.14	0.57 - 7.87	[394]
Sato	2010	313.11 - 330.03	3.62 - 10.71	[395]
Pinto	2011	303.15 - 313.15	3.24 - 7.82	[396]
Schueler	2012	299 - 327	0.1 - 0.1	[397]
Hamada	2012	323.2 - 323.2	0.99 - 9.79	[398]
Pinto	2012	303.15 - 343.15	3.24 - 12.4	[399]
Lei	2013	313.2 - 333.2	0.74 - 6.2	[400]
Kariznovi	2013	303.2 - 323.2	1.02 - 5.95	[401]
Dai	2015	228.2 - 273.2	0.15 - 3.02	[402]
Jalili	2015	298.15 - 313.15	0.02 - 3.77	[403]
Qureshi	2017	298.15 - 298.15	2.97 - 5.64	[97]
Braga	2017	303.1 - 353.1	5.12 - 10.69	[404]
Lyu	2018	213.15 - 273.15	0.1 - 3.35	[343]
Hoehler	2018	258.2 - 298.3	0.14 - 5.73	[405]
Taheri	2018	313.2 - 353.2	1.03 - 6.25	[406]
Wang	2019	243.15 - 323.15	0.52 - 3.18	[407]

Authors	Year	T / K	p / MPa	Ref
Matsukawa	2021	313 - 343	1.94 - 12.7	[408]
Braga	2022	303 - 333	3.52 - 11.05	[409]
This Work	2025	230.00 - 298.15	0.5 - 6.1	

Detailed discussion of every available data source for this mixture is excluded for brevity, with the overarching details listed in Table 3.3, though some aspects will be revisited in Section 5.3. Further details are also available within existing reviews of CO_2 + alcohols [342, 401, 402, 410, 411] and CO_2 more generally [258, 326-330]. As the literature gaps at lower temperatures have already been discussed, attention is now turned to higher temperatures. Near ambient temperatures are the most frequently investigated, however there is substantial disagreement. Figure 3.3 shows the literature data available at 298.15 K to illustrate this, where there are 250/112 *pTx*/*y* points, yet some are plainly inaccurate (*eg* exceeding the saturated vapour pressure of pure CO_2) and others appear self-consistent while disagreeing with alternative sources by up to ~40 mol% for a given pressure, an order of magnitude worse than was seen with isobutane + CO_2. Roughly 50% of datapoints for either phase are for temperatures between (270 and 320) K. Only 34/30 *pTx*/*y* datapoints across 3 studies are available above 400 K and the highest temperature with available data is 477.6 K, 35 K below the critical point of methanol. There is significant scatter to the vapour data at these temperatures.

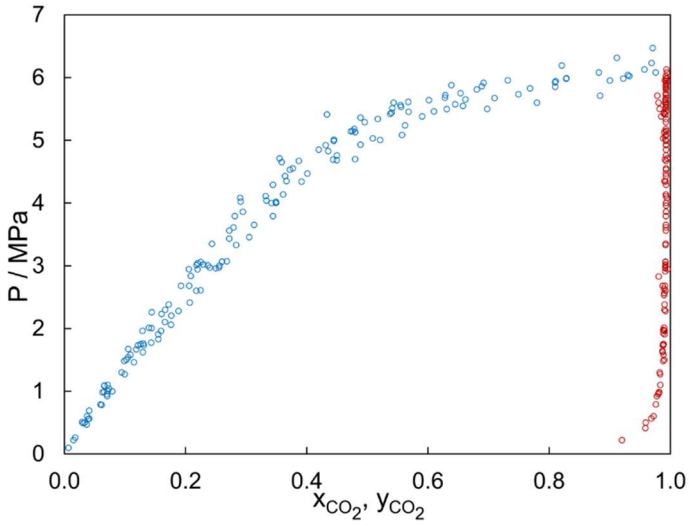


Figure 3.3: pxy projection for methanol + CO_2 at T = (298.15 ± 0.03) K showing the data available in the literature. Note that for clarity all datasets are represented by the same symbol

While this work is focussed on phase behaviour, density data for liquid-like phases are of next most importance in model optimisation. Such data are especially important in situations where there is ambiguity regarding potential phase separations or near-critical effects, thus there is value in discussing what is present in the literature for methanol + CO_2. As discussed in the previous chapter, accurate description of liquid phase densities is a challenge for engineering models (such as cubic EoS); the densities of pure methanol and CO_2 are especially troublesome and their mixtures even more so, where simple volume translations are inadequate.

Nine studies are available in total, summarised in Table 3.4. The majority of the data lies at temperatures between (298.15 and 323.2) K, primarily in the form of saturated liquid density data. Only one dataset, the earliest [363], is present for temperatures greater than 323.2 K, while only two/three (explained momentarily) are present for temperatures below 298.15 K [377, 383, 412]. The work of Bezanehtak *et al* [383] extends to the lowest temperatures with four closely spaced isotherms, though there is significant scatter to the data. The other low temperature study is that of Chang *et al*, initially published [377] with unusually low density values then published again [412] with more reasonable values, the data are identical except for an unspecified (non-constant) offset applied to the densities and no apparent acknowledgement of the adaptation. Both versions were featured in comparisons by Bezanehtak *et al* [383], though erroneously identified as data from unique measurement campaigns. It is most likely that the change is as a result of an updated calibration of the densimeter, however it has not been addressed. As such, there are effectively no reliable data at temperatures below 298.15 K. There are likely to be strong association and clustering effects present in the liquid phase at these temperatures, the proper elucidation of which require reliable density data. There have been molecular dynamic studies into such behaviours at temperatures near to the critical point temperature of CO_2 [393, 413], observing significant clustering under CO_2-rich conditions. Only three studies investigated single-phase density, focussed on liquid-like states for supercritical fluid extraction and chromatography [375, 414, 415].

Table 3.4: Previous investigations into the density of methanol + CO_2 including the temperature ranges covered and whether the data are for saturated vapour (SV), liquid (SL), or compressed fluid single-phase (CF) density

Authors	Year	T / K	Type	Ref
Brunner	1987	298.15 - 373.15	SL	[363]
Berger	1990	303.15	CF	[414]
Kodama	1996	313.15	SV,SL,CF	[375]
Chang	1997/8	291.15 - 313.14	SV,SL	[377, 412]
Bezanehtak	2002	278.15 - 308.15	SL	[383]
Smith	2002	313.2 - 323.2	CF	[415]
Aida	2010	313.15	SL	[393]
Kariznovi	2013	303.2 - 323.2	SL	[401]
Jalili	2015	298.15 - 313.15	SL	[403]

3.3 Mixtures with H_2

3.3.1 General Phase Behaviour of H_2 Mixtures

The overall behaviour of hydrogen mixtures has not received as much attention as other "families" of mixtures, such as the systems containing CO_2 or water, but there have been periods of greater interest and attempts to understand the underlying trends. Most notably, in the 1940s, following the work of Kay [416] and his contemporaries, who highlighted the unusual behaviour of these systems, and in the work of Streett and colleagues [417-426] during the 1960s to early 1980s, whose extensive investigations of light hydrogen binaries are

valuable for understanding the overall phase space. Since then, little work has focussed on understanding the fluid phase behaviour seen specifically in hydrogen mixtures, though progress has been made on hydrogen clathrates [427, 428]. Additionally, work on global phase diagrams has supplanted some interest in specific families, though progress on this front remains dependent on experimental studies of specific mixtures [238, 319]. A thorough review of the phase behaviour of hydrogen mixtures has been conducted, as data are generally scarce, no broad reviews were available, and progress on understanding the high pressure fluid behaviour had stalled. Note that this section is adapted from a review currently in preparation for publication.

The substantial asymmetry between hydrogen and almost all possible chemical species results in similar qualitative fluid phase behaviour across the vast majority of hydrogen mixtures. These mixtures display limited miscibility typical of type III systems according to the system of van Konynenburg and Scott [319, 322] or type $1^{C}X^{X}$ by the system of Bolz et al. The only mixtures here not displaying type III behaviour are those of hydrogen isotopes, which display type I/1^{P} behaviour, and hydrogen with neon isotopes, which display type II/ $1^{P}A\mathit{l}^{X}$ behaviour. These exceptions will be discussed further below.

As previously mentioned, type III mixtures should also exhibit a region of three fluid equilibria connecting an upper critical end point to the critical point of the more volatile component; however, this is masked for all known type III hydrogen mixtures by the formation of a solid phase at higher temperatures. The behaviour near to the critical point of hydrogen is only known in the mixture with helium (an exceptional case), as such it is not currently possible to fully classify the Bolz type (hence the X^{X} designation).

Few investigations into solid-fluid equilibria of hydrogen mixtures exist. Those that do can be considered to fall into three broad categories: solid-fluid equilibria between hydrogen and other light molecules under extreme conditions of temperature and/or pressure, equilibria between hydrogen and conventionally-solid compounds intended to contain hydrogen (*eg* materials that may be used in pressure vessels), and hydrogen-containing clathrates.

Solid-fluid equilibria can be found in the phase space of any hydrogen mixture at sufficiently high pressure and industrially relevant temperatures. For cryogenic processes, especially those utilising liquified hydrogen, the pressures required are not high. Understanding solid freezeout is increasingly important for determining processing requirements and impurity tolerances, but current knowledge is deficient. At moderate pressures, the onset of solid formation usually occurs within several kelvin of the triple point of the less volatile component, with hydrogen generally depressing the freezing point except towards lower pressures [429]. At higher pressures, the three phase SFFE line diverges further from the melting line of the pure component, typically, but not exclusively [420], maintaining a positive slope [419, 421, 422, 424, 426].

Further complicating the behaviour is the formation of hydrogen clathrates, which may occur under conditions far from the conventional solid regions of the pure components. The formation of clathrates in flowing systems is problematic, long a source of trouble for the extraction and processing of hydrocarbons [428] and just as detrimental in hydrogen-based

systems. Conversely, there is interest in the use of hydrogen clathrates as an energy dense store [427], as substantial hydrogen contents have been demonstrated [430, 431], though the gigapascal scale pressures currently required limit applicability.

Finally, understanding the interaction between fluid hydrogen and solids intended to contain it is of the upmost importance in the development of infrastructure for the widespread use of hydrogen, most significantly for hydrogen pipelines and storage vessels. Initially such systems were at low pressure, including for airships [432], now focus is placed on high pressure systems, such as pipeline linings [433]. The immense size asymmetry between hydrogen and any such material results in complex effects, with hydrogen able to diffuse into solids, embrittling metals [434] and permeating through polymers [435].

3.3.2 Introduction to Literature Data for H_2 Mixtures

As with much of this work, the literature has focussed on the fluid phase behaviour of binary mixtures of hydrogen with relevant compounds. A limited number of datasets exist for ternary and higher order mixtures and these are neglected for brevity. The mixtures considered cover a wide variety of chemical families and functional groups. For hydrocarbons, this includes straight chained and isomeric alkanes, alkenes, cycloalkanes, aromatics, and alcohols, while non-hydrocarbons include diatomic molecules, noble gases, and polar compounds. Many of the datasets can be found through databanks such as DETHERM [436], though standard precautions are advised with regards to the presence of duplicated or erroneous datasets.

Table 3.5: Availability of data for considered binary mixtures of hydrogen with different groups of molecules

Group	# Considered	# With Data	# Datasets	# Datapoints
Alkanes	10	9	33	3447
Iso-Alkanes	8	3	6	536
Alkenes	4	2	6	718
Cyclics	12	2	5	481
Aromatics	8	5	9	624
Alcohols	8	5	10	501
Diatomics	8	4	16	1088
Polar Inorganics	5	5	20	1242
Noble Gases	6	4	18	2132
Total	**70**	**39**	**123**	**10769**

An overview of the mixtures for which data are present is provided in Table 3.4, and a list of the available datasets and information about the number of datapoints and the range of conditions explored is provided in Table 3.5. In general, studies listed are those which contain composition data for both phases, preferably for more than ten state points. This excludes approximately half of the datasets available, but a much smaller fraction of the overall datapoints. Small datasets are less useful when fitting models, as are those which contain data for only one of the coexistence phases (most commonly solubility in the liquid), though a small number of low uncertainty measurements across a suitably large span of conditions may

still be useful when model overfitting can be avoided. Additionally, many of the excluded datasets consist only of a single point at ambient temperature and pressure. What is especially desirable is data in regions displaying more complex behaviour or where compositions change rapidly, such as the near critical regions. In total, data were sought for mixtures of hydrogen with 70 different compounds, of which only 39 contained noteworthy amounts of data for both phases. Note that, for all the groups listed except noble gases, many (typically larger) molecules are considered unlikely to have data with reasonable confidence (though occasional exceptions are expected) but are not discussed here.

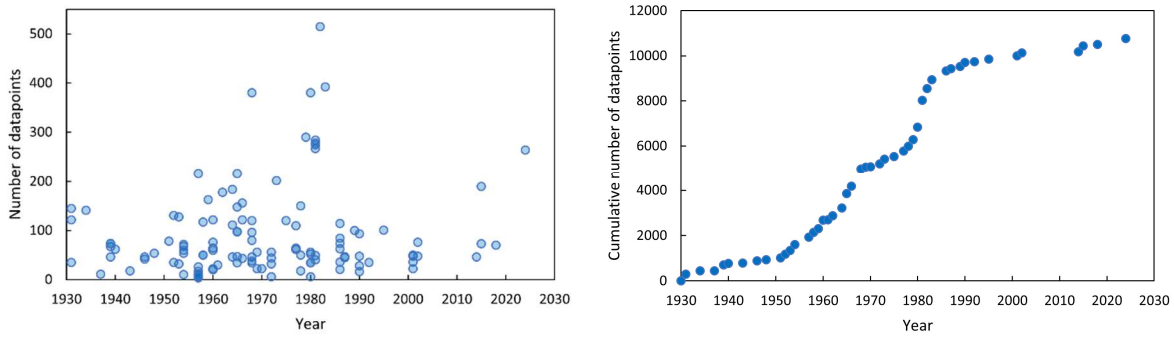


Figure 3.4: Distribution of the datasets published over time, showing (a) the year and number of datapoints included and (b) the cumulative number of datapoints as a function of time over the past century

When considering the data produced each year over almost the last century, as is shown in figure 3, a clear and concerning tread is visible. Initially there is a slow rise which accelerates in the mid-20th century with the development of measurement techniques and equipment and the concurrent growth of the chemical and energy industries, then plateaus towards the end of the century. Since then, in juxtaposition to the rapidly growing importance of hydrogen in the net zero transition, few experimental works have been published. The majority of datapoints produced in the 21st century come from only two publications [138, 305], one from this work and the other from a preceding work, using largely the same apparatus and technique. This is a significant issue, as older experimental techniques were often less accurate and expectations and standards for reporting experimental uncertainties were lower. Additionally, at temperatures below 200 K the ortho/para ratio changes meaningfully, but the ratios were rarely measured and this is occasionally blamed for experimental disagreements, as in the case of hydrogen + neon [418].

Table 3.6: Overview of available data sets for the phase behaviour of binary mixtures with hydrogen

Hydrogen +	Authors	Year	T_{range} / K	P_{range} / MPa	# Points	Ref
methane	Freeth	1931	90.6 - 90.7	1.71 - 20.82	35	[437]
	Fastovskii	1940	90.3 - 127.0	3.14 - 22.95	62	[438]
	Benham	1957	116.5 - 172.0	3.38 - 27.58	26	[439]
	Augood	1957	111.7	2.28 - 17.93	5	[440]
	Kirk	1965	66.9 - 116.6	1.03 - 12.69	97	[441]
	Yorizane	1968	103.2 - 163.2	1.01 - 15.20	46	[442]
	Sagara	1972	103.2 - 173.7	1.02 - 10.83	56	[443]

Hydrogen +	Authors	Year	T_{range} / K	P_{range} / MPa	# Points	Ref
methane (*cont.*)	Tsang	1980	92.3 - 180.0	0.22 - 137.98	380	[422]
	Yorizane	1980	93.2	10.13 - 15.20	6	[444]
	Hong	1981	108.1 - 183.1	0.08 - 28.41	284	[445]
	Hu	2014	100.1 - 120.5	0.24 - 2.27	46	[446]
	Lin	2018	100.1 - 130.7	0.24 - 3.11	70	[447]
ethane	Levitskaya	1939	158.2 - 188.2	0.03 - 7.82	67	[448]
	Williams	1954	144.3 - 199.8	3.45 - 6.89	10	[449]
	Cohen	1969	143.5 - 199.4	0.71 - 13.79	56	[450]
	Sagara	1972	148.2 - 223.2	2.03 - 8.11	32	[443]
	Heintz	1982	92.5 - 280.2	3.18 - 559.50	515	[424]
	Hiza	1995	80.0 - 189.7	0.27 - 15.60	101	[451]
propane	Burriss	1953	277.6 - 360.9	0.54 - 52.76	128	[452]
	Bolshakov	1954	248.2 - 298.2	1.52 - 20.27	54	[453]
	Williams	1954	172.1 - 297.1	1.72 - 55.12	72	[449]
	Trust	1968	88.2 - 348.2	0.69 - 20.68	380	[454]
butane	Nelson	1943	297.1 - 388.8	2.25 - 10.72	18	[174]
	Aroyan	1951	144.3 - 297.0	2.11 - 53.43	78	[173]
	Augood	1957	213.6 - 273.2	9.06 - 18.99	12	[440]
	Klink	1975	327.7 - 394.3	2.78 - 16.88	120	[175]
pentane	Freitag	1986	273.2 - 373.2	0.35 - 27.59	63	[455]
hexane	Nichols	1957	277.6 - 477.6	0.01 - 68.95	216	[456]
heptane	Peter	1960	424.2 - 498.9	0.38 - 78.45	64	[457]
	Zernov	1990	423.2 - 473.2	0.37 - 4.05	48	[458]
octane	Connolly	1965	463.2 - 553.2	0.46 - 13.79	148	[459]
	Connolly	1989	463.2 - 543.2	1.01 - 15.04	100	[460]
decane	Sebastian	1980	462.5 - 583.5	1.93 - 25.52	52	[461]
isobutane	Dean	1946	310.9 - 394.3	3.45 - 20.69	42	[176]
	This Work	2024	189.9 - 400.0	1.08 - 19.93	264	[138]
2,3-dimethylbutane	Connolly	1986	393.2 - 483.2	1.46 - 9.08	74	[462]
2,2,4-trimethylpentane	Dean	1946	310.9 - 423.4	1.21 - 34.92	46	[176]
	Peter	1960	424.0 - 499.4	0.35 - 107.87	76	[457]
	Laugier	1980	499.2 - 523.2	3.00 - 36.80	34	[463]
ethene	Likhter	1939	158.2 - 188.2	0.05 - 8.00	74	[464]
	Williams	1954	158.2 - 255.4	1.67 - 53.35	68	[449]
	Hiza	1968	80.0 - 169.8	0.20 - 15.91	80	[465]
	Sagara	1972	123.2 - 248.2	2.03 - 8.11	44	[443]
	Heintz	1983	114.2 - 247.2	4.03 - 599.83	392	[425]
propene	Williams	1954	199.9 - 297.1	1.72 - 55.12	60	[449]
cyclohexane	Krichevskii	1958	293.2 - 333.2	4.90 - 68.80	117	[466]
	Thompson	1965	338.7 - 394.3	0.69 - 69.04	34	[467]
	Berty	1966	310.9 - 410.9	0.02 - 65.72	156	[468]
	Connolly	1986	413.2 - 523.2	0.91 - 14.52	114	[462]
methylcyclohexane	Peter	1960	424.2 - 498.7	0.34 - 88.26	60	[457]
benzene	Ipatev	1948	298.2 - 423.2	0.01 - 294.20	54	[469]

Hydrogen +	Authors	Year	T_{range} / K	P_{range} / MPa	# Points	Ref
benzene (*cont.*)	Connolly	1962	433.2 - 533.2	0.71 - 20.69	178	[470]
	Connolly	1965	433.2 - 533.2	1.90 - 17.80	98	[459]
	Thompson	1965	338.7 - 433.2	0.53 - 68.93	47	[467]
methylbenzene	Simnick	1978	461.9 - 575.2	2.02 - 25.37	50	[471]
	Laugier	1980	542.2 - 568.2	3.46 - 32.70	56	[463]
1,3-dimethylbenzene	Connolly	1986	513.2 - 593.2	1.21 - 11.09	84	[462]
1,4-diethylbenzene	Connolly	1986	533.2 - 573.2	1.14 - 12.59	36	[462]
phenol	Gillespie	1986	316.5 - 560.9	0.69 - 13.79	21	[472]
methanol	Michels	1953	297.6 - 372.5	8.51 - 81.06	32	[473]
	Brunner	1987	298.2 - 373.2	3.44 - 110.30	47	[363]
	d'Angelo	2001	314.4 - 476.6	4.49 - 10.98	48	[474]
	Bezanehtak	2002	278.2 - 308.2	2.00 - 11.02	48	[383]
ethanol	Brunner	1990	298.2 - 508.2	0.50 - 33.75	93	[475]
	d'Angelo	2001	299.9 - 476.5	3.70 - 9.03	36	[474]
1-propanol	d'Angelo	2001	299.9 - 513.6	3.64 - 10.19	50	[474]
1-butanol	Tyvina	1977	313.2 - 473.2	0.41 - 30.40	61	[476]
	d'Angelo	2001	295.3 - 524.9	3.91 - 8.82	22	[474]
2-methyl-1-propanol	Tyvina	1977	313.2 - 473.2	0.41 - 30.40	64	[476]
N_2	Verschoyle	1931	63.1 - 88.2	0.01 - 22.78	122	[477]
	Gonikberg	1939	79.0 - 109.0	0.12 - 17.75	73	[478]
	Shtekkel	1939	90.0 - 113.0	1.61 - 9.55	46	[479]
	Augood	1957	67.0 - 77.7	2.62 - 17.79	17	[440]
	Akers	1960	83.2 - 122.0	2.17 - 13.79	20	[480]
	Maimoni	1961	90.0 - 95.0	0.36 - 4.60	30	[481]
	Yorizane	1968	77.4 - 88.2	1.67 - 19.05	34	[442]
	Streett	1978	63.2 - 110.3	1.03 - 57.22	150	[420]
	Xiao	1990	100.0	1.39 - 3.42	16	[482]
CO	Verschoyle	1931	68.1 - 88.2	0.03 - 22.79	145	[477]
	Augood	1957	81.4	9.52 - 18.06	8	[440]
	Akers	1960	83.2 - 122.0	2.17 - 13.79	22	[480]
	Yorizane	1968	77.4 - 123.2	0.61 - 15.20	38	[442]
	Tsang	1981	70.0 - 125.0	0.49 - 52.94	267	[423]
D_2	Newman	1958	18.0 - 28.5	0.07 - 0.35	50	[483]
HD	Newman	1958	18.0 - 28.5	0.07 - 0.35	50	[483]
CO_2	Augood	1957	239.7	18.48 - 19.17	6	[440]
	Kaminishi	1966	233.2 - 298.2	5.08 - 19.99	43	[484]
	Spano	1968	219.9 - 289.9	1.08 - 20.32	96	[485]
	Yorizane	1970	273.2	6.08 - 37.49	22	[486]
	Tsang	1981	220.0 - 290.0	0.93 - 171.79	278	[426]
	Bezanehtak	2002	278.2 - 298.2	4.81 - 19.25	76	[383]
	Fandino	2015	218.2 - 303.2	0.56 - 15.44	190	[305]
	Tenorio	2015	252.8 - 302.9	2.04 - 10.57	73	[487]
water	Zoss	1952	273.2 - 606.5	6.89 - 20.68	35	[488]
	DeVaney	1978	366.5 - 588.7	1.38 - 11.03	18	[489]

Hydrogen +	Authors	Year	T_{range} / K	P_{range} / MPa	# Points	Ref
water (*cont.*)	Gillespie	1980	310.9 - 477.6	0.34 - 13.79	34	[490]
	Seward	1981	? - 713.2	? - 250.00	?	[491]
SO_2	Augood	1957	263.2 - 293.2	10.34 - 19.13	12	[440]
H_2S	Augood	1957	213.6	10.34	4	[440]
	Yorizane	1969	243.2 - 273.2	1.01 - 5.07	22	[349]
ammonia	Wiebe	1934	298.2 - 373.2	5.07 - 101.33	141	[492]
	Wiebe	1937	273.2	5.07 - 101.33	11	[493]
	Augood	1957	293.2 - 293.7	8.76 - 19.03	12	[440]
	Reamer	1959	277.6 - 394.3	1.54 - 41.69	163	[494]
	Heise	1972	298.2	2.89 - 20.22	6	[495]
helium	Smith	1952	17.4 - 21.8	0.19 - 5.87	131	[496]
	Sonntag	1964	20.4 - 31.5	0.24 - 3.45	111	[497]
	Streett	1964	15.5 - 32.5	0.24 - 3.45	184	[417]
	Sneed	1968	15.5 - 29.8	2.36 - 10.36	120	[498]
	Streett	1973	26.0 - 100.0	0.59 - 917.00	202	[419]
	Hiza	1981	20.0 - 28.0	0.09 - 2.06	49	[499]
	Pashkov	1981	14.7 - 30.0	0.01 - 15.41	274	[500]
	van den Bergh	1987	148.7 - 353.9	1610 - 7120	45	[324]
	Yamanishi	1992	15.9 - 20.1	0.06 - 0.16	35	[501]
helium-3	Hiza	1981	22.0 - 28.0	0.16 - 1.54	40	[499]
neon	Streett	1965	24.6 - 33.7	0.04 - 1.39	216	[418]
	Heck	1966	26.0 - 42.5	0.21 - 2.51	122	[502]
argon	Augood	1957	87.4	11.51 - 18.27	7	[440]
	Volk	1960	87.0 - 140.0	1.70 - 10.24	122	[503]
	Mullins	1964	87.0 - 105.0	2.03 - 12.19	46	[504]
	Ostronov	1977	85.9 - 112.8	0.51 - 4.05	110	[505]
	Calado	1979	83.1 - 141.4	0.08 - 51.80	290	[421]
	Xiao	1990	100.0	0.64 - 4.62	28	[482]

3.3.3 Mixtures with Organic Compounds

Normal alkanes are a natural place to start, structurally simple molecules that are well studied in comparison to other homologous series. The stability of these molecules permits experiments up to high temperatures for heavy alkanes, and the historical need to process and separate the wide range of carbon chains found in fossil fuels incentivised much research.

A clear trend is visible when examining the number of available datasets for hydrogen + n-alkane binaries as a function of carbon number. The smaller compounds, whose closer volatility to hydrogen increases the need for optimised separations, are better studied, while above a carbon number of four there are no more than two datasets available, with no data available for hydrogen + nonane and most n-alkanes longer than decane. Some solubility data are available for a few heavy n-alkanes, including up to n-hexatetracontane (C46) [506].

The system of hydrogen + methane is one of the best studied hydrogen mixtures, with the greatest number of VLE datasets available and only slightly fewer points than hydrogen + helium. Data are available for the entire region of the phase space enclosed by the methane saturation curve, the mixture critical curve, and the three phase SFFE curve, from the work of Tsang et al [422], as such this mixture may be considered well studied. Eleven other studies of the mixture are also available [437-447], though two [440, 444] have few points and are included only because they also include data for other mixtures. The work of Cosway and Katz [507] on higher order mixtures is occasionally listed as an additional source [508], though this simply collated three individual points from other sources.

The binary mixture with ethane is also well studied with six datasets [424, 443, 448-451], with the work of Heintz and Streett [424] covering up to the intersection of the critical curve with the three phase SFFE curve at pressures up to 560 MPa. As with all other studies that went up to great pressures with hydrogen, there is no available alternative dataset in the very high pressure regime for comparison. Propane [172, 449, 452, 453] and butane [173-175, 440] both have four sets of data available, including a limited amount of data in the near critical regime, though no data is available in the very high pressure regime. Only a single dataset is available for each of the hydrogen binaries with pentane [455], hexane [456], and decane [461], though some liquid solubility data is available. The data situation is only mildly better for heptane [457, 458] and octane [459, 460] with two studies for each.

Isomeric alkanes are less well studied than their normal counterparts, especially when considering the number of options that arise through combinatorics for larger molecules. Of the many possibly binary mixtures with hydrogen, only three have data for both phases.

There are only two datasets are available for the simplest isomeric alkane, isobutane, [138, 176]. The older work, that of Dean and Tooke, has relatively few points, and uses a troubled apparatus from 1937 [509], however there is still acceptable agreement for liquid phase compositions with the more recent work while a consistent difference is visible between the vapour compositions. The more recent study, produced as part of this work [138], covers a substantially broader range of temperatures and examined the near critical regime much more closely, while providing a thorough uncertainty analysis, in what is the single largest dataset for hydrogen phase behaviour published in the last four decades. There has since been a study on interfacial tension for isobutane + H_2, which erroneously states that there are no available EoS and overlooked the preceding work, limiting the analysis that could be conducted [181]. This is but one of many cases in which research communication shortcomings (not only data shortcomings) have been observed for hydrogen mixtures.

There is no data available for the two isomers of pentane, unfortunate given the value of 2,2-dimethylpropane (neopentane) for understanding the impact of quaternary carbon groups. Connolly and Kandalic [462] provide liquid solubility and full VLE composition data for 2,3-dimethylbutane in a broad study that examined several lesser investigated mixtures. No data could be found for other hexane isomers. Dean and Tooke, in the previously mentioned work [176], also used an improved apparatus to investigate the mixtures with 2,2,4-trimethylpentane, the fuel additive commonly known as isooctane, and an unspecified mixture of isomeric dodecane, with some characterisation for the latter provided but insufficient for

use. Peter and Reinhartz [457] and Laugier et al [463] also investigated hydrogen + 2,2,4-trimethylpentane, the former extending into the near critical region, albeit with few points. While isobutane and isooctane alone can be used to determine interaction parameters for the CH and C functional groups, 2,2-dimethylpropane would be a more appropriate choice for the C group. Some high pressure liquid phase solubility data are available for squalane, a long chain branched hydrocarbon that is generally well characterised among heavy hydrocarbons.

The mixtures of hydrogen with alkenes are especially poorly studied, in spite of the relevance of these mixtures to hydrogenation and dehydrogenation reactions. There are regions of the phase space where reactions would occur uncatalyzed for some of these mixtures, though this has not been stated as the limiting factor in any of the literature investigations. Only for the simplest alkene, ethene, is there a substantial amount of data, across five datasets [425, 443, 449, 464, 465], including the work of Heintz and Streett [425] who covered the entire vapour-liquid coexistence region in a follow up work to the earlier experiments with ethane [424]. Williams [449] also reported data for the mixture with propene. Additionally, the mixture critical curve for both the ethene and propene systems was investigated by Chen et al [510], but data in the two phase region is not reported. Scant data is available for heavier alkenes, though one study [511] produced data on the solubility of hydrogen in alkenes up to a carbon number of 17. This absence is greatly inconvenient, not only due to the industrial relevance of these mixtures, but also because these alkenes, such as 2-butene, display cis-trans isomerism, often not considered well in models, partly due to complexity but also due to the lack of data for many systems.

Little data are available for mixtures of hydrogen with cyclic or aromatic components. For the latter, data are only available for cyclohexane and methylcyclohexane, with no data available for other ring sizes nor for other cyclohexane based molecules like ethylcyclohexane or the three dimethylcyclohexane isomers. These mixtures with a hexyl ring are relevant to liquid organic hydrogen carriers and in hydrogenation and dehydration reactions involving aromatics more generally. At present the lack of data for cyclics and their corresponding aromatics presents a significant barrier to assessing the economic viability of LOHCs. Four sets of data [462, 466-468] are present for cyclohexane, though no data is available in the near critical region. Meanwhile, only Peter and Reinhartz [457] investigated the mixture with methylcyclohexane. Several small datasets for liquid solubility, mostly at ambient conditions, have been published in recent years due to the increased interest in LOHCs.

The data situation is only mildly better for aromatic hydrocarbons. There are four datasets available for hydrogen + benzene [459, 467, 469, 470], with the work of Ipatev et al extending to almost 300 MPa, though the small number of points and age of the data make it difficult to interpret more than just rough trends. Two datasets [463, 471] are available for methylbenzene (toluene), the aromatic counterpart to methylcyclohexane. Of the three dimethylbenzene isomers, only 1,3-dimethylbenzene (meta-xylene) has any data, in the work of Connolly and Kandalic [462]. Beyond this, the only available data is solubility in the liquid phase for unspecified mixed xylene isomers. Connolly and Kandalic also investigated the system with 1,4-diethylbenzene, though no data is available for the corresponding cyclic. No data is available for ethylbenzene. One study [472] is available for the mixture with phenol.

The final category of organic molecules discussed here is hydrogen with alchols. The polarity and potential for hydrogen bonding in alcohol results in a greater degree of asymmetry than seen with the preceding mixtures. Large regions of the pressure/temperature space available to common phase behaviour apparatuses have extremely low mutual solubilities. Still, there great value in the compositions of the vapour phase at low pressures where the composition changes rapidly, as well as near critical data for both phases, both of which are relatively accessible and relevant to industrial processes.

There are four datasets are available for methanol [363, 383, 473, 474]. One of these, the work of Brunner et al [363], follows and earlier investigation by Brunner [512] which contains the only available data on the mixture critical curve, though the critical compositions are not provided. Brunner, with Hültenschmidt, [475] later investigated the binary with ethanol and also produced three points of data on the critical curve, this time with compositions listed. The only other dataset for ethanol is that of d'Angelo [474] who produced VLE data for hydrogen with the first four primary alcohols, including the only dataset for hydrogen + 1-propanol. There are data for 1-butanol and 2-methyl-1-propanol in the work of Tyvina [476]. No data are available for mixtures of hydrogen with 2-propanol or with 2-butanol or 2-methyl-2-propanol.

3.3.4 Mixtures with Inorganic Compounds

Mixtures of hydrogen with organic molecules are prevalent in industry both historically (with fossil fuels) and in future (with green alternatives), however, the importance of the mixtures with inorganic compounds should not be overlook. Binary mixtures of hydrogen with other diatomic molecules are a clear example; diatomic molecules are typically very volatile, as illustrated by hydrogen itself, and as such are prone to needing rigorous separation processes. The most relevant in the context of hydrogen are nitrogen, carbon monoxide, oxygen, and, to a much lesser extent, the isotopes of hydrogen.

The most frequently studied of the hydrogen + diatomic family and one of the most well studied hydrogen binaries overall is the mixture with nitrogen. Nine studies are available [420, 440, 442, 477-482] spanning almost the entire fluid coexistence region. Streett and Calado [420], as with the related works, attempted to go to low enough temperatures and high enough pressures to reach the onset of solid formation, though did not manage to in this case, even at temperatures barely above the triple point of pure nitrogen, implying the three phase SFFE line leaves the triple point with a negative slope.

In non-reactive contexts, carbon monoxide is remarkably similar to nitrogen due to their similar diatomic structure and approximately equal molecular mass. As such, the behaviour of carbon monoxide mixtures does not differ greatly from that of nitrogen mixtures when the volatility of the other components is substantially higher or lower, as is the case with hydrogen. This similarity, combined with the toxicity and corrosivity associated with carbon monoxide, discourages experimental investigations, though the prevalence of the mixture in syngas has balanced this somewhat. Interestingly, though perhaps unsurprisingly given the similar conditions of relevance, four [440, 442, 477, 480] of the five available datasets for hydrogen with carbon monoxide come from publications that also featured the binary with nitrogen, and

the fifth, the work of Tsang and Streett [423], is a follow up to Streett and Calado's investigation with nitrogen.

Next less volatile is oxygen. Mixtures containing hydrogen and oxygen are present in effectively all processes that extract energy from hydrogen, from combustion cycles to fuel cells. The reaction between hydrogen and oxygen to form water is highly energetic and easily initiated, occurring spontaneously under sufficiently high temperatures and pressures. The reactive nature of is mixture renders high pressure experiments challenging and raises safety concerns when handling hydrogen [513]. While data exists for non-equilibrium behaviour like flame properties [514], no data exists at high pressures for phase equilibrium. Studies have modelled this behaviour in a predictive manner [515] based upon pure component properties, and comparisons to mixtures of hydrogen with similar diatomic molecules, such as nitrogen or carbon monoxide, can provide further improvements. Under some circumstances deviations from expected behaviour likely occur, such as under the influence of strong magnetic fields due to the paramagnetic nature of oxygen, however this applies almost exclusively to astrophysics.

The last H_2 + diatomic mixtures considered are the isotopic mixtures of hydrogen involving protium, deuterium, and tritium. The molecules formed by these combinations are sufficiently different to experience fluid phase separations, though are close enough to have behave in a near-ideal manner, with some quantum considerations, as a type $I/1^P$ mixture. Little data is available in the open literature for these mixtures. There are no studies of the phase behaviour of hydrogen with tritium, nor with hydrogen tritide or deuterium tritide. One single study is available for the mixtures of hydrogen with deuterium and with hydrogen deuteride [483], however the data is presented partially graphically and partially as deviations from Raoult's law for smoothed data. Some studies are available on real and simulated cryogenic distillation processes [516].

The "polar" opposite of the exceptional type I mixtures of hydrogen isotopes are, unsurprisingly, those involving polar compounds. Looking first to CO_2, with a substantial quadrupolar moment, the binary mixture with hydrogen has seen the most studies published in the 21st century, albeit only three [305, 383, 487], due to its central role in the net zero transition. Five studies preceded these [426, 440, 484-486], including one [426] which covered what is suspected to be the entire coexistence region. The critical curve of the mixture either intersects the three phase SFFE curve or comes remarkably close, in either case there is ambiguity as to if a region of FFE exists at higher temperatures and pressures. There is also an old study which at the time was suspected to perhaps include such a region, though this was likely experimental error. A recent study [517] examined the vapour compositions and densities, though not the liquid compositions.

The most strongly polar compound considered is water, whose mixture with hydrogen is relevant to many industrial processes as well as underground hydrogen storage and the extraction of naturally occurring hydrogen (and orange hydrogen [113]). This mixture is can be difficult to investigate as one nears the critical point of water, due to the high corrosivity of water under such conditions and the tendency for hydrogen to cause embrittlement, with substantial diffusion of hydrogen into containing vessel and occasional explosive rupturing of

pressure transducers reported in the work of Seward and Franck [491]. Theirs is the only investigation in the vicinity of the water critical point and extends to 250 MPa, though the publication focusses on the critical curve and states that the full dataset would be subject to further publication, which unfortunately could not be located, perhaps having never been published, and it is recommended that efforts be made to rediscover this extensive and unique dataset. Three other VLE datasets are available [488-490], though none particularly large, believed to have fewer points combined than the dataset of Seward and Franck. One other notable study on this system, although it only provides rough bounds on phase boundaries, is that of Bali et al [108] which went to temperatures up to 1473 K and 2.6 GPa with an unorthodox technique, showing the fluid demixing continues far above the critical point of water. A wide variety of aqueous solutions are also important, such as brines found in geological formations, but data is even more scarce for these mixtures. One recent study [518] reported the solubility of hydrogen in water and formation brine, wherein references to other studies on solubility in aqueous salt solutions can also be found.

While water is the most strongly dipolar molecule considered here, several other relevant compounds also have significant dipoles and are listed in order of their polarity. There is SO_2, whose dipole moment is close to that of methanol, then ammonia, then H_2S, and then the far weaker moment of carbon monoxide [519]. SO_2 has only a single small dataset available, the broad work of Augood [440], who also produced one of two datasets available for H_2S. Yorizane [349] produced a slightly larger dataset for H_2S, but combined there are only 13 points available for each phase, though a potential new SO_2 dataset has been mentioned [327]. H_2S is the second lightest compound in the family of dihydrogen chalcogenides after water, so understanding its behaviour would be beneficial to understanding the anomalous properties of water.

Mixtures of hydrogen with ammonia are highly industrially important mixture, most notably in the production of ammonia to be reacted further to produce fertilisers, and there is growing interest in ammonia as a hydrogen-derived energy carrier and low carbon fuel. One might expect there to be extraordinarily detailed studies of the behaviour of this mixture, and the ternary with nitrogen, due to the extreme pressure conditions under which Haber-like processes favour and the subsequent discovery of type III phase behaviour in the system of nitrogen + ammonia, however, data are extremely scarce. Only one large dataset is available, the work of Reamer and Sage [494], though this data appears to be partly smoothed. Augood [440] and Heise [495] report a couple of datapoints, beyond this only solubility data is available, most notably the work of Weibe and Tremearne [492] up to 100 MPa and a short follow up [493]. Attempts have been made to address this shortcoming through molecular dynamic simulations [520], but these are no substitute for accurate experimental measurements. Additionally, rough measurements in a diamond anvil cell by Chidester and Strobel [521] found that, at room temperature, hydrogen and ammonia were immiscible up to the point of solid formation at 1.2 GPa.

The final hydrogen mixtures discussed here are those involving noble gases. The noble gases are all monoatomic molecules, providing the closest approximation to spherical molecules possible with real chemicals with minimal additional effects such as reactivity and polarizability. As spherical molecules form the foundation of many equations of state, from the

classical van der Waals equation to modern SAFT-type models, experimental measurements of the behaviour of hydrogen with noble gases provides important validation for what are, at first approximation, mixtures of simple molecules. Data are available for the lightest three noble gases, helium, neon, and argon, while no data available for mixtures of hydrogen with krypton or with xenon (though some SLE data is available for the latter), nor with radon or heavier noble gases, due to their high radioactivity and short half-lives.

Mixtures of hydrogen with helium differ from all other possible hydrogen mixtures, as here hydrogen is the less volatile component. Strictly speaking, this is not quite true should one consider hypothetical mixtures of hydrogen with unconventional matter, such as with neutrons, but these are of no industrial relevance and are exclusively mixtures that are either unstable or exist under conditions where quantum mechanical and gravity effects dominate, as is the case in neutron stars. The binary mixture of hydrogen + helium is notable not only for being the lightest mixture of chemically different compounds, but also for being the mixture that has been investigated over the broadest range of reduced temperatures and pressures. The low masses of both hydrogen and helium, coupled with the low temperatures at which processes like their cryogenic separation take place, results in pronounced quantum effects. Close to absolute zero, at temperatures below those at which a hydrogen-rich solid phase forms, helium-rich phases may transition to a superfluid Bose-Einstein condensate. This mixture also displays the barotropic effect, as was first noted by Kamerlingh Onnes. It has the greatest number of available datapoints of the hydrogen binaries, with nine datasets [324, 417, 419, 496-501], the most recent of which also features helium + HD and D_2, although it is limited to low pressures. Streett [419] went up to pressures of 917 MPa at 100 K for FFE and up until the onset of hydrogen-rich solid formation. Van den Bergh et al [324] extended this up to 7.12 GPa at 353.9 K and observed experimentally the formation of a helium-rich solid phase, later performing calculations of the phase behaviour up to 100 GPa [522].

Neon, of volatility next closest to hydrogen, is the only mixture presenting type II/$1^{P}A\ell^{X}$ phase behaviour, with a liquid-liquid separation, as well as an azeotrope. Two studies are available in the literature [418, 502], with a third that only presents the data graphically [523]. Studies also available for deuterium + neon [524, 525]. The isotopic purity of the neon used is consistently unspecified, presumably the natural earthly abundance. Knowledge of the differing behaviour of hydrogen with pure neon-20 and neon-22 would be valuable for understanding the onset of the liquid-liquid separation and designing highly tailored cryogenic cycles.

Mixtures of hydrogen with argon are similarly studied to those with carbon monoxide and nitrogen, covering the entire fluid coexistence region [421]. Five studies are available with data for both phases [421, 440, 482, 504, 505], with another one with >100 points of just liquid data [503], but with data for D_2 + argon as well.

3.3.4 Critical Behaviour of H_2 Mixtures

The mixture critical behaviour has been mentioned for several of the above mixtures, with the critical curve followed until the onset of solid formation in some of the lightest mixtures. For

the others, the situation is less clear, though trends are visible, especially when considering the paths of the critical curves in terms of reduced temperatures and pressures. These paths are shown for several selected mixtures in Figure 3.5, where the dashed lines are traces based on literature data, while the solid line is a model prediction; to be discussed in a later chapter (5.2.3) but raised here as an example (that should be viewed critically compared to the others that are well-supported by experiments).

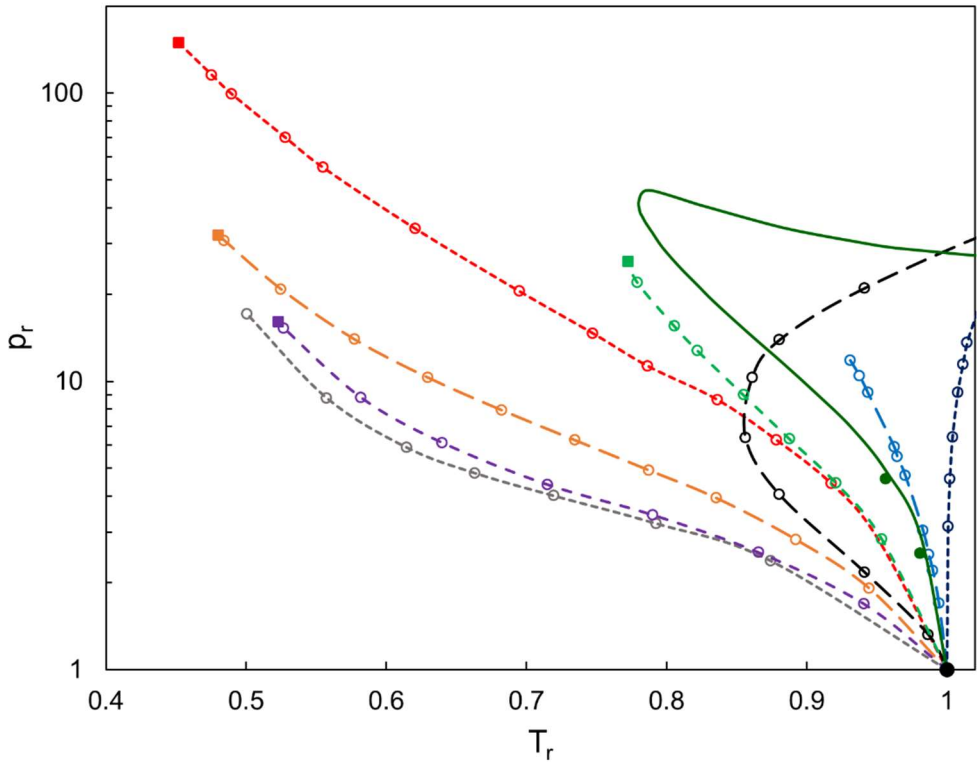


Figure 3.5: Mixture critical curves of several hydrogen binaries as a function of reduced temperature and pressure. — — Helium [419], - - - N_2 [420], – – CO [423], — — methane [422], - - - ethane [424], – – CO_2 [426], — — methanol [512], - - - water [491], —— isobutane (this work, discussed later in Section 5.2.3), ○ represents experimental data (filled ● in the case of data from this work), ■ represents the estimated intersection of the critical curve with the SFFE line, and ● represents the critical point of the less volatile component, please note this is hydrogen in the case of hydrogen + helium

Two significant open questions remain regarding the critical behaviour of all the mixtures except those of hydrogen isotopes, necessitating the use of X (unknown route or target) in their Bolz classifications. The first of these questions applies to those mixtures which are not known to have an intersection of the critical curve with the SFFE region: whether the critical curves ultimately tend to higher temperatures and pressures.

As the asymmetry between hydrogen and the other component grows so does the steepness of the critical curve, as can be seen in Figure 3.5. The steepness also increases as the critical curve proceeds to lower temperatures, becoming almost vertical in the case of CO_2 (though this is less apparent with the log scaled y-axis). It may be reasonable to expect that the curves would continue nearly vertically towards enormous pressures, before inevitably intersecting

with a three phase SFFE line, closing the fluid coexistence region. However, the critical curves of many type III mixtures never intersect the SFFE line [325, 526], at least under conceivable conditions where conventional molecular structures remain stable [527]. This is known to be the case for two highly asymmetric hydrogen mixtures, those with helium [324, 419] and with water [108, 491]. For the former, the critical curve proceeds towards great temperature and pressure, via a temperature minimum. For the latter, ambiguity remains due to experimental uncertainties as the curve begins by rising sharply, though if there is a temperature minimum it must be on the order of several Kelvin. Only for hydrogen + water is there not certainly an initial trend towards lower temperatures, the regions of the critical curve that have been explored for the various other type III mixtures discussed invariably display the same trend as hydrogen + helium does prior to its temperature minimum, differing only in scale (as expected from theory). As such, it appears that for some hydrogen mixtures, where the critical curve is far detached from the melting line of the less volatile component, the critical curve will almost surely reach a temperature minimum and the region of fluid-fluid equilibria will persist to high temperatures and pressures. This is to say that, from current understanding of global phase diagrams, the probability that there is no greater set of real hydrogen mixtures whose critical curves display temperature minima may be reasonably said to be zero, while a finite probability is retained in model systems (*eg* the ideal gas model).

Equation of state models can offer some insights, for instance the curve for isobutane in Figure 3.5 was produced using PR-vdW. However, all current models struggle to accurately recreate the behaviour of fluids at high pressures with high molar densities, though this shortcoming may perhaps be resolved in future decades. Without accurate predictive models suitable for these conditions and lacking experimental data in the regions of interest, a wide range of behaviours can be calculated [528-530], including unphysical ones [531]. For some predictions, a lack of physicality may be readily apparent, though for examples like the one shown for isobutane, conclusive assessment may not be possible. Some models produce critical curves that proceed near vertically to pressures well beyond those where solid formation for both components should occur, others show a temperature minimum and gradual rise to higher temperatures not exceeding the critical temperature of the less volatile component before probable solidification, while in other cases the equilibria predicted continues to supercritical temperatures. This highlights a clear need for more data in the near critical region of hydrogen mixtures up to high pressures.

The second open question is regarding what happens to the phase equilibria beyond the onset of solid formation. This expansive region is rarely considered as it is easily damaging to both instruments and industrial process equipment. Such measurements often must be made in a diamond anvil cell, where mixing is challenging and pressure measurements have high uncertainties, though both are engineering problems that may be resolved with further development. It may be possible for a region of fluid-fluid equilibria to re-emerge at higher temperatures and pressures in situations where the mixture critical curve intersects the solid region, for example with hydrogen + CO_2 where such an intersection may only just barely occur. New experimental data will be required to determine if this is possible, especially as currently existing models are much less capable of describing solid-fluid equilibria, with only one continuous model available, which is not yet applicable to mixtures nor real fluids [223]. The solid-fluid equilibria involving the solid phase rich in the less volatile component is rarely

investigated, let alone in detail, and the data situation is even worse for the more volatile component, perhaps only investigated in the exceptional case of hydrogen + helium system [324]. There are also transitions in the solid phase coexisting with the fluid, such as the transition from ammonia-rich solid phase III to solid phase IV in equilibrium with a hydrogen-rich fluid [521].

While the behaviour discussed in this subsection typically occur under temperature and pressure conditions outside of those used industrially today, there may be viable opportunities to extend these ranges to take advantage of the critical behaviour. Near to the critical curve, especially in the vicinity of inflection points, rapid changes in properties such as saturation compositions and densities occur. The effects may be further amplified by the addition of separation enhancing agents, for instance the addition of a small quantity of helium or water to a mixture of hydrogen with an alcohol would greatly shift the phase space to promote separation under conditions where it would not conventionally be feasible. Such changes can be utilised to produce efficient separation processes, with potential incentives over classical processes which may require high thermal duties, such as cryogenic distillations. While the pressures involved would normally incur high compression costs, hydrogen may be obtained at pressures up to 70 MPa from pipelines or up to ~200 MPa by warming liquid hydrogen to ambient temperature, such that the primary limiting factor is the increased capital cost of using high pressure equipment. However, no technoeconomic assessment and comparison has been made for hydrogen mixtures in such processes thus far, limited in no small part by a lack of experimental data.

Chapter 4: Experimental Methods

“Anything that interacts with its environment is effectively performing a measurement; what makes it useful is knowing precisely what is being measured.”

— Paraphrasing of Carlo Rovelli’s Relational Quantum Mechanics

4.1 Phase Behaviour Apparatus

4.1.1 Apparatus as Presented Initially

The apparatus used in this work has been adapted/developed from one that has been described previously [305, 306, 532, 533], so it shall be described in terms of how it was presented at the start of this work, then how it was modified during the course of investigations. Focus is placed not only on the form of the apparatus, but also on the methodology behind its application. The means by which one takes knowledge of physical properties and dispatches them to perform measurements is known as metrology. The principle from the previous chapters, that many forms of energy and/or work may be present but not all are significant in a specified context, is extended and realised here.

Rigour and standardisation are of great importance, as measurements are rarely truly direct and instead emerge from an often-recursive series of many smaller measurements. Take, for example, the measurement of temperature by means of resistance thermometry. The system to be measured must be brought into thermal contact with a thermometer (and both, practically speaking, are in thermal contact with the ambient environment), such that intermolecular interactions may allow for the conduction of heat and attainment of thermal equilibration between the system and the thermometer. The thermometer itself contains a length of wire across which a potential difference may be raised to produce an electric current flowing through the wire, opposed by an electrical resistance. The resistance of the wire (as with any material) is a function of many variables, however, for a good thermometer, it is especially sensitive to temperature (such that a high signal to noise ratio may be achievable with minimal complex corrections). Overlooking, for simplicity, the means by which the resistance itself is measured, one must then relate the resistance to the temperature. Sufficient knowledge of physical properties may permit absolute *ab initio* relation (at least, following the redefinition of the SI units), but relation to fixed points is more practical. For a pure simple component, such a fixed point is the triple point. The classical phase rule necessitates that there be no degrees of freedom wherever three phases (in this case, solid, vapour, and liquid) are present, thus the realisation of the three phase system ensures that the temperature is exactly the triple point temperature. Observing the resistance of the wire at this temperature therefore provides a practical (though complex) route to indirectly perform measurements with low uncertainty.

The exact mechanisms behind many of the more basic aspects of the metrology applied here are excluded for brevity, especially where it is of little relevance (for instance, the complex electrophysics underlying the working of various microcontrollers within the equipment used are ultimately unimportant).

There are two overarching types of phase behaviour measurement techniques, known as analytical and synthetic methods. The details of the various subtypes, their implications, and the works that have employed them across recent decades can be found in the series of detailed review papers of Dohrn and colleagues [534]. The primary difference is that analytical methods realise a system in multiphase equilibrium and then interact with it to gain information on the state, while synthetic methods gain information from interactions during the creation or modification of a state; it is the former that are primarily employed in this work. Analytical *pTxy*

measurements of phase behaviour require that the fluid/mixture of interest be introduced to a volume and maintained at the measurement state points, such that composition may be analysed.

The volume in this case is a high pressure cell, shown within the overall (simplified) piping and instrumentation diagram (P&ID) in Figure 4.1 and in detail, as it was after modification, in Figure 4.3. The cell has a maximum working temperature and pressure of 473 K and 20 MPa, respectively, and an internal volume of approximately 143 cm^3. The cell consists of monobloc pot with a flat-plate closure, machined out of stainless steel 316L, sealed by compressing an O-ring retained between the body and lid of the cell by a seal retaining ring. To ensure compatibility with a wide range of fluids that may swell or attack polymeric seals, a hollow, nitrogen-pressurised, stainless steel O-ring, plated in silver to improve surface finish, was used (Trelleborg). Gold plated rings (Busak and Shamban, Wills Ring, type O) were used in earlier investigations, however the surface finish was of lower quality, appearing matt, whereas the silver plating had a mirror finish. Three fluid ports, one 1/8″ and two 1/16″, in the lid connect the cell to the other fluid facing volumes.

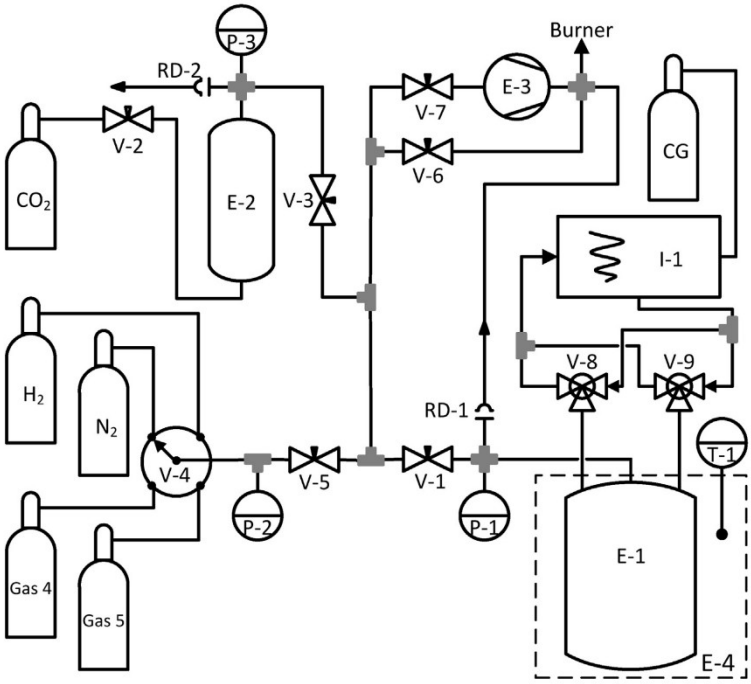


Figure 4.1: Simplified P&ID diagram of the VLE apparatus used in this work as it was initially, as shown in [305], reproduced with permission

The temperature of the cell and its contents was measured using a secondary-standard platinum resistance thermometer (PRT) (Fluke model 5615), housed within a blind hole in the wall of the cell, and connected to a digital readout unit (Fluke 1502A). The PRT was calibrated according to the International Temperature Scale of 1990 [535] between (77 and 693) K, with the calibration checked before each measurement campaign in a triple point of water cell. This description of temperature is currently considered to be within 10 mK of the thermodynamic temperature and can be reevaluated *ad hoc* as standards improve [536]. The cell was immersed in a thermostatic bath (Lauda Proline RP890) capable of operating between (183 and 473) K, allowing the cell temperature to be held constant to within ±10 mK. Three different

bath fluids were used to cover the range of temperatures explored in this work. Ethanol was used for all measurements below 311 K, deionised water was used for the measurements between (311 and 363) K, and silicone oil for the higher temperatures.

Pressure measurements were made by the combination of a gauge pressure sensor (Keller PA-33X, 30 MPa full scale), connected to the cell, and an absolute pressure sensor for the atmospheric pressure (Keller PAA-21Y, 0.2 MPa full scale). Mixing inside the cell was promoted by a polytetrafluoroethylene (PTFE) encapsulated magnetic stirrer bar magnetically coupled to an external permanent magnet and gear assembly driven by a motor above the bath.

Samples were withdrawn from the cell through two electromagnetic rapid on-line sample injector (ROLSI) valves (MINES-ParisTech ROLSI Evolution IV) [537-539]. These were connected to the cell via the two 1/16″ ports with 1.59 mm OD x 0.13 mm ID capillaries that extend into the cell. One passed near to the bottom of the cell while the other stopped near the top, such that two phases could sampled should their interface lie within the middle ~75% of the cell. The sampling valves could be opened for durations from 10 ms to several seconds, allowing a sample, on the order of micromoles, to be drawn into the valve and swept into the gas chromatograph (GC, Agilent 7890A) by carrier gas. The small sample size relative to the cell volume minimised disturbances to the equilibrium. To avoid condensation, the valves were fitted with cartridge resistance heaters and were insulated with glass-filled PTFE shells. The ROLSI valves were arranged in a parallel configuration and connected to the GC via a bespoke heated transfer line. The shared sections of the tubing were insulated and heated, though the short split sections immediately upstream and downstream of ROLSI valves were not. The sample facing surfaces were passivated (SilcoTek Sulfinert) to the greatest extent possible.

The GC allowed for the components to be separated on up to two packed columns and quantified with a thermal conductivity detector (TCD) or a flame photometric detector, for the detection of trace amounts of sulphurous compounds. In this work, only one column (Porapak Q) was required for separation and the TCD was used for all quantification. Notably, the GC was not equipped with any form of inlet septum, commonly used to inject samples in standard chromatographic processes. Instead, samples could be injected either through ROLSI valves or via two gas sample loops, of nominal volumes 0.05 and 0.25 cm^3, respectively which were housed within the GC's valve oven. A P&ID of the GC setup is shown in Figure 4.2. The GC and TCD allowed for composition measurements down to ~50 ppm (on a molar basis) under optimised conditions.

Filling and emptying of the cell was accomplished with a fluid handling system. A series of valves allowed for the cell to be filled with up to four different fluids from gas cylinders, as well as CO_2 via a 500 cm^3 reservoir, a vacuum pump (Vacuubrand MZ 2D NT) to evacuate the system, and a vent line to empty the system. The vacuum pump and vent line led to a flare system consisting of a propane-fired Bunsen burner within an exhaust stack, allowing hazardous fluids such as H_2S to be safely disposed of. A pressure sensor connected to the CO_2 reservoir allowed roughly known amounts of CO_2 to be transferred to the cell, determined

through the use of *pVT* relations, though in this work it was simply used as an intermediate store of CO_2.

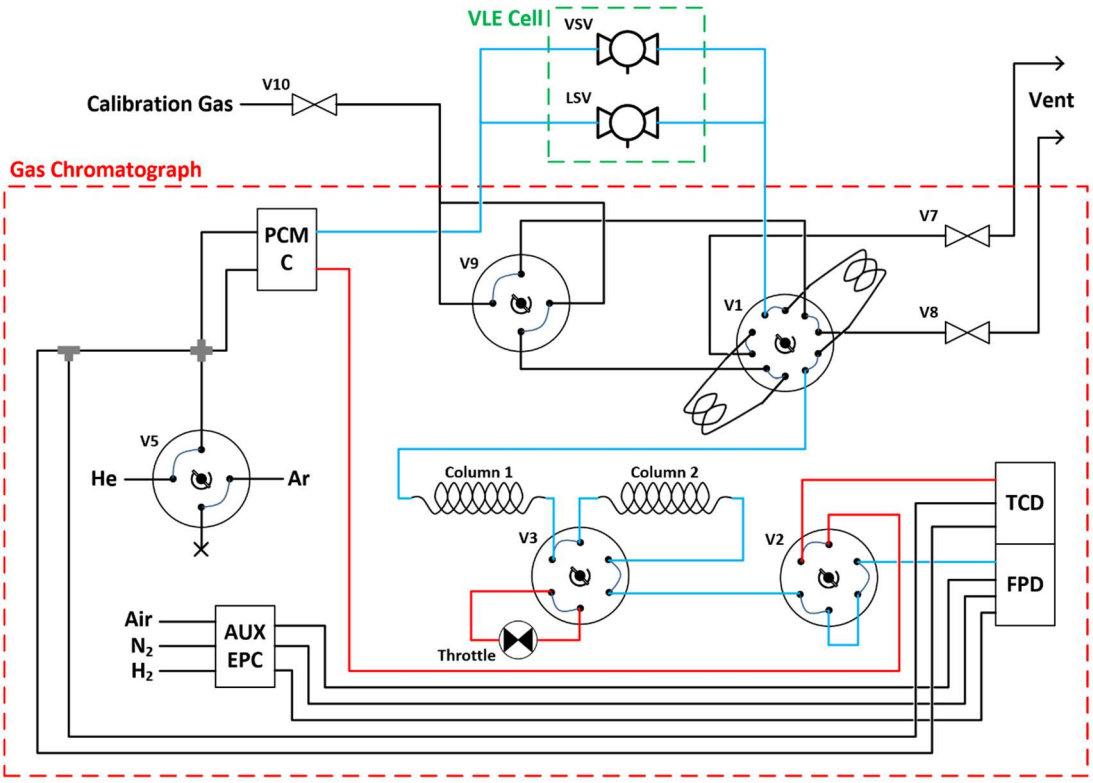


Figure 4.2: P&ID of the GC setup, showing the switching valves in their off position and numbered as they are in the GC itself, with the main carrier gas stream highlighted blue. In this work V2 and V3 were on the on position, such that column 2 was bypassed and the TCD used as the detector

Several safety features were also present, most importantly a rupture-disc device connected to the cell and specified to rupture prior to any part of the cell and its connected volume approaching their yield stresses; this was necessary because it is possible for unacceptable pressures to be generated in the event of a power failure while the cell is at low temperatures and high pressures. The CO_2 reservoir was fitted with a similar rupture disc, and the path to the vacuum pump fitted with a proportional relief valve. A constant nitrogen flow into the space above the cell in the bath was used to purge any potential leaks from the cell, as well as to keep atmospheric oxygen away to prevent any potential for ignition when using flammable bath fluids such as ethanol.

4.1.2 Modifications Made to the Apparatus

Originally, the apparatus was designed for the study the vapour equilibrium of mixtures containing CO_2 and a light gas and with possible addition of trace H_2S. Measurements of systems containing less volatile compounds that are liquids at ambient conditions required several modifications.

It was expected that the pressure difference between the cell and the high pressure cylinders, containing either compressed gas or liquid CO_2, would be used to fill the cell, which could later be emptied simply by venting to the atmosphere (possibly via the burner). Some further amount of control could be achieved using temperature swings, for instance to obtain pressures higher than cylinder pressures when at temperatures sufficiently above the minimum operating temperature of the bath or its fluid (whichever is higher). This approach also limited the accuracy with which the contents of the cell could be estimated. To overcome this would require a pump or compressor, as recommended in the preceding work [533].

Best suited for this task is a high pressure syringe pump (Teledyne ISCO 100 DM), which may be used to precisely meter fluid in and out of the cell. In this case, an Isco 100DX pump was used, with a working volume of 103 cm^3, volume resolution of 0.00001 cm^3, and maximum working pressure of 68.95 MPa. A thermostatic jacket around the cylindrical body allowed for temperature regulation and more convenient filling of the pump with condensable gases. The jacket was used in combination with a thermostatic circulating bath filled with deionised water. A K-type thermocouple on the exterior of the allowed for online temperature monitoring. Electronic inlet and outlet valves allowed the pump to be used in various automated measurement processes. The outlet valve of the pump was connected to two further valves, one leading to a vent or a liquid waste catch pot or to a vacuum pump (as desired), and the other leading to the cell. To use the pump to fill the cell would be relatively simple, but to withdraw liquid or control pressure in multiphase systems required access to the bottom of the cell, otherwise retracting the piston in the pump could draw vapour into the pump, resulting in a system that is harder to analyse and control. This was achieved by running a 0.79 mm OD x 0.50 mm ID (1/32″ nominal diameter) tube coaxially through the existing 3.18 mm OD x 1.75 mm ID inlet/outlet line and port to the cell and extended near to the bottom.

A 250 ml glass bottle with a four port lid, placed upon a magnetic stirrer plate, was used to introduce liquids to the Isco pump. Two of the ports were sealed, one was connected via PTFE tubing to the inlet valve of the Isco pump and a valve leading to a second vacuum pump (Vacuubrand MZ 2D NT). The vacuum pump could be used to degas the liquid under vacuum and stirring (with a PTFE stir bar), as well as to assist in evacuating the Isco pump. The final port in the lid of the bottle was connected to a 60 ml plastic syringe clamped above the bottle. Two valves allowed the syringe to be detached and refilled without exposing the contents of the bottle or syringe to atmosphere. This syringe would be filled with dry nitrogen, needed to provide a pressure gradient for liquid to flow into the evacuated pump. A portion of this nitrogen inevitably dissolves into the otherwise degassed liquid, however there was no stirring at this stage and the upper 10-20 % of the liquid would be left in the bottle, minimising nitrogen content to negligible levels (and no nitrogen peaks were observed by the detector upon sampling). When introducing low pressure condensable gases, like isobutane, the bottle was not used and instead the cylinder containing the gas was connected to the tubing leading the Isco and vacuum pumps. The Isco pump temperature would then be reduced to sub-ambient (typically to 283 K) such that fluid from the supply cylinder would condense inside the pump.

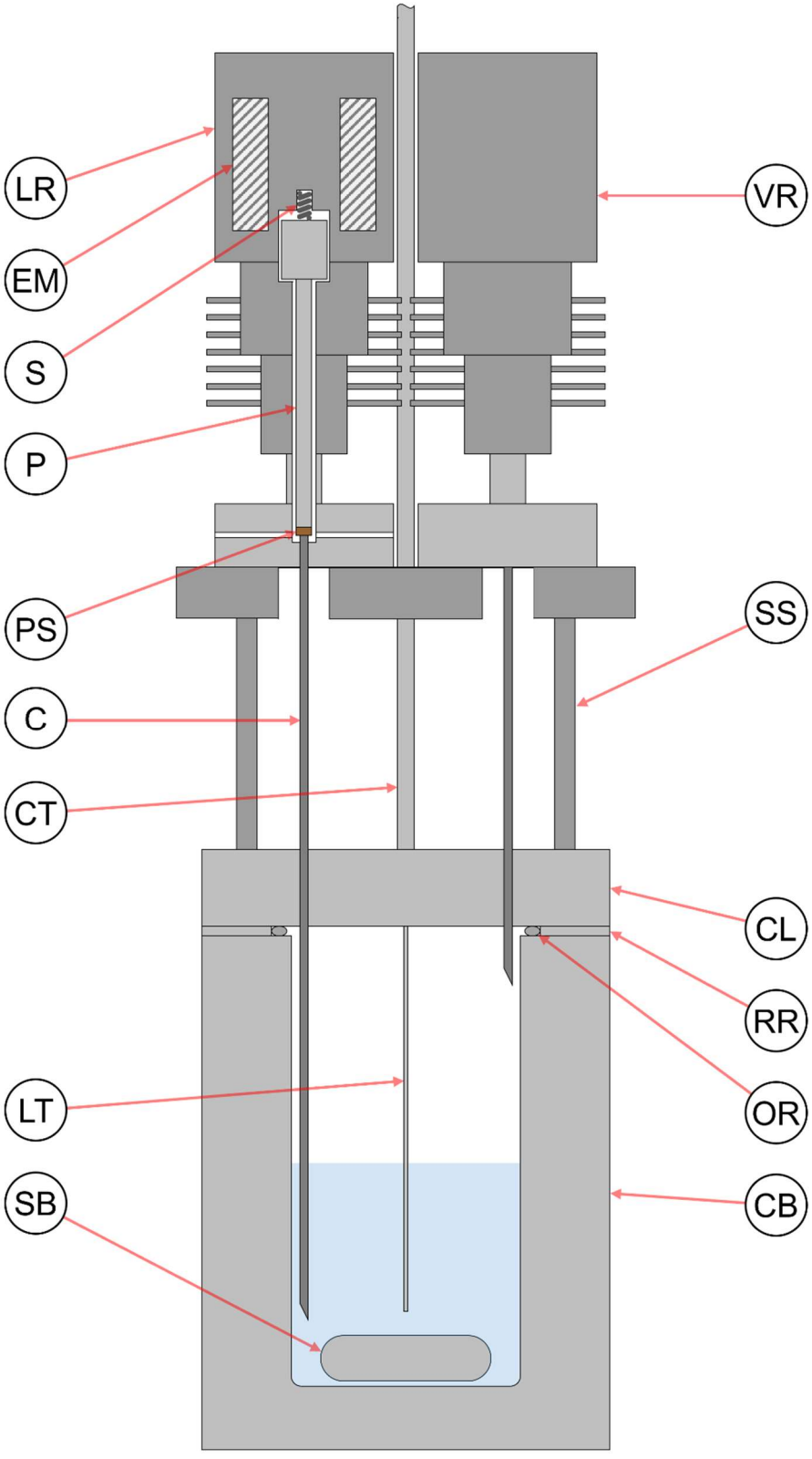


Figure 4.3: Simplified cutaway view of the cell and ROLSI valves. LR: liquid ROLSI, VR: vapour ROLSI, EM: electromagnet, S: spring, P: piston, PS: piston seal, C: capillary, CT: coaxial tube, LT: liquid tube, SB: stirrer bar, SS: supporting structure, CL: cell lid, RR: retaining ring, OR: O-ring, CB: cell body. The pressure fittings, bath structure and working fluid, ROLSI insulation, and heated lines are not shown and the scale of the ROLSI internals has been exaggerated for visibility

The Isco pump, secondary vacuum pump, and liquid in/out section were placed into the fume cupboard, requiring that the flare system and some control equipment be removed, the former being decommissioned entirely in favour of venting to atmosphere (via the fume cupboard airflow).

The heated line, connecting the ROLSI valves to the GC, present at the beginning of the work, had to be replaced. An attempt was made to run the heated line at its maximum service temperature (473 K, which was set by material stability rather than power and thermal performance) during initial attempts to make measurements of the methanol + CO_2 system, however it was unable to achieve this temperature at its maximum power level. Further insulation was added to reduce heat loses, but a section of the line overheated before reaching the setpoint, resulting in a short circuit. It was identified that the cause was poor thermal contact between the heating element (PTFE insulated nichrome wire) and the 1/16″ tubing, and imbalanced power density between the area where the controlling thermocouple was located and an adjoining section, exacerbated by poor heat conductance along the line.

A new design, consisting of three individually controllable heated sections, was selected and produced in house. Now, the tubing that delivered carrier gas to the ROLSI valves would be unheated until the split section immediately upstream of the parallel valves, so that the carrier gas enters the ROLSI valves preheated, while heating further upstream would have no meaningful impact. Heating was provided by a cartridge heater inserted into an aluminium block, whose shape is reminiscent of a flanged cylindrical bobbin, around which the tubing to be heated was wound and retained by a cylindrical aluminium cover wrapped in silicone sponge insulation. The tubing that returned the carrier gas and samples to the GC was heated in two separate sections, the split section immediately downstream of the valves and the longer common section, such that heating could be applied to almost the entire sample return path even in the case that one sampling valve is connected (as was the case in the initial methanol + CO_2 calibrations using gravimetrically prepared mixtures sampled from the VVC). The 1/16″ tubing in the split section was inserted into a 6 mm copper tube alongside two 1/8″ copper tubes, producing a snug fit. Around the outer copper tube was tightly wound thin PTFE insulated nichrome wire (acting as the heating element), sleeved in FEP heat shrink to ensure thermal contact. A K-type thermocouple inserted into the copper tubing was used for temperature measurement and control. The low dead volume tee union connecting both arms of the split section together, and with which it could be connected to the common section, had several windings of wire around it, but was otherwise only in thermal contact with the rest of the assembly via the 1/16″ tubing and thin wire. While this is presumed to be a slight cold spot in the line (and would be difficult to address without introducing the risk of overheating a section), it represents only a couple of centimetres of the ~1.5 m length of the return path and is insulated together with the rest of split section. A similar design was used for the common section of the sample return path, again using 6 mm copper tubing to house the 1/16″ tubing, along with one 1/8″ copper tube and a pair of long rod resistance heaters (powered in series) to provide heating, which took up the remaining loose space within the outer tube. Again, a K-type thermocouple inserted into the tubing was used for temperature control, and the entire length of the assembly insulated. This line passed into the GC and terminated within the heated valve box, such that the only section of sample facing surfaces between the ROLSI valves and the detector within the GC that weren't directly thermally controlled were the

lengths of tubing covered by the pressure fitting bolts and the minimum length of tubing required to make and unmake the connection.

A system to vent the vapour phase in a remote/automatic manner was added during the measurements of isobutane + H_2. This consisted of a pneumatically-operated inverted-bellows valve (Swagelok Nupro HB Series), actuated using a solenoid valve connected to the nitrogen supply line, downstream of a 2 m long x 0.13 mm ID capillary to help regulate the flow to a controllable rate and a filter to prevent blockages. This was initially connected to the cell via the fluid handling system's vent line, see V-16 in Figure 4.4.

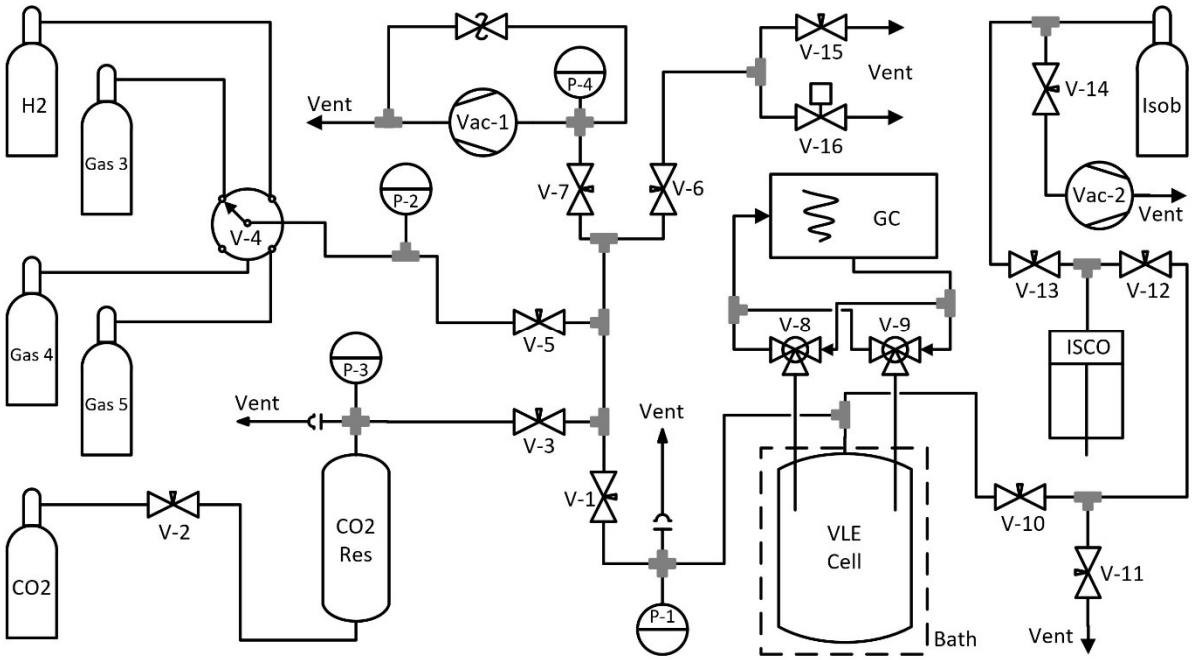


Figure 4.4: Simplified P&ID diagram of the VLE apparatus used in this work as it was during measurements of isobutane with CO_2 and with H_2, adapted from [305], as shown in [138]

When servicing the apparatus following the measurements of isobutane systems it was discovered that wear between the stirrer and the bottom of the bottom of the cell had produced a thin dusting of grey debris composed of PTFE and steel, suspected to be the cause of several ROLSI capillary blockages. This problem would likely be exacerbated for mixtures of methanol with CO_2, which can cause significant swelling and decompression damage to polymers such as PTFE, so alternative materials were considered. Initially a glass encapsulated magnetic stirrer bar was tried, sleeved in a thin layer of FEP heat shrink to reduce friction and wear, however the glass cracked after several uses and resulting debris eventually blocked both ROLSI capillaries. This was then substituted by a stainless-steel encapsulated magnetic stirrer, again sleeved in FEP. Alternative stirrer geometries were also considered during this time to aid in equilibration, such as the design of Bruno & Rybowiak [540], however issues with rotational stability in testing and concerns that prolonged entrainment could affect vapour samples prevented further consideration.

Further changes were made for the measurements of methanol + CO_2, with the final P&ID shown in Figure 4.5. Thick sponge insulation was added around the fluid jacket and head

(excluding the pressure sensor) of the Isco pump. The K-type thermocouple on the jacket was replaced with a stick-on 4-wire PRT. The thermocouple was moved to hang in the air in the fume cupboard near to the tubing downstream of the pump, providing a rough value of the ambient temperature to supplement the existing ambient temperature measurement made by the PRT inside the cell's pressure sensor, which was near to the exhaust of the fans in the thermostatic bath (Huber CC1) and could be several degrees hotter than other regions of the apparatus.

The PTFE tubing at the inlet of the Isco pump was replaced with stainless steel tubing to allow for filling at high pressures, and connected via a cross union and valves to a PTFE liquid inlet tube, the secondary vacuum pump, and the gas portion of the fluid handling system via the connection that had previously led to the venting system. The venting system was instead connected to the end of the coaxial inlet above the cell.

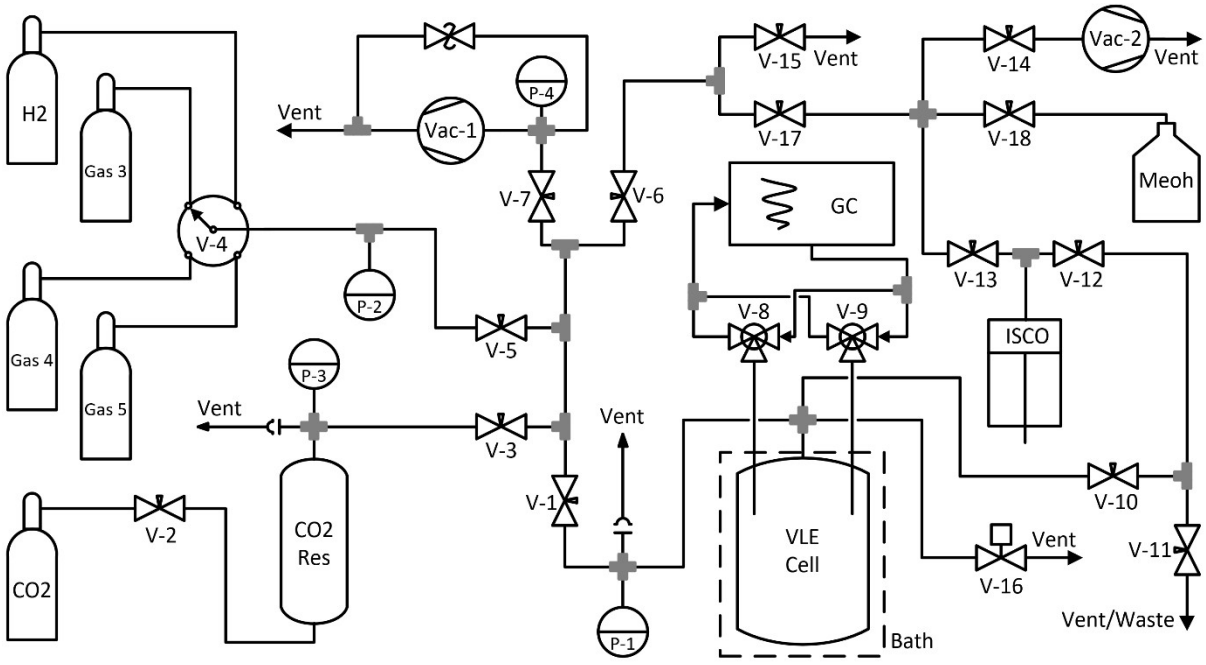


Figure 4.5: Simplified P&ID diagram of the VLE apparatus used in this work as it was during measurements of methanol with CO_2, adapted from [138, 305]

4.1.3 General Operating Procedure

The general operating procedure of the apparatus in the form it was in at the end of experimental work (see Figure 4.5), following the investigations of methanol + CO_2, is provided. This procedure assumes a binary mixture, though modification for higher order mixtures is straightforward so long as all components are fluids at or near standard conditions.

First, the entirety of the system to be used in a given experiment would be evacuated and then flushed with one of the fluids under investigation (typically CO_2). This would be repeated several times to ensure a clean system before returning to a rough vacuum (measured as 0.3 kPa at the vacuum pump inlet).

Two options exist for the procedure following this and these shall be described first for when investigating systems and/or state points where the mixture behaviour (specifically the equilibrium compositions and densities) is known approximately, whether through literature data or modelling.

The less volatile component would be drawn into the Isco pump. For liquids, the liquid would be degassed under vacuum before being allowed to enter the pump aided by a pressure gradient provided by dry nitrogen, while for condensable liquids, the liquid would be condensed in the pump under reduced temperature, and gases would simply be allowed to flow in from the supply cylinder. The fluid in the pump would then be compressed and allowed to flow into the volume between V-10 to V-12 and to equilibrate to determine the initial amount of substance. V-10 would then be opened to meter fluid into the cell, before being closed and the pump fluid recompressed to determine the swept volume and, by extension, the metered amount. Next, the more volatile component would be allowed to flow into the cell through V-1 to raise the pressure in the cell to the desired initial point.

In the alternative case, where the system cannot be sufficiently predicted *a priori*, the Isco pump would first be filled with the more volatile component and metered into the cell before filling the Isco pump with the less volatile component as before, such that the overall system composition would be set instead of the cell pressure.

In both cases, the maximum amount of the more volatile component would be present in the cell at the beginning of the measurement sequence, while the minimum amount of the less volatile component would be present in the cell, with the remainder that will eventually be needed held within the Isco pump. At this stage, the pressure inside the cell should be close to the vapour pressure of the more volatile component if at temperatures below its critical point, the mixture critical pressure if above its critical temperature, or the maximum working pressure (20 MPa) if the critical pressure exceeds the accessible pressure range. Similarly, the mole fraction of the more volatile component should be close to one or to the mixture critical composition. If pressures greater than the cylinder pressure are required, pressure could be raised further using the using the pump (though this only works in certain cases) or by filling the cell first at lower temperature and carefully allowing it to heat isochorically.

The mixture inside the cell would be allowed to equilibrate under stirring until the temperature and pressure were steady to within their respective repeatabilities. The internal volume of the cell should then contain two fluid phases (typically a vapour and a liquid) in equilibrium, though the procedure may also be applied to other multi-phase equilibria with appropriate considerations, including those with three or more phases that may include solids. Stirring would then be stopped to avoid issues like a vortex covering/uncovering the end of a capillary or liquid droplets entrained in the vapour.

Samples would be taken of the equilibrium phases, typically the liquid first to allow the vapour more time to settle. Typically, three to five samples may be withdrawn in a short period first to flush the capillary with fresh sample, followed by 10 to 25 measurement samples, depending on the conditions and time to obtain steady sample composition. In some cases it was

preferable only to perform the rapid capillary flushing for the liquid capillary, as the process can disrupt the equilibrium in ways that are difficult to anticipate and has been observed both in this work and in literature [201, 202].

Once sampling was completed, stirring would be resumed and one could vent a portion of the vapour phase and/or inject more fluid from the Isco pump to adjust the pressure and overall composition to the next measurement point. This procedure could be performed manually or, preferably, automatically, until the entire range of conditions for that particular sequence of measurements was completed. The cell would then be depressurised and emptied. In the case that the components are all gas-like at ambient pressure this may be done simply by opening to atmosphere, otherwise the remaining fluid may be removed by flushing with CO_2 or by evacuation, with a small flow of gas also allowed to flow into the vacuum pump (either from the atmosphere or from a cylinder) to act as a purge to prevent condensation in the vacuum pump.

4.2 Detector Calibration

4.2.1 Theory of the Composition Measurement Method

The composition of phase(s) inside the cell is determined analytically; by withdrawing samples, separating their constituents, and then quantifying the amounts sampled.

The sample is withdrawn/injected into the flow path of a heated carrier gas stream, such that the sample flashes (vaporising in the case where a liquid is sampled) and is swept along towards the GC, effectively creating a pulse with a high local concentration of the sampled components surrounded by pure carrier gas. The sample flows through the chromatographic column wherein the differing affinities of the components to the stationary phase result in their separation. The width of the pulse for a component widens due to diffusion and the interactions with the stationary phase, such that it leaves the column as a broader, skewed distribution that may have a significant tail.

The sample components, diluted in carrier gas, are then passed through a detector for quantification. In this case, a hot-wire thermal conductivity detector is used, consisting of a thin metal wire housed within a thermostatic chamber. A current is passed through the wire, maintaining it at a constant temperature that is higher than that of the surrounding chamber and gas. The temperature gradient results in a heat flux from the wire into the gas, requiring a continuous power that is a function of the thermal conductivity of the gas. Since their introduction as the katharometer [432], two wires have typically been used, forming two arms of a Wheatstone bridge, with the main carrier gas stream passed over one wire while additional pure carrier gas is passed over the other wire as reference. In the case of the TCD used in this work, a single wire is used, with the main and reference streams alternatively passed over the wire, switching at a rate of 5 Hz. In either case, the measurement principle remains the same: when the composition of the gas flowing over the wire changes so does its thermal conductivity, changing the power required to maintain the wire temperature, resulting in a

measurable signal, in this case a change in voltage from a baseline value (in this case ranging from approximately 10 μV up to 0.75 V).

While there are somewhat rigorous descriptions for the signal produced in both steady state and transient hot-wire TCDs [541-543], their use as a chromatographic detector does not require such formality. Instead, empirical relations may be used, avoiding excessive use of corrections and benefiting from the high degree of linearity of the detector response with respect to the sampled amount. The general form of these relations is as follows: the signal *s* produced by a detector is a function of the concentration *c* of component *i* at the detector at time *t*

$$s = f(c_i) \tag{4.1}$$

It may equally be described as a function of related properties, such as partial pressure or density. The area *A* of the resulting peak is

$$A = \int s dt \tag{4.2}$$

and the number of moles *n* of component *i* are

$$n_i = \dot{Q} \int c_i dt \tag{4.3}$$

Here, $\dot{Q}$ is the volumetric flow rate through the detector. If a mixture was sampled, then the mole fraction x_i is

$$x_i = \frac{n_i}{\sum n_i} = \frac{\int c_i dt}{\sum \int c_i dt} \tag{4.4}$$

Usage of these equations requires that the functional form of equation 4.1 be known, or, at least, ascribed/assumed. The simplest case would be to assume the signal is a linear function of concentration, such that

$$s = a_i c_i \tag{4.5}$$

Where a_i is a component specific calibration constant. It is also specific to the GC and detector used. The peak area produced by a given component is now

$$A_i = a_i \int c_i dt \tag{4.6}$$

Which may be rearranged and substituted into equation 4.3 to yield the number of moles

$$n_i = \frac{\dot{Q}}{a_i} A_i \tag{4.7}$$

As $\dot{Q}$ is held constant, it may be combined with the component specific calibration constant so that

$$n_i = a_i^* A_i \tag{4.8}$$

and the sample composition is

$$x_i = \frac{a_i^* A_i}{\sum a_i^* A_i} \tag{4.9}$$

This can also be rewritten in terms of the relative response factor r_j of the detector to component *j* compared to component *i*

$$r_j = \frac{A_i x_j}{A_j x_i} \tag{4.10}$$

The linear description is very convenient due to its simplicity, however its applicability is limited as TCDs exhibit significant nonlinearity. A simple correction is to make the amount of substance a quadratic function of the peak area

$$n_i = a_i^* A_i + b_i^* A_i^2 \tag{4.11}$$

where b_i is an additional component specific calibration constant.

This approach has been applied successfully before [305, 306, 532, 544-547], and is used in much of this work, but is not without its own limitations. Most notably, it cannot capture the effects of varying peak shapes, such that an infinitely sharp peak and an infinitely broad peak of equal area would be treated the same way, which is not representative of the real non-linear detector response. When peaks retain a similar shape regardless of sample size this may still be a reasonable treatment, however the peak shapes are known to change quite significantly, initially broader before becoming increasingly sharp and tailed, then eventually broader as they approach the maximum measurable sample size, as shown in Figure 4.6, although sample size in that case was limited to below the point at which peaks broaden again. Additionally, the source of the sample and the way it is injected into the GC may also effect the shape, though it is possible for the shape effects to be captured by this simple approach should the calibration peaks be representative of the measurement peaks.

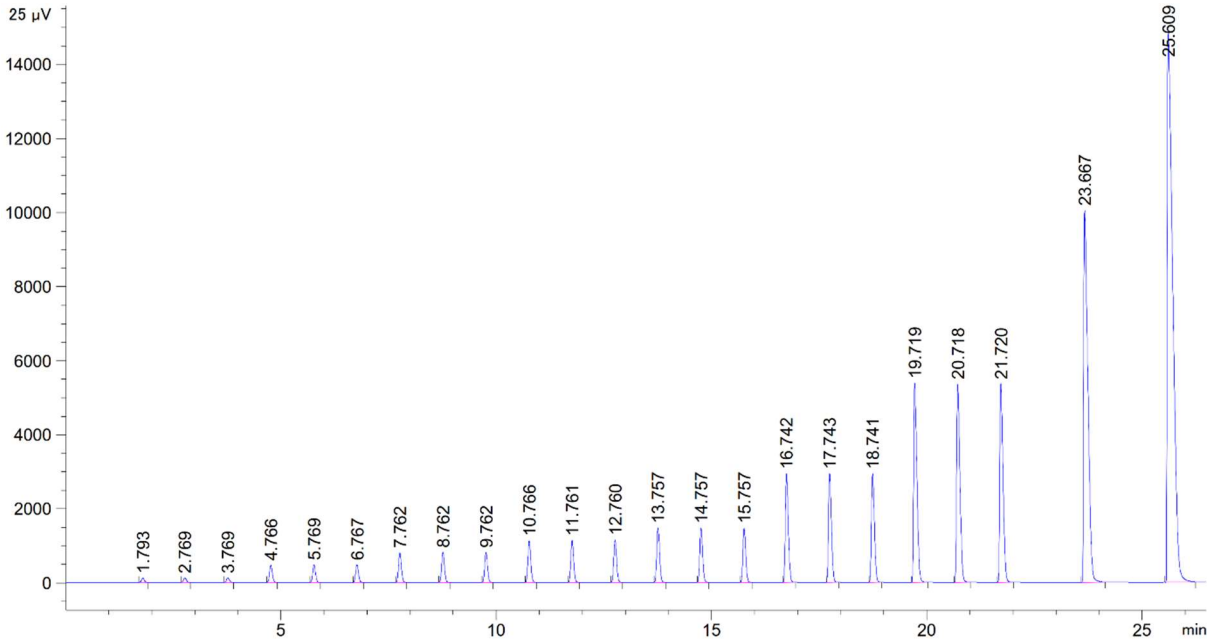


Figure 4.6: Chromatogram showing peaks produced by CO_2 samples withdrawn through a ROLSI valve with increasing valve opening time, with sample size ranging from approximately 35 nmol to 8.5 µmol

Alternatively, the signal can be expressed as a quadratic function of concentration

$$s = a_i c_i + b_i c_i^2 \tag{4.12}$$

where b_i is an additional component specific calibration constant. The peak area takes the form

$$A_i = a_i \int c_i \, dt + b_i \int c_i^2 \, dt \tag{4.13}$$

The number of moles now requires knowledge of how the composition varies as a function of time, which can be expressed in terms of the signal as

$$c_i = \frac{-a_i + \sqrt{a_i^2 + 4b_i s}}{2b_i} \tag{4.14}$$

To proceed further one must now either be reading the detailed real time signal or use a model to describe the peak based on some based on some form of shape parameters, such as the statistical moments of the peak. Neither normal distributions nor skewed normal distributions accurately capture the shape of chromatographic peaks, however, they may be approximated as an exponentially modified gaussian (EMG) distribution [548, 549], which models an ideal column followed by a mixing chamber, allowing the signal to be described as

$$s = \frac{h\sigma}{\tau}\sqrt{\frac{\pi}{2}}\exp\left(\frac{1}{2}\left(\frac{\sigma}{\tau}\right)^2 - \frac{t-\mu}{\tau}\right)\operatorname{erfc}\left(\frac{1}{\sqrt{2}}\left(\frac{\sigma}{\tau} - \frac{t-\mu}{\sigma}\right)\right) \tag{4.15}$$

where μ is the mean, σ the standard deviation, τ the exponent relaxation time, h is a scaling factor, and erfc is the complimentary error function

$$\operatorname{erfc}(x) = 1 - \operatorname{erf}(x) = \frac{2}{\sqrt{\pi}}\int_x^\infty \exp(-y^2)dy \tag{4.16}$$

In practice this equation is often rewritten in the form

$$s = \frac{h\sigma}{\tau}\sqrt{\frac{\pi}{2}}\exp\left(-\left(\frac{\mu-t}{\sigma}\right)^2\right)\operatorname{erfcx}\left(\frac{1}{\sqrt{2}}\left(\frac{\sigma}{\tau} + \frac{\mu-t}{\sigma}\right)\right) \tag{4.17}$$

where erfcx is the scaled complimentary error function

$$\operatorname{erfcx}(x) = \exp(x^2)\operatorname{erfc}(x) \tag{4.18}$$

The EMG distribution parameters may be estimated from the mean retention time m, variance s_p^2, and skewness γ of the peak

$$\mu = m - s_p\left(\frac{\gamma}{2}\right)^{\frac{1}{3}} \tag{4.19}$$

$$\sigma^2 = s_p^2\left(1 - \left(\frac{\gamma}{2}\right)^{\frac{2}{3}}\right) \tag{4.20}$$

$$\tau = s_p\left(\frac{\gamma}{2}\right)^{\frac{1}{3}} \tag{4.21}$$

The concentration can now be expressed in terms of the peak shape and the component specific calibration constants a_i and b_i

$$c_i = \frac{1}{2b_i}\left(-a_i + \sqrt{a_i^2 + \frac{2\sqrt{2\pi}b_i h\sigma}{\tau}\exp\left(-\left(\frac{\mu-t}{\sigma}\right)^2\right)\operatorname{erfcx}\left(\frac{1}{\sqrt{2}}\left(\frac{\sigma}{\tau} + \frac{\mu-t}{\sigma}\right)\right)}\right) \tag{4.22}$$

The concentration with respect to time may be integrated numerically to yield the number of moles

$$n_i = \frac{\dot{Q}}{2b_i}\int\left(-a_i + \sqrt{a_i^2 + \frac{2\sqrt{2\pi}b_i h\sigma}{\tau}\exp\left(-\left(\frac{\mu-t}{\sigma}\right)^2\right)\operatorname{erfcx}\left(\frac{1}{\sqrt{2}}\left(\frac{\sigma}{\tau} + \frac{\mu-t}{\sigma}\right)\right)}\right)dt \tag{4.23}$$

which may then be used to calculate the mole fraction, as previously. A simple method of performing the numeric integration of the above integral is the trapezoid rule

$$\int f(x)dx \approx \sum \frac{f(x_{k-1})+f(x_k)}{2}(x_k - x_{k-1}) \qquad (4.24)$$

Overall, this approach requires more computation, including an optimisation for each peak, than the simple quadratic function of area, however, it remains cheap and fast to compute in absolute terms for any computer.

The effect of peak shape can now be evaluated to provide some insight into the potential errors introduced when using simpler expressions. Figure 4.7 shows four modelled peaks, each with an area of 40000 units (the units in this case being 25μVs as is standard for the particular make of detector used, though this is immaterial for the purposes of this work, provided the units are consistent) but with varied values of the peak variance and skew. In practice, the peaks obtained in this work lie between these rather extreme examples.

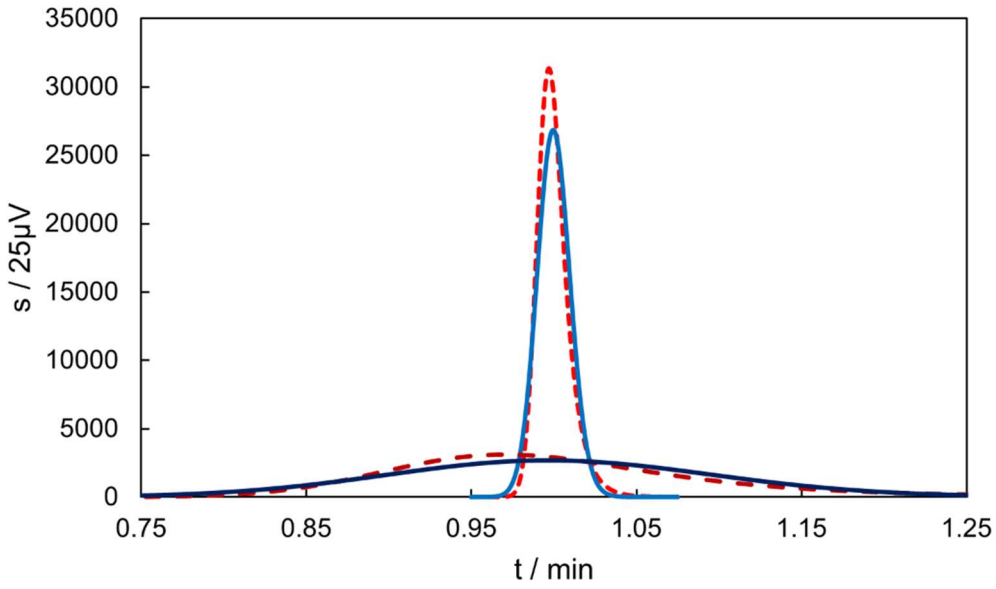


Figure 4.7: Calculated peaks using the EMG distribution with an area of 40000 units for varied values of variance and skewness, — s_p^2 = 0.0001 γ = 0.1, — s_p^2 = 0.01 γ = 0.1, - - s_p^2 = 0.0001 γ = 1, — — s_p^2 = 0.01 γ = 1

The impact of varied peak shape on the calculated amount is shown in Figure 4.8. It is apparent that the greatest differences occur when peaks are especially sharp. A peak with s_p^2 = 0.0001 and γ = 1 corresponds to an amount 19 % larger than for s_p^2 = 0.1, with skewness having little effect for broad peaks. The actual impact of these peak shape effects on real composition measurements is more complicated, and must be assessed on a case-by-case basis, however it provides an idea of the magnitude of the error that may be introduced in the worst case.

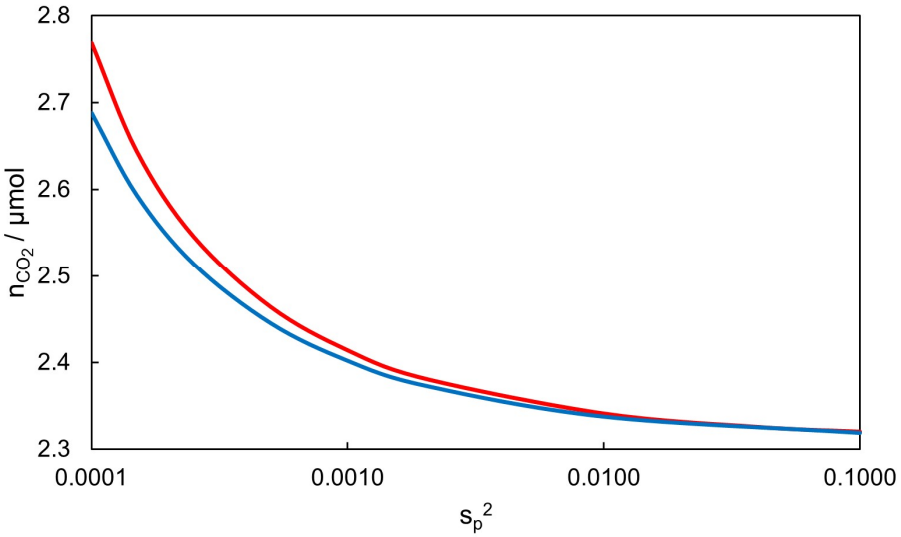


Figure 4.8: Sample amount calculated for varied values of variance and skewness for a peak of area 40000 units, using the optimised parameters for CO_2 (a_i = 2885, b_i = -50.36), — γ = 0.1, — γ = 1, note the x-axis is log scaled

Further considerations for deviations from ideal chromatographic peaks can be found in literature, such as for Taylor dispersion measurements of diffusion coefficients [550], where there are many similarities in the analysis, but the impacts on phase behaviour measurements specifically has historically been neglected.

Regardless of the exact calibration equations used, the parameters must be regressed from calibration measurements that contain sufficient information about the sampled amounts and/or compositions. Two different calibration methods were used: firstly, calibration using gas sample loops, as the apparatus was originally designed for, and then calibration against synthetic mixtures, required for calibration with methanol.

4.2.2 Calibration with Gas Loop Sampling

The GC is equipped with two gas sample loops, connected to a multiport switching valve (V1 in figure 4.2) such that they may be filled with vapour samples of known composition (typically pure fluids). The contents of either loop may be injected into the main flow path of the GC downstream of the ROLSI valves through the actuation of the switching valve. These loops were different sizes, nominal volumes 0.05 cm^3 and 0.25 cm^3, so that the calibration can cover a broader range of sample sizes.

The temperature and pressure of each of these loops are measured, the former in two places using K-type thermocouples whose values are averaged and the latter with an in-line pressure sensor (Keller PAA-21Y, 0.6 MPa full scale). The temperature and pressure are then used to calculate the density of the sample inside the loop, which may be done with low uncertainty for pure fluids using multiparameter equations of state. These models were used as implemented in REFPROP 10.0 [292, 293], and are listed in Table 4.1 along with their stated

relative expanded uncertainties (k = 2) for the relevant *pT* region. The density can be used as a proxy for the amount of substance, such that

$$\rho_i = \frac{a_i}{V_j} A_i + \frac{b_i}{V_j} A_i^2 \tag{4.25}$$

where ρ_i and V_j are the gas density in and volume of loop *j*, respectively. The volumes are constant, thus may be combined with the parameters a_i and b_i to give new effective parameters, and cancel out in the calculation of mole fraction for a mixture, so their value is unimportant. The parameters themselves were regressed by the minimisation of the sum squared error *S* between the filling density ρ_{loop} and density calculated from the calibration equation ρ_{calc}

$$S = \sum (\rho_{loop} - \rho_{calc})^2 \tag{4.26}$$

The loops could be filled at pressures in the range of (0.1 to 0.3) MPa, providing sufficient information to fit the calibration constants, albeit over a limited range of sample sizes. Considering also that the loops were different sizes, the calibration can cover sample sizes over a little more than one order of magnitude, corresponding to approximately (2 to 30) µmol. It was not possible to calibrate for smaller samples with this method without instead relying on mixtures where the component has been diluted, though doing so should not introduce additional uncertainties provided the calibration equation used is valid over the measurement range.

Table 4.1: Equations of state used to calculate gas loop densities for calibration, their relative uncertainties, and references

Chemical Name	EoS	$U_r(\rho)$ / %	Ref
Isobutane	Bücker & Wagner	0.1	[284]
Carbon Dioxide	Span & Wagner	0.03	[207]
Hydrogen	Leachman *et al.*	0.04	[282]

Fandino, Trusler, & Vega-Maza [305] validated the apparatus, as it was originally constructed, by sampling purchased gas mixtures of known composition for both of the mixtures investigated in that work, using both the gas sampling loops and the ROLSI valves. Two were an equimolar mixture of CO_2 with N_2 (obtained from different suppliers), while the third was CO_2 with H_2 (x_{CO2} = 0.1). The compositions measured were within the uncertainties specified by the supplier for both mixtures for both sampling methods. Later, Souza [533] used two high purity gas mixtures, one a binary mixture of CO_2 with CO (x_{CO2} = 0.5) and the other CO_2 with CH_4 (x_{CO2} = 0.95), to revalidate the calibration approach. The measured compositions were again within the uncertainties of the mixture compositions specified by the suppliers, though it was not specified if the mixtures were sampled using the gas sample loops, from the cell via the ROLSI valves, or both. It was not convenient to use this approach for the mixtures investigated in this work due to the low vapour pressures of isobutane and methanol at ambient temperatures.

Further validation has been provided by measuring the phase behaviour of mixtures whose behaviour is well studied in literature. Previously, Fandino, Trusler, & Vega-Maza performed measurements of CO_2 + N_2 [305], and in this work isobutane + CO_2 was used for validation,

as published in [138]. This form of validation is important as it is necessary to demonstrate that the calibration approach remains applicable during phase behaviour measurements wherein the samples may be vapours or liquids and the cell temperature and pressure vary greatly.

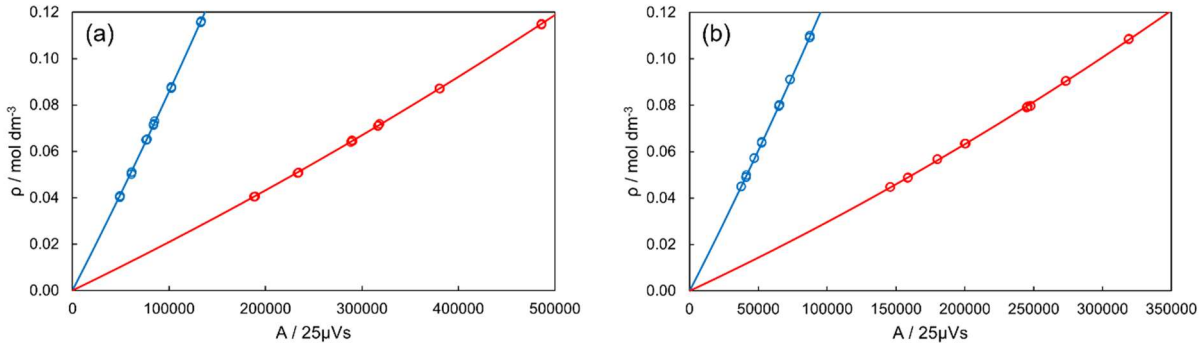


Figure 4.9: Gas loop filling density against peak area for (a) isobutane and (b) CO_2 when using helium as the carrier gas, showing experimental points ○ and the calculated calibration curves, — loop 1, — loop 2

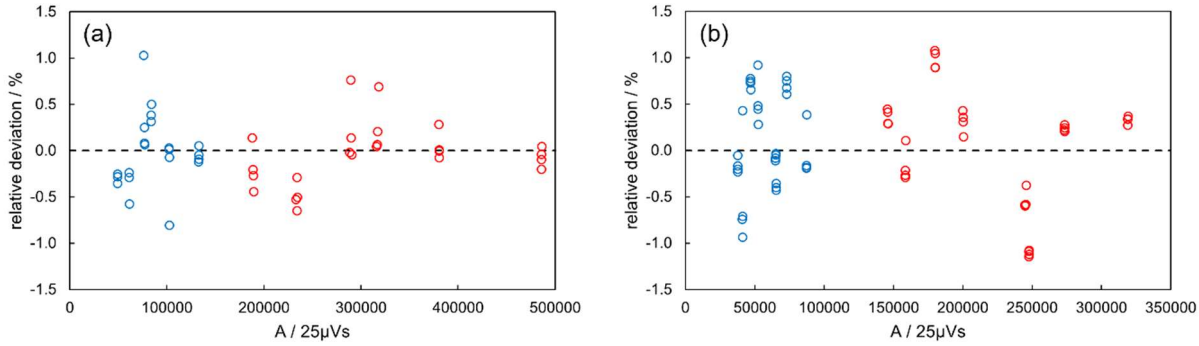


Figure 4.10: Relative deviations of the measured loop filling densities from the calibration equation for (a) isobutane and (b) CO_2 when using helium as the carrier gas

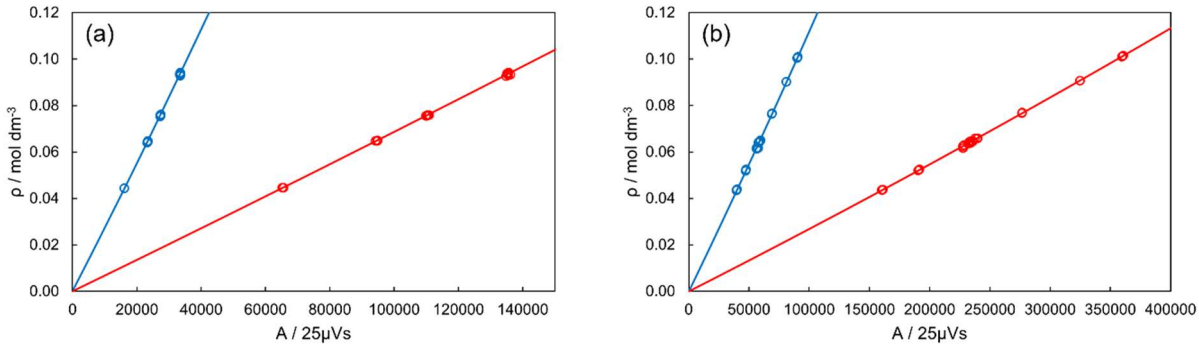


Figure 4.11: Gas loop filling density against peak area for (a) isobutane and (b) H_2 when using argon as the carrier gas, showing experimental points ○ and the calculated calibration curves, — loop 1, — loop 2

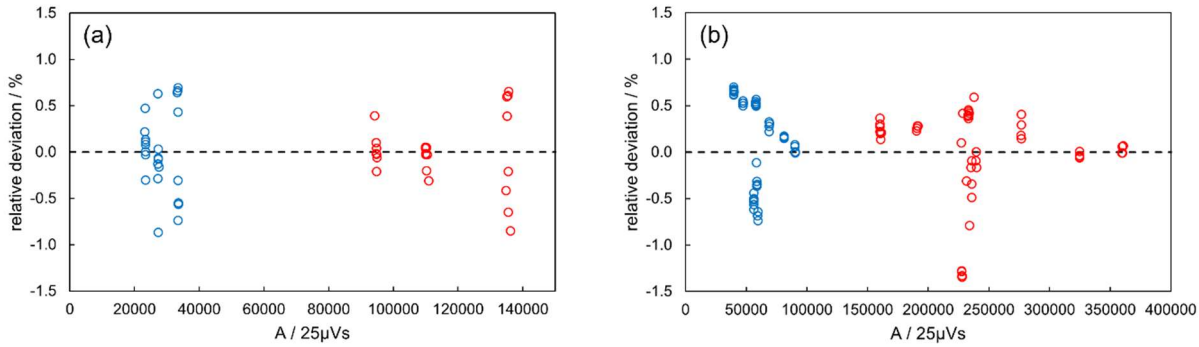


Figure 4.12: Relative deviations of the measured loop filling densities from the calibration equation for (a) isobutane and (b) H_2 when using argon as the carrier gas

It was found that there was a positive deviation from linearity for all analyte/carrier gas combinations, though the non-linearity was greater when using helium as the carrier gas, as can be seen in figures 4.9 and 4.11. The relative deviations of the calibration equations from the experimental data are shown in figures 4.10 and 4.12. In all cases, deviations did not exceed 1.5 % and rarely exceeded 1 %. There do not appear to be any systematic deviations except for hydrogen with argon, wherein a negative, rather linear, deviation is present for loop 1 for most of the points. It is interesting to note that the points for that loop which do not follow that trend, as well as the points with negative relative deviations for loop 2, all belong to an earlier batch of calibration measurements, possibly as a result of drift in one or more of the sensors involved in the calibrations. The optimised calibration parameters are shown in Table 4.2.

The calibration method was identified early on in the apparatus's life as a significant source of uncertainty that could likely be reduced [305].

Table 4.2: Optimised calibration constants for the components investigated in this work with their respective carrier gases

Analyte/Carrier	Loop 1		Loop 2	
	$a_{1,i}$ / mol dm^{-3}	$a_{2,i}$ / mol dm^{-3}	$a_{1,i}$ / mol dm^{-3}	$a_{2,i}$ / mol dm^{-3}
Isobutane/He	8.09 x 10^{-7}	4.68 x 10^{-13}	2.01 x 10^{-7}	7.23 x 10^{-14}
Isobutane/Ar	2.69 x 10^{-6}	3.07 x 10^{-12}	6.72 x 10^{-7}	1.37 x 10^{-14}
CO_2/He	1.16 x 10^{-6}	1.12 x 10^{-12}	2.77 x 10^{-7}	1.93 x 10^{-13}
H_2/Ar	1.07 x 10^{-6}	4.64 x 10^{-13}	2.64 x 10^{-7}	4.88 x 10^{-14}

A portion of the uncertainty comes from determining the amount of a component contained within the loop, and this could be reduced by improving the accuracy of the measurement of the pressure and temperature through lower uncertainty sensors (for example, the use of PRTs instead of K-type thermocouples). However, the temperature regulation of the gas sample loops would remain a significant issue. Currently, heating is applied electrically to a plate at the base of the insulated GC valve box, conducting through to the sample loops via the ten port valve. The valve box is not perfectly insulated and there are gas flows both through the ten port valve and the other valves in the valve box connected to the plate, which change periodically throughout calibrations and measurements, producing temperature gradients. It is

for this reason that the temperatures of each loop are measured in two locations, near to the middle and one end of the loop, and averaged to estimate the average temperature of the gas inside, albeit imperfectly.

Regardless of the uncertainties in the amount contained within the sample loops, two major limitations remain for the gas loop calibration method. Firstly, the samples are not introduced the same way in calibrations as they are in measurements, and secondly, compounds that are liquid at ambient temperature and pressure (or more practically, 0.2 MPa) cannot be introduced to the sample loops. The former allowed for sampling artefacts to be introduced, such as peak shape effects, reducing accuracy, while the latter presented a more drastic roadblock for the measurement of methanol systems.

4.2.3 Calibration Against Synthetic Mixtures

The alternative approach used in this work was to prepare a synthetic compressed liquid mixture, of known composition and take samples of varying size. The calibration parameters for both (or all in the case of a higher order mixture) components may be regressed simultaneously by minimising the sum squared error in composition in effectively the same manner as before. While it is not possible to directly determine the amount of substance sampled in absolute terms, this remains immaterial to the final value of the composition. In practice, the amount may be determined whenever at least one component is suitable for calibration with gas sample loops, albeit with a higher uncertainty than the composition uncertainty.

Two approaches were taken to the preparation and sampling of synthetic methanol + CO_2 mixtures. The first approach, which would go on to be abandoned due its limitations, was to prepare the mixtures gravimetrically.

The cell was too heavy to be used with the high accuracy balance available, limited to 5 kg, so an existing variable volume cell [551] was modified and equipped with a similar ROLSI valve to the ones on the cell. This VVC would be evacuated, weighed, filled with some amount of methanol via a syringe, reweighed, filled with some amount of CO_2 via a HPLC pump, then weighed a final time. The pressure would then be raised above the bubble point by compressing the variable volume with nitrogen. The VVC would be placed onto a magnetic stirrer plate, driving a PTFE encapsulated stirrer bar inside, and allowed to equilibrate.

The composition of a binary mixture inside the VVC could be calculated simply using the following equation

$$x_1 = \frac{(m_1 - m_0)M_2}{(m_1 - m_0)M_2 + (m_2 - m_1)M_1} \tag{4.27}$$

Where m_0 is the mass when evacuated, m_1 the mass after adding component 1, m_2 the mass after adding component 2, and M_1 and M_2 are the molar masses of the components. Corrections would be required to account for the dead volume at the inlet to the VVC and for the effects of buoyancy when weighing [552], based upon the ambient temperature, pressure,

and humidity while weighing. The magnetic stirrer bar inside the cell could interfere with the weighing, though the impact on the measured mass was of the order of a milligram.

CO_2 is well known to swell polymers [553] and methanol can also have compatibility issues with a range of polymers. The combination of them was found to cause problems for the polymeric materials in the VVC. The two O-rings used to form the dynamic seal around the piston needed to be replaced after each use, explosively decompressing upon the piston's removal after depressurising and emptying the VVC (typically one or both O-rings would unseat and come away from the piston rapidly) with visible signs of swelling and associated damage (for both materials used, FKM and NBR). This raised some concerns about the possibility of composition changes if methanol or CO_2 entered the O-rings or the void between them preferentially. Changes to the design and materials of the piston seals could reduce these effects, but was not pursued further. The PTFE encapsulating the stirrer bar was observed to swell, the first one used ruptured after several uses.

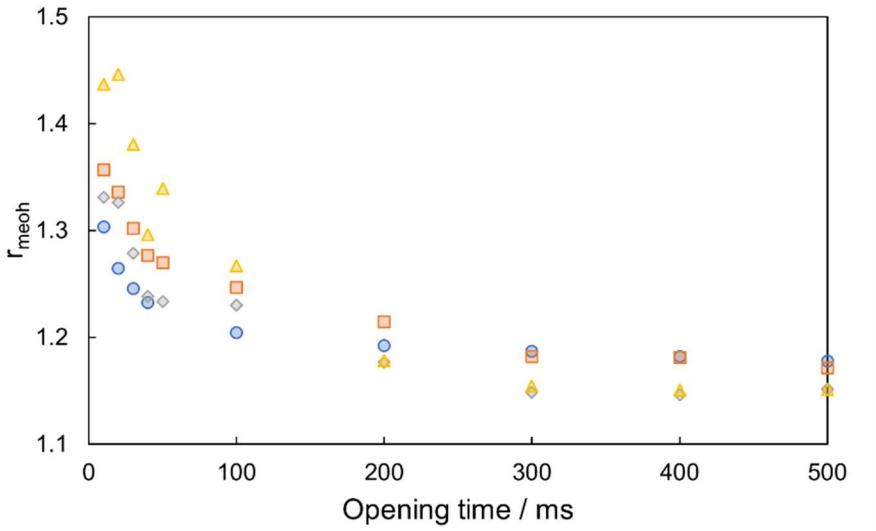


Figure 4.13: Relative response factor of methanol compared to CO_2 as a function of ROLSI valve opening time for four mixtures prepared in the VVC, x_{CO2} = ● 0.268, ■ 0.400, ♦ 0.499, ▲ 0.600

An unexpected trend was observed in the response measured at the detector as a function of the opening time (and by extension, though not exactly proportionally, the sample size). It appeared as though the detector was far less sensitive to small quantities of methanol than larger ones, as can be seen from the rise in the detector's relative response factor to CO_2 compared to methanol shown in Figure 4.13. This effect was not consistent with the behaviour upon sampling any previously investigated mixtures (wherein, it should be noted, CO_2 was generally one of the components, but no such unusual trends were observed). It would be possible for a highly non-linear relationship between the thermal conductivity of analyte + carrier gas mixtures, such as that seen with hydrogen + helium, to cause such an effect, however this should not be the case for methanol + helium. Instead, it appeared that the sample was being altered between sampling and detection, such that an apparent highly non-

linear detector response was observed even though the actual detector response remained only mildly non-linear.

It has been demonstrated in the literature previously [554-556] that oxygenated volatile organic chemicals like methanol can adsorb readily to the surfaces of sample pathways in gas chromatography. On stainless steel, strong adsorption was observed at low temperatures while at elevated temperatures, where compounds may quickly desorb, the methanol appeared to be destroyed and could not be detected [556]. A much weaker, but still detectable, adsorption was observed onto passivated surfaces featuring the same sulfinert treated components used in the majority of the sample pathway in this work. The suspicion, therefore, was that the quantity of methanol withdrawn upon sampling was sufficiently small to be meaningfully affected by the adsorption.

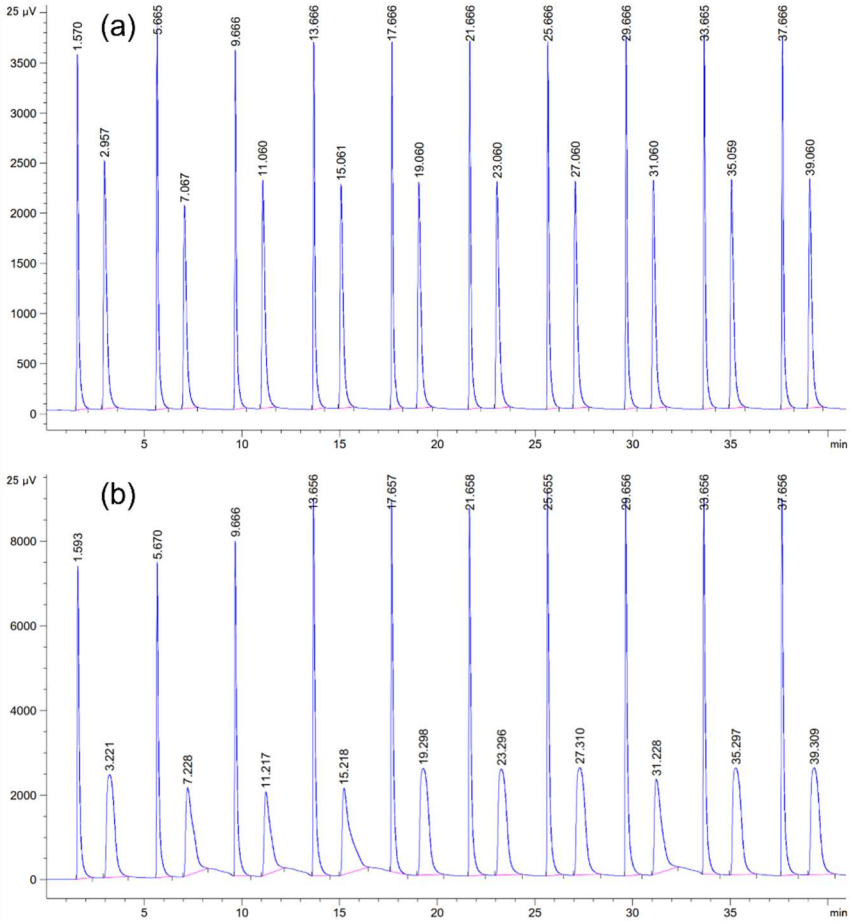


Figure 4.14: Example chromatograms from VVC methanol + CO_2 calibrations (a) with and (b) without heating the sample return path, showing peaks produced by repeated sampling. Note that CO_2 has the lower retention time (ie it is the first in each pair of peaks) and that the sample sizes were not the same for (a) and (b) so the absolute magnitude of the signal should not be compared here

Samples withdrawn without heating of the sample pathway did indeed show effects consistent with adsorption, CO_2 peaks remained sharp while methanol peaks were broad and inconsistent, unsuitable for accurate measurements, as can be seen in Figure 4.14. The methanol peaks were much sharper, consistent with other the peaks produced by other

compounds, when the entire sample pathway was heated. However, the presence of unpassivated stainless steel surfaces on the interior of the ROLSI valves, as well as on pressure fittings, parts of the GC switching valves, the throttle (which had originally been sulfinert coated, but was replaced with a standard stainless steel version prior to this work), and the detector assembly, meant that a portion of methanol would be lost before reaching the detector.

When repeatedly withdrawing methanol-containing samples, less methanol would be detected in the earliest samples before reaching a steady value, implying that the system first needs to reach a quasi-steady state in which the amount of methanol adsorbed from each subsequent sample is equal to the amount released from the adsorption sites from the preceding samples. If methanol were to be destructively adsorbing then the reaction must produce degradation products, and, as adsorption continues even after many samplings, the reaction must occur such that the products then leave the adsorption site or act as an equivalent site. No degradation products were observed reaching the detector, nor mentioned in similar literature, so it is likely that they were either immobile or somehow undetectable, though few compounds would allow for the latter. If hydrogen was produced then it could conceivably produce a signal small enough to be lost in noise as a result of the minimal change in thermal conductivity of helium upon the addition of small quantities of hydrogen, similarly if any product had approximately the same retention time as CO_2 or methanol it would have an unresolvable peak, though few candidate compounds fit this criterion. Alternative products such as CO or heavier compounds would produce properly resolvable peaks and would have been observed.

Accurate measurements of methanol containing mixtures would require a means of accounting for the adsorbed methanol. Adding a constant offset c_i in the calibration equation, such as

$$n_i = a_i A_i + b_i A_i^2 + c_i \tag{4.28}$$

could approximate the adsorption for larger methanol samples, where the amount adsorbed is roughly constant, however it would not be applicable for small samples where the amount of methanol was within an order of magnitude of the amount that could be adsorbed, where a more physically based description of the adsorption process would be required.

As a form of chemisorption was suspected, it was likely that the adsorbed methanol would only form a monolayer, whereas multilayer adsorption would likely occur in the case of physisorption alone. This is convenient, as monolayer adsorption is simpler to model. Langmuir adsorption theory [557] was applied:

$$\theta_i = \frac{K_i p_i}{1 + K_i p_i} \tag{4.29}$$

where θ_i is the fraction of adsorption sites occupied by component i, K_i is the adsorption equilibrium constant for that component, and p_i is its partial pressure in the gas phase. The partial pressure of methanol was not measurable directly in this apparatus. Instead, the peak area is used as a proxy for the partial pressure

$$\theta_i = \frac{K_i A_i}{1 + K_i A_i} \tag{4.30}$$

Such that the overall calibration equation is

$$n_i = a_i A_i + b_i A_i^2 + c_i \left(\frac{K_i A_i}{1 + K_i A_i} \right) \tag{4.31}$$

The Langmuir adsorption equilibrium constant here is no longer the same as in the classical version, though its role remains the same. Furthermore, the ability to perform direct comparisons to formal adsorption measurements would be of limited usefulness as the sample is passed over a range of surfaces with differing compositions, surface roughness, and temperature, such that the constant determined is an effective equilibrium constant representing the entire system, though primarily representing the adsorption onto stainless steel.

There are five significant assumptions made in this model. Firstly, it is assumed that adsorbing molecules only form a monolayer, a reasonable approximation in this case but nevertheless not strictly accurate, especially given the diversity of sample facing surfaces. The second, related, assumption is that all the adsorption sites that participate are equivalent, effectively representing an average of the real sites. Third, no changes occur to the adsorption sites as a result of adsorption or potential reactions that occur to any adsorbed molecules, which is hard to prove but is consistent with the experimental observations. Fourth, the adsorption behaviour is treated as if it is in equilibrium or quasi-equilibrium and any time dependencies can be neglected, such as the effect of the finite and varied ROLSI valve opening time. Finally, the adsorption behaviour is dependent only on the presence of methanol and uninfluenced by the presence of carrier gas or other components. The second and fifth of these assumptions shall be examined more below.

It should be noted that the adsorption phenomenon believed to be occurring is not limited only to the methanol withdrawn in sampling, and should also occur within the cell itself at high temperatures, where the reaction products may interfere with the equilibrium or go on to cause further reactions with other components present in the cell. This did not cause any issue within this work, as temperatures for the methanol + CO_2 system were limited to 298.15 K, however it is expected to play a role at higher temperatures and had not previously been recognised in the literature as an increased source of experimental uncertainty for methanol-containing systems in analytical and synthetic measurements alike. The extent to which this may influence measurements has not been assessed within this work, though can be expected to have the greatest effect in near-critical regimes at high temperatures.

The occurrence of adsorption exacerbated the issue of introducing calibration and measurement samples via different means. The ROLSI valve on the VVC would certainly be more representative of samples withdrawn through the ROLSIs on the cell than the gas sample loops would be, however, differences between the individual ROLSIs and the way carrier gas was flowed through them remained. The flowrate through either ROLSI on the cell, in their parallel configuration, would be approximately half of that experienced by the ROLSI on the VVC, resulting in different residence times within the steel surfaced interior of the valves and different concentration distributions. As such, it is expected that both the c and K_{eq} would differ between the three different ROLSI valves across the VVC and cell.

In view of this, the decision was made to calibrate the detector against synthetic mixtures prepared volumetrically in the cell and sampled with the ROLSIs in the same manner that they would be used during measurements. The Isco pump used to meter in a precise quantity of both components, with the amount injected determined from the swept volume at constant temperature and pressure along with dead volume corrections. The procedure was similar to those used in synthetic bubble point measurements, differing only in that the filling process does not end at the bubble point but instead proceeds further into the one phase region (typically exceeding the bubble pressure by 5 MPa), such that there is no risk of the system re-entering the two phase region. If desired, the approach also allows for bubble point measurements to be performed during the filling and compressed liquid density measurements to be made beyond that point.

A slight modification was made to the apparatus whenever a calibration was conducted, two of the ports on the cross union above the cell were plugged to reduce the dead volume. These would normally lead to the venting valve (V-16 in figure 4.5) and to V-1 along with the cell's pressure sensor and bursting disc. Pressure measurements now depended on the Isco pump's pressure sensor, meaning that the cell pressure could only be monitored up until the point that the mixture preparation is completed. In this configuration, all fluid facing surfaces were stainless steel, silver (in the case of the cell's O-ring), or glass (for the first two mixtures where the glass encapsulated stirrer bar was used) except for the thin FEP sleeving around the stirrer bar and the PEEK piston seals in the ROLSI valves (although only a minute area was exposed to the fluid in the cell and mass transfer would be extremely limited as a result of the thin internal diameter of the capillaries). Unknown quantities of CO_2 and methanol would be lost within the FEP sleeving, though the potential impact of this on the composition of the bulk mixture within the cell is negligible compared to the other sources of uncertainty.

First the system would be evacuated. The Isco pump is then filled with liquid CO_2 by condensing at reduced temperature before warming back to 298 K and allowed to equilibrate at a pressure of 10 MPa. At this stage, the CO_2 is occupying the measured volume of the Isco pump, the dead volume in the pump, and the volume between the pump and the cell. CO_2 is then allowed to flow into the cell. CO_2 is now also within the cell, as well as a dead volume upstream of the cell and another volume downstream of the cell. The pressure in the pump (and connected/associated volumes) is returned to 10 MPa to determine the volume swept, before being evacuated. The Isco pump is then filled with methanol, which would be injected into the cell in the same manner as with CO_2. The cell and Isco pump would be maintained at 298.15 K, approximately the ambient temperature, to minimise the effect of temperature gradients in dead volumes.

If starting with the cell containing both vapour and liquid in equilibrium the volume of liquid would rise as methanol is injected (though strictly the liquid level at the calibration temperature of 298 K was not a monotonic function of the amount of methanol injected, it quickly passes its minimum and the level rises) until the entire cell is full of mixed methanol + CO_2. The pressure begins at the vapour pressure of CO_2 and reduces, following the mixture bubble curve, as methanol is injected. At this stage the volume upstream of the cell contains liquid methanol, while the volume downstream of the cell (a short thin length of tubing immediately above the cell) contained effectively pure CO_2 vapour, as mixing in this volume was limited to

diffusion and the under the calibration conditions the vapour phase of the mixture was near pure CO_2 anyway ($y_{CO2} > 0.99$). As more methanol is injected the liquid mixture begins to enter the downstream dead volume, compressing the CO_2 vapour until it condenses into liquid CO_2. This can be observed as the pressure slowly rising until the entire system is in a liquid state, at which point the pressure begins to rise rapidly.

The amount of first component, in this case CO_2, in the cell, can be reasonably approximated as

$$n_1 = \Delta V_{1,p} \rho_{1,p}(p, T_{1,p}) - V_{1,d} \rho_{1,d}(p_{BP}, T_{1,d}) \tag{4.32}$$

where $\Delta V_{1,p}$ is the change in pump volume when injecting the first component, $\rho_{1,p}$ is the density of that component at the pump pressure p and temperature $T_{1,p}$, $V_{1,d}$ is the relevant dead volume, in this case the volume downstream of the cell (relative to the pump), and $\rho_{1,d}$ is the density within this dead volume at the ambient temperature $T_{1,d}$ and the pressure at which the cell was entirely filled with liquid p_{BP}.

The amount of the second component, methanol, is given by

$$n_2 = \Delta V_{2,p} \rho_{2,p}(p, T_{2,p}) - V_{2,d} \rho_{2,d}(p_c, T_{2,d}) \tag{4.33}$$

where the dead volume $V_{2,d}$ in this case is volume upstream of the cell and $\rho_{2,d}$ is the density within this dead volume at the ambient temperature $T_{2,d}$ and the final pressure within the cell p_c.

In reality, the composition inside the cell is also affected by the mixed liquid entering the downstream dead volume after the cell fills while the second component is injected. This is difficult to determine because it requires knowledge of the mixture density as well as an assumption about how well mixed the cell contents were during the process, however, as the cell volume is much larger (>100x) than this dead volume, the composition of the mixture entering the dead volume does not vary significantly during this process and the impact on the final composition in the cell is negligible.

The densities of the pure fluids were determined using multiparameter equations of state, as was done with the gas sample loops, using the model of Span & Wagner for CO_2 [207] and of de Reuck & Craven for methanol [283].

Four calibration mixtures were prepared in the cell over the course of the investigation of methanol + CO_2, with a total of approximately three thousand samples taken. Their compositions are reported in Table 4.3 as determined from the synthetic mixture preparation and the average value of the samples withdrawn through the ROLSI valves after optimising the calibration parameters. The calibration parameters are listed in Table 4.4. Different parameters for methanol were used for the liquid and vapour ROLIs, as systematic deviations were visible when using the same parameters for both, which is assumed to be a result of differences between the valves and the carrier gas flow through them. Calibrations 1 and 2 were made while using the glass encapsulated stirrer bar, which blocked the ROLSI capillaries upon its breakup, and so different (though nominally identical) capillaries were used for calibrations 3 and 4, with no apparent effect on the calibration. The preparation procedure for calibration 4 was slightly different to the others, the amount of CO_2 required was greater than could be introduced with one filling of the Isco pump, so, in order to keep uncertainties to a

minimum, the system was initially completely filled with liquid CO_2 and the amount was determined through compressibility measurements.

Table 4.3: Compositions of the methanol + CO_2 calibration mixtures, as determined from the preparation of the synthetic mixture $x_{CO2,synth}$ as well as the average values obtained from sampling with the liquid $x_{CO2, Liq\ ROLSI}$ and vapour $x_{CO2, Vap\ ROLSI}$ ROLSI valves

Cal #	$x_{CO2, synth}$	$x_{CO2, Liq\ ROLSI}$	$x_{CO2, Vap\ ROLSI}$
1	0.4802	0.4810	0.4797
2	0.4132	0.4117	0.4122
3	0.5703	0.5710	0.5716
4	0.9480	0.9470	0.9478

The sample sizes ranged from (1 to 31) µmol, for 10 ms increments of ROLSI opening time from 10 ms to 100 ms, corresponding to a range of sample sizes of (1 to 18) µmol of CO_2 and (0.05 to 13) µmol for methanol. The broad range of sizes for methanol was especially important for capturing the effects of adsorption, achieving a good fit across more than two orders of magnitude in sample size and three orders of magnitude of peak area.

Table 4.4: Optimised calibration constants for CO_2 and methanol using the adsorption corrected calibration equation, helium as the carrier gas, and different values for either ROLSI valve for methanol

Analyte	a_i / µmol	b_i / µmol	c_i / µmol	K_i
CO_2	6.50×10^{-5}	-6.05×10^{-12}	-	-
Methanol, Liq	6.95×10^{-5}	-3.14×10^{-11}	1.75×10^{-1}	4.54×10^{-4}
Methanol, Vap	7.46×10^{-5}	-5.09×10^{-11}	1.19×10^{-1}	5.59×10^{-4}

It is interesting to note that the calibration parameters for CO_2 regressed against the synthetic mixtures are not the same as those obtained from the gas sample loops, even after converting to matching units. Most notably, the deviation from linearity was found to be negative, as was the deviation for methanol, while all calibrations with the gas sample loops across this work and the preceding works had positive deviations from linearity. This is most likely the result of peak shape effects and the higher uncertainties in the density in the gas loops, and suggests that the uncertainty for calibration with pure substances using gas sample loops is likely underestimated, though determining the extent of this underestimation is non-trivial and beyond the scope of this work. Such a difference was not observed in the previously mentioned validations by Fandino, Trusler, & Vega-Maza [305], however those validations were performed with gas phase samples at lower pressure and density, among other differences.

Deviations from expected compositions where within 0.45 mol% for liquid valve and within 0.5 mol% for vapour valve across the relevant range. For the fourth calibration mixture and the shortest opening time (10 ms), where adsorption had the greatest effect due to the low amount of methanol, deviations reached 0.67 mol%, though the amount of methanol in that case was below the range of any peaks observed during the phase behaviour measurements. Ultimately, no vapour samples were reported in this work for methanol + CO_2 due to the low fraction of methanol in the vapour phase for the conditions covered, so, for simplicity and to

avoid redundancy, discussion shall focus specifically on the calibration for the liquid ROLSI valve.

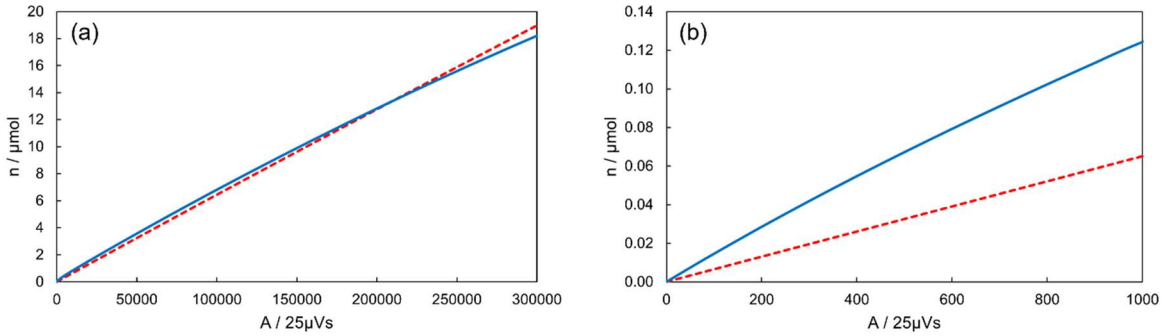


Figure 4.15: Calibration curves for methanol — and CO_2 - - (a) across the entire relevant range and (b) for small peak areas, where the non-linearity due to adsorption is most notable

The calibration curves for methanol and CO_2 when using helium as the carrier gas are shown in Figure 4.15. The extreme effective non-linearity in the detector response for method is readily apparent in Figure 4.15b. Deviations from the expected compositions as a function of the methanol peak area are shown in Figure 4.16 for several different modifications to a quadratic function of peak area; neglecting adsorption with and without using the parameters for CO_2 determined using the gas calibration loops, using a simple offset to account for adsorption, and when considering adsorption using the Langmuir-like term.

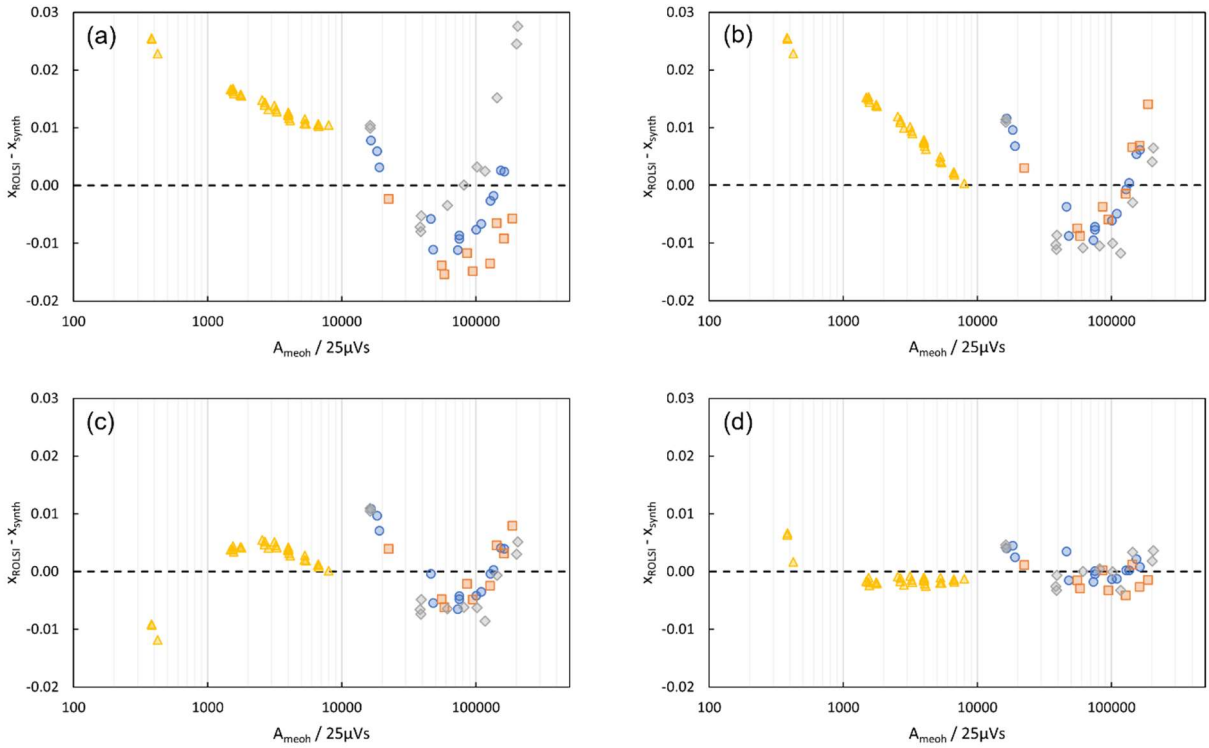


Figure 4.16: Deviations of sampled compositions from the synthetic mixture compositions for different optimised versions of the calibration equation, (a) no adsorption and CO_2 parameters taken from gas sample loop calibrations, (b) no adsorption and CO_2 parameters also

regressed, (c) adsorption treated with a simple constant offset, (d) adsorption modelled using a Langmuir-like term. Each point represents the average of a sequence of samplings, typically consisting of 25 samples, x_{CO2} = ● 0.4802, ■ 0.4132, ♦ 0.5703, ▲ 0.9480

Two variations of the calibration equation were considered, addressing some of the underlying assumptions in the adsorption term. First, addressing the real heterogeneity of the sample facing surfaces, was a dual site Langmuir model for methanol

$$n_i = a_i A_i + b_i A_i^2 + c_{i,1}\left(\frac{K_{i,1}A_i}{1+K_{i,1}A_i}\right) + c_{i,2}\left(\frac{K_{i,2}A_i}{1+K_{i,2}A_i}\right) \tag{4.34}$$

which added two more adjustable parameters, $c_{i,2}$ and $K_{i,2}$. When optimised, the second adsorption equilibrium constant was large, acting effectively as a constant offset rather than a meaningful function of sample size, with no methanol samples in the calibrations being sufficiently small to assess the validity properly.

The second variation was to consider the competitive adsorption between methanol and CO_2, as CO_2 would realistically experience some adsorption which would reduce the number of sites available for methanol to adsorb to. The calibration equation in this case becomes

$$n_i = a_i A_i + b_i A_i^2 + c_i\left(\frac{K_i A_i}{1+K_i A_i + K_j A_j}\right) \tag{4.35}$$

where A_j is the peak area of the co-adsorbing component and K_j its particular adsorption equilibrium constant.

As CO_2 lacks the strong interactions that allow methanol to adsorb strongly, and as no loss of CO_2 through adsorption was been observed in any of the measurements, it is understood that it should only experience physisorption and may desorb quickly. Attempts to fit the competitive adsorption model with or without the subsequent desorption of CO_2 produce similar results, with slightly varied parameters, so ultimately CO_2 was treated as though all of it desorbs and ultimately reaches the detector (ie the sampled amount can be described without the adsorption term), but CO_2 adsorption still plays a role in preventing methanol from adsorbing. The equilibrium constant for CO_2 was found to be 31 times smaller than that of methanol, considered consistent with the expected behaviour. Furthermore, the adsorption of CO_2 is sufficiently limited that it is reasonable to treat it also as monolayer adsorption, while, most strictly, it would be expected to ultimately form multiple layers requiring a different adsorption description and a reconciliation of the two competing types of adsorption, which was not necessary in this work.

The performance of these two alternatives models was found to be similar, and shall be compared on the basis of the standard deviation of the deviations from the average composition measured for each mixture. The single site adsorption of methanol only, as shown in Figure 4.16d, achieved a standard deviation of 0.238 mol%, while the dual site adsorption achieved a standard deviation of 0.155 mol% and best performance was seen with the competitive single site adsorption with a standard deviation of 0.139 mol%, nearly half that of the simpler model. The fact that the latter was most accurate, despite introducing one fewer adjustable parameter than the dual site model, is taken to indicate that the competitive adsorption is the more physically accurate description. A comparison between the

performance of the two single site models is shown in Figure 5.17. It should be noted that the differences between the three adsorption models are driven primarily by the ability to describe the smallest methanol samples in the presence of large amounts of CO_2, and within the range of sample sizes observed during phase behaviour measurements the single site adsorption of methanol alone may be adequate, though the competitive adsorption was ultimately preferred. As the deviations from the average sampled compositions (not the expected composition, which would also be effected by the uncertainty in the mixture preparation) were normally distributed, it is reasonable to expect that ~68 % of compositions measured upon sampling would be within 0.14 mol% of the actual sample composition, and ~95 % would be within 0.28 mol%, recalling here that the sample composition is not necessarily perfectly representative of the composition of the equilibrium phases in the cell.

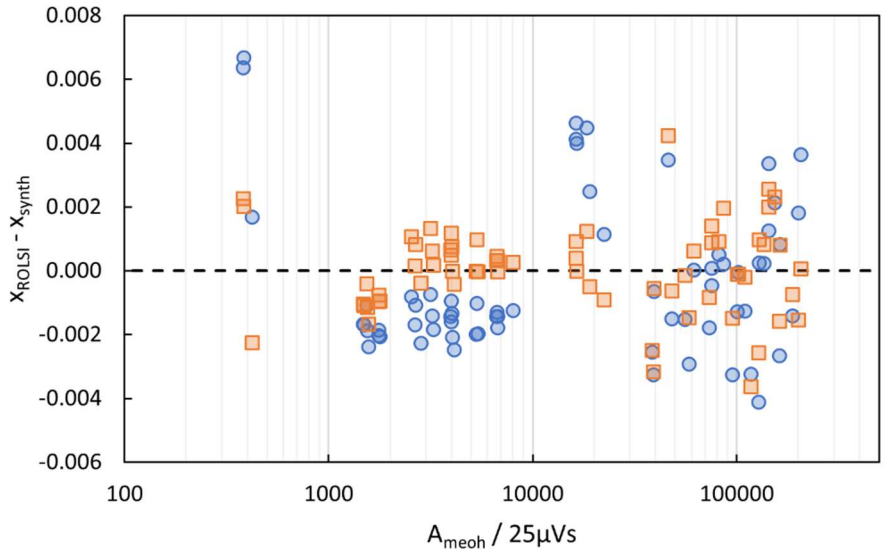


Figure 4.17: Comparison between the deviations for the single site adsorption of methanol alone ● and for the competitive single site adsorption of both methanol and CO_2 ■, as a function of the methanol peak area

While the calibration and measurement samples were now sampled in the same way, and thus more representative than in the case of gas sample loop calibration, there remain some differences between these samples. All calibration were compressed liquid samples, whereas in measurements the samples would be saturated liquids and vapours. Additionally, the temperatures and pressures within the cell, as well as the properties of the fluids within it (such as density and viscosity) would not be the same as during the calibrations. Ultimately, deviations in calibration were sufficiently low that it is unlikely that shape effects had caused significant deviations, so the use of a quadratic function of concentration paired with an EMG distribution was considered unnecessary.

Table 4.5: Optimised conditions for the GC and sampling system used in methanol + CO_2 measurements and the resultant retention times for each component

Condition	Value/Name
Oven temperature	473 K
Valve box temperature	363 K
Detector temperature	553 K
ROLSI temperature	373 K
Heated line temperature	373 K
Carrier gas	Helium
GC upstream pressure	0.25 MPa
Carrier gas flow rate	10 mL/min
Reference gas flow rate	20 mL/min
Make up gas flow rate	2 mL/min
Separation column	Porapak Q
Methanol retention time	3.2 min
CO_2 retention time	1.5 min

4.3 Additional Considerations

4.3.1 Materials

The source and purity of the samples are described in Table 4.6, along with any purifications performed. The gases were obtained from BOC and were used as supplied without further purification, while methanol was obtained in two batches of different quality, from Sigma Aldrich and VWR, and degassed under vacuum prior to use.

Helium was used as the carrier gas for the measurements of CO_2 with isobutane and with methanol, generally an ideal carrier gas when using a TCD because it has a much greater thermal conductivity than most other compounds, providing a strong response to those three compounds. Hydrogen is the only gas with a higher thermal conductivity than helium and the thermal conductivity of mixtures of hydrogen and helium does not vary as a monotonic function of mole fraction. Therefore, helium is not a suitable carrier gas when detecting hydrogen using a TCD and argon was used in its place for the isobutane + H_2 measurements. The thermal conductivity of argon is much lower than that of hydrogen and approximately half that of isobutane, meaning that a strong response was obtained for the former while an acceptable response was obtained for the latter.

Both carrier gases and the hydrogen were available at excellent purity of 0.99999, and the CO_2 just below at 0.99995. Isobutane could only be obtained at a purity of 0.995; the main impurity is understood to be n-butane, whose properties are relatively close to those of isobutane. The methanol batches had specified purities of 0.9975 and 0.999, though tested higher according to the certificates of analysis for their respective lots, as detailed in Table 4.7.

Table 4.6: Description of the materials used and their mole fraction purities

Chemical Name	Source	Purity As Supplied	Purification Method
Isobutane	BOC	0.995	None
Carbon Dioxide	BOC	0.99995	None
Hydrogen	BOC	0.99999	None
Helium	BOC	0.99999	None
Argon	BOC	0.99999	None
Methanol 1	Sigma Aldrich	0.9975	Vacuum degassed under stirring
Methanol 2	Avantor via VWR	0.999	Vacuum degassed

The first batch of methanol would be briefly exposed to the atmosphere upon decanting methanol from the supplied bottle into the apparatus's liquid inlet bottle before being degassed under stirring, allowing some air and some moisture to enter the methanol, the former quickly removed in degassing. The time between breaking the seal on the supplied bottle and beginning to degas was approximately ten seconds each time. The second batch did not use the liquid inlet bottle, instead, the supplied bottle was used directly. Two septum ports on the supplied bottle were used to connect it to the tubing to the Isco and vacuum pumps and to the syringe of dry nitrogen. The supplied bottle remained sealed from the atmosphere throughout the procedure, though this meant it was not possible to add a stirring bar to aid in degassing, preventing exposure to ambient humidity. For both batches, each bottle would only be used once to ensure minimal risk of contamination. The Isco pump would be filled with the amount required for a given experiment or series of experiments then raised above ambient pressure, typically 10 MPa, for the duration of the experiment(s) to ensure air or moisture would not be able to mix into the methanol through any small leaks.

Table 4.7: Quality of the methanol batches as specified and as per the certificate of analysis for their particular lots, given on a mass fraction basis to the resolution provided

	Specification		Certificate of analysis	
	Batch 1	Batch 2	Batch 1	Batch 2
Purity	0.9975	0.999	0.9983	1.000
Water content	0.00005	0.000020	<0.00001	0.000010
Residue after evaporation	0.000003	0.000003	0.000003	0.000003

The purity and especially the water content of the methanol is important to the quality of the measurements and has been demonstrated in studies of other properties to have a significant effect [558]. Impurities may be responsible for some of the disagreements in literature for methanol + CO_2 phase behaviour. In this work, the water contents of either batch were similar and sufficiently low for the methanol to be considered anhydrous for all practical purposes, and no differences were observed during measurements or calibrations with either batch, nor were any impurity peaks observed by the GC.

4.3.2 Control, Data Acquisition & Processing, and Automation

There are several aspects to the control of the apparatus, with the subprocesses ranging from entirely manual to entirely automatic. Most of the more minor aspects are trivial, such as the manual operation of valves by the operator (when filling or emptying the system) or the maintaining of a setpoint by an offline controller (such as the PID controllers that maintain the temperature of the sections of the heated sample line), and as such shall not be discussed in detail. The more critical aspects are discussed below, as one of the objectives within this work was to increase in the degree of automation in the measurement procedure, to move from a setup where the sampling at one state point was fully automated to one where measurements of entire sets of isotherms could be automated.

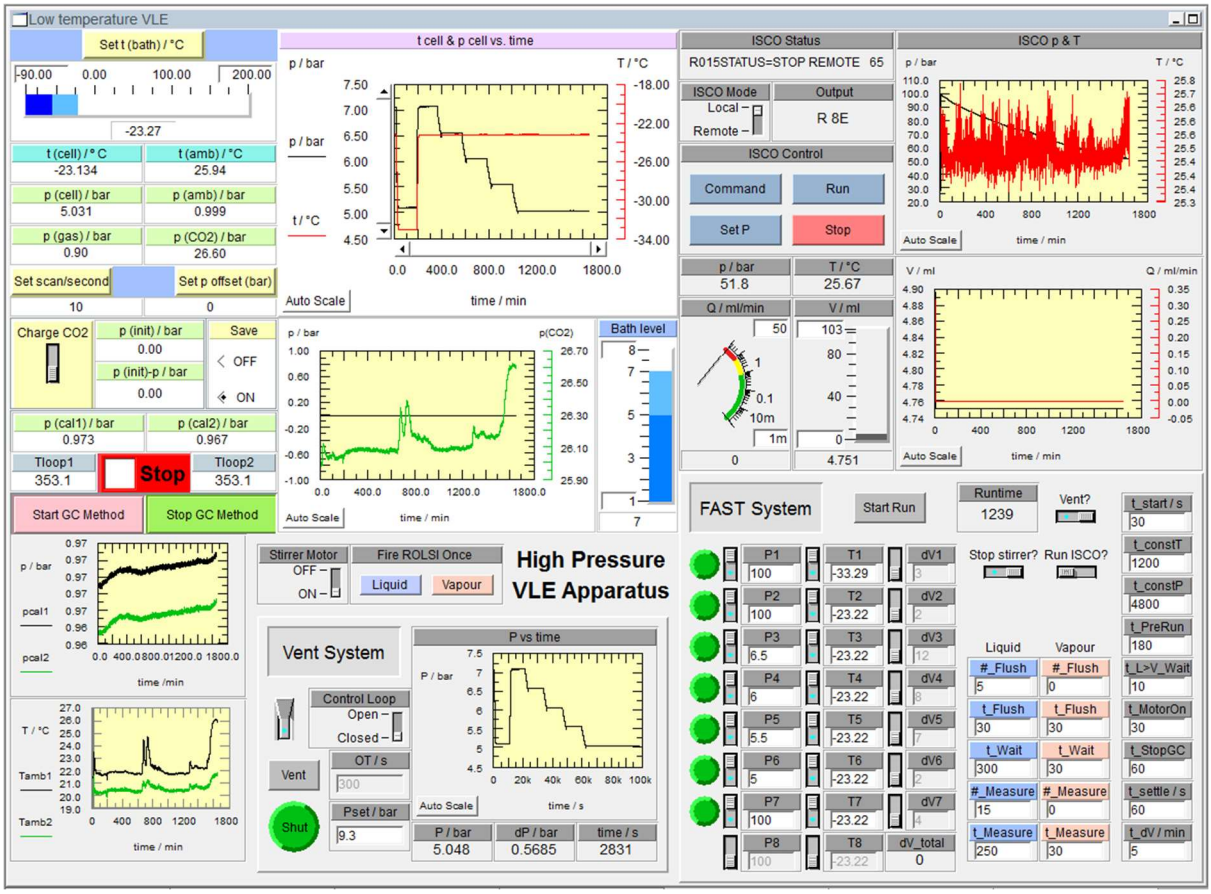


Figure 4.18: The main control panel of the control and data acquisition program, as it appeared at the end of a sequence of low temperature methanol + CO_2 measurements across 7 state points. Part of this panel was developed by Souza [533], while the majority was added in this work (note that the underlying workings are not visible in this view)

The apparatus was primarily controlled using a computer program implemented in Keysight VEE (similar to the more widely used LabVIEW), the main control panel for this program is shown in Figure 4.18. This program was originally designed for the purposes of data acquisition and control of the sampling system. The former involved the computer being connected to the various instruments and readout units, many connected via a data acquisition unit (DAU) (Agilent 34970A), where the program would periodically poll the current value of system properties from the appropriate unit, at a rate sufficiently high to capture the necessary

information but sufficiently low to not overwhelm any part of the system nor to wear out switches or relays too rapidly. In this work a rate of 0.1 Hz was used for measured values, except for in the venting valve control system, which used a variable rate dependant on the derivative of the difference between the current value and the set point. The control of the sampling system was managed through the use of a switching board in the DAU, which could send signals to the relays that powered the ROLSI valves or to the GC to start or finish running the GC method. The remainder of interactions with the GC were handled using the manufacturers proprietary software ChemStation and the onboard controllers within the GC.

The modifications made to the apparatus in this work facilitated a much greater degree of automation, requiring careful consideration of safety and feasibility of a given run path. The Isco pump, with its variable volume, permitted metering of fluids in or out of the cell (using its in-built features), while the venting system provided another avenue for removing fluids (controlled with a simple on-off controller implemented in software, with a variable refresh rate and a one iteration predictive time horizon for improved reliability). Additionally, the bath was able to be controlled remotely, though the capabilities this afforded had not been utilised in the preceding works.

The first step in implementing automation is to understand the implications of its meaning; for actions to be done without thought, exactly as commanded, and with reduced oversight. An automated system is no less capable of inflicting damage upon itself than a person using a manual one, and knows less. The high pressure syringe pump and temperature changes in the cell are especially capable of generating pressures in excess of the safe working limit. In the simplest implementation, the methodology of automated measurements mirrors that of manual measurements though adaptations are typically required due to differences in how a program may interact with the apparatus compared to a human.

It is preferable to keep the number of things controlled automatically to an absolute minimum, as the complexity of automated systems grows exponentially with increasing number of controllable parameters as a result of combinatorics. For example, the apparatus had, at the end of this work, thirty one two-position valves and one four-position valve (excluding cylinder valves, check valves, and pressure or flow regulators) such that there were more than eight billion unique combinations of valve positions. In practice, only the solenoid valve that actuates the venting valve, the ROLSI valves, and the Isco pump inlet/outlet valves were directly controlled by the control program (this excludes several valves controlled automatically by the GC's own software, though none actuate during standard measurements), such that the number of combinations was limited to thirty two, massively reducing the possibility of serious deviations from nominal operation due to control shortcomings. If one were also to consider the many variable parameters (such as bath temperature or carrier gas flow rate), limited only by the resolution of their controllers, the number of unique states the apparatus may reach easily exceeds the number of atoms in the observable universe, the majority of which would result in serious damage to the apparatus.

Convenient movement through the (p,T,x,y) phase space that one may wish to cover in their measurements is achieved by movement through (p,T,n_1,n_2) space (at least, for a two phase binary system), subject to some constraints in natural and composite dimensions, such as that

the fluid-fluid interface inside the cell must lie between the two capillaries. This requires an understanding of the behaviour of the mixture; the more accurately one can evaluate the internal state of the cell (whose opaque steel walls prevent direct observation), the more confidently one may proceed with a predetermined sequence of measurements.

The thermodynamic models being optimised as a research output were applied to predict the mixture behaviour, generally the PR-mWS-NTRL model though the PR-vdW model was used wherever there were issues with convergence, as in the case of isobutane + H_2. A complete description of the internal state of the cell, when within the two phase region, is provided whenever the amount of one component is known, supplemented by the measured temperature, pressure, and equilibrium phase compositions. In this case, changes in Isco pump volume provide knowledge of the amount of a component entering the cell, and modelling provides an estimation of the amount leaving the cell when venting mixed fluid. The liquid level inside the cell was determined using a mass balance, relying on the densities predicted by the thermodynamic model. Note that when the amounts of both components in the cell are known, the system is over-defined, which can provide an avenue for determining the densities of one of the phases.

Movement through the (p,T,n_1,n_2) space may be done in a variety of ways or in different directions, the optimal route typically needs to be evaluated on a case-by-case basis. When injecting one component and venting a mixed phase, more control is afforded by venting the phase which may be richest in one of the components. Frequently this phase is the vapour, rich in the more volatile component, whose mole fraction approaches one in many cases for asymmetric mixtures and is often less varied across experimentally relevant ranges of pressure than for the liquid phase. Thus, it is generally most convenient to have the pump filled with the less volatile component in normal operation, and to vent the mixed vapour phase, as such this was the primary approach used in this work.

The determination of the measurement sequence was done *a priori* in this work, leaving the control to rely on dead reckoning. This is not strictly necessary, and the required operations to have a more adaptive approach were all tested to various degrees during the investigations of methanol + CO_2, but the procedure remains largely the same and simply involves closing an otherwise open feedback loop. The hardest adaption is the on-the-fly optimisation of the thermodynamic model, though this is readily achievable for models with few adjustable parameters. For example, a PR-vdW model, with two binary interaction parameters, k_{ij} and l_{ij}, implemented in the VEE program, may be optimised by means of a grid search and reliably achieve the global optimal prediction within the time taken to move between state points. This capability was partially demonstrated but not fully employed before the end of experiments. Processing of the chromatographic data was done in Microsoft Excel following a sequence of measurements, but could instead be done by the control program following each state point or analysed in real time by connecting the analogue output of the GC to the program.

The most advanced level of automation achieved was in the measurement of methanol + CO_2 at 230, 240 and 250 K. Here, the system was prepared by filling the cell with a metered amount of CO_2 from the syringe pump, then refilling the pump with methanol, such that contents of the cell were known precisely until the first venting of the vapour phase. A small quantity of

methanol would be injected into the cell, measurements made at the three different temperatures in sequence, then repeating until the estimated liquid level inside the cell grew close to its limit, at which point the vapour phase would be vented periodically as well, until measurements had been made of three isotherms from near the saturated vapour pressure of CO_2 down to the lower limit of the sampling system, with a single initial charge of the system.

Automatic detector calibration is also achievable, when using the method of calibration against volumetrically prepared synthetic mixtures described previously, by intentionally leaving the two phase region after a series of measurements.

4.3.3 Uncertainty

The uncertainty analysis in this work follows largely the same methodology as the preceding [305, 306, 532] and related works [545], with modifications for the new calibration method and the determination of densities, guided by the methods and definitions of the 'Evaluation of Measurement Data – Guide to the Expression of Uncertainty in Measurement' [559-561], commonly known simply as GUM.

In the determination of the composition z_i of the liquid x_i or vapour y_i phases, the measured quantities were the temperature T, pressure p, and the chromatographic peak areas A_i, the standard uncertainties of which are provided in Table 4.8. The combined standard uncertainty in mole fraction $u_c(z_i)$ is calculated from these quantities through the expression

$$u_c(z_i) = \sqrt{u^2(z_i) + \left[\left(\frac{\partial z_i}{\partial T}\right)u(T)\right]^2 + \left[\left(\frac{\partial z_i}{\partial p}\right)u(p)\right]^2} \tag{4.36}$$

where $u(z_i)$ is the uncertainty in the calculated mole fraction of component i (which, in the case of a binary mixture, is the same for both components), $u(T)$ is the uncertainty in temperature, and $u(p)$ is the uncertainty in pressure. A key assumption here is that the measured quantities are independent of each other, which is often the case [559] and can reasonably be expected to be here. A second assumption is that the partial derivatives are constant, which less guaranteed (primarily for the derivatives of composition with respect to temperature and pressure in the above equation, and more guaranteed for the derivatives mentioned below), however, the extension of the analysis to exceptions is challenging and requires the use of higher order derivatives that are hard to evaluate. The temperature and pressure uncertainties dominate in regions of the phase space where the composition changes rapidly, such as in near-critical regions and in the high pressure region of the bubble curve for methanol + CO_2 (when below the critical temperature of CO_2). In other regions, the uncertainty in mole fraction is the main contribution.

From this point, a distinction is made between the uncertainty in measured mole fraction for the two calibration methods employed. For the calibration with gas sample loops, the existing description is used, where $u(z_i)$ is given by

$$u^2(z_i) = \left[z_i(1 - z_i)\right]^2 \sum \left[u_r^2(A_i) + u_r^2(a_i)\right] \tag{4.37}$$

where $u_r(A_i)$ is the relative standard uncertainty in peak area and $u_r(a_i)$ is the relative standard uncertainty in the detector response factor a_i, assuming a linear function of area is used for

the calibration equation. This approximation is not exactly correct, but avoids the difficulty in separating the uncertainties in the linear and non-linear calibration parameters. This uncertainty comes from the calibration measurements may be described as

$$u_r^2(a_i) = \left[u_r^2(n_i) + u_r^2(A_i)\right]_{cal} \tag{4.38}$$

where $u_r(n_i)$ is the relative standard uncertainty in the amount of substance n_i. The calibration and area uncertainties have remained effectively unchanged since previous evaluations and, as such, $u(z_i)$ reduces to the same simple quadratic expression

$$u(z_i) = 0.011 z_i (1 - z_i) \tag{4.39}$$

For calibration against volumetrically prepared synthetic mixtures a different approach is taken, relying on the fact that the calibration parameters have been regressed against compositions (not amounts) for many samples, such that

$$u^2(z_i) = \left[z_i(1 - z_i)\right]^2 \sum \left[u^2(z_{cal}) + u^2(z_{synth})\right] \tag{4.40}$$

where $u(z_{cal})$ is the uncertainty in sampled compositions observed during calibration (ie the standard deviation of the measured compositions from their average value) and $u(z_{synth})$ is the uncertainty in the composition of the synthetic mixture as a result of its preparation.

In preparing a mixture within the cell, the relevant measured quantities are the temperature, pressure, and volume of the Isco pump, and the volumes of two dead volumes, one upstream and one downstream of the cell. The uncertainty in which these as measured directly affect the final value of the mole fraction inside the cell. The pump temperature and pressure are also used to calculate the densities of the pure fluids injected, using models which themselves have an uncertainty. Overall, the synthetic mixture uncertainty is given by

$$\begin{aligned} u^2(z_{synth}) = &\left[\left(\frac{\partial z_i}{\partial T_1}\right)u(T_p)\right]^2 + \left[\left(\frac{\partial z_i}{\partial p_1}\right)u(p_p)\right]^2 + \left[\left(\frac{\partial z_i}{\partial V_1}\right)(u_r(V)\times V_1)\right]^2 + \left[\left(\frac{\partial z_i}{\partial \rho_1}\right)(u_r(\rho_1)\times \rho_1)\right]^2 + \left[\left(\frac{\partial z_i}{\partial V_{d,1}}\right)u(V_{d,1})\right]^2 \\ &+ \left[\left(\frac{\partial z_i}{\partial T_2}\right)u(T_p)\right]^2 + \left[\left(\frac{\partial z_i}{\partial p_2}\right)u(p_p)\right]^2 + \left[\left(\frac{\partial z_i}{\partial V_2}\right)(u_r(V)\times V_2)\right]^2 + \left[\left(\frac{\partial z_i}{\partial \rho_2}\right)(u_r(\rho_2)\times \rho_2)\right]^2 + \left[\left(\frac{\partial z_i}{\partial V_{d,2}}\right)u(V_{d,2})\right]^2 \end{aligned} \tag{4.41}$$

where $u(T_p)$ and $u(p_p)$ are the uncertainties in the Isco pump temperature and pressure, respectively, $u_r(V)$ is the relative uncertainty in the pump volume, V_i is the pump volume swept when injecting component i, $u_r(\rho_i)$ is the relative uncertainty in the model used to predict the density of that component, and $u(V_{d,i})$ is the uncertainty in the dead volume relevant to component i.

It should be noted that the dead volume terms cause $u(z_{synth})$ to no longer be a symmetric function of composition and it is discontinuous at the limits of the pure components, however this does not carry through to $u(z_i)$ due to the nature of the finite number of synthetic mixtures used in the calibration.

Overall, $u(z_i)$ again reduces to a simple quadratic function of composition

$$u(z_i) = 0.0081 z_i (1 - z_i) \tag{4.42}$$

It can be seen that the composition uncertainty with this method is approximately 75 % of the previous method. This method should also provide a more accurate value of the uncertainty, as the calibration method is reflective of how measurement samples are taken, whereas the uncertainty of the previous method is likely underestimated.

Not all uncertainties can be captured, primarily due to shortcomings in the ability to reliably describe them quantitatively. The most significant is the uncertainty in how representative the withdrawn sample if of the actual equilibrium phases, driven especially by the ability for entrained liquid in the vapour phase to be unknowingly sampled. Another example would be the possible effects of unrecognised temperature gradients within the cell, though these are expected to have a negligible effect for this apparatus. The fact that the measurements are made in the presence of gravitational acceleration leads to hydrostatic pressure effects that cause a pressure gradients that cannot be accurately quantified without knowledge of the liquid level inside the cell and the densities of the equilibrium phases, though discussion of this uncertainty can be found in literature [307].

Contributions from further detached uncertainties, such as the influence of ambient relative humidity, have been neglected as their magnitude is negligible compared the uncertainty contributions discussed above.

Table 4.8: Standard uncertainties of the relevant measured quantities

Contribution	Symbol	Uncertainty	Units
Cell Temperature	T	0.006	K
Cell Pressure	p	0.009	MPa
Peak Area*	A	0.5	%
Gas Loop Temperature	T_{GL}	1	K
Gas Loop Pressure	p_{GL}	0.0009	MPa
Pump Temperature	T_p	0.3	K
Pump Pressure	p_p	0.02	MPa
Pump Volume*	V	0.3	%
Dead Volume 1	Vd,1	0.1	cm^3
Dead Volume 2	Vd,2	0.25	cm^3

*Relative uncertainty

Chapter 5: Results & Discussion

“The most exciting phrase to hear in science, the one that heralds new discoveries, is not ‘Eureka!’ but ‘That’s funny…’”

— Isaac Asimov

5.1 Isobutane + CO_2

5.1.1 Experimental Results

The phase behaviour of isobutane + CO_2 was investigated at three temperatures: (240, 280, and 310) K, with data tabulated in Table 5.1 and shown graphically in Figure 5.1. Please note that, wherever values are indexed numerically (*eg* x_1), component 1 is the more volatile component (in this case CO_2). Also note that the results for isobutane + CO_2, as with isobutane + H_2 in the next section, have been published already [138] and are partially reproduced here, with some adaptation and further analysis. Similarly, the results of methanol + CO_2, in the section after, are subject to publication after the time of writing. There were three literature data sources available around 310 K, one at 310 K [337] and two at 310.93 K [333, 334], and one source of literature data available at 280 K [332], allowing for direct comparisons. The data obtained in this work for those two isotherms were found to be in very good agreement with the literature data, providing revalidation for the apparatus and technique, previously validated [305, 533] before the modifications discussed in the previous chapter were made. It can be seen that the vapour composition at 3.34 MPa from Weber's 280 K [332] measurements is probably erroneous, though the other measurements appear to be of high quality. The 240 K isotherm is 10 K lower than in the next lowest temperature source [332], extending the available data further into the range of relevance for refrigeration. At 240 K the pressures were nearing the lower limit of pressure at which the sampling system could function and required long ROLSI valve opening times, up to 10 seconds for the vapour phase, also meaning no measurements were made at lower still temperatures. Even at these low pressures, the results appear consistent with the model predictions and higher temperature data.

Table 5.1: Experimental phase behaviour data for [CO_2 (1) + isobutane (2)], the temperature, T, pressure, p, liquid, x_1, and vapour, y_1, compositions and their combined standard uncertainties, $u_c(x_1)$ and $u_c(y_1)$

T / K	p / MPa	x_1	y_1	$u_c(x_1)$	$u_c(y_1)$
310.003	6.8206	0.8690	0.9199	1.25×10^{-3}	8.11×10^{-4}
310.003	6.5503	0.8336	0.9123	1.53×10^{-3}	8.80×10^{-4}
309.996	6.2706	0.7930	0.9066	1.81×10^{-3}	9.32×10^{-4}
310.003	5.9435	0.7569	0.8970	2.02×10^{-3}	1.02×10^{-3}
309.995	5.4556	0.6760	0.8835	2.41×10^{-3}	1.13×10^{-3}
309.998	4.9009	0.6025	0.8708	2.63×10^{-3}	1.24×10^{-3}
309.993	4.0123	0.4614	0.8370	2.73×10^{-3}	1.50×10^{-3}
309.994	3.0092	0.3192	0.7894	2.39×10^{-3}	1.83×10^{-3}
310.004	2.0185	0.1869	0.7175	1.67×10^{-3}	2.23×10^{-3}
310.006	1.4631	0.1158	0.6180	1.13×10^{-3}	2.60×10^{-3}
310.004	1.0426	0.0640	0.4885	6.59×10^{-4}	2.75×10^{-3}
310.005	0.7233	0.0251	0.2315	2.70×10^{-4}	1.96×10^{-3}
280.001	3.8865	0.9325	0.9773	6.92×10^{-4}	2.44×10^{-4}
280.003	3.7361	0.8878	0.9699	1.10×10^{-3}	3.21×10^{-4}
280.009	3.5536	0.8436	0.9592	1.45×10^{-3}	4.30×10^{-4}
280.006	2.9466	0.6381	0.9338	2.54×10^{-3}	6.80×10^{-4}

T / K	p / MPa	x_1	y_1	$u_c(x_1)$	$u_c(y_1)$
280.007	2.5491	0.5227	0.9165	2.74×10^{-3}	8.41×10^{-4}
280.007	2.0678	0.3894	0.8947	2.62×10^{-3}	1.04×10^{-3}
280.005	1.5569	0.2630	0.8586	2.13×10^{-3}	1.34×10^{-3}
279.998	1.1188	0.1700	0.8058	1.55×10^{-3}	1.72×10^{-3}
279.999	0.9060	0.1274	0.7555	1.22×10^{-3}	2.03×10^{-3}
280.002	0.7034	0.0889	0.6953	8.91×10^{-4}	2.33×10^{-3}
240.008	1.2106	0.9148	0.9854	8.58×10^{-4}	1.59×10^{-4}
239.997	1.1347	0.8052	0.9770	1.73×10^{-3}	2.47×10^{-4}
240.003	1.0450	0.6645	0.9667	2.45×10^{-3}	3.54×10^{-4}
240.010	0.9379	0.5185	0.9599	2.75×10^{-3}	4.23×10^{-4}
240.013	0.8361	0.4179	0.9484	2.68×10^{-3}	5.39×10^{-4}
240.008	0.7374	0.3349	0.9434	2.45×10^{-3}	5.87×10^{-4}
240.005	0.6187	0.2581	0.9302	2.11×10^{-3}	7.14×10^{-4}

Standard uncertainties are $u(T)$ = 0.006 K, $u(p)$ = 0.009 MPa

5.1.2 Modelling Results

Both PR-vdW and PR-mWS-NRTL were found to describe the behaviour of isobutane + CO_2 very closely, the accuracy primarily only limited by the scatter of the literature data. A marginally better fit could be obtained for PR-mWS-NRTL, with an average absolute deviation in mole fraction of 0.0071 compared to 0.0094, however the simpler PR-vdW would be sufficient in most cases. The former may predict the liquid phase density more accurately [217], however this was not able to be assessed. It had been intended that measurements of the compressed liquid phase would be made for this mixture and for isobutane + H_2 using an existing vibrating tube densimeter apparatus [551]; however, a failure of the pump seal occurred during testing and a small leak persisted after servicing. The pump piston featured a double seal arrangement like in the VVC (discussed in the previous chapter) and similar concerns about the possibility of composition changes applied, especially as it was found that CO_2 swelling slowed the leak over time.

Comparisons of the predictions of the PR models with those of EPPR78, SAFT-γ-Mie, and GERG-2008 can also be seen in Figure 5.1. At temperatures of (280 and 310) K, the predictions of EPPR78 and GERG-2008 are relatively similar to each other and are almost in agreement with the experimental data, however the bubble pressure is consistently underpredicted. At T = 240 K, the differences between them are more pronounced, with EPPR78 overpredicting the bubble pressure while GERG-2008 underpredicts it. The vapour compositions for these three isotherms are in close agreement between the PR models, EPPR78, and GERG-2008, though PR-mWS-NRTL just outperforms the others, more so with the liquid compositions. SAFT-γ-Mie has the most marked difference in its predictions. At T = 310 K, the predicted compositions are more isobutane-rich, especially for the liquid phase, and the critical pressure is slightly underpredicted. At T = 280 K an unphysical azeotrope appears, also predicted at T = 240 K, and the liquid phase especially remains overly isobutane-rich with bubble pressures significantly overpredicted. A prediction of VLLE is also visible, which was not found to occur during experiments. If a three phase (VLLE) line were to

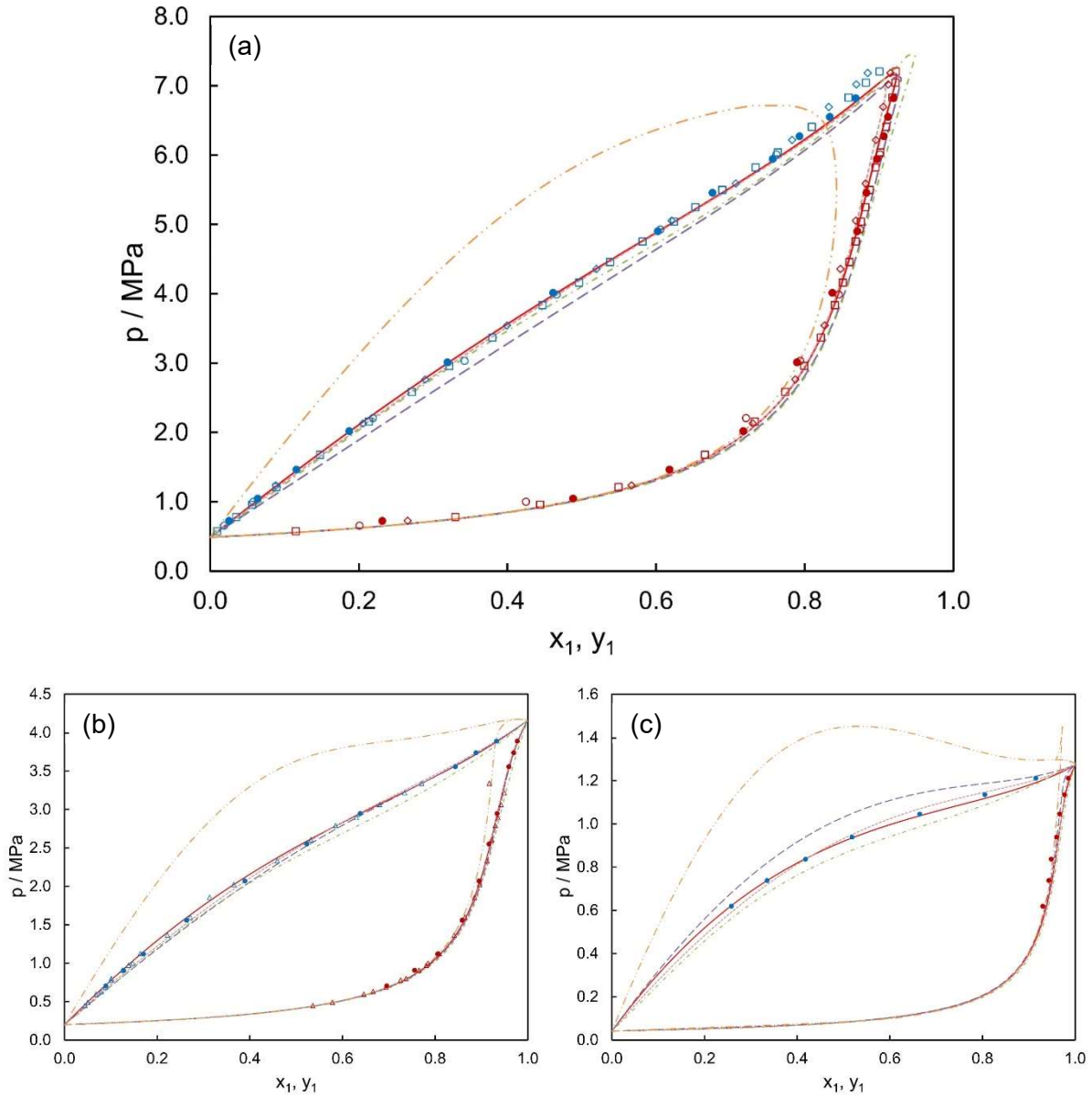


Figure 5.1: pxy diagrams for [CO_2 (1) + isobutane (2)] at (a) 310 K, (b), 280 K, and (c) 240 K, showing the experimental data from this work ●, as well as the data of Nagata et al [337] at 310 K ○, Besserer and Robinson [334] at 310.93 K ◇, Weber [332, 333] at 310.93 K □ and 280 K △. Also shown are the predictions of PR-vdW - - - and PR-mWS-NRTL — and those of EPPR78 – –, SAFT-γ-Mie – ·· –, and GERG-2008 – · –

Table 5.2: Optimised constants for the temperature dependent binary interaction parameters for the two PR EoS models for isobutane + CO_2

Model	Parameter	c_1	c_2	c_3
PR-vdW	k_{ij}	1.40×10^{-1}	-3.30×10^{-4}	8.00×10^{-7}
	l_{ij}	7.83×10^{-3}	-5.01×10^{-5}	-
PR-mWS-NRTL	k_{ij}	3.03×10^{-1}	-1.00×10^{-3}	1.61×10^{-6}
	τ_{12}	7.72×10^{-1}	-3.42×10^{-3}	-
	τ_{21}	2.72×10^{0}	-5.43×10^{-3}	-

exist, it is likely that this would be at temperatures lower than those at which solid formation, not normally considered in fluid thermodynamic models, occurs. As such, from a practical perspective, one could consider the mixture to exhibit type I phase behaviour according to the classifications of van Konynenburg & Scott [322], as has been done for other CO_2 + alkane mixtures [562]. For n-alkanes, it is only for heptane and beyond that the VLLE curve appears, so this treatment may be reasonable. The SVLE curve for most of these CO_2 + light alkane binaries has not been traced far enough to rule out the possibility of a disconnected LLE region, though for isobutane (and n-butane) it is unlikely. As the van Konynenburg & Scott types do not consider solid formation, from a fluid theory perspective one could perhaps view the mixture differently. Determination of the mixture type from interaction parameters alone is difficult for real mixtures; the idealised analysis of van Konynenburg & Scott [322] suggests that the mixture should be classified as type II but is not strictly applicable here. The only physically meaningful difference (outside of metastable subcooled states) would be the existence of Widom-like lines and accompanying critical enhancements (at least, per contemporary understanding), however for this mixture a hypothetical liquid-liquid critical curve would be too far detached from the region of real fluid coexistence to be significant. That said, one cannot place excessive emphasis on this without acknowledging that the van Konynenburg & Scott lose some meaning when applied in such a way. The classifications of Bolz *et al* [321] are less ambiguous, the mixture is at least type 1^{P} or at most type $1^{P}X^{X}$ (to indicate uncertainty as to the potential for LLE to exist under conditions unseen, perhaps as type $1^{P}l^{X}$), but the lack of standardisation regarding solid phases still presents a problem.

The binary interaction parameters used in this work were described as functions of temperature in the following manner:

$$X = c_1 + c_2(T/\mathrm{K}) + c_3(T/\mathrm{K})^2 \tag{5.1}$$

where X stands for k_{ij}, l_{ij}, τ_{ij}, ε_{kl}, or λ^{r}_{kl}, as appropriate, and c_1, c_2, and c_3 are constants regressed by the minimisation of the sum squared error between the measured compositions and the model predictions, shown in Tables 5.2, 5.4, 5.9, and 5.10.

5.2 Isobutane + H_2

5.2.1 Experimental Results

The phase behaviour of isobutane + H_2 was investigated at nine temperatures: (190, 240, 280, 311, 339, 363, 390, and 400) K, with data tabulated in Table 5.3 and shown graphically in Figure 5.2. These measurements span almost the entire range from the lower temperature limit of the apparatus to the critical point of isobutane, 71% of the range between the triple point and critical point temperatures of isobutane. They also constitute the largest dataset for a hydrogen binary mixture produced in the past four decades, by number of datapoints and range of conditions spanned. For the (390 and 400) K isotherms the mixture critical pressure was within the operating range of the apparatus, allowing for measurements to be made in the near critical region. Two isotherms, (311 and 339) K, could be directly compared to literature data [176], finding surprisingly close agreement for the liquid compositions while there is a pronounced difference for the vapour compositions, with consistently lower hydrogen mole

fractions found in this work than in literature. This is not unusual, given that the one prior study was conducted long ago with rudimentary techniques with documented troubles [176, 509].

Table 5.3: Experimental phase behaviour data for [H_2 (1) + isobutane (2)], the temperature, T, pressure, p, liquid, x_1, and vapour, y_1, compositions and their combined standard uncertainties, $u_c(x_1)$ and $u_c(y_1)$

T / K	p / MPa	x_1	y_1	$u_c(x_1)$	$u_c(y_1)$
399.989	9.1782	0.2011	-	8.25×10^{-3}	-
		0.1995	-	8.25×10^{-3}	-
399.994	8.9165	-	0.2489	-	2.14×10^{-3}
399.987	8.8297	0.1647	0.2489	1.87×10^{-3}	2.10×10^{-3}
399.984	8.6578	0.1552	0.2515	1.71×10^{-3}	2.09×10^{-3}
399.988	8.5031	0.1480	0.2521	1.62×10^{-3}	2.09×10^{-3}
399.977	8.2699	0.1385	0.2507	1.51×10^{-3}	2.08×10^{-3}
399.991	7.9605	0.1269	0.2484	1.22×10^{-3}	2.05×10^{-3}
399.991	7.6946	-	0.2461	-	2.04×10^{-3}
399.986	7.4167	0.1094	0.2379	1.07×10^{-3}	1.99×10^{-3}
399.985	7.1132	0.1002	0.2304	9.92×10^{-4}	1.95×10^{-3}
399.996	7.0312	0.0974	0.2288	9.67×10^{-4}	1.94×10^{-3}
399.982	6.6041	0.0858	0.2150	8.63×10^{-4}	1.86×10^{-3}
399.981	5.9999	0.0696	0.1921	7.12×10^{-4}	1.71×10^{-3}
399.994	5.8940	-	0.1883	-	1.68×10^{-3}
399.996	5.8239	-	0.1852	-	1.66×10^{-3}
399.979	5.6957	0.0617	0.1783	6.37×10^{-4}	1.61×10^{-3}
399.979	5.2926	0.0513	0.1582	5.35×10^{-4}	1.46×10^{-3}
399.991	5.2190	-	0.1560	-	1.45×10^{-3}
399.980	4.9934	0.0438	0.1413	4.61×10^{-4}	1.33×10^{-3}
399.981	4.6905	0.0362	0.1224	3.84×10^{-4}	1.18×10^{-3}
399.981	4.2873	-	0.0944	-	9.40×10^{-4}
399.983	3.9891	-	0.0718	-	7.33×10^{-4}
390.001	16.4992	0.3375	0.4233	3.84×10^{-3}	3.82×10^{-3}
390.001	16.2475	0.3148	0.4434	2.72×10^{-3}	2.93×10^{-3}
390.003	16.0043	0.3004	0.4541	2.51×10^{-3}	2.83×10^{-3}
390.003	15.8044	0.2908	0.4600	2.41×10^{-3}	2.80×10^{-3}
390.004	15.5051	0.2802	0.4632	2.32×10^{-3}	2.78×10^{-3}
390.003	15.2538	0.2707	0.4692	2.26×10^{-3}	2.78×10^{-3}
390.001	15.0003	0.2618	0.4717	2.20×10^{-3}	2.77×10^{-3}
390.002	14.8025	0.2556	0.4732	2.16×10^{-3}	2.77×10^{-3}
390.004	14.5060	0.2465	0.4761	2.10×10^{-3}	2.77×10^{-3}
390.004	14.2558	0.2393	0.4763	2.06×10^{-3}	2.77×10^{-3}
390.002	14.0042	-	0.4773	-	2.77×10^{-3}
390.002	13.5007	0.2201	0.4746	1.89×10^{-3}	2.74×10^{-3}
390.003	13.0006	0.2075	0.4726	1.81×10^{-3}	2.74×10^{-3}
390.003	12.4980	0.1954	0.4693	1.73×10^{-3}	2.74×10^{-3}
390.002	11.9938	-	0.4643	-	2.74×10^{-3}
390.014	11.4921	0.1732	0.4602	1.58×10^{-3}	2.73×10^{-3}
390.014	10.9891	0.1622	-	1.49×10^{-3}	-

T / K	p / MPa	x_1	y_1	$u_c(x_1)$	$u_c(y_1)$
390.013	10.4842	0.1514	-	1.41×10^{-3}	-
389.998	9.4606	0.1304	-	1.25×10^{-3}	-
390.000	9.2051	0.1251	-	1.20×10^{-3}	-
390.000	8.9506	0.1199	-	1.16×10^{-3}	-
389.998	8.7462	0.1158	-	1.13×10^{-3}	-
390.001	8.4521	0.1101	-	1.08×10^{-3}	-
390.000	8.2097	0.1052	-	1.04×10^{-3}	-
389.999	7.9565	0.1002	-	9.92×10^{-4}	-
390.008	7.7552	0.0967	0.3582	9.61×10^{-4}	2.53×10^{-3}
390.005	6.8458	0.0791	0.3194	8.01×10^{-4}	2.39×10^{-3}
390.006	5.9292	0.0618	0.2700	6.38×10^{-4}	2.17×10^{-3}
390.008	5.1509	0.0466	0.2120	4.89×10^{-4}	1.84×10^{-3}
390.005	4.0009	0.0253	0.1489	2.71×10^{-4}	1.39×10^{-3}
374.989	19.9277	0.2703	0.6701	2.17×10^{-3}	2.43×10^{-3}
374.991	19.5304	0.2648	0.6704	2.14×10^{-3}	2.43×10^{-3}
374.989	19.0294	0.2564	0.6696	2.10×10^{-3}	2.43×10^{-3}
374.988	18.5257	0.2485	0.6678	2.05×10^{-3}	2.44×10^{-3}
374.989	18.0255	0.2405	0.6657	2.01×10^{-3}	2.45×10^{-3}
374.991	17.5275	0.2328	0.6610	1.96×10^{-3}	2.46×10^{-3}
374.988	17.0180	0.2250	0.6590	1.92×10^{-3}	2.47×10^{-3}
374.987	16.5157	0.2172	0.6576	1.87×10^{-3}	2.48×10^{-3}
374.987	16.0145	0.2094	0.6542	1.82×10^{-3}	2.49×10^{-3}
374.988	15.5118	0.2016	0.6499	1.77×10^{-3}	2.50×10^{-3}
374.994	15.0206	0.1947	0.6447	1.72×10^{-3}	2.52×10^{-3}
374.992	14.5125	0.1869	0.6381	1.67×10^{-3}	2.54×10^{-3}
374.996	14.0201	0.1795	0.6361	1.62×10^{-3}	2.55×10^{-3}
374.993	13.5080	0.1718	0.6277	1.56×10^{-3}	2.57×10^{-3}
374.995	13.0143	0.1641	0.6232	1.51×10^{-3}	2.58×10^{-3}
374.993	12.5032	0.1567	0.6166	1.45×10^{-3}	2.60×10^{-3}
374.994	12.0074	0.1489	0.6080	1.39×10^{-3}	2.62×10^{-3}
374.988	9.9708	0.1186	0.5703	1.15×10^{-3}	2.70×10^{-3}
374.988	8.9630	0.1035	0.5457	1.02×10^{-3}	2.73×10^{-3}
374.988	8.4584	0.0958	0.5307	9.53×10^{-4}	2.74×10^{-3}
375.005	7.4120	0.0812	0.5177	8.21×10^{-4}	2.75×10^{-3}
375.006	7.0097	0.0753	0.5004	7.66×10^{-4}	2.75×10^{-3}
375.007	6.5050	0.0680	0.4744	6.97×10^{-4}	2.74×10^{-3}
375.007	6.0019	0.0606	0.4461	6.27×10^{-4}	2.72×10^{-3}
375.001	5.4958	0.0533	0.4081	5.55×10^{-4}	2.66×10^{-3}
374.994	4.9914	0.0456	-	4.79×10^{-4}	-
374.996	4.4892	0.0383	-	4.05×10^{-4}	-
374.995	3.9859	0.0302	-	3.22×10^{-4}	-
363.147	18.9980	0.2225	0.7543	1.90×10^{-3}	2.04×10^{-3}
363.145	17.9877	0.2099	0.7494	1.82×10^{-3}	2.07×10^{-3}
363.145	16.9809	0.1973	0.7439	1.74×10^{-3}	2.10×10^{-3}
363.148	16.6861	0.1933	0.7442	1.72×10^{-3}	2.09×10^{-3}
363.148	16.3844	0.1897	0.7425	1.69×10^{-3}	2.10×10^{-3}

T / K	p / MPa	x_1	y_1	$u_c(x_1)$	$u_c(y_1)$
363.148	16.1824	0.1867	0.7408	1.67×10^{-3}	2.11×10^{-3}
363.147	15.9836	0.1848	0.7296	1.66×10^{-3}	2.17×10^{-3}
363.147	15.7828	0.1823	0.7388	1.64×10^{-3}	2.12×10^{-3}
363.148	15.4819	0.1784	0.7359	1.61×10^{-3}	2.14×10^{-3}
363.147	14.9828	0.1719	0.7332	1.57×10^{-3}	2.15×10^{-3}
363.147	14.4770	0.1655	0.7271	1.52×10^{-3}	2.18×10^{-3}
363.148	14.2760	0.1626	0.7309	1.50×10^{-3}	2.16×10^{-3}
363.149	13.9738	0.1597	0.7249	1.48×10^{-3}	2.19×10^{-3}
363.148	13.7766	0.1571	0.7217	1.46×10^{-3}	2.21×10^{-3}
363.148	13.5711	0.1545	0.7207	1.44×10^{-3}	2.21×10^{-3}
363.149	13.3723	0.1519	0.7195	1.42×10^{-3}	2.22×10^{-3}
363.149	13.1738	0.1495	0.7154	1.40×10^{-3}	2.24×10^{-3}
363.146	12.9620	0.1458	0.7178	1.37×10^{-3}	2.23×10^{-3}
363.147	11.9555	0.1335	0.7047	1.27×10^{-3}	2.29×10^{-3}
363.146	10.9556	0.1211	0.6863	1.17×10^{-3}	2.37×10^{-3}
363.157	9.4536	0.1022	0.6588	1.01×10^{-3}	2.47×10^{-3}
363.154	8.9856	0.0958	0.6482	9.53×10^{-4}	2.51×10^{-3}
363.148	8.4388	0.0892	0.6400	8.94×10^{-4}	2.53×10^{-3}
363.148	7.9675	0.0834	0.6248	8.41×10^{-4}	2.58×10^{-3}
363.143	5.3536	0.0499	0.5159	5.22×10^{-4}	2.75×10^{-3}
363.145	4.9518	0.0446	0.4925	4.69×10^{-4}	2.75×10^{-3}
363.145	4.7009	0.0413	0.4760	4.36×10^{-4}	2.74×10^{-3}
363.145	4.4490	0.0394	0.4609	4.16×10^{-4}	2.73×10^{-3}
338.710	19.7239	0.1875	0.8549	1.68×10^{-3}	1.36×10^{-3}
338.711	18.0148	0.1728	0.8465	1.57×10^{-3}	1.43×10^{-3}
338.710	15.9917	0.1529	0.8372	1.43×10^{-3}	1.50×10^{-3}
338.711	14.9931	0.1439	0.8321	1.35×10^{-3}	1.54×10^{-3}
338.700	13.2959	0.1272	0.8288	1.22×10^{-3}	1.56×10^{-3}
338.700	11.9938	0.1187	0.8223	1.15×10^{-3}	1.61×10^{-3}
338.700	10.4888	0.1047	0.8132	1.03×10^{-3}	1.67×10^{-3}
338.703	7.1078	0.0657	0.7562	6.76×10^{-4}	2.03×10^{-3}
338.704	3.9616	0.0332	0.6430	3.54×10^{-4}	2.53×10^{-3}
338.704	2.1000	0.0126	0.4224	1.37×10^{-4}	2.68×10^{-3}
310.919	16.1656	0.1281	0.9220	1.23×10^{-3}	7.91×10^{-4}
310.926	12.5358	0.1009	0.9177	9.98×10^{-4}	8.30×10^{-4}
310.926	8.8101	0.0713	0.8970	7.28×10^{-4}	1.02×10^{-3}
310.925	5.5123	0.0441	0.8529	4.64×10^{-4}	1.38×10^{-3}
310.925	2.9979	0.0228	0.7529	2.45×10^{-4}	2.05×10^{-3}
310.936	1.5339	0.0094	0.5996	1.02×10^{-4}	2.64×10^{-3}
279.994	19.7308	0.1267	0.9690	1.22×10^{-3}	3.30×10^{-4}
279.991	16.9987	0.1073	0.9697	1.05×10^{-3}	3.23×10^{-4}
280.000	14.1845	0.0909	0.9668	9.09×10^{-4}	3.53×10^{-4}
280.003	11.0385	0.0723	0.9629	7.38×10^{-4}	3.93×10^{-4}
279.987	7.5495	0.0501	0.9534	5.23×10^{-4}	4.89×10^{-4}
279.989	4.6215	0.0287	0.9321	3.07×10^{-4}	6.97×10^{-4}
279.990	2.1057	0.0124	0.8755	1.35×10^{-4}	1.20×10^{-3}

T / K	p / MPa	x_1	y_1	$u_c(x_1)$	$u_c(y_1)$
279.992	1.0852	0.0057	0.7770	6.21×10^{-5}	1.91×10^{-3}
239.995	19.7104	0.0941	0.9928	9.38×10^{-4}	7.86×10^{-5}
239.995	16.1565	0.0837	0.9916	8.43×10^{-4}	9.17×10^{-5}
239.996	12.5402	0.0623	0.9857	6.43×10^{-4}	1.55×10^{-4}
239.997	9.0786	0.0452	0.9857	4.75×10^{-4}	1.55×10^{-4}
239.997	5.5076	0.0265	0.9870	2.84×10^{-4}	1.42×10^{-4}
239.998	2.3701	0.0115	0.9764	1.25×10^{-4}	2.53×10^{-4}
239.995	1.0844	0.0057	0.9526	6.25×10^{-5}	4.97×10^{-4}
189.948	19.4572	0.0584	0.9995	6.05×10^{-4}	5.50×10^{-6}
189.950	15.8934	0.0490	0.9992	5.13×10^{-4}	8.39×10^{-6}
189.934	12.0480	0.0362	0.9993	3.84×10^{-4}	7.69×10^{-6}
189.947	8.9784	0.0291	-	3.11×10^{-4}	-

Standard uncertainties are $u(T)$ = 0.006 K, $u(p)$ = 0.009 MPa

There were some complications with the measurements, most notably issues with sampling the vapour phase. Liquid samples were generally unproblematic (both for this mixture and the others investigated), near identical samples of the liquid phase could be obtained immediately after a short flushing, while equivalently consistent samples of the vapour frequently required up to twenty five samplings, sometimes still varying unsatisfactorily even after that point. It is believed that these issues were the result of disruptions to the equilibrium upon sampling, where small amounts of liquid could become entrained in the vapour and even accumulate on the capillary for the vapour sampling ROLSI valve. These effects, and the extent of their inconvenience, have been detailed in some depth in the literature [201, 202] where windowed cells have allowed for visual observation. In such a situation, the system is effectively in temperature and pressure equilibrium but not in surface equilibrium. The energetic effects are subtle, such that would require exceptionally precise temperature and pressure measurements for the occurrence of this effect to produce a noticeable signal.

Direct visual observation is insufficient to confirm whether entrainment has occurred, for two major reasons. The first, expected to be less common, is that the refractive indices of the phases may be very similar and change as compositions equilibrate, allowing for droplets to appear and disappear from sight, as has been encountered in interfacial tension measurements [563]. The second issue, pertinent to any attempt at observation (visual or otherwise, with the partial exception of light and matter scattering techniques), is that the effect may produce droplets of size down to nanometre-scale (nanodrops). Nanodrops are far longer lived than larger scale droplets due to their low effective surface tension [187, 564]. For H_2 mixtures the effect may be even more pronounced, as the thermal de Broglie wavelength of hydrogen is non-negligible [565]. Furthermore, at the nano-scale, there is also no immediately apparent metric by which an experimentalist may assess if agglomerations of molecules are nanodrops (that will proceed to slowly coalesce until they are a macroscopic bulk phase), colloids (that may remain suspended indefinitely), transient clusters (that are commonplace wherever meaningfully supercritical (*ie* neither strictly liquid-like or gas-like) fluids are present), or simply stable configurations of the fluid which are inhomogeneous at the molecular level (recall here the concept of two fluid models). This is, in part, due to insufficient definition. Further discussion of nanodrops, their relation to supercritical fluids, and the theoretical

shortcomings of the definitions of both surface tension and fluid states (including colloids) is excluded for brevity.

In some instances, such as some moderate pressures at T = 390 K, liquid compositions are given while vapour compositions are not, as no steady vapour sample composition could be obtained despite the liquid samples remaining well behaved. A small number of state points are missing a liquid or vapour composition due to complications with liquid level. While implementing and testing the automated system, the liquid level inside the cell would sometimes exceed the working limits, especially when only using the syringe pump to increase the pressure (before the venting system was implemented). This was amplified by uncertainties from the model affecting estimates of the liquid level. This issue was normally exhibited as the first and/or last state point, in a sequence of measurements, sampling the same phase with both ROLSIs. This data was included when there was confidence that the contents of the cell were still in the two phase region, and excluded wherever it was likely that only one phase was present.

The lowest temperature explored, 190 K, was sufficiently low for the ortho-para ratio of hydrogen to change from its high temperature limit, differing by approximately 3 %. The mixture was left to equilibrate for several days at this temperature before measurements across the isotherm began (which itself was spread across several days), so it is reasonable to suspect that the equilibrium ratio may have been reached. No measurements were made of the ortho-para ratio, and contemporary understanding of the conversion (taking on the order of days in the simple case of pure hydrogen in the absence of external fields) is insufficient to assess with certainty what the conversion rate would be in the presence of isobutane and the dynamic magnetic field produced by the stirring system. It is likely that any divergences from the equilibrium ratio would have had negligible effect (which cannot be said if one proceeded to lower temperatures still).

5.2.2 Modelling Results

The near critical data obtained were very important for modelling purposes, as accuracy in this region can provide insights into a model's performance and allow for better fitting. Predictions of this region were found to be much more variable when regressing BIPs only from the lower temperature isotherms, where the liquid composition varies relatively linearly as a function of pressure, akin to the idealistic Henry's law, and the top of the phase envelope is far out of sight.

A quality of fit like that seen with isobutane + CO_2 using the PR models could not be achieved with isobutane + H_2. For PR-vdW, predictions of the vapour phase compositions are generally accurate, however, at higher temperatures, most notably (363 and 375) K, a difference in trend is visible at high pressures. The accuracy of the predicted liquid phase compositions varies less consistently across the temperature range, over-predicting the H_2 mole fractions at (390 and 400) K, under-predicting them from (280 to 363) K, then notably over-predicting them again at 190 K. This is believed to be an artifact of the temperature dependant BIPs, especially given the good agreement between liquid compositions measured in this work and the

literature for the comparable isotherms. Unfortunately, numerical problems were encountered when trying to regress the BIPs for PR-mWS-NRTL for isobutane + H_2, and no useful results could be obtained with this model. The highly asymmetric nature of this mixture greatly increases the difficulty in converging the flash algorithms, resulting in frequent, though unpredictable, failures to converge to a valid solution. It is suspected that the capacity of this mixture (like all hydrogen binaries, other than mixtures with its own isotopes) to exhibit molar density inversions was not handled well by the flash algorithm, exacerbating convergence difficulties.

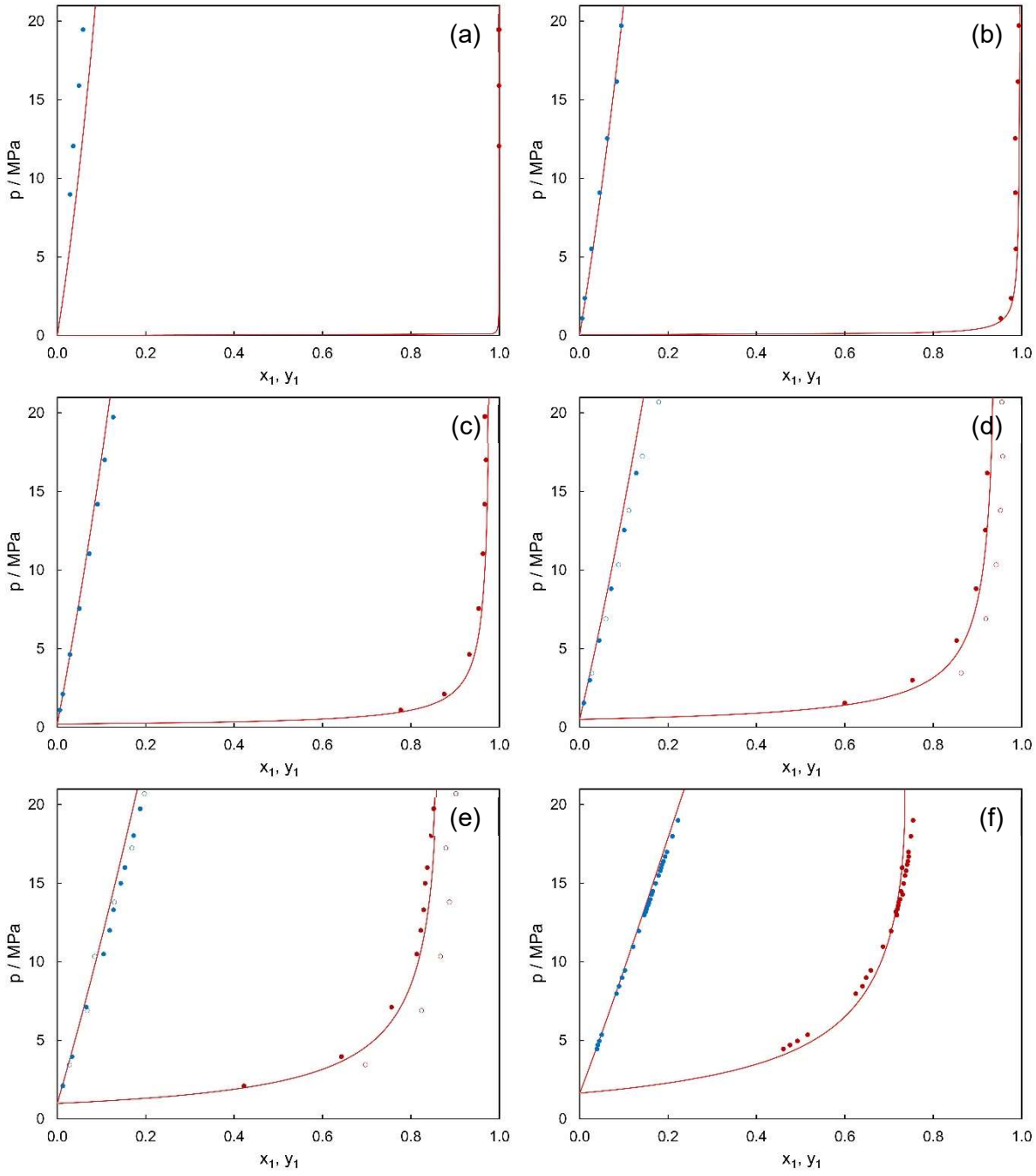


Figure 5.2: pxy diagrams for [H_2 (1) + isobutane (2)] at (a) 190 K, (b), 240 K, (c) 280 K, (d) 311 K, (e) 339 K, (f) 363 K, (g) 375 K, (h) 390 K, and (i) 400 K, showing the experimental data from this work ●, as well as the data of Dean and Tooke [176] at (311 and 339) K ○ and the predictions of PR-vdW — (Figure continues on next page)

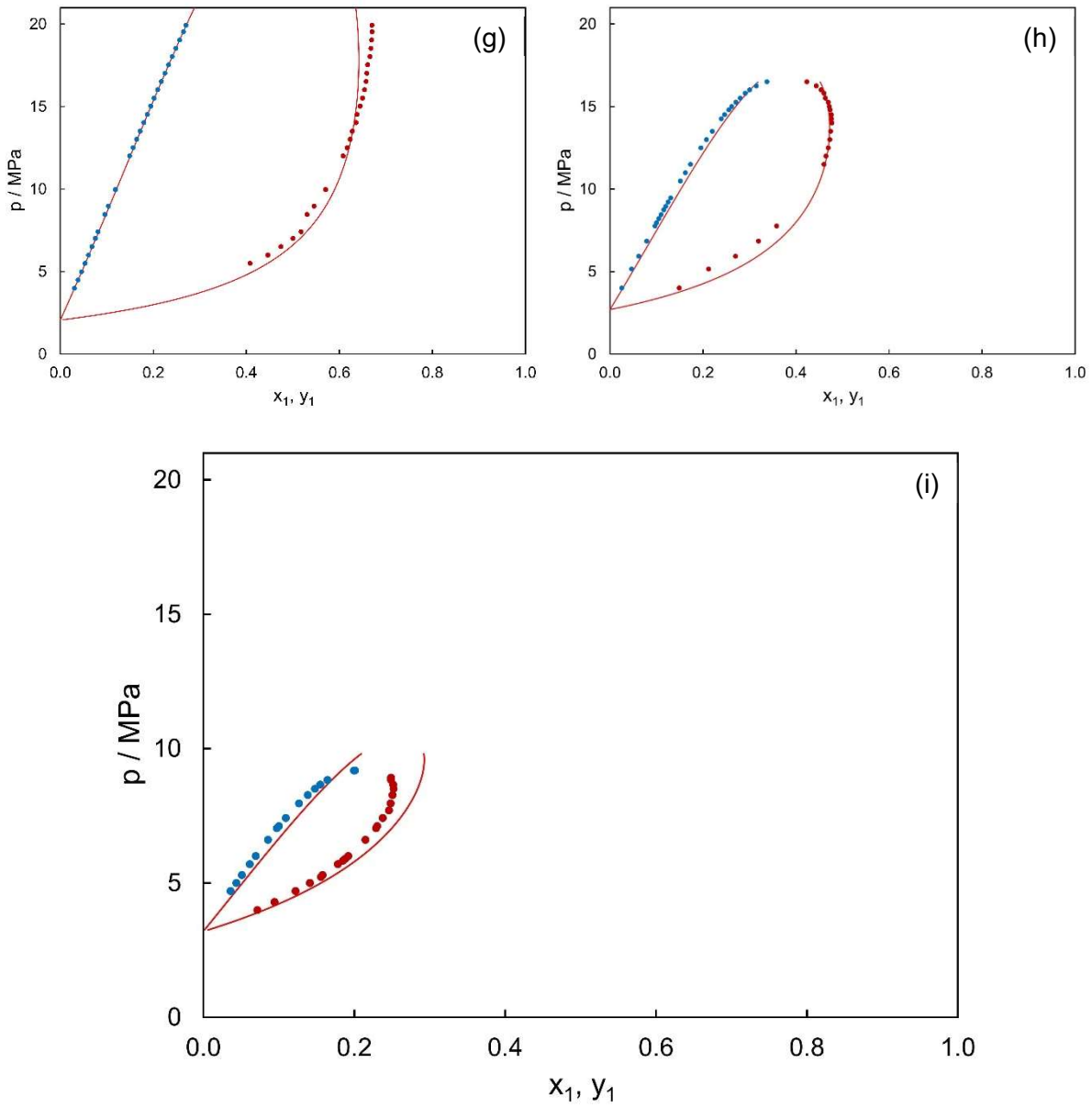


Figure 5.2: pxy diagrams for [H_2 (1) + isobutane (2)] at (a) 190 K, (b), 240 K, (c) 280 K, (d) 311 K, (e) 339 K, (f) 363 K, (g) 375 K, (h) 390 K, and (i) 400 K, showing the experimental data from this work ●, as well as the data of Dean and Tooke [176] at (311 and 339) K ○ and the predictions of PR-vdW — (Continued from previous page)

Despite the challenges in modelling isobutane + H_2 with PR-vdW and PR-mWS-NRTL, a significantly better fit is obtained with PR-vdW than with the alternative models, as can be seen in Figure 5.3. As mentioned previously, SAFT-γ-Mie cannot currently be used for this mixture, however EPPR78 and GERG-2008 could be. At T = 390 K, EPPR78 systematically underpredicts the isobutane mole fraction in both phases while overpredicting the critical pressure. While imprecise, the predictions are still reasonable and the trends as expected, the same statement cannot be made about the predictions of GERG-2008. At T = 390 K, the predicted phase envelope is much larger than found in experiments, with the liquid excessively isobutane-rich and the vapour excessively H_2-rich, and does not close at high pressures. The shortcomings are most visible when examining the pressure-temperature plot of the mixture

critical loci, as shown in Figure 5.4. The experimentally estimated critical points and those predicted by PR-vdW and EPPR78 all depart from the critical point of isobutane with a negative slope and tend quickly towards great pressure, while GERG-2008 predicts that the critical loci depart with a positive slope before passing a temperature maximum and turning back to lower temperatures and higher pressures. This prediction is unphysical and a known shortcoming of GERG-2008 in the description of hydrogen mixtures [288, 531]. The departure with positive slope is seen almost exclusively with helium mixtures [218], while the temperature maximum is more unusual still. Neither EPPR78 or GERG-2008 produce sufficiently accurate predictions for real world use, and there is clear room for their parameters to be refined. Additionally, the group interaction parameters for the CH group with H_2 in SAFT-γ-Mie can and should be optimised with the new experimental data, though this is outside the scope of this work.

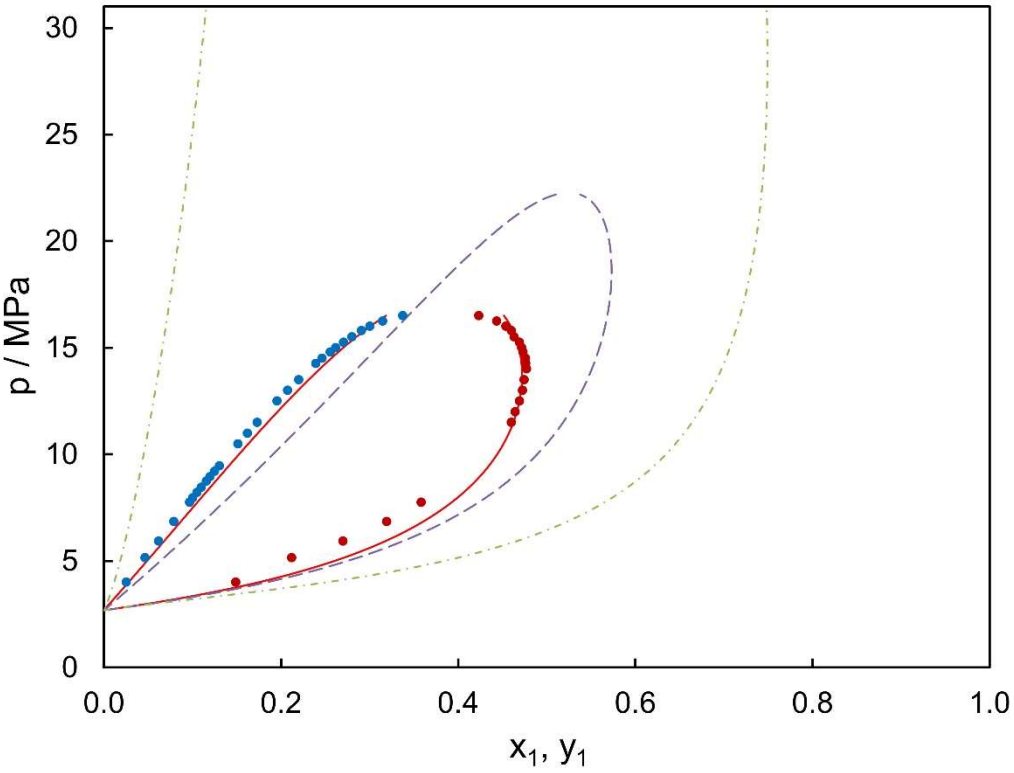


Figure 5.3: pxy diagram for [H_2 (1) + isobutane (2)] at 390 K, showing the experimental data from this work ●, as well as the predictions of PR-vdW — and those of EPPR78 – – and GERG-2008 – · –

Table 5.4: Optimised constants for the temperature dependent binary interaction parameters for PR-vdW EoS model for isobutane + H_2

Model	Parameter	c_1	c_2	c_3
PR-vdW	k_{ij}	3.07×10^{0}	-1.00×10^{-2}	-7.71×10^{-6}
	l_{ij}	5.61×10^{-1}	-2.12×10^{-3}	-

5.2.3 Critical behaviour

The binary mixture of isobutane + H_2 was found to unambiguously display type III/1$^{C}X^{X}$ phase behaviour, as could reasonably be expected for a mixture of such dissimilar molecules [325]. The mixture critical loci can be seen to rise sharply from the critical point of isobutane, though its path at very high pressures is unknown. The melting line of isobutane, near to which the three phase vapour-liquid-solid equilibrium line is expected to follow if consistent with other hydrogen mixtures [420, 422, 425, 526], is far separated from the critical loci. It is perhaps unlikely that the two should ever meet, if so it would be at enormous pressure, however the critical loci may instead eventually turn back towards higher temperatures, as is known to occur for other type III mixtures [218, 324, 419]. Prediction of the phase behaviour in regions so detached from experimental data is challenging, and the cubic equations of state used in this work may not be capable of describing some aspects of it [566], though alternative models such as Carnahan-Starling-type, and (beyond it) SAFT-type, equations of state may overcome this issue.

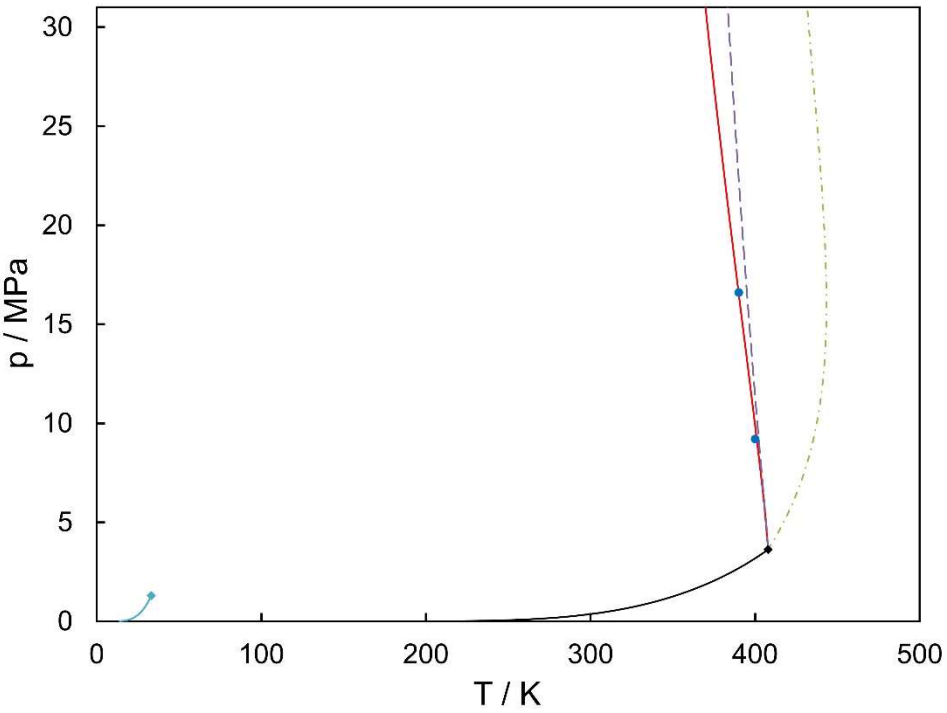


Figure 5.4: pT diagram for isobutane + H_2, showing the vapour curves of pure isobutane — and H_2 — predicted by the EoS of Bücker & Wagner and of Leachman et al, the critical points of pure isobutane ◆ and H_2 ◆, the experimentally estimated mixture critical points ●, and the mixture critical loci predicted by PR-vdW —, EPPR78 – –, and GERG-2008 – · –

Critical scaling laws were applied in order to determine the critical point at (390 and 400) K, given in Table 5.5, using the following equation [567] for binary mixtures:

$$z_1 = z_{1,c} + \left(\lambda_1 + \varepsilon\frac{\lambda_2}{2}\right)(p_c - p) + \varepsilon\frac{\mu}{2}(p_c - p)^{\beta} \qquad (5.2)$$

where z_1 is the mole fraction of H_2 in the liquid, where $\varepsilon = 1$, or vapour, where $\varepsilon = -1$, p is the pressure, $z_{1,c}$ is the critical composition, p_c is the critical pressure, $\beta = 0.325$, and λ_1, λ_2, and μ are scaling parameters. $z_{1,c}$, p_c, λ_1, λ_2, and μ have been described as a linear function of temperature, in order to allow for the calculation of $(\partial z_i/\partial T)$ in the combined composition uncertainties, according to the equation:

$$M = a_{M,1} + a_{M,2}\left(T / K\right) \tag{5.3}$$

where M stands for $z_{1,c}$, p_c, λ_1, λ_2, or μ, while a_1 and a_2 are constants are regressed against experimental data by minimising the sum squared error in composition, the values of which are listed in Table 5.6.

Table 5.5: Estimated critical pressure, p_c, and composition, $z_{1,c}$, for [H_2 (1) + isobutane (2)] at experimental temperatures, T

T / K	p_c / MPa	$z_{1,c}$
390.003	16.598	0.3829
399.986	9.191	0.2153

Table 5.6: Values of the parameters used in the determination of critical points using the critical scaling laws and estimation of near critical uncertainties

Parameter	a_1	a_2
λ_1	4.58×10^{-1}	-1.20×10^{-3}
λ_2	-2.24×10^{-1}	5.79×10^{-4}
μ	-2.51	5.96×10^{-3}
$z_{1,c}$	6.92	-1.68×10^{-2}
p_c	305.44	-7.41×10^{-1}

The points at 9.18 MPa for the 400 K isotherm were initially excluded from the parameter fitting as both ROLSI valves had sampled the same phase and it was not certain if the system was still in the two phase region. These points were found to lie almost exactly on the curve predicted by the equations, as can be seen in Figure 5.5 and so were ultimately included in the fitting, to minimal effect. The quality with which the critical scaling laws could be aligned with the near critical data is taken as an indication that the data in this region are thermodynamically consistent and self-consistent.

The most fascinating result of the investigation of isobutane + H_2 was only observed after publication of the main results, a fitting demonstration of how challenging it can be to ensure that a phase space has been fully explored (even when modelling). The PR-vdW parameters optimised in the work predict a temperature minimum in the critical curve. This had not been noticed originally, despite interest in the potential occurrence, as a result of the choice of flash algorithm; while most of this work used *pT* flashes, comparisons in Clapeyron used *Tx* flashes which struggled with the inflection points in composition as a function of pressure.

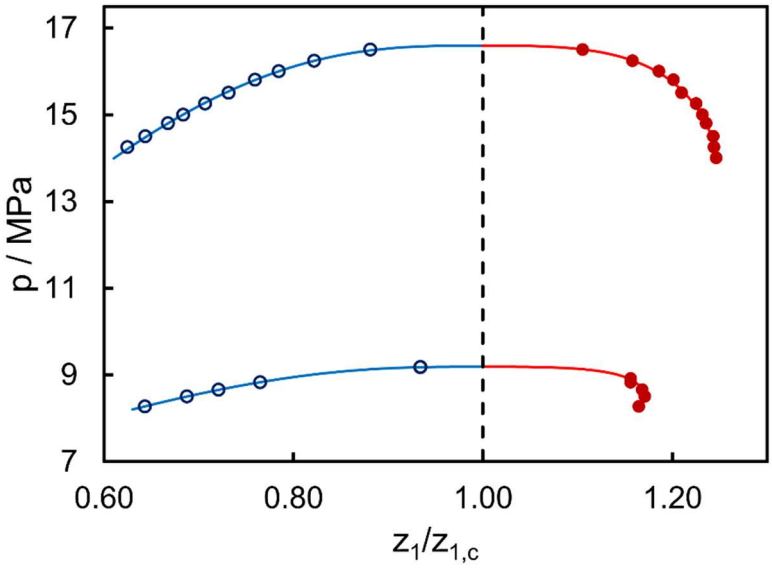


Figure 5.5: Near critical region of [H_2 (1) + isobutane (2)] at (390 and 400) K in terms of the pressure p and reduced critical composition $z_1/z_{1,c}$, showing the predictions of the scaling law — as well as the experimental data for the liquid ○ and vapour ● compositions

The mixture critical curve predicted by the optimised PR-vdW model, when extended to higher pressures than were investigated experimentally (by an order of magnitude), displayed the trend shown in Figure 5.6. The prediction of a temperature minimum itself is not surprising, as has been alluded to in the general discussion of hydrogen mixtures, however this is followed shortly by pressure maximum and, further along, by a pressure minimum (albeit at temperatures beyond those used in optimisation, *ie* T > 400 K). At first glance, the critical curve predicted looks much like a mixture isopleth that has been mirrored horizontally.

The predicted behaviour is unusual, discussion of such behaviour was not found in the literature. That no such behaviour has been observed or described for any binary mixtures cannot be said with certainty, however the extensive search of hydrogen binaries specifically is considered exhaustive. The critical curve is continuous, such that it is topologically identical to any other type III mixture, though the region persisting to high temperatures and pressures appears almost like the intersection of a normal type III or $1^{C}X^{X}$ critical curve (tending to high pressures) with a u type (per the Bolz classifications) critical curve descending from high pressures. Further work will be required to ascertain if this prediction is plainly unphysical. Cursory examinations of the properties predicted under these conditions found no obvious signs of unphysicality, for instance the molar volumes did not excessively encroach on the co-volumes (though this is for the vdW rule with $l_{ij} \neq 0$). To assess the validity of the behaviour with low uncertainty will most likely require the renewal of hydrogen fluid phase behaviour research at pressures in excess of 100 MPa, largely abandoned in the years following the works of Streett and coworkers. That said, there is little reason not to pursue such measurements regardless of this observation; for instance, the pressures are not far beyond those seen in H_2 pipelines or when allowing liquid hydrogen to heat isochorically.

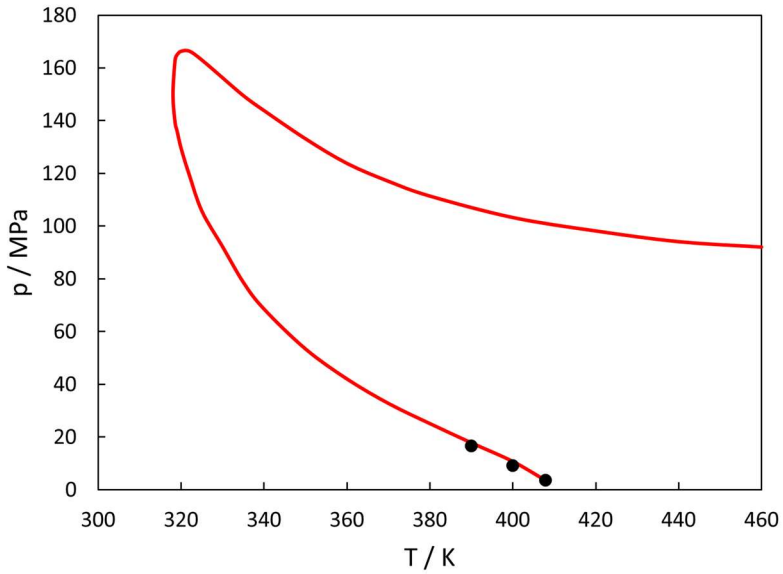


Figure 5.6: pT projection of the mixture critical curve – for isobutane + H_2 predicted by the PR-vdW EoS using BIPs optimised against the experimental data up to 20 MPa, including the isobutane critical point and the two experimentally estimated mixture critical points ●

Given that research into the behaviour of hydrogen-containing solids (primarily hydrogen clathrates) is a field of active investigation, typically at pressures in excess of 1 GPa and with high uncertainties (especially in pressure and composition), it appears not only reasonable but also necessary to examine the fluid phase behaviour up to such pressures. It is unclear from the literature if such research has been neglected for some intentional (albeit perhaps no longer justifiable) reason or if it has stalled due to the more/some practical realities of research. It is evident that research from the time of Kay and contemporaries was driven by practical process development needs for the petrochemical industry, with ancillary curiosity about behaviour in regions of the phase space yet to be explored spurred by the recent developments in the behaviour of nitrogen + ammonia, the first practically demonstrated type III mixture [185]. The rapidly growing scale of petrochemical usage, prompting studies of common industrial mixtures, then coupled well with the period wherein researchers like Streett and Brunner placed much attention in extension of data to high pressures.

Attention appears to have since diverged, partly going to high pressure solid phase behaviour (*eg* with diamond anvils), though otherwise simply ceasing out of sight. The growing importance of in hydrogen in the net zero transition will certainly spur new studies (as it did with this work), however the time taken to foster interest and conduct experiments remains a significant hurdle. Given the harsh constraints and wide ranging knowledge gaps, it would be pertinent to address the nascent known unknowns and regions with potential for unknown unknowns preferentially. It will not be possible to appreciate the space within which process engineering problems can be solved without this.

5.3 Methanol + CO_2

5.3.1 Experimental Results

The phase behaviour of methanol + CO_2 was investigated at five temperatures: (230, 240, 250, 273.15, and 298.15) K, with data tabulated in Table 5.7 and shown graphically in Figures 5.7 and 5.8. Data is provided only for the liquid phase, as the fraction of methanol in the vapour is nearly zero while the measurement uncertainty resulting from the adsorption of methanol is significant. Attempts were made to measure the vapour composition at T = 298.15 K, where the methanol fraction was at its highest of the all the measured temperatures, and samples were occasionally withdrawn at the lower temperatures to confirm that the vapour was still present. Ultimately there was insufficient value to these measurements, as several sets of literature data were available and, more importantly, model predictions under these conditions are accurate. The liquid phase composition was of much greater value, as the behaviour in this region is difficult to capture and the disagreements in the literature prevent accurate model optimisation.

Comparisons to literature data are also shown in Figures 5.7 and 5.8. Data at temperatures within ± 3 K have also been included in Figure 5.7 to supplement the data scarcity at low temperatures, though caution should be taken to infer too much from those comparisons as the bubble curve shifts rapidly with temperature under those conditions. In general, there are substantial disagreements between the numerous literature sources, though the trends are consistent for all (at least, for datasets of non-trivial size). At temperatures near and below the critical temperature of CO_2 the liquid curve has two distinct regimes. At low pressures, starting from the saturated vapour pressure of methanol, the composition is a roughly linear function of pressure, close to the behaviour of Henry's law. More complex behaviour is seen at high pressures, near to the saturated vapour pressure of CO_2 (or the CO_2 widom lines for supercritical temperatures), with the curve flattening significantly, before increasing in slope for $x_{CO2} \geq 0.9$.

Table 5.7: Experimental phase behaviour data for [CO_2 (1) + methanol (2)], the temperature, T, pressure, p, liquid, x_1, compositions, their standard uncertainties, $u(x_1)$, and their combined standard uncertainties, $u_c(x_1)$

T / K	p / MPa	x_1	$u(x_1)$	$u_c(x_1)$
298.151	6.106	0.9410	4.50×10^{-4}	2.80×10^{-3}
298.149	6.061	0.9286	5.37×10^{-4}	3.18×10^{-3}
298.152	6.007	0.8986	7.38×10^{-4}	4.38×10^{-3}
298.151	5.967	0.8752	8.85×10^{-4}	5.66×10^{-3}
298.153	5.939	0.8474	1.05×10^{-3}	7.60×10^{-3}
298.150	5.915	0.8188	1.20×10^{-3}	9.82×10^{-3}
298.149	5.892	0.7946	1.32×10^{-3}	1.12×10^{-2}
298.149	5.870	0.7725	1.42×10^{-3}	1.14×10^{-2}
298.149	5.849	0.7485	1.52×10^{-3}	1.05×10^{-2}
298.148	5.824	0.7274	1.61×10^{-3}	9.19×10^{-3}
298.147	5.799	0.7075	1.68×10^{-3}	7.85×10^{-3}
298.148	5.770	0.6880	1.74×10^{-3}	6.67×10^{-3}

T / K	p / MPa	x_1	$u(x_1)$	$u_c(x_1)$
298.148	5.739	0.6664	1.80×10^{-3}	5.59×10^{-3}
298.147	5.705	0.6474	1.85×10^{-3}	4.85×10^{-3}
298.142	5.668	0.6288	1.89×10^{-3}	4.29×10^{-3}
298.142	5.630	0.6139	1.92×10^{-3}	3.93×10^{-3}
298.143	5.590	0.5990	1.95×10^{-3}	3.63×10^{-3}
298.146	5.548	0.5822	1.97×10^{-3}	3.36×10^{-3}
298.149	5.503	0.5701	1.99×10^{-3}	3.20×10^{-3}
298.154	5.223	0.4972	2.02×10^{-3}	2.62×10^{-3}
298.155	5.192	0.4903	2.02×10^{-3}	2.59×10^{-3}
298.155	4.984	0.4560	2.01×10^{-3}	2.44×10^{-3}
298.155	4.772	0.4263	1.98×10^{-3}	2.33×10^{-3}
298.154	4.251	0.3724	1.89×10^{-3}	2.16×10^{-3}
298.156	3.902	0.3369	1.81×10^{-3}	2.04×10^{-3}
298.155	3.595	0.3058	1.72×10^{-3}	1.93×10^{-3}
298.154	3.297	0.2750	1.61×10^{-3}	1.81×10^{-3}
298.154	2.993	0.2487	1.51×10^{-3}	1.71×10^{-3}
298.155	2.696	0.2222	1.40×10^{-3}	1.59×10^{-3}
298.155	2.394	0.1960	1.28×10^{-3}	1.48×10^{-3}
298.155	2.120	0.1723	1.15×10^{-3}	1.36×10^{-3}
298.155	1.988	0.1608	1.09×10^{-3}	1.31×10^{-3}
298.154	1.794	0.1443	1.00×10^{-3}	1.23×10^{-3}
298.155	1.592	0.1274	9.00×10^{-4}	1.15×10^{-3}
298.154	1.419	0.1129	8.11×10^{-4}	1.08×10^{-3}
298.154	1.214	0.0961	7.04×10^{-4}	1.00×10^{-3}
298.154	1.012	0.0804	5.99×10^{-4}	9.36×10^{-4}
298.154	0.910	0.0734	5.51×10^{-4}	9.08×10^{-4}
298.155	0.807	0.0631	4.79×10^{-4}	8.71×10^{-4}
298.154	0.705	0.0580	4.43×10^{-4}	8.54×10^{-4}
298.155	0.604	0.0503	3.87×10^{-4}	8.31×10^{-4}
298.155	0.503	0.0446	3.45×10^{-4}	8.16×10^{-4}
273.141	3.412	0.9832	1.34×10^{-4}	6.80×10^{-3}
273.142	3.396	0.9656	2.69×10^{-4}	7.69×10^{-3}
273.137	3.374	0.9321	5.13×10^{-4}	9.93×10^{-3}
273.147	3.355	0.9121	6.49×10^{-4}	1.17×10^{-2}
273.149	3.342	0.8772	8.72×10^{-4}	1.56×10^{-2}
273.152	3.341	0.8803	8.53×10^{-4}	1.52×10^{-2}
273.150	3.326	0.8445	1.06×10^{-3}	2.01×10^{-2}
273.152	3.313	0.8104	1.24×10^{-3}	2.38×10^{-2}
273.154	3.298	0.7804	1.39×10^{-3}	2.42×10^{-2}
273.157	3.282	0.7438	1.54×10^{-3}	2.06×10^{-2}
273.157	3.265	0.7114	1.66×10^{-3}	1.60×10^{-2}
273.147	3.221	0.6628	1.81×10^{-3}	1.05×10^{-2}
273.148	3.100	0.5706	1.98×10^{-3}	5.31×10^{-3}
273.153	2.992	0.5209	2.02×10^{-3}	4.12×10^{-3}
273.155	2.845	0.4698	2.02×10^{-3}	3.39×10^{-3}
273.144	2.688	0.4244	1.98×10^{-3}	2.98×10^{-3}

T / K	p / MPa	x_1	$u(x_1)$	$u_c(x_1)$
273.148	2.535	0.3858	1.92×10^{-3}	2.71×10^{-3}
273.150	2.398	0.3587	1.86×10^{-3}	2.56×10^{-3}
273.152	2.277	0.3374	1.81×10^{-3}	2.44×10^{-3}
273.155	2.092	0.3042	1.71×10^{-3}	2.28×10^{-3}
273.162	1.125	0.1675	1.13×10^{-3}	1.67×10^{-3}
273.167	1.019	0.1520	1.04×10^{-3}	1.61×10^{-3}
273.161	0.915	0.1376	9.61×10^{-4}	1.55×10^{-3}
273.163	0.813	0.1216	8.65×10^{-4}	1.50×10^{-3}
273.165	0.711	0.1056	7.65×10^{-4}	1.46×10^{-3}
273.169	0.608	0.0901	6.64×10^{-4}	1.42×10^{-3}
273.171	0.506	0.0738	5.54×10^{-4}	1.40×10^{-3}
250.014	1.751	0.9563	3.38×10^{-4}	2.12×10^{-2}
250.013	1.745	0.9268	5.49×10^{-4}	2.83×10^{-2}
250.013	1.739	0.8901	7.92×10^{-4}	4.12×10^{-2}
250.014	1.736	0.8566	9.95×10^{-4}	5.54×10^{-2}
250.016	1.731	0.8287	1.15×10^{-3}	6.37×10^{-2}
250.016	1.726	0.8022	1.29×10^{-3}	6.28×10^{-2}
250.017	1.722	0.7760	1.41×10^{-3}	5.41×10^{-2}
250.014	1.715	0.7516	1.51×10^{-3}	4.36×10^{-2}
250.001	1.708	0.7287	1.60×10^{-3}	3.46×10^{-2}
250.007	1.701	0.7106	1.67×10^{-3}	2.87×10^{-2}
250.004	1.687	0.6745	1.78×10^{-3}	2.02×10^{-2}
250.005	1.672	0.6447	1.86×10^{-3}	1.55×10^{-2}
250.006	1.602	0.5542	2.00×10^{-3}	8.22×10^{-3}
250.006	1.568	0.5270	2.02×10^{-3}	7.10×10^{-3}
250.007	1.530	0.4981	2.02×10^{-3}	6.18×10^{-3}
250.009	1.403	0.4307	1.99×10^{-3}	4.76×10^{-3}
250.007	1.313	0.3877	1.92×10^{-3}	4.18×10^{-3}
250.009	1.220	0.3533	1.85×10^{-3}	3.81×10^{-3}
250.008	1.112	0.3163	1.75×10^{-3}	3.49×10^{-3}
250.010	1.051	0.2959	1.69×10^{-3}	3.34×10^{-3}
250.008	0.931	0.2592	1.56×10^{-3}	3.10×10^{-3}
250.011	0.811	0.2256	1.41×10^{-3}	2.91×10^{-3}
250.013	0.710	0.1969	1.28×10^{-3}	2.78×10^{-3}
250.012	0.659	0.1809	1.20×10^{-3}	2.71×10^{-3}
250.013	0.607	0.1685	1.14×10^{-3}	2.66×10^{-3}
250.013	0.557	0.1539	1.05×10^{-3}	2.62×10^{-3}
250.013	0.505	0.1392	9.71×10^{-4}	2.58×10^{-3}
239.997	1.257	0.9234	5.73×10^{-4}	4.80×10^{-2}
239.997	1.253	0.8932	7.72×10^{-4}	6.45×10^{-2}
239.997	1.252	0.8568	9.94×10^{-4}	8.47×10^{-2}
239.998	1.249	0.8279	1.15×10^{-3}	9.05×10^{-2}
240.001	1.246	0.7992	1.30×10^{-3}	8.19×10^{-2}
240.000	1.243	0.7757	1.41×10^{-3}	6.85×10^{-2}
240.000	1.239	0.7516	1.51×10^{-3}	5.44×10^{-2}
240.001	1.228	0.7145	1.65×10^{-3}	3.74×10^{-2}

T / K	p / MPa	x_1	$u(x_1)$	$u_c(x_1)$
239.999	1.208	0.6472	1.85×10^{-3}	2.03×10^{-2}
239.999	1.158	0.5642	1.99×10^{-3}	1.14×10^{-2}
240.000	1.105	0.5059	2.02×10^{-3}	8.40×10^{-3}
240.002	1.014	0.4443	2.00×10^{-3}	6.52×10^{-3}
240.003	0.948	0.3928	1.93×10^{-3}	5.50×10^{-3}
240.003	0.880	0.3582	1.86×10^{-3}	5.00×10^{-3}
240.003	0.803	0.3222	1.77×10^{-3}	4.58×10^{-3}
240.003	0.758	0.2995	1.70×10^{-3}	4.36×10^{-3}
240.003	0.672	0.2623	1.57×10^{-3}	4.06×10^{-3}
240.004	0.584	0.2300	1.43×10^{-3}	3.85×10^{-3}
240.004	0.512	0.1993	1.29×10^{-3}	3.69×10^{-3}
230.008	0.875	0.9572	3.32×10^{-4}	5.71×10^{-2}
230.009	0.869	0.9194	6.00×10^{-4}	1.03×10^{-1}
230.008	0.875	0.8581	9.86×10^{-4}	1.98×10^{-1}
230.009	0.874	0.8291	1.15×10^{-3}	1.70×10^{-1}
230.010	0.872	0.7996	1.30×10^{-3}	1.19×10^{-1}
230.011	0.870	0.7741	1.42×10^{-3}	8.47×10^{-2}
230.010	0.868	0.7515	1.51×10^{-3}	6.38×10^{-2}
230.011	0.859	0.7230	1.62×10^{-3}	4.64×10^{-2}
230.010	0.853	0.6810	1.76×10^{-3}	3.13×10^{-2}
230.010	0.846	0.6609	1.82×10^{-3}	2.67×10^{-2}
230.010	0.810	0.5779	1.98×10^{-3}	1.58×10^{-2}
230.010	0.792	0.5535	2.00×10^{-3}	1.40×10^{-2}
230.010	0.772	0.5349	2.02×10^{-3}	1.29×10^{-2}
230.013	0.661	0.4024	1.95×10^{-3}	8.22×10^{-3}
230.013	0.613	0.3645	1.88×10^{-3}	7.49×10^{-3}

Standard uncertainties are $u(T)$ = 0.006 K, $u(p)$ = 0.009 MPa

At T = 298.15 K, the experimental data is consistently within the scatter of the literature data, as is visible in Figure 5.8. For T = (230 to 273.15) K, shown in Figure 5.7, the data is in close agreement with the (admittedly scant) literature in the high pressure regime, however, the liquid phase was consistently richer in CO_2 compared to literature at lower pressures (or conversely, the bubble pressure was lower in this work for given composition). This not immediately apparent from Figures 5.7a-c, as the data in the lower pressure regime are consistently for temperatures (1 to 3) K lower than in this work, while it is pronounced in Figure 5.7d as the majority of the data are within 0.5 K.

The discrepancy is consistent with the presence of likely impurities in the “pure” components used by literature studies: water and “permanent” gases (note that this is a historical term which has since lost its literal interpretation) such as hydrogen, nitrogen, carbon monoxide, or methane. Great care was taken when handling the “pure” components used in this work, data were found to be consistent across two batches of methanol (of certified purity) from different suppliers, and no likely impurities would cause the differences observed should they have been present during the measurements in this work. As such, it is deemed likely that the disagreement originates with the literature datasets (themselves frequently disagreeing, providing further credence). There is a non-zero possibility that a systematic deviation in

measured pressure and/or composition in this work could instead be responsible, however, this is deemed unlikely as it is inconsistent with observations in the measurement of other mixtures (such as isobutane + CO_2) and the calibration procedure was rigorous and of low uncertainty (and the calibration measurements were self-consistent across broad ranges of composition and sample size). Furthermore, the many of the literature studies are old and lacking detailed experiment uncertainty analysis; many of the newer literature studies were simply performing short campaigns to validate an apparatus against methanol + CO_2 and have high uncertainties [405, 408, 409]. This work finds that most such validations should be deemed invalid and that they contribute to a cycle in which the presence of many (low quality) measurements promotes further low quality measurements, cluttering the literature and hindering process development. A tendency of works featuring such “validations” to only compare their data to less than 10% of the available literature data [408, 409], with no acknowledgement or justification of the narrow selection, is noted. Future works seeking to validate an apparatus and/or methodology must be rigorous in doing so; the presence of thorough open-access works (now including this work) featuring low uncertainty measurements and detailed reviews of the literature leaves no excuse for such a lack of rigor.

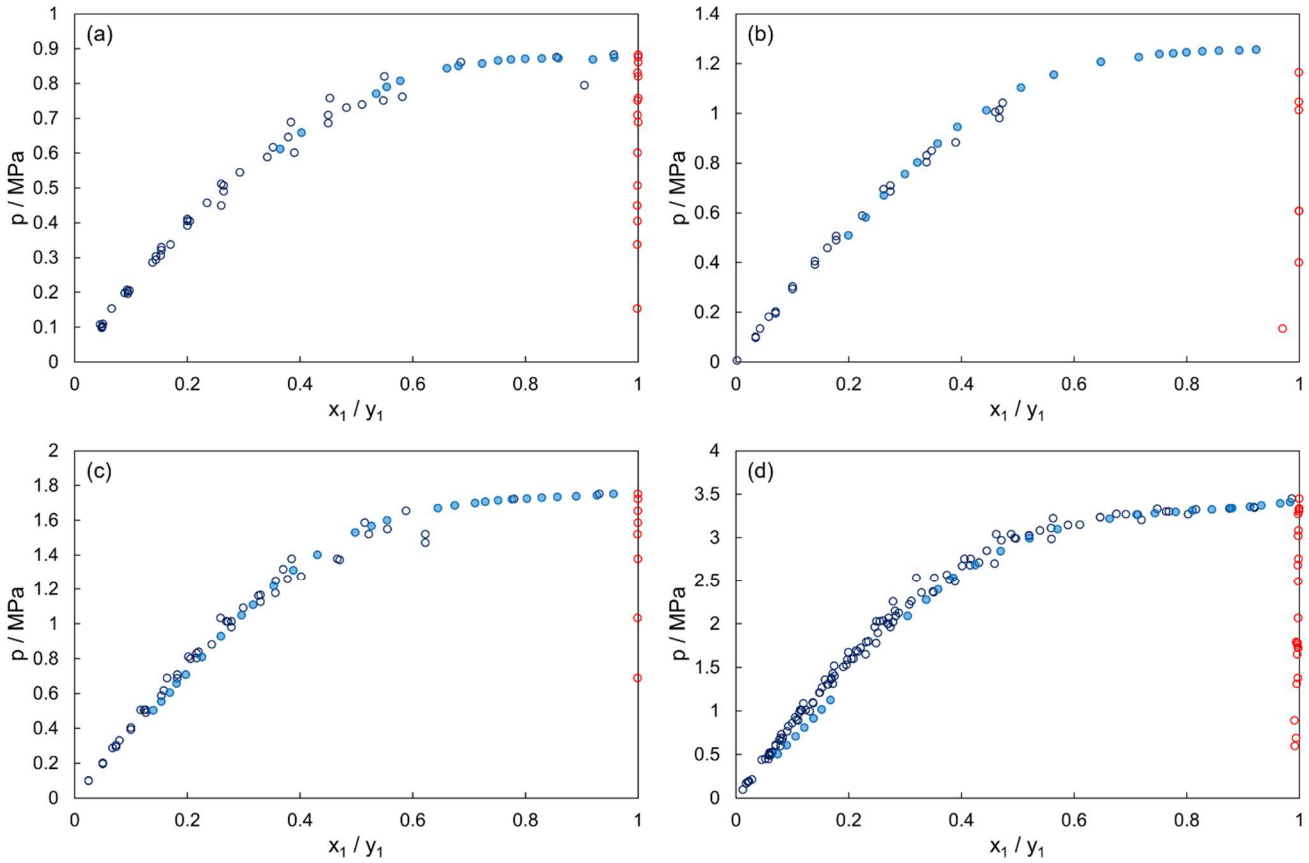


Figure 5.7: pxy diagrams for [CO_2 (1) + methanol (2)] at temperatures of (a) (228 to 231) K, (b), (237 to 242) K, (c) (247 to 251) K, (d) (272 to 274) K, showing the experimental data from this work ●, as well as the values available in literature ○/○

For reference (and to recap), to produce data on methanol + CO_2 of sufficiently low uncertainty to be worth publishing, presented herein, required: years of work dedicated to this specific mixture, exploration of several potential calibration techniques, development of novel

calibration equations, strict “pure” component handling (and batch/supplier comparisons), thorough heating and passivation of sample-facing surfaces, abandonment of vapour measurements (where y_{meoh} < 0.01), and layers of validation. This validation included: measurements of related systems with multiple agreeing low uncertainty datasets available in the literature (both when the apparatus was originally constructed, with CO_2 + N_2, and upon the initiation of this work, with isobutane + CO_2), reproducible measurements of synthetic single-phase mixtures of known composition with the exact same sampling approach used in the primary measurements (originally gas phase mixtures but, in this work, extended to liquid phase mixtures), detailed evaluation of the validity of the theory associated with the composition measurement method, comparison to synthetic bubble point measurements made in the same apparatus, and periodic assessment of the PRT against the triple point of water followed by comparison of the pressure measurements against the vapour pressure of “pure” CO_2 across the fluid coexistence region (using the reverified PRT and an exceptionally low uncertainty EoS).

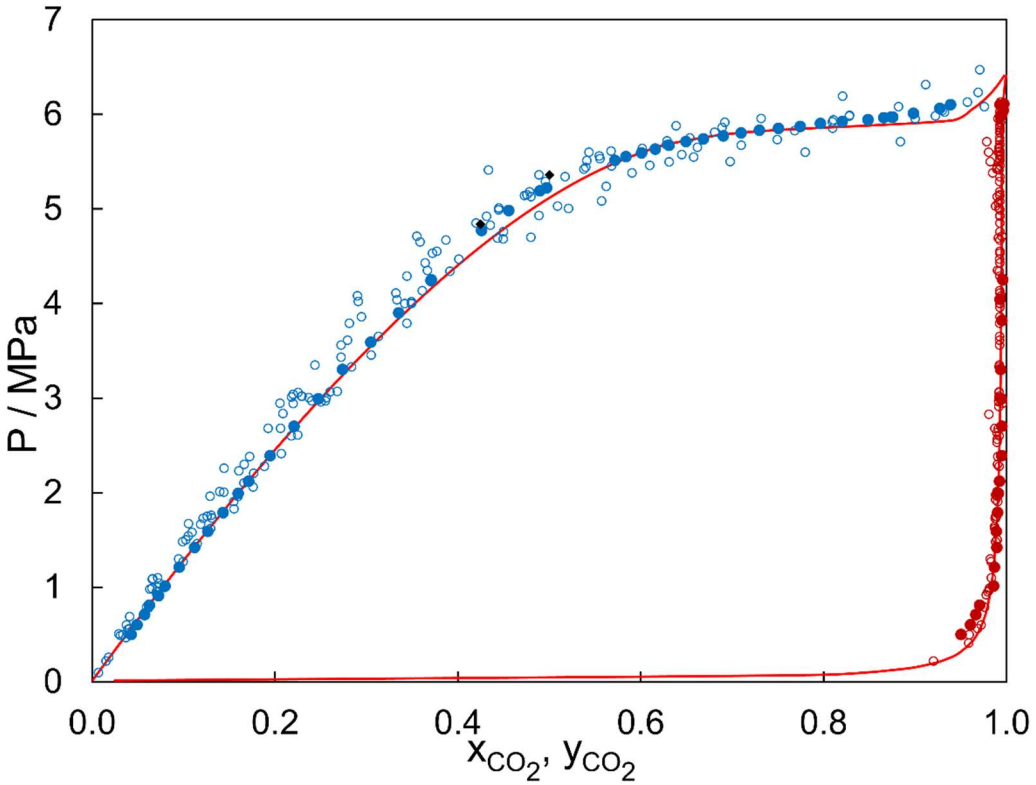


Figure 5.8: pxy diagrams for [CO_2 (1) + methanol (2)] at 298.15 K, showing the experimental analytical liquid ● and vapour ● data and synthetic ◆ data from this work, as well as the values available in literature ○/○, and the best fit obtained with PR-mWS-NRTL — (near to the limit where unphysical VLLE predictions appear). Please note that the vapour data shown were ultimately not included in the final dataset

The majority of studies utilising a synthetic technique report high temperature and/or pressure uncertainties [408, 409] (an order of magnitude higher than in this work, or greater). The majority utilising analytical techniques either take large samples (typically three to six orders of magnitude larger than in this work), disrupting equilibrium greatly, and/or (for those that also use chromatographic analysis) do not discuss the issues with methanol adsorption and/or

degredation [343, 405, 406]. There are some welcome exceptions, such as the work of Hong & Kobayashi [365], wherein the calibration was performed in such a way that adsorption, including possibly competitive adsorption, could be accounted for [568], though no details are provided for the impact this had for methanol + CO_2 specifically. Additionally, most studies utilising analytic techniques don't provide detailed information regarding calibrations, such as the calibration equation used and/or assessments of the deviations of the calibration equation from calibration measurements [343, 405, 406].

There is a gap between approximately (1 to 2) MPa for the 273.15 K isotherm in this work, though there is little deviation from linearity at these pressures and thus little impact on model optimisation. The data at higher pressures come from an earlier series of measurements, which, along with the T = 298.15 K isotherm, used the 99.75% methanol. The data at lower pressures having been produced in a later run, following the (230 to 250) K measurements, using the 99.9% methanol. More specifically, data produced using the purer methanol batch all used the same charge of methanol, helping to further ensure consistency (a benefit of the highly automated methodology). The data produced in this work are self-consistent across the temperatures measured and within each individual isotherm. Closely spaced measurements were made to demonstrate the low scatter, and repeats were made for approximately one third of the points (with minimal disagreement, thus the averages are reported). The lower operating limit for the sampling system (~0.5 MPa) was restrictive, especially at T = 230 K, however the relative flatness of the liquid curve meant measurements could be made across the majority of the composition range.

An important observation was that no evidence of liquid-liquid separation was observed, confirming long standing suspicions for which there had previously been insufficient supporting data. The liquid curve flattens significantly as temperature decreases, such that at T = 230 K it is horizontal within the uncertainty of the pressure sensor, though a monotonic increase in pressure with composition is still seen except for a single point (which differs by less than half the pressure uncertainty). This one exceptional point should not be taken to imply the possibility that LLE was likely encountered, it is simply a demonstration that the pressure uncertainty is not insignificant at low pressure (as expected for a pressure sensor designed for high pressure service), and indeed a similar (but less immediately apparent) deviation of approximately equal magnitude is also visible at p = 0.857 MPa. Note further that the method by which the measurements proceed and the accuracy with which the cell contents were known at this point are considered sufficient to render unlikely the possibility of having entered the required overall density and composition ranges to realise LLE. There remains a non-zero possibility that a (rather specific) combination of uncertainties and mixture behaviour would allow for LLE to have been theoretically by masked in practice by a single metastable liquid phase. This hypothetical disequilibrium liquid would need to have been metastable for a duration greater than (at least) two hours in the absence of stirring, and with minimal effect on temperature and pressure as it evolved (*eg* coalescing from nanodrops of one liquid suspended in the other). The likelihood that this occurred is believed to be negligible, especially when considering the overall trends (supported by the self-consistency of the data across all temperatures covered), but is noted for completeness. Furthermore, if an unusually metastable liquid phase were to be physical, then few applications (*eg* large scale static storage) would need be concerned about the eventual separation into two stable phases; for

instance, the residence times of fluids in separation units are well within the minimum metastable lifetime.

A span of ~13 K remains between the lowest temperatures measured in this work and the triple point temperature of CO_2, thus the possibility of a liquid-liquid separation in this region remains. It was not observed in the work that extended to temperatures below the triple point temperature of CO_2 [343], however that work lacks the required number of points in the region of interest to be conclusive by any means. Complex interactions, especially when considering potential association between methanol and CO_2 molecules, could contribute to such a separation being avoided. For yet greater confidence regarding the presence or absence of LLE, mixing enthalpies and free energy analysis could be investigated.

5.3.2 Volumetric Data

The preparation of synthetic mixtures in the cell during calibration inherently allowed for density measurements, though knowledge of the cell volume (not only the dead volumes) was of material importance for knowledge of the density. The calibration procedure allowed for measurements of the liquid density from the point of saturation and into the compressed liquid region. In this work, the capability to measure both saturated and compressed liquid density within a single calibration mixture preparation was not realised, however both were demonstrated individually. The combination was not demonstrated only because the capacity to do so with low uncertainty was not appreciated until the fourth calibration run, wherein the target composition required that the system start in the one phase region.

The volumes of the different sections of the sample containing volumes were regressed from measurements of the isothermal compressibility of CO_2 using the Isco pump. The overall sample volume was subdivided into the variable volume within the Isco pump, the (partially dead) volume at the head of the pump and the connections to the inlet and outlet valves, the volume beyond the outlet valve of the Isco pump leading to the valve to the cell and an outlet valve, the volume after the valve to the cell up to the end of the 1/32” tube within the cell, the internal volume within the cell (excluding the volume of the stirrer bar, 1/32” tube, and ROLSI capillaries), and the volume in the short section of 1/8” tubing and pressure fitting above the cell through which the 1/32” tube passed.

The volumes leading from the pump up to the valve to the cell could be physically subdivided and measured sequentially. The latter three volumes could not be isolated from each other, as such it was only possible to measure the combined volume, so the subvolumes were determined through computer-aided design (CAD) modelling. The sum of the estimated volumes was found to be in agreement with the measured total volume to within the measurement uncertainty and thus the estimated volumes were used. Rough assessment of the first of these volumes, terminating at the end of the 1/32” tube within the cell, was conducted by periodically sampling from the cell (initially filled with pure compressed liquid CO_2) while injecting methanol in a stepwise fashion. The appearance of methanol peaks within the sample chromatograms occurred as expected, and pressure and temperature changes in the cell were observed that further corroborated this. The cell pressure as a function of the

volume of methanol swept from the pump is presented in Figure 5.9. The second and third points are model calculations (shown in orange), assuming that no mixing occurs and that the methanol injected (up until the entire subvolume was filled) simply compressed the liquid CO_2, as the valve to the cell was closed after the first two methanol injections. This was necessary to minimise the risk of back-flow (and the impact of diffusion) and these injections needed to be sufficiently large as to sweep fluid with minimal mixing in the small volume within the valve.

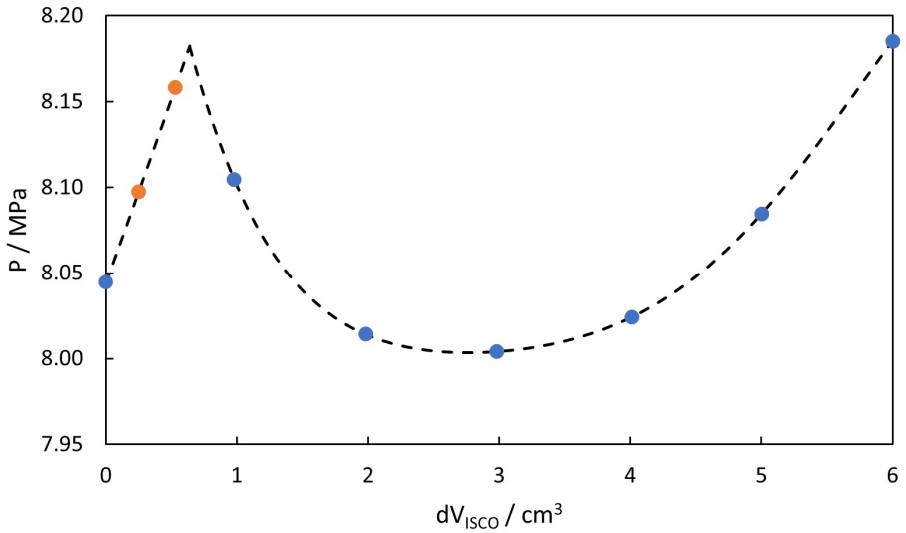


Figure 5.9: Cell pressure as a function of the volume of methanol swept by the pump, showing measured points ●, model calculations ●, and polynomial best fits – –

Conservative values for the uncertainties in the estimated volumes and for the values of ambient temperature were used, both for density measurements and in calculating calibration mixture compositions, as previously listed in Section 4.3.3. These conservative values may be reduced by a factor of two or more in future if further validation is conducted.

Table 5.8: Rough saturated liquid density data obtained in this work at T = 298.15 K

p / MPa	x_{CO2}	ρ_{sat} / (kmol/m^3)
4.77	0.4247	22.97
5.25	0.5002	22.63
5.61	0.6061	21.60

The saturated liquid densities were extracted from the data from synthetic mixture preparations made under flow, as such their quality is not reflective of the capabilities of the apparatus nor could a realistic uncertainty be quantified. However, they have been included for completeness and to supplement the scarce literature data, and are listed in Table 5.8. Minor adjustments to the procedure, such as the more standard approach involving discrete steps through volume or pressure, would yield notable improvements. It should be noted that stepping through pressure setpoints, with minimal changes to procedure, is complicated for mixtures like methanol + CO_2 as the cell pressure typically decreases upon the addition of methanol. The rough saturated liquid densities obtained were in agreement with the literature data, as shown in Figure 5.10, although there are substantial deviations between the three

(discounting the earlier version [377] of the dataset from Chang *et al*) literature sources [363, 383, 412] and the data of Benzanehtak *et al* [383] show significant scatter.

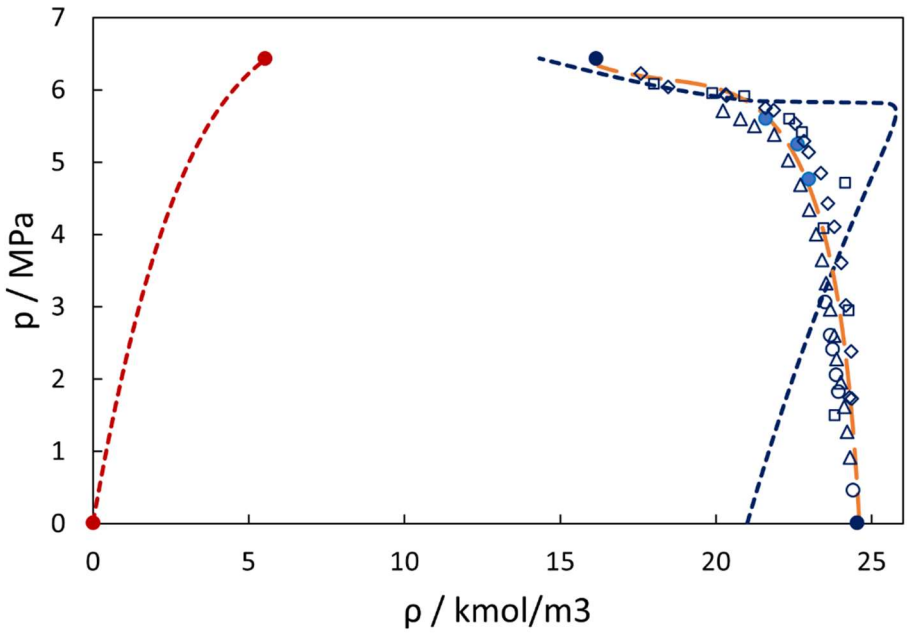


Figure 5.10: Saturated liquid densities for methanol + CO_2 at T = 298.15 K, showing the pure component vapour ● and liquid ● densities, experimental measurements ●, literature data of Brunner [363], Chang et al [412], and Benzanehtek et al [383], and an example of typical PR-vdW model predictions –/– encountered during optimising only for pTxy data, in this case without volume translation to emphasise the difficulty in capturing liquid densities with cubic EoS (note that a prediction of liquid-liquid separation appears as a horizontal line). Also shown are the predictions of SAFT-γ-Mie – – using the literature parameters

Table 5.9: Low uncertainty compressed liquid density data obtained in this work at T = 298.15 K during preparation of the fourth synthetic calibration mixture, including the expanded (k = 2) uncertainties in composition and density, as well as relative expanded uncertainties for the latter

p / MPa	x_{CO2}	$U(x_{CO2})$	ρ_{CF} / (kmol/m^3)	$U(\rho_{CF})$ / (kmol/m^3)	$U_r(\rho_{CF})$ / %
8.10	0.9948	0.0020	17.837	0.050	0.283
8.01	0.9850	0.0019	18.014	0.050	0.278
8.00	0.9755	0.0019	18.190	0.050	0.273
8.02	0.9659	0.0019	18.370	0.049	0.268
8.08	0.9569	0.0019	18.544	0.049	0.264
8.19	0.9480	0.0019	18.718	0.049	0.260

The compressed liquid density measurements were conducted with greater intent and in a stepwise manner. The results are tabulated in Table 5.8 and shown in Figure 5.11. The densities expected in the case of ideal mixing (*ie* a linear transition between the densities of the pure components) are also shown, though it should be noted that they do not immediately appear to be linear as the pressure is not constant. There are no literature data sources for methanol + CO_2 compressed liquid densities available for comparison at 298.15 K, with the

closer proximity of the few literature data to the critical point of CO_2 presenting a significant barrier to comparison by extrapolation or thermodynamic modelling. Significant clustering effects were observed in molecular dynamic studies at those higher temperatures for CO_2-rich mixtures [393, 413], thus the new data generated here may help to extend and assess such molecular-scale behaviours to lower temperatures.

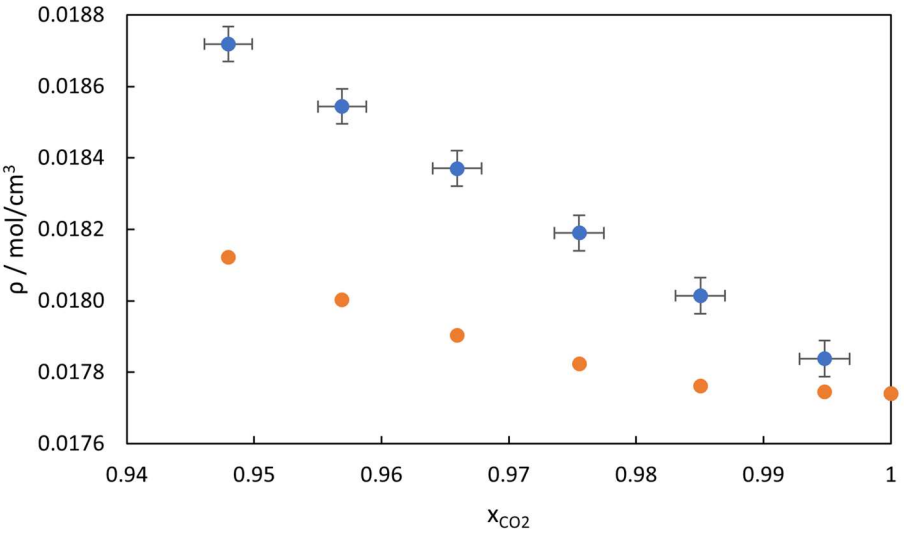


Figure 5.11: Density of compressed liquid methanol + CO_2 against composition during cell filling at T = 298.15 K, showing measured densities ● (with expanded (k = 2) uncertainties) and the densities expected in the case of ideal mixing ●

The ability to obtain density measurements, like those presented, effectively for free alongside low uncertainty calibrations, which may themselves simply be the final step in an automated sequence progressing through an isotherm (or through the phase space via more complex vectors), is inviting. The uncertainties are not as exemplary as are achievable with vibrating tube densimeters [569], however they remain of high quality. Minor modifications to operating procedure and/or hardware (especially regarding dead volumes), effectively extending the developments made thus far, could reasonably be expected to reduce uncertainties by a factor of two or greater. Furthermore, in light of the data shortcomings pervading industrially relevant mixtures, an opportunity to generate additional data that is unlikely to ever be redundant should not be overlooked.

5.3.3 Modelling Results

The modelling of methanol + CO_2 presented a significant challenge, most notably in relation to avoiding the prediction of unphysical liquid-liquid separations. The significant asymmetry and presence of association, both the certain self-association of methanol and the possible cross-association with CO_2, are difficult to capture in models.

Meaningful quantification of model performance was also especially difficult for this mixture. The near flat regions of the bubble curve cause the difference between assessing error in composition and in pressure to be more pronounced. The occurrence of LLE further

exacerbates differences and difficulties, including in how to penalise unphysical LLE predictions and to what extent. Comparisons of the error between different isotherms is also challenging, as isotherms with few points (especially when they are in the low pressure regime/region) can achieve extremely low errors on a per point basis (as with similar bases) while not necessarily being consistent with the overall trends. Any isotherm with more than one dataset typically contains non-negligible disagreement and scatter, such that an error metric will be unusually higher than the same metric for an isotherm with only a single dataset (despite the fact that isotherms with multiple datasets are typically, but not exclusively, more reliable), even a very good fit could be obtained for the datasets individually. At temperatures near or below the critical temperature of CO_2 there are, with the addition of the data produced in this work, sufficiently reliable and closely spaced data to get a clear picture of the expected behaviour and the behaviour of regions of the BIP space with respect to temperature, whereas at higher temperature the greater spacing and scatter increase uncertainties.

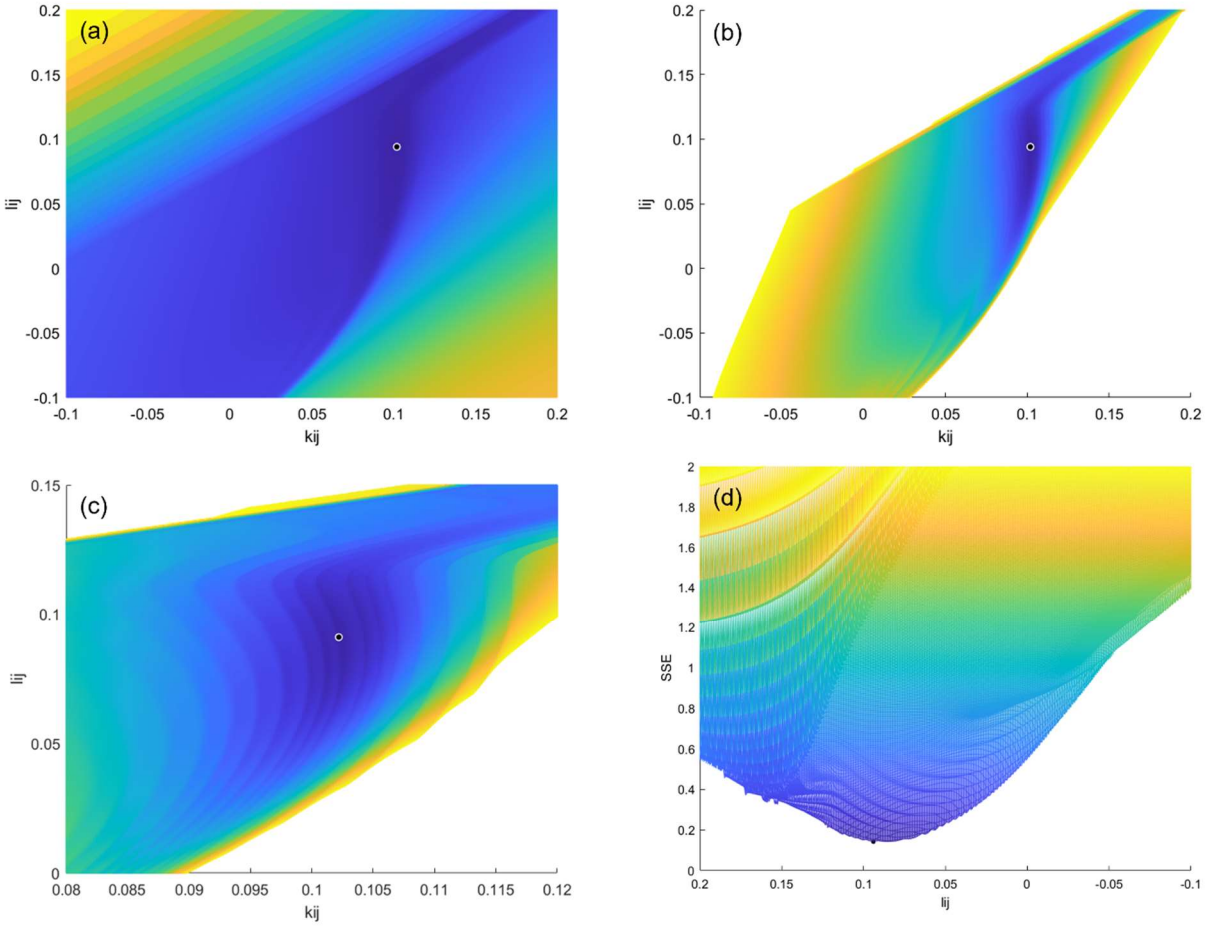


Figure 5.12: Parameter space for PR-vdW at T = 298.15 K when minimising the sum squared error in composition against the data produced in this work, shown as (a-c) an error heatmap increasingly focussed on the near-optimal region and (d) projected l_{ij} – error plane, with multiple local minima visible. Regions of lower error are shown in dark blue (note colour bars are excluded as relative values are of greater importance here) and the located minimum ● is indicated

The PR-vdW model was simplest to optimise, as seen with the other mixtures, and benefitted further now from grid searching. Grid searching revealed features of the error surface/space that explained some of the difficulties experienced when using the non-linear GRG algorithm. There were frequently many local minima present, as can be seen in Figure 5.12d, with local minima with respect to k_{ij} being more common than with l_{ij}. It was observed that the number of local minima depended greatly on resolution, and certain resolutions would produce many more minima with respect to l_{ij} especially. This would create a problem for optimiser/solver algorithms that will encounter or avoid local minima unpredictably; consistent with the repeatedly observed failure of the non-linear GRG algorithm to locate the near optimal solutions (which might be found quickly with grid searching).

Even when high resolutions and strict convergence tolerances were used, multiple ridges/waves would be observed in the parameter/error space, as shown in Figures 5.12a-c. Note that the heatmap is effectively a phase diagram when the error values are neglected, with regions without values representing the single-phase states. These appear to correspond in some cases to the intersection of the predicted liquid curve with an experimental datapoint, and in some cases the region in which a point ceases to converge properly (and has an effect regardless of whether one considers total or average errors). This behaviour is expected to be dependent on the mixture, experimental data, flash algorithm, and error assessment used; error calculations using orthogonal distance regression may potentially avoid some of these issues. It is noted that in all cases where a single self-consistent dataset was used, the ridges display shapes that resemble *pV* isotherms (as can be seen when viewing Figure 5.12c from its side), and vary in a way that appears consistent with the link of the (nominally dimensionless) BIP to the *a* and *b* terms in cubic EoS. If there is any meaning or benefit to this observation is unclear, though it appears to provide some indication of data self-consistency (appearing less clearly when data is more scattered).

It was consistently possible to locate the one apparent global minimum for a given temperature (though near-optimal local minima were common, as seen in Figure 5.12d). The optimal values of both k_{ij} and l_{ij} were found to be readily apparent functions of temperature, and varied significantly more at temperatures above the critical temperature of CO_2. The parameter l_{ij}, which is frequently neglected (*ie* set to zero or not included at all) was found to be consistently non-zero, except at one point where l_{ij} changes sign. The located optimal parameter values for each temperature group (sets of datapoints within ±0.5 K of each other) are shown in Figure 5.13, along with the optimised function of temperature. A quadratic function of temperature for both parameters was found to be sufficient to capture the behaviour to approximately the greatest extent possible, noting that the "optimal" performance is overall subpar by several metrics. Higher order polynomials encountered issues with the scatter of the literature data and, more critically, the relative lack of high temperature data. The parameters for the optimised polynomials for k_{ij} and l_{ij} are provided in Table 5.9 and comparison to the (230 to 298.15) K data from this work shown in Figure 5.13.

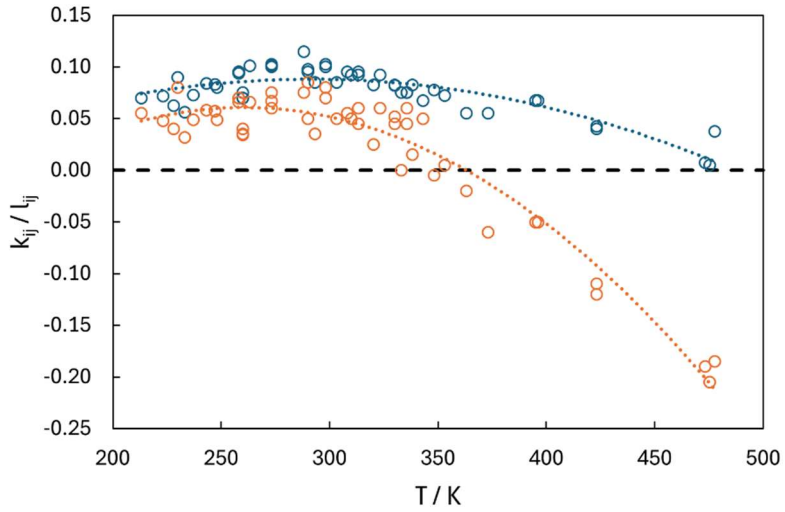


Figure 5.13: Optimal values of the BIPs k_{ij} ○ and l_{ij} ○ in the PR-vdW model as a function of temperature (for ~1 K groupings), showing the optimised polynomial functions of temperature ···/···. Note for T > 450 K there is an additional point where the (473.15 and 477.6) K data have been grouped together, to supplement the data scarcity and scatter in that region

Table 5.10: Optimised constants for the temperature dependent binary interaction parameters for the PR-vdW EoS for methanol + CO_2 across the entire temperature range

Model	Parameter	c_1	c_2	c_3
PR-vdW	k_{ij}	-1.99×10^{-2}	1.01×10^{-3}	-2.10×10^{-6}
	l_{ij}	-1.80×10^{-1}	2.50×10^{-3}	-5.64×10^{-6}

It was not possible to obtain any near-optimal fits for temperatures near or below the critical point temperature of CO_2 that did not involve a prediction of LLE. A good fit to the composition data in the low pressure regime was consistently achievable for a broad range of BIP values, though this is not an uncommon occurrence even for simple models and was not necessarily associated with good (or physical) behaviour at higher pressures. At temperatures above the critical temperature of CO_2, especially once more than approximately 20 K above it, the apparent quality of the predictions of PR-vdW increase significantly. The unphysical LLE disappears (though it was not possible to assess rigorously that it did not remain present at very high pressures) and the shape of the phase envelope can be captured adequately (especially given the experimental uncertainties/data shortcomings). This may relate to the lower liquid densities and weaker association at higher temperatures bringing the behaviour more in line with what the simple PR-vdW model is able to capture. Caution should be applied when using PR-vdW for this mixture (or similarly any model that may readily predict LLE) as different results may be obtained in regions near any potential predictions of LLE depending on the flash algorithm used (*eg pT* or *Tx* flashes, minimisation of Gibbs free energy or simply equality of fugacity) and strictness of convergence. The difficulty in obtaining acceptable results for composition meant that an accurate description of the liquid densities was effectively unachievable, regardless of any reasonable attempts to correct with a volume translation.

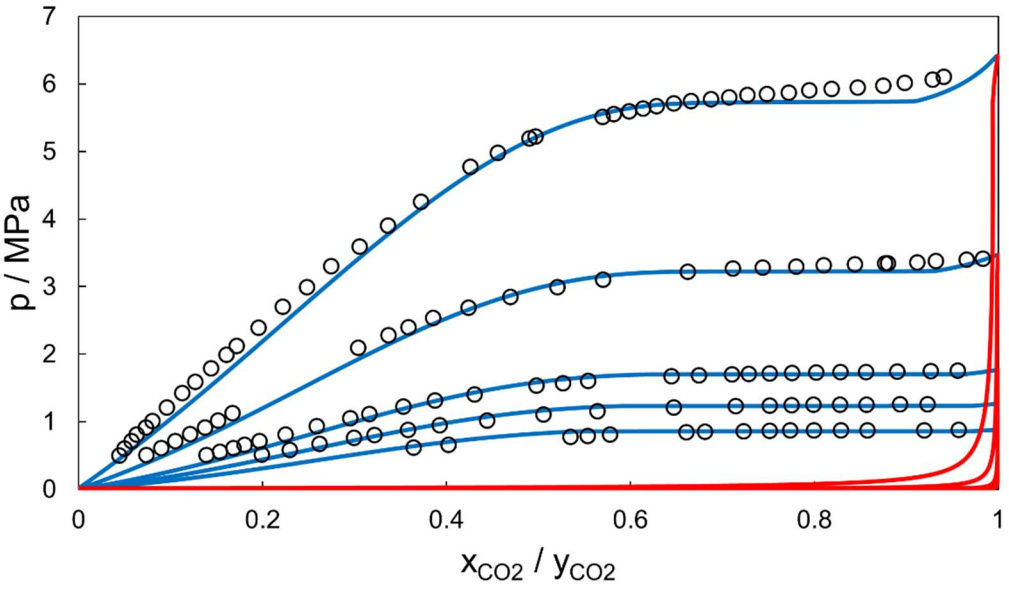


Figure 5.14: pxy diagram for methanol + CO_2 at (230 to 298.15) K, showing experimental data from this work O and predictions of PR-vdW –/–

The PR-mWS-NRTL model was found to produce significantly improved predictions, though it was challenging to fit as a result of its greater number of adjustable parameters. Focus was placed on the temperatures experimentally investigated in this work, where the greatest potential for meaningful improvements over PR-vdW was expected.

For positive values of α_{ij}, near-optimal results could be obtained by using PR-mWS-sNRTL in all cases examined. This approach, wherein k_{ij}, α_{ij}, and one of the τ_{ij} parameters would be adjusted, was found to outperform the standard approach in PR-mWS-NRTL where k_{ij} and both of the τ_{ij} parameters would be adjusted, with α_{ij} held constant at 0.3 (similar results were found for alternative values but not explored exhaustively). This result does not appear to be physically-based; instead, it is likely a result of accounting for shortcomings in the underlying theory of the model. The difference was less pronounced for negative values of α_{ij}, however these are generally less desirable as it is not known conclusively what broader effects the sign has on other (*eg* derivative) properties. The observation noted in literature [254, 255] that a non-randomness factor of negative one, plainly unsensible in the theoretical framework, can produce good results was consistent with observations both of this mixture and (cursory) analyses of other mixtures. A value of zero produced consistently poor results, as expected given the all-but-assured local composition heterogeneity when an associating component is present.

The best results with PR-mWS-NRTL were, unsurprisingly, obtained when simultaneously optimising all four BIPs. Clear improvements over PR-vdW were achievable, as was visible in Figure 5.8 for T = 298.15 K, compared to Figure 5.14. Notably, it was possible to obtain near-optimal results at low temperatures (such as 250 K) without the prediction of LLE, however the flash algorithm used made it challenging to penalise this prediction reliably. It would be simplest to obtain a polynomial function of temperature for k_{ij} and hold the other parameters constant (as can be done when parameters for NRTL are preexisting [217, 251], not the case

with CO_2). There is no theoretical basis for a requirement that α_{ij} and τ_{ij} do not vary with temperature, and in the case where association is present the opposite may be reasonably expected. The large parameter space and range of options for temperature-dependent BIP functions has prevented optimised functions being finalised at this time and is subject to future work.

For SAFT-γ-Mie (identical to SAFT-VR-Mie for this mixture, though the former term is used for consistency with the subsequent comparison) there were existing parameters available in the literature from the work of Papaioannou et al [570], which covered 9 groups generally, optimised parameters for 24 binary mixtures, and did not focus particularly on methanol + CO_2 (though it did illustrate the impressive capability of SAFT-γ-Mie to capture the density of pure methanol, rivalled only by multiparameter EoS). The unlike repulsive exponent λ^r_{kl} reported is unusually low compared to either of the pure components (43 % of λ^r_{kk} for methanol, 32 % of λ^r_{kk} for CO_2) and is an outlier compared to the other group interactions optimised in that work. Similarly, the unlike interaction energy parameter ε_{kl} was also lower than that of either of the pure components and low compared to other binary pairs, though to a lesser degree. The literature work considered the cross association of water and CO_2 (without allowing for unphysical self-association of CO_2) but did not include a similar cross association for methanol with CO_2, a phenomenon which is not well established to occur but would not be unreasonable given the similarity of methanol to water.

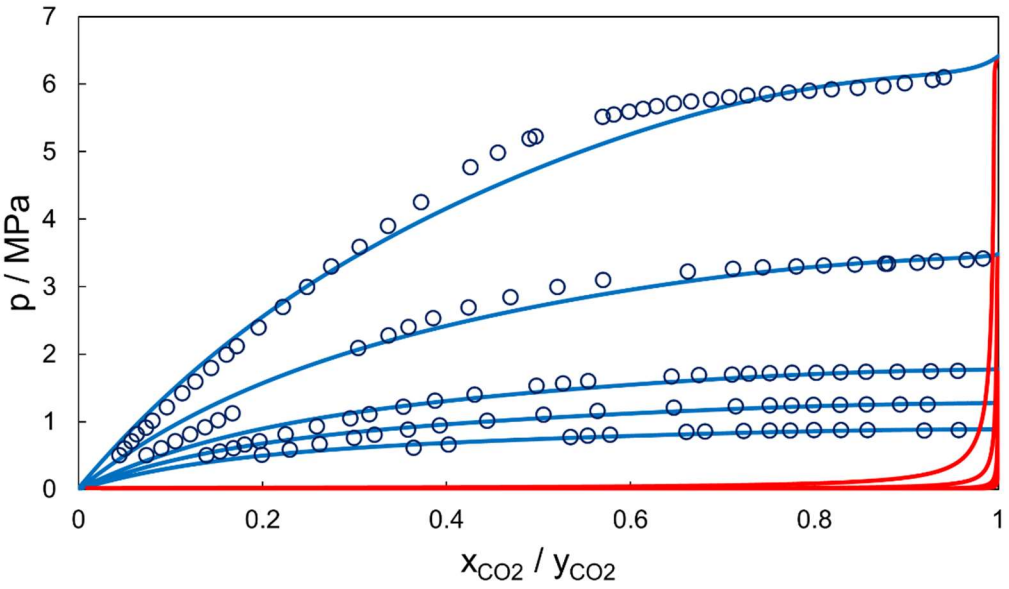


Figure 5.15: pxy diagram for methanol + CO_2 at (230 to 298.15) K, showing experimental data from this work O and predictions of SAFT-γ-Mie –/– when using literature unlike interaction parameters [570]

These literature parameter values were found to perform sub-optimally, but they do avoid any unphysical LLE predictions. The poor performance of this model, otherwise expected to perform well, coupled with shortcomings of the other models, promoted attempts to fit improved parameters in this work. Optimisation was based on a similar grid searching algorithm as used for the PR models. Significantly improved performance was possible; reductions in the sum squared error in pressure of (73 to 94) % were readily achievable at

temperatures between (230 and 273.15) K. Optimised parameters for this temperature range are given in Table 5.10. Note here the Clapeyron software was used for the modelling, which by default prefers *Tx* flashes, thus the convenient error metric to calculate is the (sum squared) error in pressure; somewhat inconvenient for direct comparisons with the PR models, however in many cases these metrics fail to fully capture qualitative behaviour (for instance whether or not LLE is predicted). A comparison at T = (230 to 273.15) K between the two parameter sets for SAFT-γ-Mie and the data generated in this work is shown in Figure 5.16. Convergence issues were encountered at 298.15 K and some higher temperatures; for this and other reasons further optimisation of SAFT-γ-Mie (*eg* across the entire coexistence region) was not pursued, but would make for valuable future work. It is noted that the parameter values provided in literature (and those in their vicinity) do not fail to converge at T = 298.15 K, so it is possible that similar convergence issues occurred in the original parameter fitting (hence the unusual values).

It was feasible to assess, at least to first approximation, whether LLE would be predicted with any particular set of parameters, by assessing the monotonicity of the liquid curve. This method is strictly only effective for connected regions of LLE, which is suitable for this case. The flash algorithm used in the SAFT calculations (a *Tx* flash) is better suited for this purpose, capable of more readily capturing the region the region of LLE and directly observing negative values of *dp/dx*, whereas the *pT* flashes typically at most show a horizontal region and *dp/dx* is not well behaved nor rigorously continuous. Furthermore, it was generally easier to avoid the prediction of LLE while still obtaining near-optimal solutions with SAFT-γ-Mie than with PR-mWS-NRTL, wherein optimisation of four parameters (as opposed to two) was required to gain a similar level of flexibility.

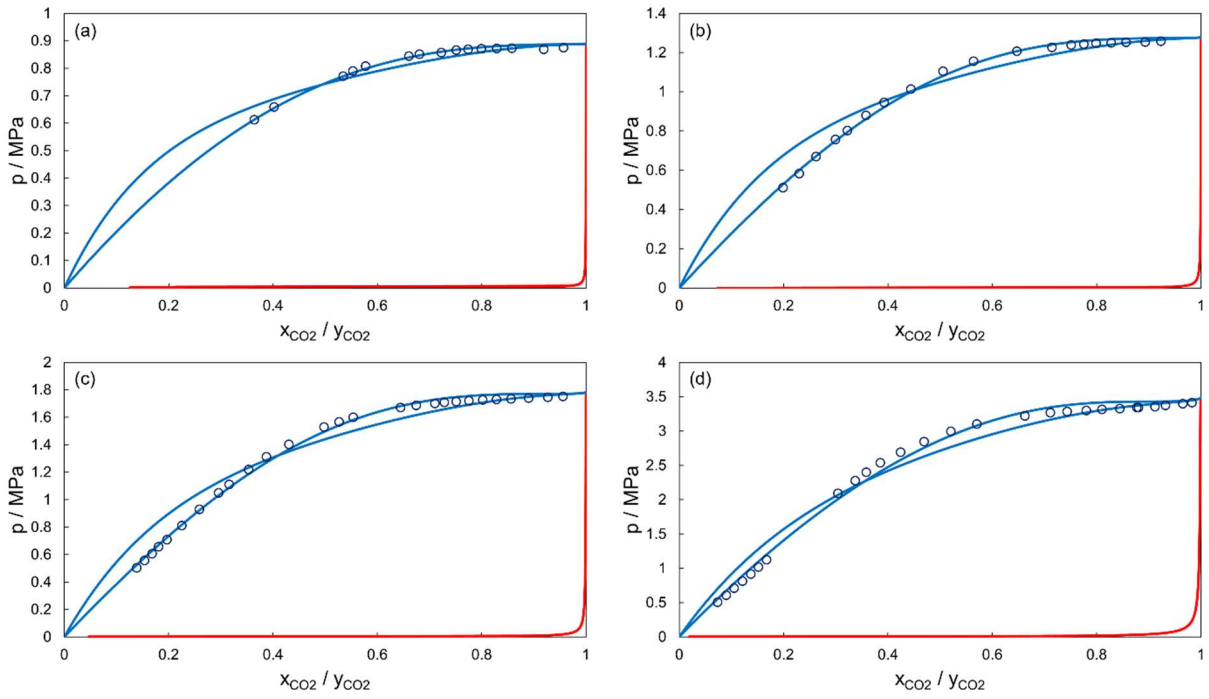


Figure 5.16: pxy diagram for methanol + CO_2 at (a) 230 K, (b) 240 K, (c) 250 K, and (d) 273.15 K showing experimental data from this work O and predictions of SAFT-γ-Mie –/– when using literature unlike parameters or when optimising both unlike parameters

Combining rules were used for several of the unlike interaction parameters as they were in literature [570]; the arithmetic mean was used for unlike segment and hard sphere diameters, and a modified geometric mean was used for the unlike attractive exponent. The unlike energy parameter ε_{kl} was optimised directly, without the use of combining rules, for greater transferability. Adaptation to any particular combining rule(s), such as the Lorentz-Berthelot rules, can be done simply by regressing a chosen BIP like k_{ij} (note that this is a different k_{ij} to those within cubic EoS) with the chosen rule against the values provided here. The unlike repulsive exponent λ^r_{kl} was optimised in a similar way, however it may be desirable (depending on application) to leave this constant (*ie* temperature independent). A clear relationship between the two parameters was observed, thus transitioning between one approach and the other is not expected to be difficult. Higher values of either parameter generally produced lower errors, however a region of LLE occurs beyond a certain point so constraining the values is necessary.

Cross-association (between an *H* site on CO_2 and an *e* site on methanol) was examined briefly, by considering four cases for the 250 K dataset. No cross-association produced excellent results (and is significantly simpler to optimise, with half the parameters), two weak cross-associations ($\varepsilon^{HB}_{kl,ab}$ = 200 and 500 for a bonding volume $K_{kl,ab}$ of 0.5 Å^3) produced similar results, such that it remains unclear if weak cross-association might produce marginally better results, and water-like cross-association (directly applying the literature values for water-CO_2 cross association [570] to methanol-CO_2) had poor results, greatly increasing the region of the parameter space where LLE was present. As such, neglecting cross association appears to be a promising avenue to accurate predictions for methanol + CO_2 (especially at temperatures < 300 K) with minimal optimisation cost for the two parameters compared to the otherwise four.

Table 5.11: Newly optimised constants for the temperature dependence of the unlike interaction parameters for SAFT-γ-Mie for methanol + CO_2 for temperatures between (230 and 273.15) K

Model	Parameter	c_1	c_2	c_3
SAFT-γ-Mie	ε_{kl}	-1.07×10^{3}	1.09×10^{1}	-2.21×10^{-2}
	λ^r_{kl}	-3.46×10^{2}	3.01×10^{0}	-6.1×10^{-3}

The two other EoS considered for analysis (noting that the range of potentially available options is large but the number of fairly comparable models with available optimisations are few) are predictive SRK (PSRK) and the multiparameter EoS of Blackham & Lemmon. Both of these models were used as standard and did not produce exceptional results, thus shall not be discussed in detail.

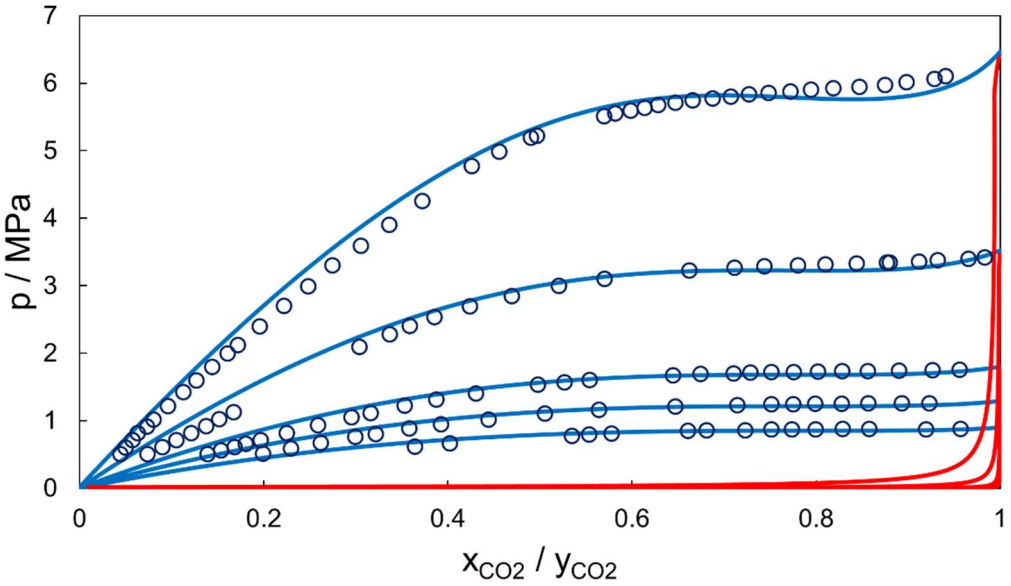


Figure 5.17: pxy diagram for methanol + CO_2 at (230 to 298.15) K, showing experimental data from this work O and predictions of PSRK –/–

The predictions of PSRK are generally substandard, better (albeit still lacking) results were achievable with the simpler optimised PR-vdW model. Similar predictions of unphysical LLE were visible, for example as is shown in Figure 5.17. PRSK should theoretically be capable of greater performance as it is a cubic + g^E model (using modified UNIFAC parameters for g^E). While it is a group contribution method, and thus often loses some performance relative to component specific equivalents, methanol and CO_2 molecules are treated as their own groups here (as with the other GC EoS discussed) so performance should not be affected.

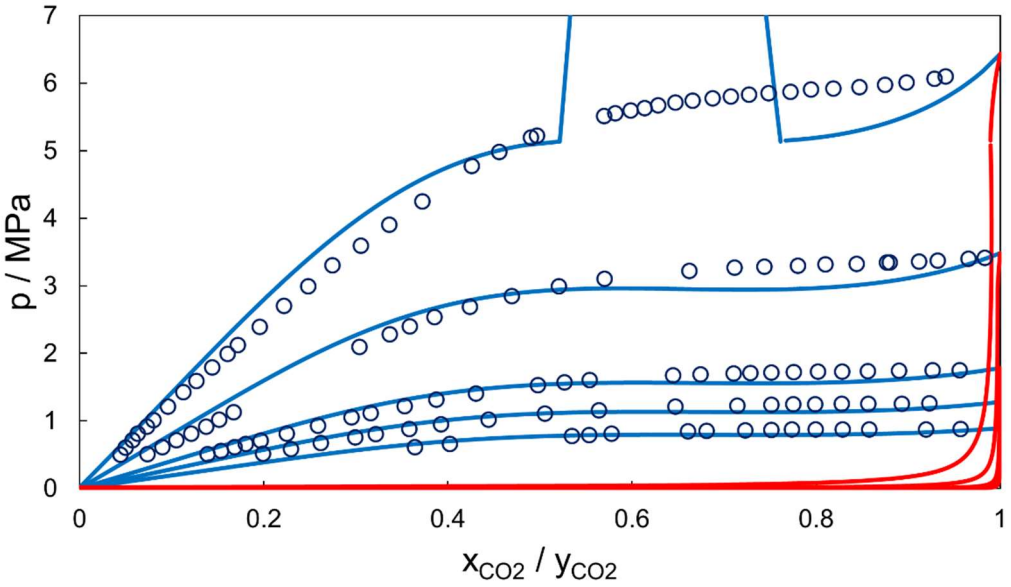


Figure 5.18: pxy diagram for methanol + CO_2 at (230 to 298.15) K, showing experimental data from this work O and predictions of the EoS of Blackham & Lemmon –/–

The multiparameter EoS of Blackham and Lemmon was the least accurate of the models discussed here, featuring unphysical LLE to a more severe degree and exhibiting large deviations from experimental data. The predictions at temperatures between (230 and 298.15) K are shown in Figure 5.18; note that, as a result of the flash algorithms implemented in REFPROP, proper visualisation of an expansive LLE region was possible at 298.15 K. Not much detail is provided about the model or it's optimisation and performance, as has been commented on in other works [558]. The poor performance as seen here is not uncommon for multiparameter EoS that have not been well optimised. Given the scattered literature data for composition, few points of density data, and general lack of other property data, this outcome is not surprising. There is clear potential for improvement, however it is not clear if there is sufficient property data available to justify pursuit of such multiparameter EoS given the quality of predictions achievable using SAFT-γ-Mie and PR-mWS-NRTL.

There is potential for PR-vdW to used in situations where only basic EoS are available/accessible, though only for the lower pressure region at temperatures below ~320 K while more broadly at higher temperatures, and it is recommended that non-zero values of l_{ij} be used. If a simple model is required but $\gamma - \varphi$ models are available, PR coupled with the Wilson activity model would produce adequate results at low temperatures (with LLE predictions prevented), as has been shown in literature for the similar SRK-vdW-Wilson model [343], but would not be applicable at temperatures above the critical temperature of CO_2. PR-based models, especially where a volume translation has been applied, would likely result in in better volumetric property predictions than SRK-based models, though would still be sub-standard for most applications.

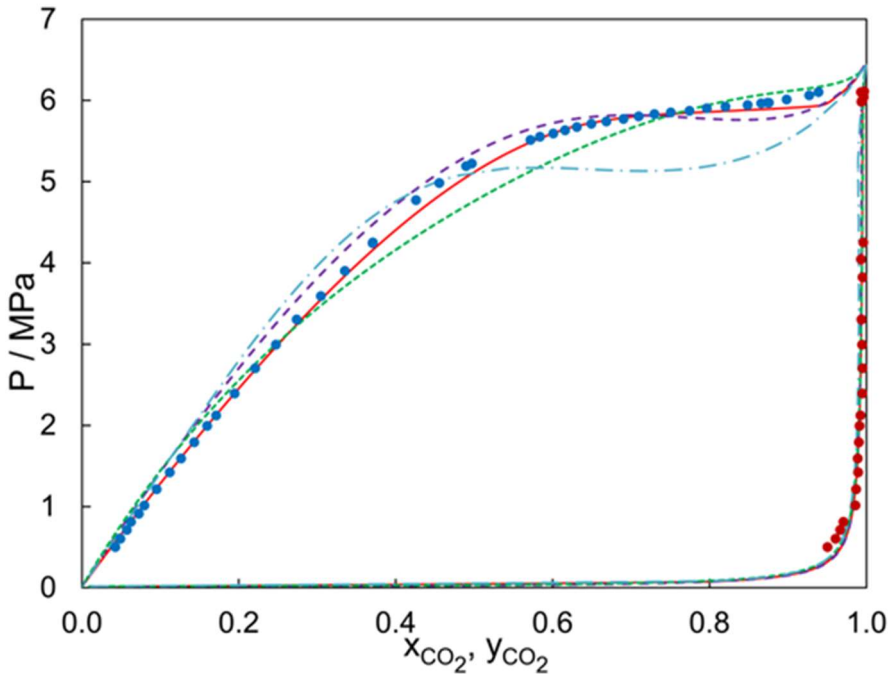


Figure 5.19: pxy diagram for methanol + CO_2 at 298.15 K, showing exp data ● and predictions of PR-mWS-NRTL —, PSRK – –, SAFT-γ-Mie - - - (with literature BIP values), and Blackham & Lemmon – · –

Model performance was generally correlated with the number of adjusted/adjustable BIPs, however, as can be seen with the performance of Blackham & Lemmon especially (*eg* in Figure 5.19), poorer results are obtained beyond a certain point (in part due to the loss of physics-based/informed relationships). It was preferable to keep the number of BIPs to be optimised to a minimum, as the marginal effort in fitting each additional parameter suffers due to cardinality. With this in mind, the best performing model could be considered to be SAFT-γ-Mie (when using newly optimised BIPs as opposed to literature values), capable of outperforming the alternative models when only optimising two BIPs. Similar performance was achievable with PR-mWS-NRTL when three BIPs were optimised, especially in the case of PR-mWS-sNRTL where α_{ij} was one of the varied parameters. It is possible that best performance is achievable when optimising PR-mWS-NRTL with all four potential BIPs, however it is inconclusive as to whether it consistently outperforms SAFT-γ-Mie due to convergence issues with the latter and optimisation issues with the former preventing full analysis and comparison. It is doubly inconclusive when one considers simultaneous optimisation of a cross-association between methanol and CO_2, wherein both models would have four BIPs. It is believed that that SAFT-γ-Mie could provide better prediction of volumetric and calorific properties, however there is insufficient data to conduct a thorough assessment.

For reliably and readily accessible (given basic familiarity with modelling and optimisation) accurate predictions of methanol + CO_2 at low temperatures, SAFT-γ-Mie is recommended, while at temperatures greater than 320 K comparable performance (at least, considering data shortcomings) may be achieved with simpler models. The growing accessibility of SAFT-type equations through open source software (previously lacking this family of models), like Clapeyron, render usage difficulty comparable to PR-vdW.

Chapter 6: Conclusions & Recommendations

“Scientia humanitatis decus et tutamen.” (“Scientific knowledge, the crowning glory and the safeguard of Humanity”)

— Modification of the Imperial College Motto

6.1 Summary and Conclusions

The need to improve process efficiencies and develop novel processes to conserve materials and energy long predates the formalised concept of a process (let alone process systems engineering). The exponential nature of technological development has caused this need to grow in scale to such an extent that global mass and energy balances are now a practically constraining factor. Just as the establishment of chemical engineering has promoted (to the benefit of society and quality of life in many ways) the rate of depletion of natural resources and the rate at which climate change progresses, so too must it now mitigate these issues through the realisation of sustainability. Chemical engineering is not the problem to which the climate demands action; instead, it is one of the central pillars upon which a solution must be built.

Achieving net zero greenhouse gas emissions, and likely net negative emissions beyond it, is an essential and realistic step in mitigating climate change. Further, when placed within the broader scope of sustainability (closing the loop on process mass balances, supported by sustainable energy sources), it is here that a solution to Jevons' pervasive paradox arises, wherein further technological development may proceed with all costs paid fairly. The engineering of these solutions must be based on physical behaviours, with the implementation supported by a healthy recognition of both past failures (such as the use of CFCs and the fugitive emissions of natural gas) and ones that may only be appreciated in the future. Some of the most fundamental of these physical behaviours fall within the purview of thermophysics, therein described through models. These models may then be used to study processes, often implemented in process simulators to improve efficiency and efficacy while minimising risks (whether economic, environmental, or societal).

Thermodynamic models do not provide exact solutions and frequently there are many options available. In some cases, a suitable model may be readily available in accessible software, however in more cases there is no such model optimised or accessible. In the latter case, optimisation, implementation, or experimental investigation may be required, none of which are trivial. The necessary dependency on reliable experimental data is consistently limiting; few industrially relevant mixtures are well studied. Knowledge of the fluid phase behaviour is especially important, yet these measurements are challenging and time consuming.

The literature has been reviewed in depth for the phase behaviour mixtures of CO_2 with isobutane and with methanol as well as practically all hydrogen binary mixtures (with extant data), with clear shortcomings identified. Of note, the review of methanol + CO_2 covers the 71 studies available in the literature, finding marked disagreements well beyond those normally encountered, exacerbated by many low quality studies. Data at low (< 270 K) and high (> 350 K) temperatures are scarce, while data at intermediate temperatures have disagreements spanning almost half the composition range. The review of hydrogen mixtures exceeds all those previously available, correcting a number of errors, discussing many more mixtures (including those without data), and examining the overall behaviour of the family of hydrogen mixtures in depth. The tools necessary to optimise accurate models and elucidate the global phase diagrams for hydrogen mixtures have been provided. The possibly of previously unrecognised potential to conduct processes at pressures beyond those seen in industry

today, taking advantage of high pressure phase equilibria, is noted and bares resemblance to that which was seen in the advent of the Haber-Bosch process.

There is significant incentive to improve the procedure and design of experiments, providing an opportunity to put the thermodynamic models being optimised to use as an experimental aid supporting automation. While the implementation is not trivial and must be done with care, it allows for measurements to be made more rapidly and in a more reproducible fashion, benefitting from machine precision. Such an approach has been realised in the automated analytical apparatus developed in this work, wherein the capability to inject and vent fluids, a rigorous data acquisition and control program, and a Peng-Robinson model allowed for careful movement through the phase space. Varying degrees of automation have been applied successfully and further refinements have been identified. The successful automated measurement of three isotherms with a single initial charge and the integration of density measurements during calibrations represent significant progressions.

Low uncertainty measurements have been made of the phase behaviour of three binary mixtures of varying degrees of asymmetry, with a total of 294/158 pTx/y datapoints produced at temperatures between (190 and 400) K and pressures between (0.5 and 20) MPa. Measurements of isobutane + CO_2 were conducted along three isotherms, two of which had literature data available for comparison while the measurements at 240 K extended the temperature range with available data. Excellent agreement was seen between the data generated in this work and the reliable data from literature, providing another layer of validation to the apparatus and methodology. The mixture displays type I/1^P phase behaviour with no indication of a liquid-liquid separation, consistent with other CO_2 + light alkane systems. The measurements of the system isobutane + H_2, conducted along nine isotherms, represent the vast majority of thermophysical property measurements ever made of this mixture and the largest work on any hydrogen mixture in four decades. Measurements in the near critical region could be made for the two highest temperature isotherms, and could be well described by critical scaling laws. The mixture was found to display type III/$1^C X^X$ phase behaviour as a result of the substantial size asymmetry, and contemporary understandings of phase behaviour have allowed greater insights than were possible in the one prior study eight decades ago. Measurements of methanol + CO_2 were conducted along five isotherms, focused on resolving disagreements at near ambient temperatures and expanding understanding at low temperature where data were previously scarce. The measurements provide the first low uncertainty evidence against liquid-liquid separation at temperatures down to 230 K, resolving a long-standing unknown. In addition to phase composition data, three rough saturated liquid density measurements were made at 298.15 K, in good agreement with the limited (and unsurprisingly scattered (given the state of the VLE data)) data. Six points of low uncertainty compressed liquid density data were produced at 298.15 K, the only such data available for this system. The mixture can, at first approximation, be considered to display type I/1^P behaviour across the conditions investigated in this work and in literature. More rigorously, it is likely to count as type II/$1^P X^X$ behaviour where the liquid-liquid separation is at least partially masked by solidification. Unequivocal determination would require the thorough tracing of the two and three phase regions, including up to pressures of 1 GPa, though this is of little industrial importance.

The difficulty in accurately modelling the behaviour varied significantly between the three mixtures. Isobutane + CO_2 could be modelled well by all models considered except for SAFT-γ-Mie, as a result of a lack of optimisation for the CH group with CO_2. PR-mWS-NRTL performed marginally better than alternatives, though PR-vdW is simpler and more easily/readily implemented and would be sufficient in most cases (when a suitable volume-translation is applied). The most apparent improvements of the PR models optimised in this work were at the lowest temperature, that had not previously been investigated, demonstrating the importance of experimental data. The situation was markedly different for isobutane + H_2. GERG-2008 performed extremely poorly and SAFT-γ-Mie (as with most SAFT-type EoS currently) lacked the necessary parameters for hydrogen mixtures, leaving EPPR78 as the only qualitatively accurate model previously available. PR-vdW produced significantly better results than EPPR78, though only performed adequately in absolute terms. Convergence issues with PR-mWS-NRTL prevented optimisation within this work, requiring more rigorous flash algorithms. The mixture of methanol + CO_2 presented the greatest technical challenge, as common unphysical predictions of a liquid-liquid separation limited even qualitative correctness in several cases. It was possible to obtain predictions with PR-vdW that were quantitatively better than all previously available models, however, these predictions were of insufficient quality for use in process at temperatures below ~330 K. The qualitative shortcoming could be overcome with PR-mWS-NRTL when simultaneously optimising all four parameters, however the computational effort required has thus far prevented parameter optimisation over the entire temperature range. Best results for this mixture at $T \leq 273.15$ K were obtained with SAFT-γ-Mie when reoptimizing the unlike interaction parameters, though flash convergence issues prevented proper assessment at higher temperatures. Overall, it appears that the PR-mWS-NRTL model is recommendable in many cases, especially as it may be reduced to PR-vdW when handling simple mixtures (whether binary or higher order), however it is clear that SAFT-γ-Mie will soon eclipse these models for asymmetric mixtures. The greater physicality and broad applicability of the group contribution concept are desirable; what remains is for the parameterisation to be completed. Multiparameter EoS appear unlikely to offer prediction improvements over PR and SAFT-type EoS for the mixtures considered due to a perennial lack of experimental data.

This work has successfully completed its objectives, meaningfully reducing the known unknowns facing the development of necessary processes while revealing new questions to be answered. The groundwork has been laid both for further improved experimental investigations and for the continued development of accurate thermodynamic models, supported by new experimental data and detailed literature reviews. It is hoped that, in the near future, the title adorning the apparatus in this work as that which has produced the most experimental data for hydrogen mixtures in decades (either by total amount of datapoints or most for a single mixture) and that which is most autonomous shall be conferred to evermore capable apparatuses. The ability to develop sustainable processes using accurate, openly-accessible models supported by sufficient data is more realisable than ever before, essential for the world to transition towards net zero.

6.2 Recommendations for Future Work

6.2.1 Further Experimental Investigations

There is no shortage of related experimental investigations that would be worth pursuing following this work. Focus is placed on those of greatest industrial and theoretical value (noting that the two are not disparate).

Of greatest, though broad, importance remains the investigation of the behaviour of mixtures containing CO_2/H_2. This work has made progress on this front yet countless binary and higher order mixtures require attention, which should ideally be placed in order of industrial importance. The behaviour under geological conditions is especially under-studied, where stored CO_2 or stored or natural H_2 may exist alongside water, dissolved salts and minerals, hydrocarbons, nitrogen, and helium. These behaviours are pertinent to large scale projects (both announced and under development), like the Northern Lights project, whose commissioning is required within a short timescale relative to the time taken to generate experimental data and develop models.

The urgent need for immediate emissions reductions and decarbonisation, regardless of how deeply broader sustainable processes have been deployed, puts such data at the forefront of importance, but the eventual need for sustainable processes (*eg* those avoiding the dependency on fossil fuels) should not be neglected. Of greatest importance of those related to this work are further methanol-containing mixtures and many of the family of H_2 mixtures more broadly.

Further investigation into the behaviour of methanol + CO_2 would be beneficial. The high temperature region, especially beyond 350 K, is lacking in reliable data despite the relevance to the conditions during methanol production. Care should be taken to ensure that techniques employed carefully consider potential adsorption and degradation/reaction of methanol both within the experimental volume and any other sample-facing surfaces. There is also value in investigating further the low temperature behaviour, at temperatures from 230 K down to the triple point of CO_2, to further conclude that LLE does not occur continuously from the region of VLE. This could then be extended further down to the triple point temperature of methanol (175.6 K), up to which SLE is present but VLE persists at ever lower pressures. These regions of the phase space are relevant to both extant (*eg* Rectisol) and nascent (*eg* methanol-based CCUS) processes. Mixtures of methanol with related compounds such as hydrogen, carbon monoxide, nitrogen, methane, water, and the associated higher order mixtures, are also in need of further investigation. These mixtures are common both within methanol production and in downstream use where they may exist as impurities (including in transport and geological storage). Investigations should ideally begin with a validation against methanol + CO_2 data (such as those within this work) to ensure proper measurement of these challenging mixtures.

Many industrially relevant hydrogen mixtures have been found to have little to no available thermophysical property data. Reducing these shortcomings is essential; considering the scale of the problem efforts would be best focussed on investigating mixtures necessary for

optimising group contribution models. Measurements along homologous families of molecules should be conducted in order of increasing complexity, as was begun in earnest for the simplest molecules (such as the first two n-alkanes and n-alkenes) by Streett and contemporaries and now for isomeric alkanes by this work. It is noted that many extant apparatuses would be capable of contributing due to the unparalleled breadth of conditions relevant to hydrogen mixtures, though near-critical conditions are of greatest utility. The critical behaviour of hydrogen mixtures with large molecules (of molar mass ≥ 100 g/mol) is virtually unstudied yet the increasingly extreme asymmetry is likely to yield unusual effects that cannot confidently be modelled yet may have industrial importance.

The extension of the measurements of isobutane + H_2 to higher pressures would be of great value to understanding the model predictions observed in this work and the critical behaviour of hydrogen mixtures overall. The phase space at temperatures between 300 and 400 K at pressures up to 1 GPa should be prioritised. This data should be accompanied by further modelling work with rigorous flash algorithms and careful minimisation of the Gibbs free energy for greater usefulness. Attempts should also be made to follow the three phase SVLE curve of the mixture from the triple point of pure isobutane up to high pressures, much as was done in the works of Streett. Should an intersection between the critical curve and SVLE curve be present, experiments should then proceed to trace the coexistence regions to higher pressures still, as to determine whether a region of FFE reemerges. Similar work should be conducted with the mixture of CO_2 + H_2, for which existing measurements effectively terminate at the first (and currently only) known intersection.

Investigations into the behaviour of mixtures of different isomeric alkanes (and isomeric molecules more broadly) with CO_2 and with H_2. Most thermodynamic models do not capture the effects of structural isomerism beyond mere differences in functional groups present, let alone more complex isomerisms, in significant part due to a lack of experimental data. The purification (and purity assessment) of isomers presents a challenge, however there is much that can likely be learned from relatively simple isomers (that are easier to separate). Such work can, in turn, improve the ability to purify isomers. Improved understanding of the structural and positional effects involving these strong covalent bonds is also beneficial for understanding the corresponding effects on fluids more generally, such as the complex networks formed by liquid and supercritical states (whether through association or weaker forces).

It is not only phase behaviour measurements that are of importance, though it is often the first step; measurements of the density, both at saturation and in the compressed liquid state, are difficult to model accurately and thus data are essential for assessment as well as many aspects of process design. Heat capacity measurements are also helpful, as thermal duties are central to much of heat integration and operating costs, and these measurements may serve to further distinguish simpler cubic EoS from cubic + G^E, SAFT-type, and multiparameter EoS. Speed of sound measurements of any saturated/coexisting or single-phase states are also of great help, both in modelling and industrial application (such as flow metering).

6.2.2 Further Apparatus Development

Further autonomy for the apparatus should be pursued. The completed implementation of all avenues demonstrated in this work would not be challenging and would significantly improve both the throughput of the apparatus and the ease with which it may be used. While the apparatus currently follows a path determined *a priori* and relies on dead reckoning, and thus is subject to the accumulation of deviations, it is possible to have more adaptive approaches suitable also for mixtures displaying initially unknown behaviour. It is now clear that the measurement of broad regions of mixture phase spaces (covering the entire coexistence region for well-bounded spaces) in a single autonomous run with a single initial charge is not only possible but preferable.

Several minor adaptations to the construction would also yield significant benefits. The dead volumes in the system could be minimised further by removing the original connect between the cell and the fluid handling system, such that all fluids are injected through the coaxial liquid inlet. This would remove the need to manually make/break connections when switching between calibration and measurements, allowing for automatic calibration to be carried out with low uncertainties. The pressure sensor could be connected directly to the port previously for the fluid handling system, allowing for improved pressure measurement during calibration (that currently relies on the pump pressure sensor). This arrangement would also facilitate changing of the pressure sensor to meet the pressure range of interest of a given system. The need for the rupture-disc could be avoided by switching the venting valve from normally closed value to a normally open valve, such that any overpressure situation is avoided either by actuation commanded by the control program or, in the event of a power failure, by the valve returning to its default state. The piezoelectric sampling valve that has been in development in the group for some years now could be well suited for such an application, inherently a normally open valve and affording exceptionally low dead volume. The potential for this valve to replace the ROLSI valves should also be explored, as promising results have been obtained thus far and the distinction between its use as a sampling valve or venting valve is mostly trivial. The decreased dead volume would allow for better synthetic bubble point and density measurements, as well as more accurate knowledge of the internal system state, convenient for extensive automated sequences.

The addition of a second high pressure syringe pump, admittedly a more substantial modification, would expand the range of conditions that could be explored on a single charge and, by extension, a single instance of operator interaction. This would be especially helpful for binary mixtures that are sufficiently asymmetric to show type II or III behaviour, or for higher order multicomponent systems (for which data are even more scarce).

6.2.3 Further Model Investigations

Parameterisation of accurate models remains a key goal, with no single model perfect for all applications (and likely such a hypothetical model would either be unwieldy or require excessive parameterisation for a given application). Simple models are desired but the appropriate model varies depending on the type of mixtures present, as has been seen to

some extent in this work. Accessible models are increasingly widely available, bolstered by the growth of open access thermodynamic software such as Clapeyron, reducing the need to use bespoke or expensive third party software for complex equations of state.

Some available models, such as EPPR78, GERG-2008, and SAFT-γ-Mie perform excellently for particular mixtures where there are more data and have been greater research focus but struggle in most other cases. Work should be pursued to optimise the pure component and interaction parameters for all nature of EoS and collate accessible databases such that they may be more widely used and readily assessed. Group contribution models, such as EPPR78 and SAFT-γ-Mie, are especially valuable as they can supplement data shortcomings (including for hard to purify compounds). Such approaches may be especially important for mixtures containing many components, where dimensionality necessitates that there will never be enough time to explore all possible mixtures exhaustively. A clear starting point is the further optimisation industrially prevalent mixtures such as those containing hydrogen, CO_2, methanol, and light alkanes, which have been observed to frequently lack optimal parameters.

The question of dealing with more structurally complex molecules remains inviting to solutions. This is necessary not just for detailed descriptions of high molar mass molecules and weakly bonded agglomerations but also for the tractable extensive of group contribution approaches to atomistic approaches. This is an area in which machine learning models that use structural descriptors (such as SMILES) are likely to excel, as such systems may reasonably be described through language games. However, there remains great value in understanding the corresponding thermophysics through physics-informed non-ML models. In (engineering) practice, a combination may be desirable, though the quality of machine learning based models will require assessment against classical models and both ultimately depend on reliable experimental data. Approaches like SAFT/perturbation theory also provide a conveniently scalable description of molecular systems, including where “strong” bonds may be made or broken (as in reactive systems).

Beyond what is effectively a matrix completion exercise for existing models, there is a need to improve the description of energetic contributions that are not captured in any current models. It is possible, and well established, to capture a degree of non-ideality in classical cubic EoS. Further flexibility is provided by often-complex mixing rules, where performance is generally guided/influenced by the accuracy of the underlying physical description, but the foundational structure of cubic EoS is inherently limited. Energy explicit models, such as those based on perturbation theory (or, to a lesser extent, multiparameter equations of state), appear best suited to capture these additional non-idealities.

A significant example is the consideration of surface energies, manifested as areas and tensions (depending on how one describes a thermodynamic space). Here, consistency across scales is important; microscopic behaviours can have meaningful effects on bulk properties. This is evident, for example, from the effectiveness of two-fluid models, whether surfaces are considered directly (as in UNIQUAC) or more implicitly (as in NRTL). Such understanding is likely essential for detailed understanding of liquid, supercritical, and colloidal systems, as well as solid formation. This is relevant not only to many classical industrial

processes, but also the equilibria for pharmaceutical applications, where melting points and latent heats are commonly required in modelling but the state of the art predictions often target order of magnitude accuracy. Significant portions of these properties of fluid and solid phases are derived from surface energies, yet theory is often either lacking or not applied to the extent possible (when considering the detailed works of researchers such as Hill, Widom, and Tolman). These shortcomings should be reconciled, regardless of whether the models they are contained within keep the mean field approximation or attempt to move beyond it.

References

[1] Jevons WS. The coal question; an inquiry concerning the progress of the nation and the probable exhaustion of our coal-mines: Macmillan; 1866.
[2] Alcott B. Jevons' paradox. Ecological Economics. 2005;54:9-21.
[3] Hiller H, Reimert R, Stönner H-M. Gas Production, 1. Introduction. Ullmann's Encyclopedia of Industrial Chemistry.
[4] Falkus ME. The British Gas Industry before 1850. The Economic History Review. 1967;20:494-508.
[5] Haber F. The synthesis of ammonia from its elements. Nobel lecture. 1920;2.
[6] Johnson B. Making ammonia: fritz haber, walther nernst, and the nature of scientific discovery: Springer Nature; 2022.
[7] Uekoetter F, Smil V. Enriching the Earth. Fritz Haber, Carl Bosch, and the Transformation of World Food Production. Environmental History - ENVIRON HIST. 2002;7.
[8] Johnson B. The Challenge of Technical Implementation. In: Johnson B, editor. Making Ammonia: Fritz Haber, Walther Nernst, and the Nature of Scientific Discovery. Cham: Springer International Publishing; 2022. p. 59-64.
[9] Hower J. Coal. Kirk-Othmer Encyclopedia of Chemical Technology: John Wiley & Sons, Inc.; 2016. p. 1-63.
[10] de Klerk A. Fischer–Tropsch Process. Kirk-Othmer Encyclopedia of Chemical Technology: John Wiley & Sons, Inc.; 2013. p. 1-20.
[11] Dincer I, Acar C. Review and evaluation of hydrogen production methods for better sustainability. International Journal of Hydrogen Energy. 2015;40:11094-111.
[12] Feldman D. Polymer History. Designed Monomers and Polymers. 2008;11:1-15.
[13] Anderegg WRL, Prall JW, Harold J, Schneider SH. Expert credibility in climate change. Proceedings of the National Academy of Sciences. 2010;107:12107-9.
[14] Neumann J. Climatic change as a topic in the classical Greek and Roman literature. Climatic Change. 1985;7:441-54.
[15] Fourier JBJ. Memoir on the temperatures of the terrestrial globe and planetary spaces. Oeuvres de Fourier: Publiées par les soins de Gaston Darboux. Cambridge: Cambridge University Press; 2013. p. 95-126.
[16] Hulme M. On the origin of 'the greenhouse effect': John Tyndall's 1859 interrogation of nature. Weather. 2009;64:121-3.
[17] Arrhenius S. XXXI. On the influence of carbonic acid in the air upon the temperature of the ground. The London, Edinburgh, and Dublin Philosophical Magazine and Journal of Science. 1896;41:237-76.
[18] Etheridge DM, Steele LP, Langenfelds RL, Francey RJ, Barnola J-M, Morgan VI. Natural and anthropogenic changes in atmospheric CO2 over the last 1000 years from air in Antarctic ice and firn. Journal of Geophysical Research: Atmospheres. 1996;101:4115-28.
[19] Lan X, Tans P, Thoning KW. Trends in globally-averaged CO2 determined from NOAA Global Monitoring Laboratory measurements. NOAA. 2025.
[20] Poynting JH. LXXIV. On Prof. Lowell's method for evaluating the surface-temperatures of the planets; with an attempt to represent the effect of day and night on the temperature of the earth. The London, Edinburgh, and Dublin Philosophical Magazine and Journal of Science. 1907;14:749-60.
[21] Very FW. XLI. The Greenhouse theory and planetary temperatures. The London, Edinburgh, and Dublin Philosophical Magazine and Journal of Science. 1908;16:462-80.
[22] Fleming J. The callendar effect: the life and work of Guy Stewart Callendar (1898-1964): Springer Science & Business Media; 2013.
[23] Keeling CD. The Concentration and Isotopic Abundances of Carbon Dioxide in the Atmosphere. Tellus. 1960;12:200-3.
[24] Cavicchioli R, Ripple WJ, Timmis KN, Azam F, Bakken LR, Baylis M, et al. Scientists' warning to humanity: microorganisms and climate change. Nature Reviews Microbiology. 2019;17:569-86.

[25] Perovich D, Meier W, Tschudi M, Hendricks S, Petty AA, Divine D, et al. Arctic Report Card 2020: Sea Ice. 2020.
[26] Ornes S. How does climate change influence extreme weather? Impact attribution research seeks answers. Proceedings of the National Academy of Sciences. 2018;115:8232-5.
[27] Rezaei EE, Webber H, Asseng S, Boote K, Durand JL, Ewert F, et al. Climate change impacts on crop yields. Nature Reviews Earth & Environment. 2023;4:831-46.
[28] Caparas M, Zobel Z, Castanho ADA, Schwalm CR. Increasing risks of crop failure and water scarcity in global breadbaskets by 2030. Environmental Research Letters. 2021;16:104013.
[29] Caminade C, Kovats S, Rocklov J, Tompkins AM, Morse AP, Colón-González FJ, et al. Impact of climate change on global malaria distribution. Proceedings of the National Academy of Sciences. 2014;111:3286-91.
[30] France-Presse A. Russia Announces Plan to 'Use the Advantages' of Climate Change. The Guardian. 2020.
[31] Weart S. Rise of interdisciplinary research on climate. Proceedings of the National Academy of Sciences. 2013;110:3657-64.
[32] Black JF. The Greenhouse Effect, Ref. No: 78PR 461. Exxon Research and Engineering Co.; 1978.
[33] Flynn C, Yamasumi E, Fisher S. The G20 Peoples' Climate Vote. United Nations Development Programme (UNDP, 2021), https://www undp org/publications/g20-peoples-climate-vote-2021. 2021;9.
[34] Sanderson BM, O'Neill BC. Assessing the costs of historical inaction on climate change. Scientific Reports. 2020;10:9173.
[35] United_Nations_General_Assembly. Report of the United Nations Conference on the Human Environment, Stockholm, 5-16 June 1972: UN; 1972.
[36] Pulselli FM. Global Warming Potential and the Net Carbon Balance. In: Jørgensen SE, Fath BD, editors. Encyclopedia of Ecology. Oxford: Academic Press; 2008. p. 1741-6.
[37] Smelser NJ, Baltes PB. Encyclopedia of the Social & Behavioral Sciences. 2001.
[38] Change UNC. Kyoto Protocol—Targets for the First Commitment Period. UN New York, NY, USA; 1997.
[39] FALKNER R. The Paris Agreement and the new logic of international climate politics. International Affairs. 2016;92:1107-25.
[40] Schiermeier Q. The Kyoto Protocol: Hot air. Nature. 2012;491:656-8.
[41] IPCC. Climate Change 2023: Synthesis Report. Contribution of Working Groups I, II and III to the Sixth Assessment Report of the Intergovernmental Panel on Climate Change. Gevena, Switzerland: IPCC; 2023.
[42] Hansen JE, Pushker K, Makiko S, George T, Joseph K, E. BS, et al. Global Warming Has Accelerated: Are the United Nations and the Public Well-Informed? Environment: Science and Policy for Sustainable Development. 2025;67:6-44.
[43] IPCC. Anthropogenic and Natural Radiative Forcing. In: Intergovernmental Panel on Climate C, editor. Climate Change 2013 – The Physical Science Basis: Working Group I Contribution to the Fifth Assessment Report of the Intergovernmental Panel on Climate Change. Cambridge: Cambridge University Press; 2014. p. 659-740.
[44] Artaxo P, Berntsen T, Betts R, Fahey D, Haywood J, Lean J, et al. Changes in atmospheric constituents and in radiative forcing. 2007.
[45] Sand M, Skeie RB, Sandstad M, Krishnan S, Myhre G, Bryant H, et al. A multi-model assessment of the Global Warming Potential of hydrogen. Communications Earth & Environment. 2023;4:203.
[46] Fennell P, Driver J, Bataille C, Davis SJ. Cement and steel - nine steps to net zero. Nature. 2022;603:574-7.
[47] IEA. Methane Tracker 2020. Paris: IEA; 2020.
[48] Ruppel CD, Kessler JD. The interaction of climate change and methane hydrates. Reviews of Geophysics. 2017;55:126-68.
[49] Howarth RW. The greenhouse gas footprint of liquefied natural gas (LNG) exported from the United States. Energy Science & Engineering. 2024;12:4843-59.

[50] IPCC. Climate Change 2021 – The Physical Science Basis: Working Group I Contribution to the Sixth Assessment Report of the Intergovernmental Panel on Climate Change. Cambridge: Cambridge University Press; 2023.
[51] IPCC. Climate Change 2022 – Impacts, Adaptation and Vulnerability: Working Group II Contribution to the Sixth Assessment Report of the Intergovernmental Panel on Climate Change. Cambridge: Cambridge University Press; 2023.
[52] IPCC. Climate Change 2022 - Mitigation of Climate Change: Working Group III Contribution to the Sixth Assessment Report of the Intergovernmental Panel on Climate Change. Cambridge: Cambridge University Press; 2023.
[53] IPCC. The Ocean and Cryosphere in a Changing Climate: Special Report of the Intergovernmental Panel on Climate Change. Cambridge: Cambridge University Press; 2022.
[54] IPCC. Climate Change and Land: IPCC Special Report on Climate Change, Desertification, Land Degradation, Sustainable Land Management, Food Security, and Greenhouse Gas Fluxes in Terrestrial Ecosystems. Cambridge: Cambridge University Press; 2022.
[55] IPCC. Summary for Policymakers. Global Warming of 15°C: IPCC Special Report on Impacts of Global Warming of 15°C above Pre-industrial Levels in Context of Strengthening Response to Climate Change, Sustainable Development, and Efforts to Eradicate Poverty. Cambridge: Cambridge University Press; 2022. p. 1-24.
[56] Holl KD, Brancalion PHS. Tree planting is not a simple solution. Science. 2020;368:580-1.
[57] Martin MP, Woodbury DJ, Doroski DA, Nagele E, Storace M, Cook-Patton SC, et al. People plant trees for utility more often than for biodiversity or carbon. Biological Conservation. 2021;261:109224.
[58] Liu H, Khan I, Zakari A, Alharthi M. Roles of trilemma in the world energy sector and transition towards sustainable energy: A study of economic growth and the environment. Energy Policy. 2022;170:113238.
[59] Marti L, Puertas R. Sustainable energy development analysis: Energy Trilemma. Sustainable Technology and Entrepreneurship. 2022;1:100007.
[60] Šprajc P, Bjegović M, Vasić B. Energy security in decision making and governance - Methodological analysis of energy trilemma index. Renewable and Sustainable Energy Reviews. 2019;114:109341.
[61] Realmonte G, Drouet L, Gambhir A, Glynn J, Hawkes A, Köberle AC, et al. An inter-model assessment of the role of direct air capture in deep mitigation pathways. Nature Communications. 2019;10:3277.
[62] Schewe J, Heinke J, Gerten D, Haddeland I, Arnell NW, Clark DB, et al. Multimodel assessment of water scarcity under climate change. Proceedings of the National Academy of Sciences. 2014;111:3245-50.
[63] Gosling SN, Arnell NW. A global assessment of the impact of climate change on water scarcity. Climatic Change. 2016;134:371-85.
[64] Bui M, Adjiman CS, Bardow A, Anthony EJ, Boston A, Brown S, et al. Carbon capture and storage (CCS): the way forward. Energy & Environmental Science. 2018;11:1062-176.
[65] Boot-Handford ME, Abanades JC, Anthony EJ, Blunt MJ, Brandani S, Mac Dowell N, et al. Carbon capture and storage update. Energy & Environmental Science. 2014;7:130-89.
[66] Hepburn C, Adlen E, Beddington J, Carter EA, Fuss S, Mac Dowell N, et al. The technological and economic prospects for CO2 utilization and removal. Nature. 2019;575:87-97.
[67] MacDowell N, Florin N, Buchard A, Hallett J, Galindo A, Jackson G, et al. An overview of CO2 capture technologies. Energy & Environmental Science. 2010;3:1645-69.
[68] Mac Dowell N, Fennell PS, Shah N, Maitland GC. The role of CO2 capture and utilization in mitigating climate change. Nature Climate Change. 2017;7:243-9.
[69] Maitland GC. Carbon Capture and Storage: concluding remarks. Faraday Discussions. 2016;192:581-99.
[70] Dixon T, McCoy ST, Havercroft I. Legal and Regulatory Developments on CCS. International Journal of Greenhouse Gas Control. 2015;40:431-48.
[71] Metz B, Davidson O, De Coninck H, Loos M, Meyer L. IPCC special report on carbon dioxide capture and storage: Cambridge: Cambridge University Press; 2005.

[72] Leeson D, Mac Dowell N, Shah N, Petit C, Fennell PS. A Techno-economic analysis and systematic review of carbon capture and storage (CCS) applied to the iron and steel, cement, oil refining and pulp and paper industries, as well as other high purity sources. International Journal of Greenhouse Gas Control. 2017;61:71-84.
[73] Eljack F, Kazi M-K. Prospects and challenges of green hydrogen economy via multi-sector global symbiosis in Qatar. Frontiers in Sustainability. 2021;1:612762.
[74] Ozkan M, Nayak SP, Ruiz AD, Jiang W. Current status and pillars of direct air capture technologies. iScience. 2022;25:103990.
[75] Budinis S, Krevor S, Dowell NM, Brandon N, Hawkes A. An assessment of CCS costs, barriers and potential. Energy Strategy Reviews. 2018;22:61-81.
[76] Sodiq A, Abdullatif Y, Aissa B, Ostovar A, Nassar N, El-Naas M, et al. A review on progress made in direct air capture of CO2. Environmental Technology & Innovation. 2023;29:102991.
[77] Low M-Y, Barton LV, Pini R, Petit C. Analytical review of the current state of knowledge of adsorption materials and processes for direct air capture. Chemical Engineering Research and Design. 2023;189:745-67.
[78] Danaci D, Bui M, Petit C, Mac Dowell N. En Route to Zero Emissions for Power and Industry with Amine-Based Post-combustion Capture. Environmental Science & Technology. 2021;55:10619-32.
[79] Hochgesand G. Rectisol and purisol. Industrial & Engineering Chemistry. 1970;62:37-43.
[80] Burr B, Lyddon L. A comparison of physical solvents for acid gas removal. Gas Processors' Association Convention, Grapevine, TX2008.
[81] Zhu X, Xie W, Wu J, Miao Y, Xiang C, Chen C, et al. Recent advances in direct air capture by adsorption. Chemical Society Reviews. 2022;51:6574-651.
[82] Hou R, Fong C, Freeman BD, Hill MR, Xie Z. Current status and advances in membrane technology for carbon capture. Separation and Purification Technology. 2022;300:121863.
[83] Porter RTJ, Fairweather M, Pourkashanian M, Woolley RM. The range and level of impurities in CO2 streams from different carbon capture sources. International Journal of Greenhouse Gas Control. 2015;36:161-74.
[84] Benson SM, Surles T. Carbon Dioxide Capture and Storage: An Overview With Emphasis on Capture and Storage in Deep Geological Formations. Proceedings of the IEEE. 2006;94:1795-805.
[85] Aydin G, Karakurt I, Aydiner K. Evaluation of geologic storage options of CO2: Applicability, cost, storage capacity and safety. Energy Policy. 2010;38:5072-80.
[86] Alvarado V, Manrique E. Enhanced Oil Recovery: An Update Review. Energies. 2010;3:1529-75.
[87] McGlade C, Sondak G, Han M. Whatever happened to enhanced oil recovery? IEA Commentaries. Paris: IEA; 2018.
[88] Chen Q. Geochemical Properties of CO2-Brine-Mineral Systems Under Carbon Storage Conditions. London, UK: Imperial College London; 2025.
[89] Ghiat I, Banu A, Bicer Y, Amhamed AI, Al-Ansari T. Circularity within carbon capture networks: A review of capture and utilization technologies. Journal of CO2 Utilization. 2025;95:103075.
[90] Sunny N, Bernardi A, Danaci D, Bui M, Gonzalez-Garay A, Chachuat B. A Pathway Towards Net-Zero Emissions in Oil Refineries. Frontiers in Chemical Engineering. 2022;4.
[91] Skocek J, Zajac M, Ben Haha M. Carbon Capture and Utilization by mineralization of cement pastes derived from recycled concrete. Scientific Reports. 2020;10:5614.
[92] Marlin DS, Sarron E, Sigurbjörnsson Ó. Process Advantages of Direct CO2 to Methanol Synthesis. Frontiers in Chemistry. 2018;6.
[93] Singh H, Li C, Cheng P, Wang X, Liu Q. A critical review of technologies, costs, and projects for production of carbon-neutral liquid e-fuels from hydrogen and captured CO2. Energy Advances. 2022;1:580-605.
[94] Ye S, Wang S, Lin L, Xiao M, Meng Y. CO2 derived biodegradable polycarbonates: Synthesis, modification and applications. Advanced Industrial and Engineering Polymer Research. 2019;2:143-60.
[95] Wang S, Guo S, Luo Y, Qin Z, Chen Y, Dong M, et al. Direct synthesis of acetic acid from carbon dioxide and methane over Cu-modulated BEA, MFI, MOR and TON zeolites: a density functional theory study. Catalysis Science & Technology. 2019;9:6613-26.

[96] Bose A, Jana K, Mitra D, De S. Co-production of power and urea from coal with CO2 capture: performance assessment. Clean Technologies and Environmental Policy. 2015;17:1271-80.
[97] Qureshi MS, Le Nedelec T, Guerrero-Amaya H, Uusi-Kyyny P, Richon D, Alopaeus V. Solubility of carbon monoxide in bio-oil compounds. The Journal of Chemical Thermodynamics. 2017;105:296-311.
[98] Fajardy M, Mac Dowell N. Can BECCS deliver sustainable and resource efficient negative emissions? Energy & Environmental Science. 2017;10:1389-426.
[99] Ason A, Dal Poz J. Contracts for difference: The instrument of choice for the energy transition: OIES Paper: ET; 2024.
[100] IEA. Global Hydrogen Review 2024. Paris: IEA; 2024.
[101] Bashmakov IA, Nilsson LJ, Acquaye A, Bataille C, Cullen JM, Can SdlRd, et al. Industry In IPCC Climate Change 2022: Mitigation of Climate Change. Contribution of Working Group III to the Sixth Assessment Report of the Intergovernmental Panel on Climate Change: IPCC; 2022.
[102] Turner JA. Sustainable Hydrogen Production. Science. 2004;305:972-4.
[103] Howarth RW, Jacobson MZ. How green is blue hydrogen? Energy Science & Engineering. 2021;9:1676-87.
[104] Romano MC, Antonini C, Bardow A, Bertsch V, Brandon NP, Brouwer J, et al. Comment on “How green is blue hydrogen?”. Energy Science & Engineering. 2022;10:1944-54.
[105] Mac Dowell N, Sunny N, Brandon N, Herzog H, Ku AY, Maas W, et al. The hydrogen economy: A pragmatic path forward. Joule. 2021;5:2524-9.
[106] Fazeli R, Beck FJ, Stocks M. Recognizing the role of uncertainties in the transition to renewable hydrogen. International Journal of Hydrogen Energy. 2022;47:27896-910.
[107] DESNZ. Hydrogen Production Delivery Roadmap. In: Zero UDfESN, editor. UK2023.
[108] Bali E, Audétat A, Keppler H. Water and hydrogen are immiscible in Earth’s mantle. Nature. 2013;495:220-2.
[109] Arcos JMM, Santos DMF. The Hydrogen Color Spectrum: Techno-Economic Analysis of the Available Technologies for Hydrogen Production. Gases. 2023;3:25-46.
[110] Newborough M, Cooley G. Developments in the global hydrogen market: The spectrum of hydrogen colours. Fuel Cells Bulletin. 2020;2020:16-22.
[111] Incer-Valverde J, Korayem A, Tsatsaronis G, Morosuk T. “Colors” of hydrogen: Definitions and carbon intensity. Energy Conversion and Management. 2023;291:117294.
[112] Ajanovic A, Sayer M, Haas R. The economics and the environmental benignity of different colors of hydrogen. International Journal of Hydrogen Energy. 2022;47:24136-54.
[113] Osselin F, Soulaine C, Fauguerolles C, Gaucher EC, Scaillet B, Pichavant M. Orange hydrogen is the new green. Nature Geoscience. 2022;15:765-9.
[114] Midilli A, Dincer I. Key strategies of hydrogen energy systems for sustainability. International Journal of Hydrogen Energy. 2007;32:511-24.
[115] Balat M. Potential importance of hydrogen as a future solution to environmental and transportation problems. International Journal of Hydrogen Energy. 2008;33:4013-29.
[116] Kovač A, Paranos M, Marciuš D. Hydrogen in energy transition: A review. International Journal of Hydrogen Energy. 2021;46:10016-35.
[117] Pathak PK, Yadav AK, Padmanaban S. Transition toward emission-free energy systems by 2050: Potential role of hydrogen. International Journal of Hydrogen Energy. 2023;48:9921-7.
[118] Kouchaki-Penchah H, Bahn O, Bashiri H, Bedard S, Bernier E, Elliot T, et al. The role of hydrogen in a net-zero emission economy under alternative policy scenarios. International Journal of Hydrogen Energy. 2024;49:173-87.
[119] Boretti A, Pollet BG. Hydrogen economy: Paving the path to a sustainable, low-carbon future. International Journal of Hydrogen Energy. 2024;93:307-19.
[120] Bade SO, Taiwo K, Ndulue UF, Tomomewo OS, Aisosa Oni B. A review of underground hydrogen storage systems: Current status, modeling approaches, challenges, and future prospective. International Journal of Hydrogen Energy. 2024;80:449-74.
[121] Ben Rhouma S. Comprehensive analysis of underground H2 storage with CO2 as a cushion gas in aquifers : Capacity assessments, thermodynamic approaches, and realistic reservoir simulations

Analyse du stockage souterrain de H2 avec le CO2 comme gaz coussin dans des aquifères : Évaluations de capacité, approches thermodynamiques et simulations réalistes de réservoir: Université de Pau et des Pays de l'Adour; 2023.
[122] Farazmand M, Saadat Z, Sameti M. Above-ground hydrogen storage: A state-of-the-art review. International Journal of Hydrogen Energy. 2024;90:1173-205.
[123] Olabi AG, bahri As, Abdelghafar AA, Baroutaji A, Sayed ET, Alami AH, et al. Large-vscale hydrogen production and storage technologies: Current status and future directions. International Journal of Hydrogen Energy. 2021;46:23498-528.
[124] Peters R, Baltruweit M, Grube T, Samsun RC, Stolten D. A techno economic analysis of the power to gas route. Journal of CO2 Utilization. 2019;34:616-34.
[125] Niermann M, Beckendorff A, Kaltschmitt M, Bonhoff K. Liquid Organic Hydrogen Carrier (LOHC) – Assessment based on chemical and economic properties. International Journal of Hydrogen Energy. 2019;44:6631-54.
[126] Bacatelo M, Capucha F, Ferrão P, Margarido F, Bordado J. Carbon-neutral cement: The role of green hydrogen. International Journal of Hydrogen Energy. 2024;63:382-95.
[127] Liu W, Zuo H, Wang J, Xue Q, Ren B, Yang F. The production and application of hydrogen in steel industry. International Journal of Hydrogen Energy. 2021;46:10548-69.
[128] Ma K, Deng J, Wang G, Zhou Q, Xu J. Utilization and impacts of hydrogen in the ironmaking processes: A review from lab-scale basics to industrial practices. International Journal of Hydrogen Energy. 2021;46:26646-64.
[129] Piselli C, Balocco C, Forastiere S, Silei A, Sciurpi F, Cotana F. Energy efficiency in the commercial sector. Thermodynamics fundamentals for the energy transition. Energy Reports. 2024;11:4601-21.
[130] Davis LW, Gertler PJ. Contribution of air conditioning adoption to future energy use under global warming. Proceedings of the National Academy of Sciences. 2015;112:5962-7.
[131] Falchetta G, Cian ED, Pavanello F, Wing IS. Inequalities in global residential cooling energy use to 2050. Nature Communications. 2024;15:7874.
[132] McLinden MO, Brown JS, Brignoli R, Kazakov AF, Domanski PA. Limited options for low-global-warming-potential refrigerants. Nature Communications. 2017;8:14476.
[133] McLinden MO, Huber ML. (R)Evolution of Refrigerants. Journal of Chemical & Engineering Data. 2020;65:4176-93.
[134] Prather M, Midgley P, Rowland FS, Stolarski R. The ozone layer: the road not taken. Nature. 1996;381:551-4.
[135] Giunta C. Thomas Midgley, Jr., and the invention of chlorofluorocabon refrigerants: It ain't necessarily so. Bulletin for the History of Chemistry. 2006;31:66-74.
[136] Egorova T, Sedlacek J, Sukhodolov T, Karagodin-Doyennel A, Zilker F, Rozanov E. Montreal Protocol's impact on the ozone layer and climate. Atmos Chem Phys. 2023;23:5135-47.
[137] IPCC. Climate change 2007: the physical science basis. IPCC. 2007;6:333.
[138] Latcham RV, Trusler JPM. Phase Behavior of Isobutane + CO2 and Isobutane + H2 at Temperatures Between 190 and 400 K and at Pressures Up to 20 MPa. International Journal of Thermophysics. 2024;45:1-27.
[139] Bhatkar VW, Kriplani VM, Awari GK. Alternative refrigerants in vapour compression refrigeration cycle for sustainable environment: a review of recent research. International Journal of Environmental Science and Technology. 2013;10:871-80.
[140] Hodnebrog Ø, Dalsøren SB, Myhre G. Lifetimes, direct and indirect radiative forcing, and global warming potentials of ethane (C2H6), propane (C3H8), and butane (C4H10). Atmospheric Science Letters. 2018;19:e804.
[141] Collins WJ, Derwent RG, Johnson CE, Stevenson DS. The Oxidation of Organic Compounds in the Troposphere and their Global Warming Potentials. Climatic Change. 2002;52:453-79.
[142] Sarkar J, Bhattacharyya S. Assessment of blends of CO2 with butane and isobutane as working fluids for heat pump applications. International Journal of Thermal Sciences. 2009;48:1460-5.
[143] Ganesan P, Eikevik TM, Hamid K, Wang R, Yan H. Thermodynamic analysis of cascade high-temperature heat pump using new natural zeotropic refrigerant mixtures: R744/R600 and R744/R601. International Journal of Refrigeration. 2023;154:215-30.

[144] Zhang X, A. C, H. D. Performance Analysis of the Natural Mixture R744/R600a Refrigeration Cycle. 2010 International Conference on Mechanic Automation and Control Engineering (MACE 2010). Wuhan, China2010.
[145] Fan XW, Ju F-J, Zhang X-P, Wang F. Thermodynamic comparision of R744/R600A and R744/R600 used in mid-high temperature heat pump system. Thermal Science. 2014;18:1655-9.
[146] Sobieraj M, Rosiński M. Experimental study of the heat transfer in R744/R600a mixtures below the R744 triple point temperature. International Journal of Refrigeration. 2019;103:243-52.
[147] Ono Y. A survey of the mechanism in catalytic isomerization of alkanes. Catalysis Today. 2003;81:3-16.
[148] Wang H, Fan S, Guo S, Wang S, Qin Z, Dong M, et al. Selective conversion of CO2 to isobutane-enriched C4 alkanes over InZrOx-Beta composite catalyst. Nature Communications. 2023;14:2627.
[149] EMPIR. 20IND10. Decarb. 2021.
[150] Romeo R, Cavuoto G, Albo PAG, Lago S. Experimental densities of hydrogen-isobutane mixtures with three different compositions. ECTP2023. Venice2023.
[151] Olah GA. Beyond Oil and Gas: The Methanol Economy. Angewandte Chemie International Edition. 2005;44:2636-9.
[152] Olah GA, Goeppert A, Prakash GKS. Chemical Recycling of Carbon Dioxide to Methanol and Dimethyl Ether: From Greenhouse Gas to Renewable, Environmentally Carbon Neutral Fuels and Synthetic Hydrocarbons. The Journal of Organic Chemistry. 2009;74:487-98.
[153] Roode-Gutzmer QI, Kaiser D, Bertau M. Renewable Methanol Synthesis. ChemBioEng Reviews. 2019;6:209-36.
[154] Bertau M, Offermanns H, Plass L, Schmidt F, Wernicke H-J. Methanol: the basic chemical and energy feedstock of the future: Springer; 2014.
[155] Tabibian SS, Sharifzadeh M. Statistical and analytical investigation of methanol applications, production technologies, value-chain and economy with a special focus on renewable methanol. Renewable and Sustainable Energy Reviews. 2023;179:113281.
[156] Bahmanpour AM, Hoadley A, Tanksale A. Formaldehyde production via hydrogenation of carbon monoxide in the aqueous phase. Green Chemistry. 2015;17:3500-7.
[157] Yang C-J, Jackson RB. China's growing methanol economy and its implications for energy and the environment. Energy Policy. 2012;41:878-84.
[158] Deniz C, Zincir B. Environmental and economical assessment of alternative marine fuels. Journal of Cleaner Production. 2016;113:438-49.
[159] Svanberg M, Ellis J, Lundgren J, Landälv I. Renewable methanol as a fuel for the shipping industry. Renewable and Sustainable Energy Reviews. 2018;94:1217-28.
[160] Fasihi M, Breyer C. Global production potential of green methanol based on variable renewable electricity. Energy & Environmental Science. 2024;17:3503-22.
[161] Sollai S, Porcu A, Tola V, Ferrara F, Pettinau A. Renewable methanol production from green hydrogen and captured CO2: A techno-economic assessment. Journal of CO2 Utilization. 2023;68:102345.
[162] Nemmour A, Inayat A, Janajreh I, Ghenai C. Green hydrogen-based E-fuels (E-methane, E-methanol, E-ammonia) to support clean energy transition: A literature review. International Journal of Hydrogen Energy. 2023;48:29011-33.
[163] Bassani A, Bozzano G, Pirola C, Ranzi E, Pierucci S, Manenti F. Low Impact Methanol Production from Sulfur Rich Coal Gasification. Energy Procedia. 2017;105:4519-24.
[164] Azhari NJ, Erika D, Mardiana S, Ilmi T, Gunawan ML, Makertihartha IGBN, et al. Methanol synthesis from CO2: A mechanistic overview. Results in Engineering. 2022;16:100711.
[165] Liu G, Hagelin-Weaver H, Welt B. A Concise Review of Catalytic Synthesis of Methanol from Synthesis Gas. Waste. 2023;1:228-48.
[166] Khojasteh-Salkuyeh Y, Ashrafi O, Mostafavi E, Navarri P. CO2 utilization for methanol production; Part I: Process design and life cycle GHG assessment of different pathways. Journal of CO2 Utilization. 2021;50:101608.
[167] Elvers B. Ullmann's encyclopedia of industrial chemistry: Verlag Chemie Hoboken, NJ; 1991.

[168] Bowker M. Methanol Synthesis from CO2 Hydrogenation. ChemCatChem. 2019;11:4238-46.
[169] Hobson C, Márquez C. Renewable methanol report. Methanol Institute, Singapore. 2018.
[170] Yahyazadeh A, Nanda S, Dalai AK. A Critical Review of the Sustainable Production and Application of Methanol as a Biochemical and Bioenergy Carrier. Reactions. 2024;5:1-19.
[171] Cordonnier J, Saygin D. Green hydrogen opportunities for emerging and developing economies: Identifying success factors for market development and building enabling conditions. OECD. 2022.
[172] Trust DB, Kurata F. Vapor-liquid phase behavior of the hydrogen-propane and hydrogen-carbon monoxide-propane systems. AIChE Journal. 1971;17:86-91.
[173] Aroyan HJ, Katz DL. Low Temperature Vapor-Liquid Equilibria in Hydrogen-n-Butane System. Industrial & Engineering Chemistry. 1951;43:185-9.
[174] Nelson EE, Bonnell WS. Solubility of Hydrogen in n-Butane. Industrial & Engineering Chemistry. 1943;35:204-6.
[175] Klink AE, Cheh HY, Amick Jr. EH. The vapor-liquid equilibrium of the hydrogen—n-butane system at elevated pressures. AIChE Journal. 1975;21:1142-8.
[176] Dean MR, Tooke JW. Vapor-Liquid Equilibria in Three Hydrogen-Paraffin Systems. Industrial & Engineering Chemistry. 1946;38:389-93.
[177] KAMINISHI G-I, ARAI Y, SAITO S, MAEDA S. Vapor-liquid equilibria for binary and ternary systems containing carbon dioxide. Journal of Chemical Engineering of Japan. 1968;1:109-16.
[178] Yokoyama C, Arai K, Saito S, Mori H. Bubble-point pressures of the H2□CO□CO2 system. Fluid Phase Equilibria. 1988;39:101-10.
[179] Ke J, Han B, George MW, Yan H, Poliakoff M. How Does the Critical Point Change during a Chemical Reaction in Supercritical Fluids? A Study of the Hydroformylation of Propene in Supercritical CO2. Journal of the American Chemical Society. 2001;123:3661-70.
[180] Fürstenberg S, Souza LFS, Trusler JPM. [unpublished] Measurement and modelling of the vapor liquid equilibrium of (CO2 + CO + H2) and (CO2 + CO + H2 + CH4 + N2) between 223 and 273 K and at pressures up to 14 MPa. 2018.
[181] Andbaeva VN, Khotienkova MN. Investigation of Surface Tension of Isobutane (R600a) and Isobutane–Hydrogen Solutions. Journal of Chemical & Engineering Data. 2024.
[182] Kontogeorgis GM, Dohrn R, Economou IG, de Hemptinne J-C, ten Kate A, Kuitunen S, et al. Industrial Requirements for Thermodynamic and Transport Properties: 2020. Industrial & Engineering Chemistry Research. 2021;60:4987-5013.
[183] de Hemptinne J-C, Kontogeorgis GM, Dohrn R, Economou IG, ten Kate A, Kuitunen S, et al. A View on the Future of Applied Thermodynamics. Industrial & Engineering Chemistry Research. 2022;61:14664-80.
[184] Assael MJ, Goodwin AR, Stamatoudis M, Wakeham WA, Will S. Commonly asked questions in thermodynamics. Boca Raton: CRC; 2011.
[185] Poling BE, O'Connell JP, Prausnitz JM. The properties of gases and liquids. 5th ed. New York: McGraw-Hill; 2001.
[186] Goodwin ARH, Sengers JV, Peters CJ. Applied thermodynamics of fluids. 1st ed. Cambridge: RSC Pub.; 2010.
[187] Bedeaux D, Kjelstrup S, Schnell SK. Nanothermodynamics: Theory and Applications: World Scientific; 2023.
[188] Alberty RA. Use of legendre transforms in chemical thermodynamics: International Union of Pure and Applied Chemistry, Physical Chemistry Division, Commission on Thermodynamics. The Journal of Chemical Thermodynamics. 2002;34:1787-823.
[189] Sun W, Powell-Palm M, Chen J. The geometry of high-dimensional phase diagrams: I. Generalized Gibbs' Phase Rule2024.
[190] IUPAC. surface tension. IUPAC Gold Book. 5.0.0 ed: International Union of Pure and Applied Chemistry (IUPAC); 2025.
[191] Kaptay G. The Generalized Phase Rule, the Extended Definition of the Degree of Freedom, the Component Rule and the Seven Independent Non-Compositional State Variables: To the 150th Anniversary of the Phase Rule of Gibbs. Materials. 2024;17:6048.
[192] Okada K. Generalized Phase Rule and Possible Singular Point Sets in Physical Systems. Progress of Theoretical Physics. 1987;78:1236-41.

[193] Dias DA, Lima FWS, Plascak JA. Generalized Gibbs Phase Rule and Multicriticality Applied to Magnetic Systems. Entropy (Basel). 2021;24.
[194] Opdam J, Peters VFD, Wensink HH, Tuinier R. Multiphase Coexistence in Binary Hard Colloidal Mixtures: Predictions from a Simple Algebraic Theory. The Journal of Physical Chemistry Letters. 2023;14:199-206.
[195] Gibbs JW. Scientific papers of J. Willard Gibbs. London: Longmans, Green and Co.; 1906.
[196] Liu MK, Wagner M, Abreu E, Kittiwatanakul S, McLeod A, Fei Z, et al. Anisotropic Electronic State via Spontaneous Phase Separation in Strained Vanadium Dioxide Films. Physical Review Letters. 2013;111:096602.
[197] Leggett AJ. Interpretation of Recent Results on He3 below 3 mK: A New Liquid Phase? Physical Review Letters. 1972;29:1227-30.
[198] Frenkel D. Order through entropy. Nature Materials. 2015;14:9-12.
[199] Peters VFD, Vis M, García ÁG, Wensink HH, Tuinier R. Defying the Gibbs Phase Rule: Evidence for an Entropy-Driven Quintuple Point in Colloid-Polymer Mixtures. Physical Review Letters. 2020;125:127803.
[200] Trusler JPM. Physical Acoustics and Metrology of Fluids. Boca Raton: CRC Press; 1991.
[201] Fourie FCvN, Schwarz CE, Knoetze JH. Analytic Setup for Multicomponent High-Pressure Phase Equilibria via Dual Online Gas Chromatography. Chemical Engineering & Technology. 2015;38:1165-72.
[202] Fourie FCvN, Schwarz CE, Knoetze JH. Analytic High-Pressure Phase Equilibria. Part II: Gas Chromatography and Sampling Method Development. Chemical Engineering & Technology. 2016;39:1475-82.
[203] Anisimov MA, Sengers JV, Levelt Sengers JMH. Chapter 2 - Near-critical behavior of aqueous systems. In: Palmer DA, Fernández-Prini R, Harvey AH, editors. Aqueous Systems at Elevated Temperatures and Pressures. London: Academic Press; 2004. p. 29-71.
[204] Liao G, Du Y, Zhang F, Jiaqiang E, Chen J, Leng E. Widom line of supercritical CO2 calculated by equations of state and molecular dynamics simulation. Journal of CO2 Utilization. 2022;62:102075.
[205] Saric D, Guevara-Carrion G, Vrabec J. Thermodynamics of supercritical carbon dioxide mixtures across the Widom line. Physical Chemistry Chemical Physics. 2022;24:28257-70.
[206] Brazhkin VV, Fomin YD, Lyapin AG, Ryzhov VN, Trachenko K. Two liquid states of matter: A dynamic line on a phase diagram. Physical Review E. 2012;85:031203.
[207] Span R, Wagner W. A New Equation of State for Carbon Dioxide Covering the Fluid Region from the Triple-Point Temperature to 1100 K at Pressures up to 800 MPa. Journal of Physical and Chemical Reference Data. 1996;25:1509-96.
[208] Boyle R. New experiments physico-mechanical, touching the spring of the air, and its effects. Oxford: Oxford; 1660.
[209] Clausius R. The Mechanical Theory of Heat: With its Applications to the Steam-engine and the Physical Properties of Bodies. Havard: J. Van Voorst; 1867.
[210] Clapeyron E. Mémoire sur la puissance motrice de la chaleur. Journal de l'École Polytechnique. 1835;XIV:153-90.
[211] van der Waals JD, Rowlinson JS. On the Continuity of the Gaseous and Liquid States, edited and with an Introduction by J.S. Rowlinson. New York: Dover Phoenix Editions; 1984.
[212] van der Waals JD. Over de Continuïteit van den Gas en Vloeistoftoestand: Leiden University; 1873.
[213] Steinhaus H. Length, Shape and Area. Colloquium Mathematicum Communications. 1954;3:1-13.
[214] Mandelbrot B. The Fractal Geometry of Nature. US: W.H. Freeman and Co.; 1982.
[215] Schwerdtfeger P, Wales DJ. 100 Years of the Lennard-Jones Potential. Journal of Chemical Theory and Computation. 2024;20:3379-405.
[216] Craig DP, Thirunamachandran T. Molecular Quantum Electrodynamics: An Introduction to Radiation-Molecule Interactions. New York: Dover Publications Inc.; 1984.
[217] Orbey H, Sandler SI. Modeling Vapor-Liquid Equilibria: Cubic Equations of State and Their Mixing Rules. Cambridge: Cambridge University Press; 1998.
[218] Rowlinson JS, Swinton FL. Liquids and Liquid Mixtures (Third Edition): Butterworth-Heinemann; 1982.

[219] Liu H. From the vapour–liquid coexistence region to the supercritical fluid: the van der Waals fluid. Molecular Physics. 2023;121:e2155260.
[220] Simeoni GG, Bryk T, Gorelli FA, Krisch M, Ruocco G, Santoro M, et al. The Widom line as the crossover between liquid-like and gas-like behaviour in supercritical fluids. Nature Physics. 2010;6:503-7.
[221] Wilhelmsen Ø, Aasen A, Skaugen G, Aursand P, Austegard A, Aursand E, et al. Thermodynamic Modeling with Equations of State: Present Challenges with Established Methods. Industrial & Engineering Chemistry Research. 2017;56:3503-15.
[222] Hammer M, Aasen A, Wilhelmsen Ø. Extrapolating into no man's land enables accurate estimation of surface properties with multiparameter equations of state. Fluid Phase Equilibria. 2024;586:114196.
[223] Chaparro G, Müller EA. Development of a Helmholtz free energy equation of state for fluid and solid phases via artificial neural networks. Communications Physics. 2024;7:406.
[224] Troncoso J, Cerdeiriña CA. Ising model for the freezing transition. Physical Review E. 2024;109:014123.
[225] Redlich O, Kwong JNS. On the Thermodynamics of Solutions. V. An Equation of State. Fugacities of Gaseous Solutions. Chemical Reviews. 1949;44:233-44.
[226] Soave G. Equilibrium constants from a modified Redlich-Kwong equation of state. Chemical Engineering Science. 1972;27:1197-203.
[227] Twu CH, Bluck D, Cunningham JR, Coon JE. A cubic equation of state with a new alpha function and a new mixing rule. Fluid Phase Equilibria. 1991;69:33-50.
[228] Boston JF, Mathias PM. PHASE EQUILIBRIA IN A THIRD-GENERATION PROCESS SIMULATOR. EFCE Publication Series (European Federation of Chemical Engineering). 11 ed1980. p. 823-49.
[229] Neau E, Hernández-Garduza O, Escandell J, Nicolas C, Raspo I. The Soave, Twu and Boston–Mathias alpha functions in cubic equations of state: Part I. Theoretical analysis of their variations according to temperature. Fluid Phase Equilibria. 2009;276:87-93.
[230] Privat R, Visconte M, Zazoua-Khames A, Jaubert J-N, Gani R. Analysis and prediction of the alpha-function parameters used in cubic equations of state. Chemical Engineering Science. 2015;126:584-603.
[231] Peng D-Y, Robinson DB. A New Two-Constant Equation of State. Industrial & Engineering Chemistry Fundamentals. 1976;15:59-64.
[232] Péneloux A, Rauzy E, Fréze R. A consistent correction for Redlich-Kwong-Soave volumes. Fluid Phase Equilibria. 1982;8:7-23.
[233] Jaubert J-N, Privat R, Le Guennec Y, Coniglio L. Note on the properties altered by application of a Péneloux–type volume translation to an equation of state. Fluid Phase Equilibria. 2016;419:88-95.
[234] Prausnitz JM. Equations of state from van der Waals theory: the legacy of Otto Redlich. Fluid Phase Equilibria. 1985;24:63-76.
[235] Gmehling J, Constantinescu D, Schmid B. Group Contribution Methods for Phase Equilibrium Calculations. Annual Review of Chemical and Biomolecular Engineering. 2015;6:267-92.
[236] Jirasek F, Hayer N, Abbas R, Schmid B, Hasse H. Prediction of parameters of group contribution models of mixtures by matrix completion. Physical Chemistry Chemical Physics. 2023;25:1054-62.
[237] Valderrama JO. The State of the Cubic Equations of State. Industrial & Engineering Chemistry Research. 2003;42:1603-18.
[238] Kontogeorgis GM, Liang X, Arya A, Tsivintzelis I. Equations of state in three centuries. Are we closer to arriving to a single model for all applications? Chemical Engineering Science: X. 2020;7:100060.
[239] Wong DSH, Sandler SI. A theoretically correct mixing rule for cubic equations of state. AIChE Journal. 1992;38:671-80.
[240] Orbey H, Sandler SI. On the combination of equation of state and excess free energy models. Fluid Phase Equilibria. 1995;111:53-70.
[241] Orbey H, Sandler SI. Analysis of excess free energy based equations of state models. AIChE Journal. 1996;42:2327-34.
[242] Renon H, Prausnitz JM. Local compositions in thermodynamic excess functions for liquid mixtures. AIChE Journal. 1968;14:135-44.

[243] van Laar JJ. Über Dampfspannungen von binären Gemischen. Zeitschrift für Physikalische Chemie. 1910;72:723-51.
[244] van Laar JJ. Zur Theorie der Dampfspannungen von binären Gemischen. Erwiderung an Herrn F. Dolezalek. Zeitschrift für Physikalische Chemie. 1913;83:599-608.
[245] Peng D-Y. Extending the Van Laar model to multicomponent systems. Open Thermodynamics Journal. 2010;4:129-40.
[246] Wilson GM. Vapor-Liquid Equilibrium. XI. A New Expression for the Excess Free Energy of Mixing. Journal of the American Chemical Society. 1964;86:127-30.
[247] Privat R, Jaubert J-N, Kontogeorgis GM. The secret of the Wilson equation. Fluid Phase Equilibria. 2024;579:114018.
[248] Abrams DS, Prausnitz JM. Statistical thermodynamics of liquid mixtures: A new expression for the excess Gibbs energy of partly or completely miscible systems. AIChE Journal. 1975;21:116-28.
[249] Maurer G, Prausnitz JM. On the derivation and extension of the uniquac equation. Fluid Phase Equilibria. 1978;2:91-9.
[250] Klamt A, Krooshof GJP, Taylor R. COSMOSPACE: Alternative to conventional activity-coefficient models. AIChE Journal. 2002;48:2332-49.
[251] Kontogeorgis GM, Coutsikos P. Thirty Years with EoS/GE Models—What Have We Learned? Industrial & Engineering Chemistry Research. 2012;51:4119-42.
[252] Orbey H, Sandler SI. Reformulation of Wong-Sandler mixing rule for cubic equations of state. AIChE Journal. 1995;41:683-90.
[253] Margules M. Über die Zusammensetzung der gesättigten Dämpfe von Misschungen. Sitzungsberichte der Kaiserliche Akadamie der Wissenschaften Wien Mathematisch-Naturwissenschaftliche Klasse II. 1895;104:1243-78.
[254] Zhao Y, Dong X, Gong M, Shen J. Reconsideration of the alpha coefficient in NRTL model on the vapor liquid phase equilibrium description of refrigerant mixtures. International Journal of Refrigeration. 2019;100:227-34.
[255] Marina JM, Tassios DP. Effective Local Compositions in Phase Equilibrium Correlations. Industrial & Engineering Chemistry Process Design and Development. 1973;12:67-71.
[256] Jaubert J-N, Privat R, Mutelet F. Predicting the phase equilibria of synthetic petroleum fluids with the PPR78 approach. AIChE Journal. 2010;56:3225-35.
[257] Jaubert J-N, Mutelet F. VLE predictions with the Peng–Robinson equation of state and temperature dependent kij calculated through a group contribution method. Fluid Phase Equilibria. 2004;224:285-304.
[258] Jaubert J-N, Qian J-W, Lasala S, Privat R. The impressive impact of including enthalpy and heat capacity of mixing data when parameterising equations of state. Application to the development of the E-PPR78 (Enhanced-Predictive-Peng-Robinson-78) model. Fluid Phase Equilibria. 2022;560:113456.
[259] Trusler JPM. 3 The virial equation of state. In: Sengers JV, Kayser RF, Peters CJ, White HJ, editors. Experimental Thermodynamics: Elsevier; 2000. p. 35-74.
[260] Wisniak J. Heike Kamerlingh - The Virial Equation of State. Indian Journal of Chemical Technology. 2003;10:564-72.
[261] Barker JA, Henderson D. Perturbation Theory and Equation of State for Fluids: The Square-Well Potential. The Journal of Chemical Physics. 1967;47:2856-61.
[262] Barker JA, Henderson D. Perturbation Theory and Equation of State for Fluids. II. A Successful Theory of Liquids. The Journal of Chemical Physics. 1967;47:4714-21.
[263] Wertheim MS. Fluids with highly directional attractive forces. I. Statistical thermodynamics. Journal of Statistical Physics. 1984;35:19-34.
[264] Wertheim MS. Fluids with highly directional attractive forces. II. Thermodynamic perturbation theory and integral equations. Journal of Statistical Physics. 1984;35:35-47.
[265] Wertheim MS. Fluids with highly directional attractive forces. III. Multiple attraction sites. Journal of Statistical Physics. 1986;42:459-76.
[266] Wertheim MS. Fluids with highly directional attractive forces. IV. Equilibrium polymerization. Journal of Statistical Physics. 1986;42:477-92.
[267] Zmpitas W, Gross J. Detailed pedagogical review and analysis of Wertheim's thermodynamic perturbation theory. Fluid Phase Equilibria. 2016;428:121-52.
[268] Chapman WG, Gubbins KE, Jackson G, Radosz M. New reference equation of state for associating liquids. Industrial & Engineering Chemistry Research. 1990;29:1709-21.

[269] Lafitte T, Apostolakou A, Avendaño C, Galindo A, Adjiman CS, Müller EA, et al. Accurate statistical associating fluid theory for chain molecules formed from Mie segments. The Journal of Chemical Physics. 2013;139.
[270] Papaioannou V, Lafitte T, Avendaño C, Adjiman CS, Jackson G, Müller EA, et al. Group contribution methodology based on the statistical associating fluid theory for heteronuclear molecules formed from Mie segments. The Journal of Chemical Physics. 2014;140.
[271] McCabe C, Galindo A. SAFT Associating Fluids and Fluid Mixtures. In: Goodwin AR, Sengers J, Peters CJ, editors. Applied Thermodynamics of Fluids: The Royal Society of Chemistry; 2010. p. 0.
[272] Müller EA, Gubbins KE. Molecular-Based Equations of State for Associating Fluids: A Review of SAFT and Related Approaches. Industrial & Engineering Chemistry Research. 2001;40:2193-211.
[273] Economou IG. Statistical Associating Fluid Theory: A Successful Model for the Calculation of Thermodynamic and Phase Equilibrium Properties of Complex Fluid Mixtures. Industrial & Engineering Chemistry Research. 2002;41:953-62.
[274] Müller EA, Jackson G. Force-Field Parameters from the SAFT-γ Equation of State for Use in Coarse-Grained Molecular Simulations. Annual Review of Chemical and Biomolecular Engineering. 2014;5:405-27.
[275] Lafitte T, Bessieres D, Piñeiro MM, Daridon J-L. Simultaneous estimation of phase behavior and second-derivative properties using the statistical associating fluid theory with variable range approach. The Journal of Chemical Physics. 2006;124.
[276] Haslam AJ, González-Pérez A, Di Lecce S, Khalit SH, Perdomo FA, Kournopoulos S, et al. Expanding the Applications of the SAFT-γ Mie Group-Contribution Equation of State: Prediction of Thermodynamic Properties and Phase Behavior of Mixtures. Journal of Chemical & Engineering Data. 2020;65:5862-90.
[277] Shaahmadi F, Hurter RM, Burger AJ, Cripwell JT. Improving the SAFT-γ Mie equation of state to account for functional group interactions in a structural (s-SAFT-γ Mie) framework: Linear and branched alkanes. The Journal of Chemical Physics. 2021;154.
[278] Deiters UK, Bell IH. Unphysical Critical Curves of Binary Mixtures Predicted with GERG Models. Int J Thermophys. 2016;41.
[279] Bell IH, Lemmon EW, Harvey AH. An Analysis of the Critical Region of Multiparameter Equations of State. International Journal of Thermophysics. 2023;44:158.
[280] Span R. Multiparameter Equations of State : An Accurate Source of Thermodynamic Property Data. 1st 2000. ed. Berlin, Heidelberg: Springer Berlin Heidelberg; 2000.
[281] Garberoglio G, Gaiser C, Gavioso RM, Harvey AH, Hellmann R, Jeziorski B, et al. Ab Initio Calculation of Fluid Properties for Precision Metrology. Journal of Physical and Chemical Reference Data. 2023;52.
[282] Leachman JW, Jacobsen RT, Penoncello SG, Lemmon EW. Fundamental Equations of State for Parahydrogen, Normal Hydrogen, and Orthohydrogen. Journal of Physical and Chemical Reference Data. 2009;38:721-48.
[283] De Reuck K, Craven R. Methanol. International Thermodynamic Tables of the Fluid State, vol. 12. IUPAC, Blackwell Scientific Publications, London. 1993.
[284] Bücker D, Wagner W. Reference Equations of State for the Thermodynamic Properties of Fluid Phase n-Butane and Isobutane. Journal of Physical and Chemical Reference Data. 2006;35:929-1019.
[285] Kunz O, Wagner W. The GERG-2008 Wide-Range Equation of State for Natural Gases and Other Mixtures: An Expansion of GERG-2004. Journal of Chemical & Engineering Data. 2012;57:3032-91.
[286] Kunz O, Klimeck R, Wagner W, Jaeschke M. The GERG-2004 wide-range equation of state for natural gases and other mixtures. Germany: VDI-Verlag, Duesseldorf (Germany); 2007.
[287] ISO. 20765-2:2015 - Natural gas - Calculation of thermodynamic properties. Part 2: Single-phase properties (gas, liquid, and dense fluid) for extended ranges of application. Geneva: International Organization for Standardization; 2015.
[288] Beckmüller R, Thol M, Bell IH, Lemmon EW, Span R. New Equations of State for Binary Hydrogen Mixtures Containing Methane, Nitrogen, Carbon Monoxide, and Carbon Dioxide. Journal of Physical and Chemical Reference Data. 2021;50.

[289] Lemmon EW, Span R. Multi-parameter Equations of State for Pure Fluids and Mixtures. In: Goodwin AR, Sengers J, Peters CJ, editors. Applied Thermodynamics of Fluids: The Royal Society of Chemistry; 2010. p. 0.
[290] Span R, Wagner W, Lemmon EW, Jacobsen RT. Multiparameter equations of state — recent trends and future challenges. Fluid Phase Equilibria. 2001;183-184:1-20.
[291] Zervidi KA. Process development and optimisation of a hybrid system for direct air capture. London: Imperial College London; 2025.
[292] Huber ML, Lemmon EW, Bell IH, McLinden MO. The NIST REFPROP Database for Highly Accurate Properties of Industrially Important Fluids. Industrial & Engineering Chemistry Research. 2022;61:15449-72.
[293] Lemmon EW, Bell IH, Huber ML, McLinden MO. REFPROP 10.0. NIST; 2018.
[294] Walker PJ, Yew H-W, Riedemann A. Clapeyron.jl: An Extensible, Open-Source Fluid Thermodynamics Toolkit. Industrial & Engineering Chemistry Research. 2022;61:7130-53.
[295] Al-Malah KIM. Aspen Plus®: Chemical Engineering Applications: John Wiley & Sons Inc.; 2016.
[296] Martin MM. Introduction to software for chemical engineers. Second edition. ed. Boca Raton: CRC Press; 2020.
[297] KBC. Petro-SIM. 7.5 ed: KBC Advanced Technologies; 2024.
[298] Tangsriwong K, Lapchit P, Kittijungjit T, Klamrassamee T, Sukjai Y, Laoonual Y. Modeling of chemical processes using commercial and open-source software: A comparison between Aspen Plus and DWSIM. IOP Conference Series: Earth and Environmental Science. 2020;463:012057.
[299] Fritzson P, Pop A, Abdelhak K, Asghar A, Bachmann B, Braun W, et al. The OpenModelica integrated environment for modeling, simulation, and model-based development. Mic; 2022.
[300] Riedemann A, Subramanian A, Viena V. ProcessSimulator.jl: A Differentiable Chemical Process Simulator. Juliacon 2024. London2024.
[301] Michelsen ML. The isothermal flash problem. Part II. Phase-split calculation. Fluid Phase Equilibria. 1982;9:21-40.
[302] Privat R, Jaubert J-N, Privat Y. A simple and unified algorithm to solve fluid phase equilibria using either the gamma–phi or the phi–phi approach for binary and ternary mixtures. Computers & Chemical Engineering. 2013;50:139-51.
[303] Michelsen ML. The isothermal flash problem. Part I. Stability. Fluid Phase Equilibria. 1982;9:1-19.
[304] Lasdon LS, Waren AD, Jain A, Ratner M. Design and Testing of a Generalized Reduced Gradient Code for Nonlinear Programming. ACM Trans Math Softw. 1978;4:34–50.
[305] Fandiño O, Trusler JPM, Vega-Maza D. Phase behavior of (CO2+H2) and (CO2+N2) at temperatures between (218.15 and 303.15)K at pressures up to 15MPa. International Journal of Greenhouse Gas Control. 2015;36:78-92.
[306] Souza LFS, Al Ghafri SZS, Trusler JPM. Measurement and modelling of the vapor–liquid equilibrium of (CO2 + CO) at temperatures between (218.15 and 302.93) K at pressures up to 15 MPa. The Journal of Chemical Thermodynamics. 2018;126:63-73.
[307] Westman SF, Stang HGJ, Løvseth SW, Austegard A, Snustad I, Størset SØ, et al. Vapor–liquid equilibrium data for the carbon dioxide and nitrogen (CO2 + N2) system at the temperatures 223, 270, 298 and 303 K and pressures up to 18 MPa. Fluid Phase Equilibria. 2016;409:207-41.
[308] Hudson DR. Density and Packing in an Aggregate of Mixed Spheres. Journal of Applied Physics. 1949;20:154-62.
[309] De Laat D, De Oliveira Filho FM, Vallentin F. Upper bounds for packings of spheres of several radii. Forum of Mathematics, Sigma. 2014;2:e23.
[310] Hopkins AB, Stillinger FH, Torquato S. Densest binary sphere packings. Physical Review E. 2012;85:021130.
[311] Schöllkopf W, Toennies JP. Nondestructive Mass Selection of Small van der Waals Clusters. Science. 1994;266:1345-8.
[312] Schneider WG. Properties of the Hydrogen Bond. The Role of Lone Pair Electrons. The Journal of Chemical Physics. 1955;23:26-30.
[313] Ludwig R. Water: From Clusters to the Bulk. Angewandte Chemie International Edition. 2001;40:1808-27.

[314] van Pelt A, Peters CJ, de Swaan Arons J, Deiters UK. Global phase behavior based on the simplified-perturbed hard-chain equation of state. The Journal of Chemical Physics. 1995;102:3361-75.
[315] Kolafa J, Nezbeda I, Pavlíček J, Smith WR. Global phase diagrams of model and real binary fluid mixtures: Lorentz–Berthelot mixture of attractive hard spheres. Fluid Phase Equilibria. 1998;146:103-21.
[316] Calado JCG, Lopes JNC. The building-up of phase diagrams. Pure and Applied Chemistry. 1999;71:1183-96.
[317] Wang J-L, Sadus RJ. Phase behaviour of binary fluid mixtures: a global phase diagram solely in terms of pure component properties. Fluid Phase Equilibria. 2003;214:67-78.
[318] Furman D, Griffiths RB. Global phase diagram for a Van der Waals model of a binary mixture. Physical Review A. 1978;17:1139-48.
[319] Privat R, Jaubert J-N. Classification of global fluid-phase equilibrium behaviors in binary systems. Chemical Engineering Research and Design. 2013;91:1807-39.
[320] V. Yelash L, Kraska T. The global phase behaviour of binary mixtures of chain molecules: theory and application. Physical Chemistry Chemical Physics. 1999;1:4315-22.
[321] Bolz A, Deiters UK, Peters CJ, Loos TWd. Nomenclature for phase diagrams with particular reference to vapour–liquid and liquid–liquid equilibria (Technical report). Pure and Applied Chemistry. 1998;70:2233-58.
[322] van Konynenburg PH, Scott RL. Critical lines and phase equilibria in binary van der Waals mixtures. Philosophical Transactions of the Royal Society of London Series A, Mathematical and Physical Sciences. 1980;298:495-540.
[323] Al Ghafri S. Phase Behaviour and Physical Properties of Reservoir Fluids Under Addition of Carbon Dioxide: Imperial College London; 2013.
[324] Van Den Bergh LC, Schouten JA, Trappeniers NJ. Fluid-fluid, fluid-solid and three-phase equilibria in the system helium-hydrogen at pressures up to 75 kbar. Physica A: Statistical Mechanics and its Applications. 1987;141:524-38.
[325] Rowlinson JS, Swinton FL. Chapter 6 - Fluid mixtures at high pressures. Liquids and Liquid Mixtures (Third Edition): Butterworth-Heinemann; 1982. p. 191-229.
[326] Li H, Dong B, Yu Z, Yan J, Zhu K. Thermo-physical properties of CO2 mixtures and their impacts on CO2 capture, transport and storage: Progress since 2011. Applied Energy. 2019;255:113789.
[327] Coquelet C, Stringari P, Hajiw M, Gonzalez A, Pereira L, Nazeri M, et al. Transport of CO2: Presentation of New Thermophysical Property Measurements and Phase Diagrams. Energy Procedia. 2017;114:6844-59.
[328] Nikolai P, Rabiyat B, Aslan A, Ilmutdin A. Supercritical CO2: Properties and Technological Applications - A Review. Journal of Thermal Science. 2019;28:394-430.
[329] Munkejord ST, Hammer M, Løvseth SW. CO2 transport: Data and models – A review. Applied Energy. 2016;169:499-523.
[330] Li H, Jakobsen JP, Wilhelmsen Ø, Yan J. PVTxy properties of CO2 mixtures relevant for CO2 capture, transport and storage: Review of available experimental data and theoretical models. Applied Energy. 2011;88:3567-79.
[331] Wang H, Li D. Measurement and correlations for vapor-liquid equilibrium data of CO2-isobutane and CO2-butene binary systems. Shiyou-Huagong. 2017;46:56-61.
[332] Weber LA. Vapour-liquid equilibria measurements for carbon dioxide with normal and isobutane from 250 to 280 K. Cryogenics. 1985;25:338-42.
[333] Weber LA. Simple apparatus for vapor-liquid equilibrium measurements with data for the binary systems of carbon dioxide with n-butane and isobutane. Journal of Chemical & Engineering Data. 1989;34:171-5.
[334] Besserer GJ, Robinson DB. Equilibrium-phase properties of isobutane-carbon dioxide system. Journal of Chemical & Engineering Data. 1973;18:298-301.
[335] Leu AD, Robinson DB. Equilibrium phase properties of the n-butane-carbon dioxide and isobutane-carbon dioxide binary systems. Journal of Chemical & Engineering Data. 1987;32:444-7.
[336] Nagahama K, Konishi H, Hoshino D, Hirata M. BINARY VAPOR-LIQUID EQUILIBRIA OF CARBON DIOXIDE-LIGHT HYDROCARBONS AT LOW TEMPERATURE. Journal of Chemical Engineering of Japan. 1974;7:323-8.

[337] Nagata Y, Mizutani K, Miyamoto H. The precise measurement of the (vapour+liquid) equilibrium properties for (CO2+isobutane) binary mixtures. The Journal of Chemical Thermodynamics. 2011;43:244-7.
[338] Hou S-X, Maitland GC, Trusler JPM. Measurement and modeling of the phase behavior of the (carbon dioxide+water) mixture at temperatures from 298.15K to 448.15K. The Journal of Supercritical Fluids. 2013;73:87-96.
[339] Yeo S-D, Park S-J, Kim J-W, Kim J-C. Critical Properties of Carbon Dioxide + Methanol, + Ethanol, + 1-Propanol, and + 1-Butanol. Journal of Chemical & Engineering Data. 2000;45:932-5.
[340] Horstmann S, Jabłoniec A, Krafczyk J, Fischer K, Gmehling J. PSRK group contribution equation of state: comprehensive revision and extension IV, including critical constants and α-function parameters for 1000 components. Fluid Phase Equilibria. 2005;227:157-64.
[341] Blackham TM, Lemmon EW. Literature reference for Carbon dioxide/Methanol in REFPROP 10.0. NIST. 2010.
[342] Sima S, Ionita S, Secuianu C, Feroiu F, Geana D. Fluid phase equilibria modelling for carbon dioxide + methanol system with cubic equations of state. Revista de Chimie -Bucharest- Original Edition-. 2014;65:272-9.
[343] Lyu Z, Ma H, Zhang H, Ying W. Solubility of carbon dioxide in methanol from 213.15 K to 273.15 K: Measurement and modeling. Fluid Phase Equilibria. 2018;471:40-54.
[344] Krichevsky I, Koroleva M. The solubility of methanol in compressed gases. Acta Physicochim URSS. 1941;15:327-42.
[345] Krichevskii IR, Lebedeva ES. Solubility of nitrogen and carbon monoxide in methanol under pressure. Zh Fiz Khim. 1947;21:715-8.
[346] Snedeker RA. Phase Equilibrium in Systems with Supercritical Carbon-dioxide: Princeton University; 1956.
[347] Bezdel L, Teodorovich V. Solubility of CO2, H2S, CH4, and C2H6 in methanol at low temperatures. Gazov Promst. 1958;8:38-43.
[348] Shenderei E, Zelvenskii YD, Ivanovskii F. Solubility of carbon dioxide in methanol at low temperature and high pressure. Khim Promst. 1959;4:328.
[349] Yorizane M, Sadamoto S, Masuoka H, Eto Y. Gas Solubilities in Methanol at High Pressure. The Journal of the Society of Chemical Industry, Japan. 1969;72:2174-7.
[350] Hemmaplardh B, King AD, Jr. Solubility of methanol in compressed nitrogen, argon, methane, ethylene, ethane, carbon dioxide, and nitrous oxide. Evidence for association of carbon dioxide with methanol in the gas phase. The Journal of Physical Chemistry. 1972;76:2170-5.
[351] Katayama T, Ohgaki K, Maekawa G, Goto M, Nagano T. ISOTHERMAL VAPOR-LIQUID EQUILIBRIA OF ACETONE-CARBON DIOXIDE AND METHANOL-CARBON DIOXIDE SYSTEMS AT HIGH PRESSURES. Journal of Chemical Engineering of Japan. 1975;8:89-92.
[352] Ohgaki K, Katayama T. Isothermal vapor-liquid equilibrium data for binary systems containing carbon dioxide at high pressures: methanol-carbon dioxide, n-hexane-carbon dioxide, and benzene-carbon dioxide systems. Journal of Chemical & Engineering Data. 1976;21:53-5.
[353] Schneider R. Experimental determination of the dynamic viscosity of mixtures of methanol with CO2, CH4, C2H6 and C3H8. Berlin: TU Berlin; 1978.
[354] Ferrell JK, Rousseau RW, Bass DG. The solubility of acid gases in methanol. Final report Oct 1976-Sep 1978. United States: North Carolina State Univ., Raleigh (USA). Dept. of Chemical Engineering; 1979. p. Medium: X; Size: Pages: 50.
[355] Semenova A, Emelyanova E, Tsimmerman S, Tsiklis D. Phase-equilibria in methanol carbon dioxide system. Zhurnal Fizicheskoi Khimii. 1979;53:2502-5.
[356] Lazalde-Crabtree H, Breedveld GJF, Prausnitz JM. Solvent losses in gas absorption. Solubility of methanol in compressed natural and synthetic gases. AIChE Journal. 1980;26:462-70.
[357] Takeuchi K, Inoue I. Present Status of the Studies on Deuterium Enrichment by Lasers. Kagaku Kogaku. 1980;44:292-300.
[358] Schmelter W. Experimental studies on the calculation of the gas solubility in the system CH3OH - CO2 - N2. Berlin: TU Berlin; 1982.

[359] Weber W, Zeck S, Knapp H. Gas solubilities in liquid solvents at high pressures: apparatus and results for binary and ternary systems of N2, CO2 and CH3OH. Fluid Phase Equilibria. 1984;18:253-78.
[360] Chang T, Rousseau RW. Solubilities of carbon dioxide in methanol and methanol-water at high pressures: experimental data and modeling. Fluid Phase Equilibria. 1985;23:243-58.
[361] Galivel-Solastiouk F, Laugier S, Richon D. Vapor-liquid equilibrium data for the propane-methanol and propane-methanol-carbon dioxide system. Fluid Phase Equilibria. 1986;28:73-85.
[362] Langhorst R. Experimental Study of the Vapor Phase in wide-boiling Mixtures and Development of a Data Bank for Phase Equilibria. Berlin: TU Berlin; 1987.
[363] Brunner E, Hültenschmidt W, Schlichthärle G. Fluid mixtures at high pressures IV. Isothermal phase equilibria in binary mixtures consisting of (methanol + hydrogen or nitrogen or methane or carbon monoxide or carbon dioxide). The Journal of Chemical Thermodynamics. 1987;19:273-91.
[364] Schroeder J. Experimental determination of the solubility of solvents in compressed gases using the systems CH3OH - CO2 and C6H5CH3. Praktikumsarbeit. 1987:1-80.
[365] Hong JH, Kobayashi R. Vapor—liquid equilibrium studies for the carbon dioxide—methanol system. Fluid Phase Equilibria. 1988;41:269-76.
[366] Suzuki K, Sue H, Itou M, Smith RL, Inomata H, Arai K, et al. Isothermal vapor-liquid equilibrium data for binary systems at high pressures: carbon dioxide-methanol, carbon dioxide-ethanol, carbon dioxide-1-propanol, methane-ethanol, methane-1-propanol, ethane-ethanol, and ethane-1-propanol systems. Journal of Chemical & Engineering Data. 1990;35:63-6.
[367] Melzer WM. A Contribution to the experimental Investigation of Gas-Liquid Phase Equilibria. Berlin: TU Berlin; 1990.
[368] Page SH, Goates SR, Lee ML. Methanol/CO2 phase behavior in supercritical fluid chromatography and extraction. The Journal of Supercritical Fluids. 1991;4:109-17.
[369] Leu A-D, Chung SYK, Robinson DB. The equilibrium phase properties of (carbon dioxide + methanol). The Journal of Chemical Thermodynamics. 1991;23:979-85.
[370] Schroedter F, Melzer WM, Knapp H. Investigation of phase equilibria in multicomponent mixtures consisting of propane, carbon dioxide, water and various organic solvents: Part I: Experimental methods, equipment and procedures; results with test systems consisting of CO2, C3H8 and CH3OH. Gas Separation & Purification. 1991;5:161-72.
[371] Yong Y, Zhangli J, Kunyuan L, Huanzhang L. Determination and Correlation of Saturated Liquid Density for Binary Systems of Carbon Dioxide with Acetone, Ethyl Ether and Methanol. Gaoxiao Huaxue Gongcheng Xuebao. 1992;6:11-8.
[372] Roškar V, Dombro RA, Prentice GA, Westgate CR, McHugh MA. Comparison of the dielectric behavior of mixtures of methanol with carbon dioxide and ethane in the mixture-critical and liquid regions. Fluid Phase Equilibria. 1992;77:241-59.
[373] Yoon JH, Lee HS, Lee H. High-pressure vapor-liquid equilibria for carbon dioxide + methanol, carbon dioxide + ethanol, and carbon dioxide + methanol + ethanol. Journal of Chemical & Engineering Data. 1993;38:53-5.
[374] Tsuji T, Hongo M. Vapor-Liquid Equilibrium of Carbon Dioxide - Methanol - Ethanol System at High Pressures. International Symposium on Thermodynamics in the Chemical Engineering Industry, Beijing. 1994:457-62.
[375] Kodama D, Kubota N, Yamaki Y, Tanaka H, Kato M. High Pressure Vapor-Liquid Equilibria and Density Behaviors for Carbon Dioxide+Methanol System at 313.15K. Netsu Bussei. 1996;10:16-20.
[376] Reighard TS, Lee ST, Olesik SV. Determination of methanol/CO2 and acetonitrile/CO2 vapor-liquid phase equilibria using a variable-volume view cell. Fluid Phase Equilibria. 1996;123:215-30.
[377] Chang CJ, Day C-Y, Ko C-M, Chiu K-L. Densities and P-x-y diagrams for carbon dioxide dissolution in methanol, ethanol, and acetone mixtures. Fluid Phase Equilibria. 1997;131:243-58.
[378] Joung SN, Yoon SJ, Park J-U, Kim SY, Yoo K-P. Single-Phase Limit for Mixtures of Tri-n-butyl Phosphate + CO2 and Bis(2-ethylhexyl)phosphoric Acid + CO2. Journal of Chemical & Engineering Data. 1999;44:1034-6.

[379] Elbaccouch MM, Raymond MB, Elliott JR. High-Pressure Vapor−Liquid Equilibrium for R-22 + Ethanol and R-22 + Ethanol + Water. Journal of Chemical & Engineering Data. 2000;45:280-7.
[380] Joung SN, Yoo CW, Shin HY, Kim SY, Yoo K-P, Lee CS, et al. Measurements and correlation of high-pressure VLE of binary CO2–alcohol systems (methanol, ethanol, 2-methoxyethanol and 2-ethoxyethanol). Fluid Phase Equilibria. 2001;185:219-30.
[381] Zhu H-G, Tian Y-L, Chen L, Feng J-J, Fu H-F. Studies on Vapor-liquid Phase Equilibria for SCF CO2 + CH3OH and SCF CO2 + C2H5OH Systems. Gaodeng Xuexiao Huaxue Xuebao. 2002;23:1588-91.
[382] Laursen T, Rasmussen P, Andersen SI. VLE and VLLE Measurements of Dimethyl Ether Containing Systems. Journal of Chemical & Engineering Data. 2002;47:198-202.
[383] Bezanehtak K, Combes GB, Dehghani F, Foster NR, Tomasko DL. Vapor−Liquid Equilibrium for Binary Systems of Carbon Dioxide + Methanol, Hydrogen + Methanol, and Hydrogen + Carbon Dioxide at High Pressures. Journal of Chemical & Engineering Data. 2002;47:161-8.
[384] Kodama D. Phase Equilibria for Mixtures with Supercritical Fluids. Osaka, Japan: Osaka University; 2002.
[385] Secuianu C, Feroiu V, Geana D. High-pressure phase equilibria for the carbon dioxide+ methanol and carbon dioxide+ isopropanol systems. REVISTA DE CHIMIE-BUCHAREST-ORIGINAL EDITION-. 2003;54:874-9.
[386] Secuianu C, Feroiu V, Geană D. High-Pressure Vapor−Liquid Equilibria in the System Carbon Dioxide and 2-Propanol at Temperatures from 293.25 K to 323.15 K. Journal of Chemical & Engineering Data. 2003;48:1384-6.
[387] Xia J, Jödecke M, Pérez-Salado Kamps Á, Maurer G. Solubility of CO2 in (CH3OH + H2O). Journal of Chemical & Engineering Data. 2004;49:1756-9.
[388] Joedecke M. Experimental and theoretical studies on the solubility of carbon dioxide in aqueous salt solutions with organic components. Germany: Kaiserslautern; 2004.
[389] Xie X, Brown JS, Bush D, Eckert CA. Bubble and Dew Point Measurements of the Ternary System Carbon Dioxide + Methanol + Hydrogen at 313.2 K. Journal of Chemical & Engineering Data. 2005;50:780-3.
[390] Schwinghammer S, Siebenhofer M, Marr R. Determination and modelling of the high-pressure vapour–liquid equilibrium carbon dioxide–methyl acetate. The Journal of Supercritical Fluids. 2006;38:1-6.
[391] Naidoo P, Ramjugernath D, Raal JD. A new high-pressure vapour–liquid equilibrium apparatus. Fluid Phase Equilibria. 2008;269:104-12.
[392] Secuianu C, Feroiu V, Geană D. Phase equilibria experiments and calculations for carbon dioxide + methanol binary system. Open Chemistry. 2009;7:1-7.
[393] Aida T, Aizawa T, Kanakubo M, Nanjo H. Relation between Volume Expansion and Hydrogen Bond Networks for CO2−Alcohol Mixtures at 40 °C. The Journal of Physical Chemistry B. 2010;114:13628-36.
[394] Tochigi K, Namae T, Suga T, Matsuda H, Kurihara K, dos Ramos MC, et al. Measurement and prediction of high-pressure vapor–liquid equilibria for binary mixtures of carbon dioxide+n-octane, methanol, ethanol, and perfluorohexane. The Journal of Supercritical Fluids. 2010;55:682-9.
[395] Sato Y, Hosaka N, Yamamoto K, Inomata H. Compact apparatus for rapid measurement of high-pressure phase equilibria of carbon dioxide expanded liquids. Fluid Phase Equilibria. 2010;296:25-9.
[396] Pinto LF, Ndiaye PM, Ramos LP, Corazza ML. Phase equilibrium data of the system CO2+glycerol+methanol at high pressures. The Journal of Supercritical Fluids. 2011;59:1-7.
[397] Schüler N, Hecht K, Kraut M, Dittmeyer R. On the Solubility of Carbon Dioxide in Binary Water–Methanol Mixtures. Journal of Chemical & Engineering Data. 2012;57:2304-8.
[398] Hamada T, Kobayashi D, Takahashi T, Shono A, Otake K, Tsuji T, et al. Phase behavior for carbon dioxide/tetraalkoxysilane systems. Fluid Phase Equilibria. 2012;322-323:135-41.
[399] Pinto LF, da Silva DIS, Rosa da Silva F, Ramos LP, Ndiaye PM, Corazza ML. Phase equilibrium data and thermodynamic modeling of the system (CO2+biodiesel+methanol) at high pressures. The Journal of Chemical Thermodynamics. 2012;44:57-65.

[400] Lei Z, Zhang B, Zhu J, Gong W, LÜ J, Li Y. Solubility of CO2 in Methanol, 1-Octyl-3-methylimidazolium Bis(trifluoromethylsulfonyl)imide, and Their Mixtures. Chinese Journal of Chemical Engineering. 2013;21:310-7.
[401] Kariznovi M, Nourozieh H, Abedi J. Experimental measurements and predictions of density, viscosity, and carbon dioxide solubility in methanol, ethanol, and 1-propanol. The Journal of Chemical Thermodynamics. 2013;57:408-15.
[402] Dai C, Wei W, Lei Z, Li C, Chen B. Absorption of CO2 with methanol and ionic liquid mixture at low temperatures. Fluid Phase Equilibria. 2015;391:9-17.
[403] Jalili AH, Shokouhi M, Samani F, Hosseini-Jenab M. Measuring the solubility of CO2 and H2S in sulfolane and the density and viscosity of saturated liquid binary mixtures of (sulfolane+CO2) and (sulfolane+H2S). The Journal of Chemical Thermodynamics. 2015;85:13-25.
[404] Braga AJO, do Carmo RP, Ndiaye PM, Tavares FW. Phase Behavior Data of (CO2 + Toluene + Phenanthrene) and (CO2 + (Methanol + Phenanthrene) Systems at High Pressure. Journal of Chemical & Engineering Data. 2017;62:2812-8.
[405] Höhler F, Deschermeier R, Rehfeldt S, Klein H. Gas solubilities of carbon dioxide in methanol, acetone, mixtures of methanol and water, and mixtures of methanol and acetone. Fluid Phase Equilibria. 2018;459:186-95.
[406] Taheri M, Dai C, Lei Z. CO2 capture by methanol, ionic liquid, and their binary mixtures: Experiments, modeling, and process simulation. AIChE Journal. 2018;64:2168-80.
[407] Wang W, Zheng K, Geng CY, Chen B, Hao X, Gu FN. Determination and thermodynamic calculation of lower hydrocarbon solubility in methanol. Huaxue-gongcheng. 2019;47:45-9.
[408] Matsukawa H, Otake K. Phase behavior of carbon dioxide/tetrapropyl orthosilicate and tetrabutyl orthosilicate systems. Fluid Phase Equilibria. 2021;548:113172.
[409] Braga AJO, Tavares FW, Ndiaye PM. A new high-pressure cell for equilibrium measurements of systems with fluid and solid phases. The Journal of Supercritical Fluids. 2022;179:105420.
[410] Staby A, Mollerup J. Mutual solubilities of mono-alcohols and carbon dioxide: A review of experimental data. Fluid Phase Equilibria. 1993;89:351-81.
[411] Polishuk I, Wisniak J, Segura H. Simultaneous prediction of the critical and sub-critical phase behavior in mixtures using equation of state I. Carbon dioxide-alkanols. Chemical Engineering Science. 2001;56:6485-510.
[412] Chang CJ, Chiu K-L, Day C-Y. A new apparatus for the determination of P–x–y diagrams and Henry's constants in high pressure alcohols with critical carbon dioxide. The Journal of Supercritical Fluids. 1998;12:223-37.
[413] Horváth RA, Horvai G, Idrissi A, Jedlovszky P. Thermodynamics of mixing methanol with supercritical CO2 as seen from computer simulations and thermodynamic integration. Physical Chemistry Chemical Physics. 2020;22:11652-62.
[414] Berger TA, Deye JF. Composition and density effects using methanol/carbon dioxide in packed column supercritical fluid chromatography. Analytical Chemistry. 1990;62:1181-5.
[415] Smith RL, Lee SB, Suzuki S, Saito C, Inomata H, Arai K. Densities of Carbon Dioxide + Methanol Mixtures at Temperatures from 313.2 to 323.2 K and at Pressures from 10 to 20 MPa. Journal of Chemical & Engineering Data. 2002;47:608-12.
[416] Kay WB. Some Peculiarities in the P-T Border Curves of Mixtures of Hydrogen and a Petroleum Naphtha. Chemical Reviews. 1941;29:501-7.
[417] Streett WB, Sonntag RE, Van Wylen GJ. Liquid—Vapor Equilibrium in the System Normal Hydrogen—Helium. The Journal of Chemical Physics. 1964;40:1390-5.
[418] Streett WB, Jones CH. Liquid Phase Separation and Liquid—Vapor Equilibrium in the System Neon—Hydrogen. The Journal of Chemical Physics. 1965;42:3989-94.
[419] Streett WB. Phase Equilibria in Molecular Hydrogen-Helium Mixtures at High Pressures. The Astrophysical Journal. 1973;186:1107-26.
[420] Streett WB, Calado JCG. Liquid-vapour equilibrium for hydrogen + nitrogen at temperatures from 63 to 110 K and pressures to 57 MPa. The Journal of Chemical Thermodynamics. 1978;10:1089-100.
[421] Calado JCG, Streett WB. Liquid—vapor equilibrium in the system H2□Ar at temperatures from 83 to 141 K and pressures to 52 MPa. Fluid Phase Equilibria. 1979;2:275-82.

[422] Tsang CY, Clancy P, Calado JCG, Streett WB. PHASE EQUILIBRIA IN THE H2/CH4 SYSTEM AT TEMPERATURES FROM 92.3 TO 180.0 K AND PRESSURES TO 140 MPa*. Chemical Engineering Communications. 1980;6:365-83.
[423] Tsang CY, Streett WB. Phase equilibria in the H2□CO system at temperatures from 70 to 125 K and pressures to 53 MPa. Fluid Phase Equilibria. 1981;6:261-73.
[424] Heintz A, Streett WB. Phase equilibriums in the hydrogen/ethane system at temperatures from 92.5 to 280.1 K and pressures to 560 MPa. Journal of Chemical & Engineering Data. 1982;27:465-9.
[425] Heintz A, Streett WB. Phase Equilibria in the H2/C2H4System at Temperatures from 114.1 to 247.1 K and Pressures to 600 MPa. Berichte der Bunsengesellschaft für physikalische Chemie. 1983;87:298-303.
[426] Tsang CY, Streett WB. Phase equilibria in the H2/CO2 system at temperatures from 220 to 290 K and pressures to 172 MPa. Chemical Engineering Science. 1981;36:993-1000.
[427] Strobel TA, Hester KC, Koh CA, Sum AK, Sloan ED. Properties of the clathrates of hydrogen and developments in their applicability for hydrogen storage. Chemical Physics Letters. 2009;478:97-109.
[428] Sloan ED, Koh CA. Clathrate hydrates of natural gases. 3rd ed. Boca Raton: CRC Press; 2008.
[429] Barwood MTJ, Metaxas PJ, Falloon PE, Milligan ASD, Wu W, May EF. Optical measurements of solid nitrogen solubility in hydrogen at cryogenic temperatures. International Journal of Hydrogen Energy. 2024;71:845-56.
[430] Ranieri U, Di Cataldo S, Rescigno M, Monacelli L, Gaal R, Santoro M, et al. Observation of the most H₂-dense filled ice under high pressure. Proceedings of the National Academy of Sciences. 2023;120:e2312665120.
[431] Harrison D, Welchman E, Thonhauser T. H4-alkanes: A new class of hydrogen storage material? International Journal of Hydrogen Energy. 2017;42:2223-8.
[432] Daynes HA, Shakespear GA, Smith SWJ. The theory of the katharometer. Proceedings of the Royal Society of London Series A, Containing Papers of a Mathematical and Physical Character. 1920;97:273-86.
[433] Zhang X, Zhai L, Li H, Qi G, Gao X, Yang W. Molecular Simulation Study on the Hydrogen Permeation Behavior and Mechanism of Common Polymers. Polymers. 2024;16:953.
[434] Ohaeri E, Eduok U, Szpunar J. Hydrogen related degradation in pipeline steel: A review. International Journal of Hydrogen Energy. 2018;43:14584-617.
[435] Menon NC, Kruizenga AM, Alvine KJ, San Marchi C, Nissen A, Brooks K. Behaviour of Polymers in High Pressure Environments as Applicable to the Hydrogen Infrastructure. ASME 2016 Pressure Vessels and Piping Conference2016.
[436] Westhaus U, Dröge T, Sass R. DETHERM®—a thermophysical property database. Fluid Phase Equilibria. 1999;158-160:429-35.
[437] Freeth FA, Verschoyle TTH. Physical constants of the system methane-hydrogen. Proceedings of the Royal Society of London Series A, Containing Papers of a Mathematical and Physical Character. 1931;130:453-63.
[438] Fastovskii W, Gonikberg M. The solubility of gases in liquids at low temperatures and high pressures. Acta Physicochim URSS. 1940;12:485-8.
[439] Benham AL, Katz DL. Vapor-liquid equilibria for hydrogen–light-hydrocarbon systems at low temperatures. AIChE Journal. 1957;3:33-6.
[440] Augood DR. The Separation of HD and H2 by Absorptive Fractionation. Trans Inst Chem Eng. 1957;35:394-408.
[441] Kirk BS, Ziegler WT. A Phase-Equilibrium Apparatus for Gas-Liquid Systems and the Gas Phase of Gas-Solid Systems: Application to Methane - Hydrogen from 66.88 to 116.53 K and up to 125 Atmospheres. Adv Cryog Eng. 1965;10.2:160-70.
[442] Yorizane M, Yoshimura S, Masuoka H, Toyama A. Low Temperature Vapor-Liquid Equilibria of Hydrogen - Containing Binaries. Proc Int Cryog Eng Conf ICEC. 1968;1:57-62.
[443] Sagara H, Arai Y, Saito S. VAPOR-LIQUID EQUILIBRIA OF BINARY AND TERNARY SYSTEMS CONTAINING HYDROGEN AND LIGHT HYDROCARBONS. Journal of Chemical Engineering of Japan. 1972;5:339-48.

[444] Yorizane M, Yoshimura S, Masuoka H, Funada I, Fu CT, Lu BCY. Phase Behavior of Three Hydrogen-Containing Ternary Systems. In: Timmerhaus KD, Snyder HA, editors. Advances in Cryogenic Engineering. Boston, MA: Springer US; 1980. p. 654-61.
[445] Hong JH, Kobayashi R. Vapor-liquid equilibrium study of the hydrogen-methane system at low temperatures and elevated pressures. Journal of Chemical & Engineering Data. 1981;26:127-31.
[446] Hu M, Lin W, Gu A, Li J. Isothermal vapor–liquid equilibrium in CH4/H2/N2 system at a cryogenic temperature range from 100.0K to 125.0K. Fluid Phase Equilibria. 2014;366:16-23.
[447] Lin W, Hu M, Gu A. Vapor-liquid equilibria for low temperature CH4/H2 mixture. International Journal of Hydrogen Energy. 2018;43:12671-9.
[448] Levitskaya E, Pryannikov K. Vapor-Liquid Equilibrium in the System Hydrogen - Ethane. Zh Tekhn Fiz. 1939;9:1849-53.
[449] Williams RB, Katz DL. Vapor-Liquid Equilibria in Binary Systems. Hydrogen with Ethylene, Ethane, Propylene, and Propane. Industrial & Engineering Chemistry. 1954;46:2512-20.
[450] Cohen AE, Hipkin HG, Koppany CR. Experimental vapor-liquid equilibria for hydrogen-nitrogen-methane-ethane-ethylene. The Canadian Journal of Chemical Engineering. 1969;47:422-6.
[451] Hiza MJ, Heck CK, Kidnay AJ. Liquid-Vapor and Solid-Vapor Equilibrium in the System Hydrogen-Ethane. In: Timmerhaus KD, editor. Advances in Cryogenic Engineering. Boston, MA: Springer US; 1995. p. 343-56.
[452] Burriss WL, Hsu NT, Reamer HH, Sage BH. Phase Behavior of the Hydrogen-Propane System. Industrial & Engineering Chemistry. 1953;45:210-3.
[453] Bolshakov PE, Linshits LR. Phase equilibria in liquid-gas systems at high pressures. Tr Gos Nauchno Issled Proektn Inst Azotn Promst Prod Org Sin. 1954;3:18-27.
[454] Trust DB. The Hetergeneous Phase Behavior of the Hydrogen - Propane, Carbon Monoxide - Propane and Hydrogen - Carbon Monoxide - Propane Systems: University of Kansas; 1968.
[455] Freitag NP, Robinson DB. Equilibrium phase properties of the hydrogen—methane—carbon dioxide, hydrogen—carbon dioxide—n-pentane and hydrogen—n-pentane systems. Fluid Phase Equilibria. 1986;31:183-201.
[456] Nichols WB, Reamer HH, Sage BH. Volumetric and phase behavior in the hydrogen–n-hexane system. AIChE Journal. 1957;3:262-7.
[457] Peter S, Reinhartz K. Das Phasengleichgewicht in den Systemen H2—n-Heptan, H2-Methylcyclohexan und H2—2,2,4-Trimethylpentan bei höheren Drucken und Temperaturen. Zeitschrift für Physikalische Chemie. 1960;24:103-18.
[458] Zernov VS, Kogan VB, Egudina OG, Kobyakov VM, Babayants TV, Kalichava LI. Phase Equilibria and Volume Ratios in the Systems Heptane - Ethylene and Heptane - Hydrogen. J Appl Chem USSR. 1990;63:1469-72.
[459] Connolly JF. Vapor-Liquid Equilibrium Ratios for Four Binary Systems. Proc Amer Petrol Inst Sec 3. 1965;45:62-7.
[460] Connolly JF, Kandalic GA. Thermodynamic properties of solutions of hydrogen in n-octane. The Journal of Chemical Thermodynamics. 1989;21:851-8.
[461] Sebastian HM, Simnick JJ, Lin H-M, Chao K-C. Gas-liquid equilibrium in the hydrogen + n-decane system at elevated temperatures and pressures. Journal of Chemical & Engineering Data. 1980;25:68-70.
[462] Connolly JF, Kandalic GA. Gas solubilities, vapor-liquid equilibria, and partial molal volumes in some hydrogen-hydrocarbon systems. Journal of Chemical & Engineering Data. 1986;31:396-406.
[463] Laugier S, Richon D, Renon H. Vapor-liquid equilibriums of hydrogen-2,2,4-trimethylpentane and hydrogen-toluene systems at high pressures and temperatures. Journal of Chemical & Engineering Data. 1980;25:274-6.
[464] Likhter AI, Tikhanovich NP. Vapor-Liquid Equilibrium in the System Ethylene - Methane - Hydrogen. I. Binary System Ethylene - Hydrogen. Zh Tekhn Fiz. 1939;9:1916-22.
[465] Hiza MJ, Heck CK, Kidnay AJ. Liquid-Vapor and Solid-Vapor Equilibrium in the System Hydrogen - Ethylene. Chem Eng Progr Symp Ser. 1968;64:57-65.
[466] Krichevskii IR, Sorina GA. The phase and volume relations in systems liquid-gas at high pressures. V: The system cyclohexane - hydrogen. Zh Fiz Khim. 1958;32:2080-6.

[467] Thompson RE, Edmister WC. Vapor-liquid equilibria in hydrogen-benzene and hydrogen-cyclohexane mixtures. AIChE Journal. 1965;11:457-61.
[468] Berty TE, Reamer HH, Sage BH. Phase Behavior in the Hydrogen-Cyclohexane System. Journal of Chemical & Engineering Data. 1966;11:25-30.
[469] Ipatev VV, Teodorovich VP, Brestkin AP, Artemovich VS. Study at High Pressures. I. Vapor-Liquid Equilibrium in the System Hydrogen - Benzene at 3000 atm. Zh Fiz Khim. 1948;22:833-45.
[470] Connolly JF. Thermodynamic Properties of Hydrogen in Benzene Solutions. The Journal of Chemical Physics. 1962;36:2897-904.
[471] Simnick JJ, Sebastian HM, Lin H-M, Chao K-C. Solubility of hydrogen in toluene at elevated temperatures and pressures. Journal of Chemical & Engineering Data. 1978;23:339-40.
[472] Gillespie PC, Owens JL, Wilson GM. Gas Solubilities and Vapor-Liquid Equilibrium Measurements of H2, CO2 and NH3 in Water - Phenol Mixtures from 110F to 550F. GPA Research Rep. 1986:1-40.
[473] Michels A, De Graaff W, Van Der Somme J. Gas-liquid phase equilibrium in the system methanol-hydrogen. Applied Scientific Research, Section A. 1953;4:105-8.
[474] d'Angelo JVH, Francesconi AZ. Gas−Liquid Solubility of Hydrogen in n-Alcohols ($1 \leqslant n \leqslant 4$) at Pressures from 3.6 MPa to 10 MPa and Temperatures from 298.15 K to 525.15 K. Journal of Chemical & Engineering Data. 2001;46:671-4.
[475] Brunner E, Hültenschmidt W. Fluid mixtures at high pressures VIII. Isothermal phase equilibria in the binary mixtures: (ethanol + hydrogen or methane or ethane). The Journal of Chemical Thermodynamics. 1990;22:73-84.
[476] Tyvina TN, Valuev KI, Vasil'eva II, Sokolov BI, Kharchenko AI. Gas-liquid equilibrium in systems formed by hydrogen with butanols. J Appl Chem USSR. 1977;50:2446-9.
[477] Verschoyle TTH, Freeth FA. The ternary system carbon monoxide-nitrogen-hydrogen and the component binary systems between temperatures of -185° and -215° C., and between pressures of 0 and 225 atm. Philosophical Transactions of the Royal Society of London Series A, Containing Papers of a Mathematical or Physical Character. 1931;230:189-220.
[478] Gonikberg MG, Fastovskii VG, Gurvich IG. The solubility of gases in liquids at low temperatures and high pressures. I. Solubility of hydrogen in liquid nitrogen at temperatures of 79.0 - 109.0 K and pressures up to 190 atm. Acta Physicochim URSS. 1939;11:865-82.
[479] Shtekkel FA, Tsinn NM. Determination of the Vapor-Liquid State-Diagrams of the System Methane - Nitrogen - Hydrogen. Zh Khim Prom. 1939;16:24-8.
[480] Akers WW, Eubanks LS. Vapor-Liquid Equilibria in the System Hydrogen-Nitrogen-Carbon Monoxide. In: Timmerhaus KD, editor. Advances in Cryogenic Engineering. Boston, MA: Springer US; 1960. p. 275-93.
[481] Maimoni A. Liquid-vapor equilibria in the hydrogen-nitrogen and deuterium-nitrogen systems. AIChE Journal. 1961;7:371-5.
[482] Xiao J, Liu K. H2 - N2 - Ar ... Huaxue Gongcheng Xi'an. 1990;18:8-12.
[483] Newman RB, Jackson LC. The P, T, x relationships of H2+HD and H2+D2 mixtures between 18° and 28°K. Transactions of the Faraday Society. 1958;54:1481-91.
[484] Kaminishi GI, Toriumi T. Vapor-Liquid Phase Equilibrium in the CO2 - H2, CO2 - N2 and CO2 - O2 System. Kogyo Kagaku Zasshi. 1966;69:175-8.
[485] Spano JO, Heck CK, Barrick PL. Liquid-vapor equilibria of the hydrogen-carbon dioxide system. Journal of Chemical & Engineering Data. 1968;13:168-71.
[486] Yorizane M, Yoshimura S, Masuoka H. Vapor-Liquid Equilibrium at High Pressure: N2 - CO2, H2 - CO2 System. Kagaku Kogaku. 1970;34:953-7.
[487] Tenorio M-J, Parrott AJ, Calladine JA, Sanchez-Vicente Y, Cresswell AJ, Graham RS, et al. Measurement of the vapour–liquid equilibrium of binary and ternary mixtures of CO2, N2 and H2, systems which are of relevance to CCS technology. International Journal of Greenhouse Gas Control. 2015;41:68-81.
[488] Zoss LM. A Study of the Hydrogen and Water and Oxygen and Water Systems at Various Pressures and Temperatures [Ph.D.]. United States -- Indiana: Purdue University; 1952.
[489] De Vaney WE, Eakin BE. High-temperature VLE measurements for substitute gas components. Proc Ann Conv Nat Gasoline Assoc Am Tech Papers. 1976;55:8-9.

[490] Gillespie PC, Wilson GM. Vapor-liquid equilibrium data on water-substitute gas components: N/sub 2/-H/sub 2/O, H/sub 2/-H/sub 2/O, CO-H/sub 2/O, H/sub 2/-CO-H/sub 2/O, and H/sub 2/S-H/sub 2/O. United States1980. p. Medium: ED; Size: Pages: 38.
[491] Seward TM, Franck EU. The system hydrogen - water up to 440°C and 2500 bar pressure. Berichte der Bunsengesellschaft für physikalische Chemie. 1981;85:2-7.
[492] Wiebe R, Tremearne TH. The Solubility of Hydrogen in Liquid Ammonia at 25, 50, 75 and 100° and at Pressures to 1000 Atmospheres. Journal of the American Chemical Society. 1934;56:2357-60.
[493] Wiebe R, Gaddy VL. The Solubility in Liquid Ammonia of Hydrogen at 0° and of Nitrogen at 0, 50, 75, 90 and 100° at Pressures to 1000 Atmospheres. Critical Phenomena of Ammonia-Nitrogen Mixtures1. Journal of the American Chemical Society. 1937;59:1984-7.
[494] Reamer HH, Sage BH. Phase Behavior in the Hydrogen-Ammonia System. Journal of Chemical & Engineering Data. 1959;4:152-4.
[495] Heise F. Flüssigkeits-Dampfgleichgewichte zwischen Ammoniak und verschiedenen Gasen. Berichte der Bunsengesellschaft für physikalische Chemie. 1972;76:938-43.
[496] Smith SR. I. Gas-Liquid Phase Equilibrium in the System He - H2. II. Development of Mass Spectrograph Techniques for Analysis of He - H2 and Their Isotopes: Ohio State University; 1952.
[497] Sonntag RE, Van Wylen GJ, Crain RW, Jr. Liquid—Vapor Equilibrium in the System Equilibrium Hydrogen—Helium. The Journal of Chemical Physics. 1964;41:2399-402.
[498] Sneed CM, Sonntag RE, Van Wylen GJ. Helium–Hydrogen Liquid–Vapor Equilibrium to 100 atm. The Journal of Chemical Physics. 1968;49:2410-4.
[499] Hiza MJ. Liquid-vapor equilibria in binary systems containing 4He or 3He with nH2 or nD2. Fluid Phase Equilibria. 1981;6:203-27.
[500] Pashkov VV, Blagoi YP, Lobko MP, Marinin VS. Vapor-Liquid Equilibrium in Helium - para-Hydrogen Solutions. Fiz Nizk Temp Kiev. 1981;7:549-59.
[501] Yamanishi T, Okuno K, Naruse Y, Sada E. Liquid-vapor equilibrium in binary systems for He in n-hydrogen, hydrogen deuteride, and n-deuterium under ordinary pressure. The Journal of Physical Chemistry. 1992;96:2284-9.
[502] Heck CK, Barrick PL. Liquid-Vapor Phase Equilibria of the Neon - Normal Hydrogen System. In: Timmerhaus KD, editor. 1965 Cryogenic Engineering Conference. Houston, Texas: Adv. Cryog. Eng.; 1965. p. 349-55.
[503] Volk H, Halsey GD, Jr. Solubility of Hydrogen and Deuterium in Liquid Argon. The Journal of Chemical Physics. 1960;33:1132-9.
[504] Mullins JC, Ziegler WT. Phase Equilibria in the Argon - Helium and Argon - Hydrogen Systems from 68 to 108 K and Pressures to 120 Atmospheres. In: Timmerhaus KD, editor. 1964 Cryogenic Engineering Conference. Philadelphia, Pa: Adv. Cryog. Eng.; 1964. p. 171-81.
[505] Ostronov MG, Shatskaya LV, Finyagina RA, Brodskaya LF, Zhirnova NA. Gas-Liquid Phase Equilibrium in the Argon - Hydrogen System at Intermediate Pressures. Russ J Phys Chem. 1977;51:1407-9.
[506] Florusse LJ, Peters CJ, Pàmies JC, Vega LF, Meijer H. Solubility of hydrogen in heavy n-alkanes: Experiments and saft modeling. AIChE Journal. 2003;49:3260-9.
[507] Cosway HF, Katz DL. Low-temperature vapor-liquid equilibria in ternary and quaternary systems containing hydrogen, nitrogen, methane, and ethane. AIChE Journal. 1959;5:46-50.
[508] Lozano-Martín D, Moreau A, Chamorro CR. Thermophysical properties of hydrogen mixtures relevant for the development of the hydrogen economy: Review of available experimental data and thermodynamic models. Renewable Energy. 2022;198:1398-429.
[509] Katz DL, Hachmuth KH. Vaporization Equilibrium Constants in a Crude Oil–Natural Gas System. Industrial & Engineering Chemistry. 1937;29:1072-7.
[510] Chen Z-h, Yao Z, Zhu F-j, Cao K, Li Y, Huang Z-m. Gas−Liquid Critical Properties of Ethylene + Hydrogen and Propylene + Hydrogen Binary Mixtures. Journal of Chemical & Engineering Data. 2010;55:2004-7.
[511] Polyakov AA, Tyvina TN, Vasileva II, Naumova AA. 1986.
[512] Brunner E. Fluid mixtures at high pressures I. Phase separation and critical phenomena of 10 binary mixtures of (a gas + methanol). The Journal of Chemical Thermodynamics. 1985;17:671-9.

[513] Alfarizi MG, Ustolin F, Vatn J, Yin S, Paltrinieri N. Towards accident prevention on liquid hydrogen: A data-driven approach for releases prediction. Reliability Engineering & System Safety. 2023;236:109276.
[514] Pohsner GM, Franck EU. Spectra and temperatures of diffusion flames at high pressures to 1000 bar. Berichte der Bunsengesellschaft für physikalische Chemie. 1994;98:1082-90.
[515] Köster A, Thol M, Vrabec J. Molecular Models for the Hydrogen Age: Hydrogen, Nitrogen, Oxygen, Argon, and Water. Journal of Chemical & Engineering Data. 2018;63:305-20.
[516] Bornea A, Zamfirache M, Stefanescu I, Preda A, Balteanu O, Stefan I. Investigation Related to Hydrogen Isotopes Separation by Cryogenic Distillation. Fusion Science and Technology. 2008;54:426-9.
[517] Tsankova G, Leusmann Y, Span R, Richter M. Dew Points, Dielectric Permittivities, and Densities for (Hydrogen + Carbon Dioxide) Mixtures Determined with a Microwave Re-Entrant Cavity Resonator. Industrial & Engineering Chemistry Research. 2019;58:21752-60.
[518] Torín-Ollarves GA, Trusler JPM. Solubility of hydrogen in sodium chloride brine at high pressures. Fluid Phase Equilibria. 2021;539:113025.
[519] Haynes WM, Lide DR, Bruno TJ. CRC handbook of chemistry and physics : a ready-reference book of chemical and physical data. 94th edition / editor-in-chief, W.M. Haynes, Ph.D. ; associate editors, David R. Lide, Ph.D., Thomas J. Bruno, Ph.D. ed. Boca Raton: CRC Press; 2013.
[520] Mace EJ, Vrabec J. High-Pressure Fluid-Phase Equilibria and Henry's Constants of Supercritical Gases in Ammonia. Journal of Chemical & Engineering Data. 2024;69:573-89.
[521] Chidester BA, Strobel TA. The Ammonia–Hydrogen System under Pressure. The Journal of Physical Chemistry A. 2011;115:10433-7.
[522] van den Bergh LC, Schouten JA. Prediction of fluid–fluid and fluid–solid equilibria in the molecular system helium–hydrogen up to 1 Mbar. The Journal of Chemical Physics. 1988;89:2336-43.
[523] Simon M. On the phase separation in the liquid system Ne-pH2. Physics Letters. 1963;5:319.
[524] Brouwer JP, Hermans LJF, Knaap HFP, Beenakker JJM. Phase separation in the liquid mixture of neon and deuterium. Physica. 1964;30:1409-20.
[525] Simon M. On the phase separation in the liquid system Ne - nD2. Physics Letters. 1962;2:234.
[526] Streett WB. Phase equilibria in gas mixtures at high pressures. Icarus. 1976;29:173-86.
[527] Streett WB. Gas-gas equilibrium: High pressure limits. The Canadian Journal of Chemical Engineering. 1974;52:92-7.
[528] Cea-Klapp E, González-Barramuño B, Gajardo-Parra NF, Karelovic A, Quinteros-Lama H, Canales RI, et al. Assessing Thermodynamics Models for Phase Equilibria and Interfacial Properties Relevant to the Hydrogenation of Carbon Dioxide. Industrial & Engineering Chemistry Research. 2024;63:12235-49.
[529] Hassanpouryouzband A, Joonaki E, Edlmann K, Heinemann N, Yang J. Thermodynamic and transport properties of hydrogen containing streams. Scientific Data. 2020;7:222.
[530] Beckmüller R, Bell IH, Thol M, Lemmon EW, Span R. New fundamental equations of state for binary hydrogen mixtures containing argon, helium, and neon. Cryogenics. 2024;140:103817.
[531] Deiters UK, Bell IH. Unphysical Critical Curves of Binary Mixtures Predicted with GERG Models. International Journal of Thermophysics. 2020;41:169.
[532] Souza LFS, Al Ghafri SZS, Fandiño O, Trusler M. Vapor-liquid equilibria, solid-vapor-liquid equilibria and H2S partition coefficient in (CO2 + CH4) at temperatures between (203.96 and 303.15) K at pressures up to 9 MPa. Fluid Phase Equilibria. 2020;522:112762.
[533] Souza LFDSD. Thermodynamic properties for pre-combustion CO2 capture and pipeline transportation. Department of Chemical Engineering: Imperial College London; 2018.
[534] Dohrn R, Fonseca JMS, Peper S. Experimental Methods for Phase Equilibria at High Pressures. Annual Review of Chemical and Biomolecular Engineering. 2012;3:343-67.
[535] Preston-Thomas H. The International Temperature Scale of 1990 (ITS-90). Metrologia. 1990;27:3.

[536] Gaiser C, Fellmuth B, Gavioso RM, Kalemci M, Kytin V, Nakano T, et al. 2022 Update for the Differences Between Thermodynamic Temperature and ITS-90 Below 335 K. Journal of Physical and Chemical Reference Data. 2022;51.
[537] Guilbot P, Valtz A, Legendre H, Richon D. Rapid on-line sampler-injector: a reliable tool for HT-HP sampling and on-line GC analysis. Analusis. 2000;28:426-31.
[538] Richon D. Experimental techniques for the determination of thermophysical properties to enhance chemical processes. Pure and Applied Chemistry. 2009;81:1769-82.
[539] Richon D. ROLSI Success Story2009.
[540] Bruno TJ, Rybowiak MC. Vapor entraining magnetic mixer for reaction and equilibrium applications. Fluid Phase Equilibria. 2001;178:271-6.
[541] Perkins R, Roder HM, Decastro CAN. A High-Temperature Transient Hot-Wire Thermal Conductivity Apparatus for Fluids. Journal of Research of the National Institute of Standards and Technology. 1991;96:247.
[542] Richmond AB. Thermal Conductivity Detectors for Gas Chromatography: A Literature Survey. Journal of Chromatographic Science. 1971;9:92-8.
[543] Gardner ELW, Gardner JW, Udrea F. Micromachined Thermal Gas Sensors-A Review. Sensors (Basel). 2023;23.
[544] Al Ghafri SZS, Forte E, Galindo A, Maitland GC, Trusler JPM. Experimental and Modeling Study of the Phase Behavior of (Heptane + Carbon Dioxide + Water) Mixtures. Journal of Chemical & Engineering Data. 2015;60:3670-81.
[545] Al Ghafri SZS, Forte E, Maitland GC, Rodriguez-Henríquez JJ, Trusler JPM. Experimental and Modeling Study of the Phase Behavior of (Methane + CO2 + Water) Mixtures. The Journal of Physical Chemistry B. 2014;118:14461-78.
[546] Forte E, Galindo A, Trusler JPM. Experimental and Molecular Modeling Study of the Three-Phase Behavior of (n-Decane + Carbon Dioxide + Water) at Reservoir Conditions. The Journal of Physical Chemistry B. 2011;115:14591-609.
[547] Forte E, Galindo A, Trusler JPM. Experimental and molecular modelling study of the three-phase behaviour of (propane+carbon dioxide+water) at reservoir conditions. The Journal of Supercritical Fluids. 2013;75:30-42.
[548] Foley JP, Dorsey JG. A Review of the Exponentially Modified Gaussian (EMG) Function: Evaluation and Subsequent Calculation of Universal Data. Journal of Chromatographic Science. 1984;22:40-6.
[549] Jeansonne MS, Foley JP. Review of the Exponentially Modified Gaussian (EMG) Function Since 1983. Journal of Chromatographic Science. 1991;29:258-66.
[550] Martin Trusler JP. Measurement of Diffusion Coefficients in Binary Mixtures and Solutions by the Taylor Dispersion Method. International Journal of Thermophysics. 2024;45:46.
[551] Tay WJ. Thermophysical Properties of Hydrocarbons with Dissolved Carbon Dioxide. London: Imperial College London; 2017.
[552] Schoonover RM, Jones FE. Air buoyancy correction in high-accuracy weighing on analytical balances. Analytical Chemistry. 1981;53:900-2.
[553] Ansaloni L, Alcock B, Peters TA. Effects of CO2 on polymeric materials in the CO2 transport chain: A review. International Journal of Greenhouse Gas Control. 2020;94:102930.
[554] Rhoderick GC, Cecelski CE, Miller WR, Worton DR, Moreno S, Brewer PJ, et al. Stability of gaseous volatile organic compounds contained in gas cylinders with different internal wall treatments. Elementa (Wash D C). 2019;7.
[555] Persijn ST, Baldan A. A new look at the sorption kinetics in reference gas standards. Measurement Science and Technology. 2023;34:115018.
[556] Baldan A. KEY-VOCs: Metrology for VOC indicators in air pollution and climate change (ENV56). EURAMET; 2017.
[557] Swenson H, Stadie NP. Langmuir's Theory of Adsorption: A Centennial Review. Langmuir. 2019;35:5409-26.
[558] Rösler M, Wedler C. Adsorption kinetics and equilibria of two methanol samples with different water content on activated carbon. Adsorption. 2021;27:1175-90.
[559] BIPM, IEC, IFCC, ILAC, ISO, IUPAC, et al. Evaluation of measurement data — Guide to the expression of uncertainty in measurement (JCGM 100:2008). JCGM Working Group 1; 2008.

[560] BIPM, IEC, IFCC, ILAC, ISO, IUPAC, et al. Basic and general concepts and associated terms. Joint Committee for Guides in Metrology (JCGM 200:2012). JCGM Working Group 1; 2012.
[561] Bernardini L, McLinden MO, Yang X, Richter M. How Accurate are Your Experimental Data? A More Accessible GUM-Based Methodology for Uncertainty Evaluation. International Journal of Thermophysics. 2024;45:164.
[562] Fall DJ, Luks KD. Liquid-liquid-vapor phase equilibria of the binary system carbon dioxide + n-tridecane. Journal of Chemical & Engineering Data. 1985;30:276-9.
[563] Pan Z, Trusler JPM, Jin Z, Zhang K. Interfacial property determination from dynamic pendant-drop characterizations. Nature Protocols. 2025;20:363-86.
[564] Kim Q, Jhe W. Interfacial thermodynamics of spherical nanodroplets: molecular understanding of surface tension via a hydrogen bond network. Nanoscale. 2020;12:18701-9.
[565] Contreras S, Martínez-Borquez A, Avendaño C, Gil-Villegas A, Jackson G. Unmasking quantum effects in the surface thermodynamics of fluid nanodrops. The Journal of Chemical Physics. 2024;160.
[566] McGlashan ML, Stead K, Warr C. Prediction of (so-called) gas–gas immiscibility in fluid mixtures. Journal of the Chemical Society, Faraday Transactions 2: Molecular and Chemical Physics. 1977;73:1889-95.
[567] Green MS, Vicentini-Missoni M, Sengers JMHL. Scaling-Law Equation of State for Gases in the Critical Region. Physical Review Letters. 1967;18:1113-7.
[568] Mraw SC, Kobayashi R. Calibration of a Chromatographic Apparatus Using a Positive Displacement Pumping Method. Journal of Chromatographic Science. 1977;15:191-5.
[569] Outcalt SL. Calibration fluids and calibration equations: How choices may affect the results of density measurements made with U-tube densimeters. Journal of Research of the National Institute of Standards and Technology. 2018;123:1.
[570] Papaioannou V, Calado F, Lafitte T, Dufal S, Sadeqzadeh M, Jackson G, et al. Application of the SAFT-γ Mie group contribution equation of state to fluids of relevance to the oil and gas industry. Fluid Phase Equilibria. 2016;416:104-19.